Deactivation of Precious Metal Steam Reforming Catalysts

A Thesis presented to the University of Glasgow for the Degree of Doctor of Philosophy

by

Claire Gillan

September 2009

Steam reforming is a well established industrial process for the formation of synthesis gas. It takes place in two reversible stages: the reforming reaction (1) followed by the water-gas shift reaction (2).

(1) $C_nH_{2n+2} + nH_2O \rightleftharpoons nCO + (2n+1)H_2$

(2) $CO + H_2O \rightleftharpoons CO_2 + H_2$

Reaction (1) is highly endothermic and is favoured at high temperatures and low pressure, while reaction (2) takes place at as low temperature as possible. One of the major problems affecting the steam reforming industry is catalyst deactivation due to sulphur poisoning. Sulphur is present in the hydrocarbon feedstock and even after desulphurisation steps some sulphur still remains, from ppb to ppm levels. Such low levels of sulphur can still poison the catalyst due to the catalyst having a significant time on stream. It is therefore desirable to produce a catalyst that exhibits sulphur resistance to prolong the lifetime of the catalyst.

In this project the behaviour of precious metal catalysts (Rh and Pt supported on La-ZrO_2, Al_2O_3 and SiO_2) towards sulphur was examined. Two major aspects were studied, the catalysts' adsorpitive behaviour towards sulphur and the effect of sulphur during the steam reforming reaction.

Low pressure pulses of H_2S and CH_3SH over the catalysts followed by gas chromatography revealed that sulphur is a very strong adsorbing species, similar to CO, and could not be displaced by the adsorption of another species as there was no mechanism to desorb the sulphur species. The alumina supported catalysts offered some protection from sulphur poisoning, evidenced during co-adsorption experiments with CO, because the support was acting as a 'sulphur sink'. Adsorption mechanisms were proposed for H_2S at the different adsorption conditions tested: a 3-site adsorption mechanism producing surface sulphides at room temperature and at higher temperatures bulk sulphides were formed.

High pressure steam reforming reactions of ethane were carried out at three different temperatures (600°C, 550°C and 500°C) to act as standards to the poisoned reactions, but also revealed interesting insights into the reforming of ethane. Each catalyst produced a unique reaction profile during steam

reforming, with the La-ZrO_2 catalyst exhibiting greatest activity. The Rh catalysts showed high selectivity towards the formation of CH_4 due to the hydrogenolysis of C_2H_6, which was not occurring over the Pt catalysts. The Pt catalysts were the least active and deactivated considerably as the result of carbon formation.

Sulphur species, hydrogen sulphide and methanthiol, were introduced into the reaction by dissolving them in the feed water. It was found the identity of the sulphur species had a significant impact upon the extent of catalyst deactivation, with methanthiol having the most detrimental effect, which was attributed to the molecule decomposing and laying down carbon. None of the catalysts tested exhibited particularly high sulphur resistance, particularly with regard to methanthiol, however Rh/ZrO_2 did recover a lot of its original activity once the poison was removed from the feed. This was due to the removal of surface carbon rather than the removal of sulphur from the catalyst, because La-ZrO_2 has a faster rate of oxygen transfer and therefore a mechanism to remove surface carbon.

It would have been an impossible task getting through my PhD without the help and support of many people who have contributed along the way. I would first like to thank my supervisor, Prof. David Jackson for giving me this opportunity, and for being supportive and helpful throughout this project. I would like to thank my industrial supervisors, Dr Martin Fowles, Dr David Birdsall and Dr Sam French, for taking regular trips up to Glasgow and always giving me very useful feedback.

A huge thank you to Ron Spence for all his help and expertise with building the rig and afterwards when the occasional problem popped up. Thanks to Andy Monaghan for BETs and TGAs and the cups of tea! To William McCormak for helping with all things glass related, this may have included a breakage or two.

Thank you to Gemma Parker for showing me how to use the glass line. Dan Rosenberg and Joe Gamman for all there help at the beginning; and those who have been there throughout my project, thank you Mark, Stuart, Fiona, Lynsey, Anne-Marie and Liam. A special thank you to my good friend from the other side (organic…), Catherine. Thanks for letting me talk so much about catalysts and listening to every presentation I have ever done.

Finally, thanks to my friends and family for always being there for me. To Emma, Melanie, Bryan and my mum and dad, I could not have done this without you!

Declaration

The work contained in this thesis, submitted for the degree of Doctor of Philophosphy, is my original work, except where due reference is made to other authors. No material within has been previously submitted for a degree at this or any other university.

Claire Gillan

Figures and Tables

1. Introduction

1.1. Hydrogen Production

Hydrogen is currently a valuable feedstock for many industries; including refineries for processes such as hydrotreating and hydrocracking, fuels cells, hydrogenations and reducing gas. More recently hydrogen has been cited as a fuel for the future. The U.S Department of Energy have devoted an entire program to developments in hydrogen-based technology: 'The National Hydrogen program'. One of the major aims of this program is for hydrogen to contribute 8-10% of the total energy market by 2025[1].

Hydrogen and synthesis gas mixtures (H_2 + CO) can be described more accurately as secondary energy vectors, an intermediate between the primary sources (coal, oil and gas) and the conversion into energy [2]. This is illustrated in figure 1 which shows the conversion routes of synthesis gas to liquid fuels [3].

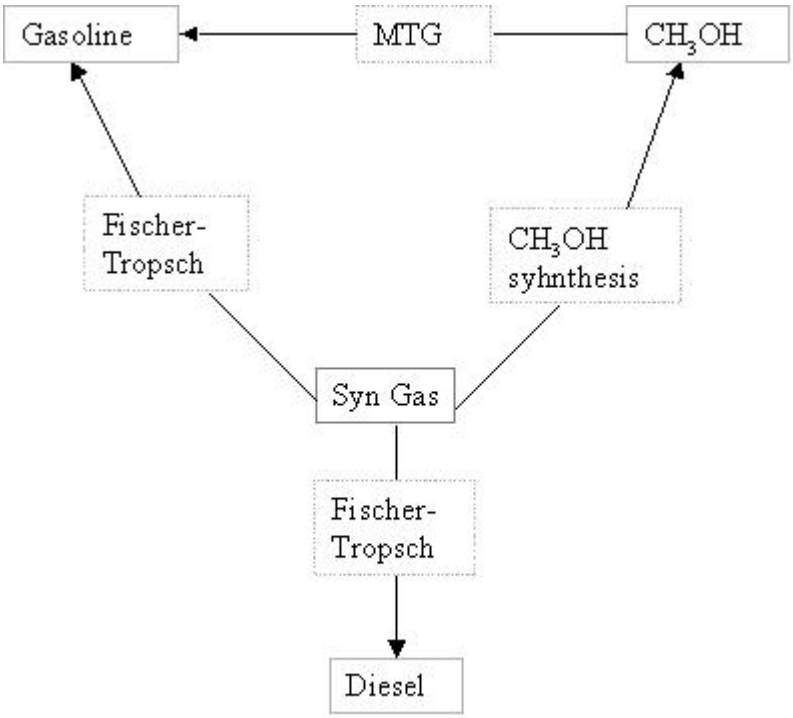

Figure 1 Conversion of synthesis gas to fuel

Large-scale conversion of natural gas into FT products may play important role in the energy economy, thereby making efficient syngas technology a necessity.

The current route for syn-gas production will not be able to cope with the demands of H_2 in the future, hence reactor design and catalyst formulation must be reviewed in order to increase the efficiency of the process [4].

1.2. Steam Reforming

There are currently a number of processes available to produce hydrogen; these include steam reforming, partial oxidation and autothermal reforming. Steam reforming is the most widely practised for the production of hydrogen, accounting for the production of 96% of on-purpose hydrogen. It is a highly endothermic reaction and is favoured at high temperatures and low pressure.

General equation:

$$C_nH_{2n+2} + nH_2O \longrightarrow nCO + (2n+1)H_2$$

Also water-gas shift reaction may occur:

$$CO + H_2O \rightleftharpoons CO_2 + H_2$$

and methanation reaction may occur:

$$CO + 3H_2 \rightleftharpoons CH_4 + H_2O$$

The reaction requires excess steam to reduce carbon formation [5]. Formation of carbon results in carbon filaments plugging catalyst pores and voids. When natural gas is used as the feedstock the steam:C ratio should be 2.5-3:1. Methane is now the feedstock preferred by industry because even at low steam:C ratios it still has a low tendency to form carbon.

The resultant gas is a mixture of H_2, CO_2, CO and CH_4. The composition will be determined by the reaction conditions. For example, the water-gas shift reaction and the methanation reaction are both favoured by low temperatures. Therefore to get a methane rich gas low temperatures and an active catalyst are required.

As mentioned above CO_2 is produced alongside H_2, so it is incorrect to suggest that its use as a fuel will result in CO_2 destruction. However the CO_2 produced is still small in comparison to the amounts evolved from power plants. The amount of CO_2 produced can be varied by changing the feedstock. The amount evolved increases when reforming higher hydrocarbons. For example, reforming methane results in a CO_2 / H_2 product ratio of 0.25. Whilst reforming pentane, results in a CO_2 / H_2 product ratio of 0.31.

A wide range of hydrocarbon feedstocks is used for the production of synthesis gas by steam reforming. The most common feedstock now is natural gas. This occurs widely throughout the world, and is the easiest feedstock to process. Natural gas consists of mainly methane, with small amounts of low molecular weight hydrocarbons, and often nitrogen and carbon dioxide. Table 1 compares the typical compositions of natural gas found in some of the major gas fields [6].

Table 1 Typical composition of natural gas found in some of the major gas fields

Component	North Sea	Groningen	Ekofisk	Indonesia
CH_4/%	93.81	81.25	85.45	84.88
C_2H_6/%	4.52	2.83	8.36	7.54
C_3H_8/%	0.38	0.41	2.85	1.60
C_4H_{10}/%	0.04	0.14	0.86	0.03
C_5H_{12}/%	0.02	0.09	0.22	0.12
N_2/%	0.73	14.23	0.43	1.82
CO_2/%	0.47	0.96	1.83	4.0
Total sulphur (H_2S)/ ppm	5		30	2

The content of the low molecular weight hydrocarbons varies depending on the source of natural gas. Also, associated gas is often used in hydrogen plants, which is less rich in methane and contains a higher percentage of higher hydrocarbons. Therefore, it is necessary not to just consider the reforming of methane, which has received a lot of attention and the mechanism fairly well

understood, but also the reforming of higher hydrocarbons. This project concerns the steam reforming of ethane as it is the simplest of the higher hydrocarbons.

1.2.1. Mechanism for Ethane reforming

Most of the literature that concerns the mechanism of the steam reforming of hydrocarbons have deduced that the reaction involves the interaction of adsorbed water species with the adsorbed hydrocarbon or fragments of the original hydrocarbon [7]. However, Yarze and Lockerbie [8] suggested the reaction proceeds by two stages:

(i) Cracking and dehydrogenation of the hydrocarbon molecules to form surface carbon.

(ii) The interaction of surface carbon with water to produce reaction products.

Kneal and Ross conducted ethane steam reforming experiments over Ni/Al_2O_3 catalysts and concluded their results were consistent with the formation of surface carbon intermediates [9]. They went on to propose the following reaction scheme for the steam reforming of ethane:

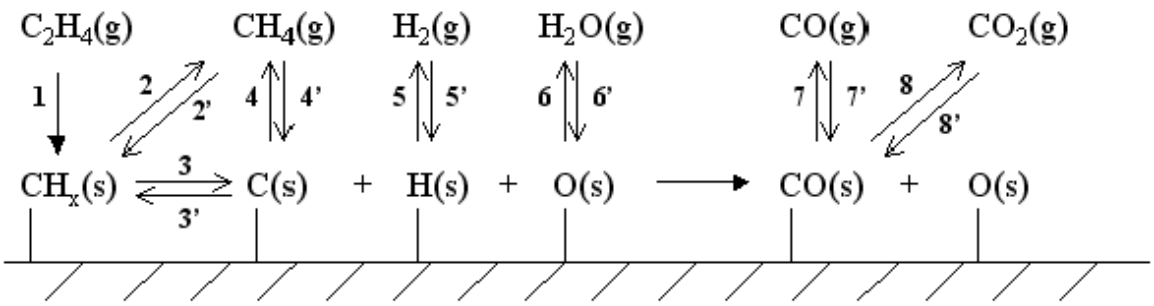

Figure 2 Mechanism for steam reforming of ethane

Ethane is adsorbed by step 1 and methane is desorbed in a disproportionation reaction in step 2. The remaining CH_2 species decomposes via step 3 and then the surface carbon species react with O(s) to form CO or CO_2, with the latter predominating. It was found that as the amount of hydrogen built up selectivity toward methane increased.

Methane was found to be one of the major products in the reforming of ethane on Rh supported on yttrium-stabilized zirconium by L. Lefferts et al [13]. In the literature, it is assumed that the methane formation in reforming of higher hydrocarbons occurs through methanation reactions [10]. L.Lefferts et al disregarded this as tests of methanation reactions on Rh/YSZ showed essentially only the WGS reaction occurs. They deduced that methane formation was due to hydrogenolysis of ethane as a consecutive reaction, figure 3.

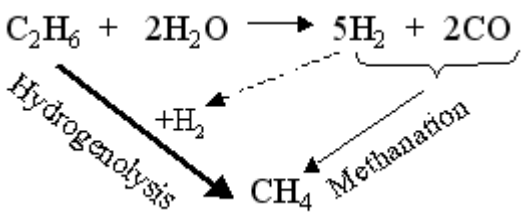

Figure 3 Reactions taking place during ethane steam reforming on Rh/YSZ

In contrast with the results obtained on Rh/YSZ, no methane was produced during steam reforming on Pt/YSZ. The authors reported that synthesis gas was the only product.

As previously mentioned, the water-gas shift reaction also occurs under steam reforming conditions, so it is necessary to have an understanding of the shift reaction in order to fully comprehend steam reforming. The activity of alumina supported metals for the WGS reaction varies as a function of their periodic position; this is demonstrated by a plot produced by Grenoble et al [11].

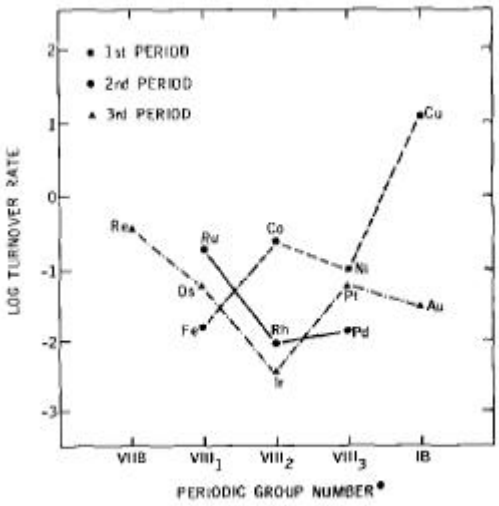

Figure 4 Periodic trends of the activity of alumina supported metals for the WGS reaction. Activities are turnover rates at 300°C and partial pressures of H_2O and CO of 31.4 and 24.3 kPa, respectively.

These trends were correlated with the heats of adsorption of CO on various metals and it was deduced that the activity depended on the strength of the CO-M interaction, since it is assumed the intermediate CO-M is involved in the surface chemistry. For a surface intermediate such CO-M there should be an optimum strength of interaction between adsorbent and adsorbate so that the interaction is strong enough to provide a sufficient concentration of the intermediate species but not strong enough to prevent subsequent reaction of the intermediate to products. For the WGS reaction, this optimum strength of interaction of CO and metal was found to be near 20 kcal/mol.

The role of the support is also key when considering WGS, as the support is believed to be the source of water activation. It has been shown that Rh/Al_2O_3 is 1.7 times more active than Rh/SiO_2 for the WGS reaction. It is concluded that the WGS reaction occurs bifunctionally in that the metal activates carbon monoxide whereas support sites are the principal sites for water activation.

1.2.2. Steam Reforming catalysts

The catalyst used universally for the steam reforming process by industry is nickel based, despite it not being the most efficient catalyst. Activities of metals supported on alumina or magnesia are of the following order: Rh, Ru > Ni, Pd, Pt > Re> Co. Rh and Ru based systems are clearly active, particularly Ru catalysts which exhibit a better selectivity towards hydrogen. However precious metal catalysts are expensive, therefore Ni catalysts are used by industry because they are relatively cheap.

Further development of the steam reforming process may lead to precious metals becoming a more attractive option. Since steam reforming is a strongly endothermic reaction, current reforming processes require a high temperature (800-900°C). To obtain higher thermal efficiencies, it is desirable for the catalyst to exhibit sufficient catalytic activity at the lowest temperature, while also performing steam reforming at low steam-to-carbon ration without carbon deposition. It has been cited that precious metals, such as Rh and Ru, have high activities at low operating temperatures (500°C)[12].

1.2.2.1. Activity of Precious metal catalysts

In two recent papers it has been found that Rh catalysts supported on yttrium-stabilised zirconia are much more active than the corresponding Pt catalysts [11,13]. The relative low reactivity of Pt is in agreement with results by Sinfielt et al. [14-16], reporting low activity of Pt in ethane hydrogenolysis compared to Rh.

The high reactivity of Rh towards C2-hydrocarbons may be explained by the following findings:

(i) Rh shows a higher binding strength towards carbon atoms than Pt, indicating a higher reactivity in C-C scission reactions [17].

(ii) Rh has a tendency to form multiple bonds to each carbon atom, which can be correlated to higher activity in C-C splitting reactions [18]. While Pt is inactive in this respect.

Due to Pt's low reactivity towards higher hydrocarbons, there is currently much interest in its potential to selectivity reform methane when the feedstock contains a mixture of hydrocarbons.

1.2.2.2. Steam reforming supports

Due to the extreme conditions involved in steam reforming, namely high temperatures and high steam partial pressure; the choice of catalyst support is somewhat restricted. High surface area γ-alumina and chromia substantially weaken and sinter at temperatures >770K and at high steam partial pressure. At high temperatures, SiO_2 becomes volatile in the presence of steam and is slowly removed from the catalyst and deposited in heat exchangers and reactors downstream of the catalyst. An alkali support is beneficial in terms of avoiding carbon formation, however at high temperatures it is also slowly removed from the catalyst. Magnesia supports are stable at high temperature but are prone to hydration at low temperature that could lead to break down of catalyst due to expansion of molecular volume [19].

The most suitable supports, regarding steam reforming conditions, are based on oxides such as α-alumina, magnesia and zirconia that have been fired at temperatures in excess of 1270K[19].

Al_2O_3 is a widely used catalyst support material due to its ability to satisfy the surface characteristics needed for almost any process. Meanwhile, ZrO_2 has attracted considerable interest more recently as a support material, specifically in regard to steam reforming. For example Igarashi et al. found that Rh/ZrO_2 had a significantly higher catalytic activity than Rh/Al_2O_3 during low temperature steam reforming of n-butane [20]. Each of the supports will be discussed more fully in the following two sections, since it is apparent the support has a large impact on catalyst activity.

1.2.2.2.1. Alumina - spillover mechanisms

γ-alumina acts as a reservoir of hydroxyl groups due to its large concentration of acid and basic sites, which favour the reverse spillover of H_2O or OH groups onto the metal surface (α-alumina is more dehydrated). These metal hydroxyls will quickly react with the carbided metal to produce H_2 and CO, as proposed by Dalmon et al. [21] for dry reforming of methane over Ni/Al_2O_3:

$$OH_{Al2O3} + M \longrightarrow M\text{-}OH$$

$$M\text{-}OH + M\text{-}C \longrightarrow CO + 1/2H_2 + M$$

The OH groups are replenished by water that is produced during the reaction.

It is proposed by Wang et al. that water molecules adsorbed onto the support during partial oxidation of CH_4 over Rh/Al_2O_3 [22] and Ru/Al_2O_3 [23] take part in the reaction mechanism. The mechanism on the support is written as:

$$H_2O + Rh\text{-}O\text{-}Al_2O_3 \rightleftharpoons OH\text{-}Al_2O_3 + H\text{-}O\text{-}Al_2O_3$$

$$OH\text{-}Al_2O_3 + H\text{-}O\text{-}Al_2O_3 \rightleftharpoons O\text{-}Al_2O_3 + H_2O\text{-}Al_2O_3$$

$$H_2O\text{-}Al_2O_3 + Rh \rightleftharpoons H_2O\text{-}Rh + Al_2O_3$$

The last step depicts H_2O spilling over from the support to the Rh metal (reverse spillover), which occurs at temperatures between 723 and 1023K. When H_2O adsorbs onto the metal it dissociates to produce $O_{(ads)}$ and $OH_{(ads)}$ which can then oxidise adsorbed CH_X species before it dissociates.

According to several authors [24,25,26] hydrogen can spillover from the metal onto the Al_2O_3 support and plays a role in the catalysis of steam reforming. The following spillover mechanism has been proposed for CO_2 reforming of CH_4 over Ni/Al_2O_3:

Firstly, CH_4 reversibly dissociates to yield CH_X and H on Ni^o with a large portion of H being spilt onto the support:

$$Al\text{-}O + Hsp \longleftrightarrow Al\text{-}OH$$

The second stage involves H-promoted CO_2 dissociation, which occurs mainly on the support.

Finally, the CH_X species reacts with H_2O to yield CH_XO and H_2; CH_XO decomposes in the metal-support interfacial region to produce H_2 and CO. The H_2O mainly comes from the support and migrates to the metal-support interface as discussed previously.

1.2.2.2.2. Zirconia

Using zirconia in place of an alumina support has been seen to result in less catalyst deactivation due to less fouling of the catalyst with carbon [27]. Souza et al. proposed three possibilities for the stability of zirconia supported Pt catalysts during CO_2 reforming of CH_4:

(i) Differences in active metal dispersion.

(ii) Strong Pt-Zr^{n+} interactions, whereby after reduction a ZrO_x species may decorate the Pt surface and diminish H_2 chemisorption capacity. This effect is known as a 'strong metal support interaction' (SMSI) and has been observed on TiO_2 supported catalysts. Ultimately this interaction was shown to decrease the CO-Pt bond strength and so inhibiting CO disproportionation (Boudouard reaction). Also, the presence of ZrO_x species over the Pt surface decreases the number of large ensembles. This would inhibit CO/CH_4 dissociation, which requires an ensemble of four or five metal atoms.

(iii) Strong Lewis basicity of ZrO_2 increasing the ability of the support to adsorb CO_2, which in turn reduces carbon deposition via Boudouard reaction [28,29]. Also Pt seemed to selectively block lewis acid sites on ZrO_2 but not on Al_2O_3. The presence Lewis acid sites are thought facilitate the cleavage of C-H bonds of CH_4, resulting in carbon formation. Souza et al. found that CH_4 turn over frequency (TOF) values were lower over Pt/ZrO_2 than Pt/Al_2O_3 and this was attributed to CH_4 activation.

The effect of the reducibility of the support on CO_2 reforming of CH_4 over Rh catalysts was examined by Wang et al [30]. In general it was found greater conversions and yields were obtained over the irreducible supported catalysts, and in particular Y-Al_2O_3. Whilst, the reducible supports, ZrO_2, were found to be unsuitable due to very long period of activation which was dependant with time on stream.

1.2.2.2.3. Doping of Support

ZrO_2 is often doped with Ce^{4+}, La^{3+} and Y^{3+} to promote redox properties and increase the stability of the support. Mattos et al. observed during CO_2 reforming of CH_4 that Pt/Ce-ZrO_2 hardly deactivated at all, whilst Pt/ZrO_2 partially deactivated [31]. It was shown that the addition of Ce to ZrO_2 resulted in a support with a greater number of oxygen vacancies in the proximity of the metal particles and a faster rate of oxygen transfer to the metal. The oxygen reacts with carbon formed from CH_4 cracking to produce CO_X species, in the absence of a reducible oxide carbon will deposit on the metal resulting in deactivation.

Al_2O_3 has also been doped with CeO_2 in a propane steam reforming study utilising a Rh catalyst, and was found to enhance both propane and steam conversion [48]. It was shown that loading 20 wt% ceria onto alumina support increases Rh dispersion and made both Rh oxide and ceria easier to reduce.

1.2.2.2.4. Promoters

Another method involves the addition of a second metal to generate a bimetallic catalyst, such as Ni-Co, Ni-Mo and Ni-Re. The Ni-Re catalyst system is particularly active [32]. It was found the activity of the bimetallic Ni-Re/Al_2O_3 catalyst is maintained much better than that of the monometallic Ni/Al_2O_3 catalyst for the oxidative reforming of gasoline. Suggesting Ni-Re/Al_2O_3 exhibits a much better coking resistance than Ni/Al_2O_3 because of the interaction between Ni and Re. XRD results indicated a new bimetallic phase may be formed by alloying Ni and Re.

There was also a change in product selectivity on using Ni-Re/Al_2O_3, methane formation decreased leading to an increased concentration in hydrogen. The use

of lower reaction temperatures are also more feasible due to the unique high activity of the bimetallic system.

Graf et al studied the infulence of adding K to Pt/Y-$ZrOr_2$ on the steam reforming of methane and ethane [10]. It was previously claimed that potassium prevents carbon formation on Ni catalysts by blocking step sites that are believed to be the nucleation sites for graphite formation [33]. However, it was found potassium improves catalyst stability but at the expense of decreasing catalyst activity.

1.3. Catalyst Deactivation

Catalyst deactivation is the loss of catalyst activity with time on stream. It is anticipated that a catalyst used for reforming will eventually deactivate. Deactivation is inevitable in any process but can be slowed and some of its consequences avoided. Moulijin et al. summarised the phenomena and their effects which lead to catalyst deactivation [34]. The summary is shown in figure 5.

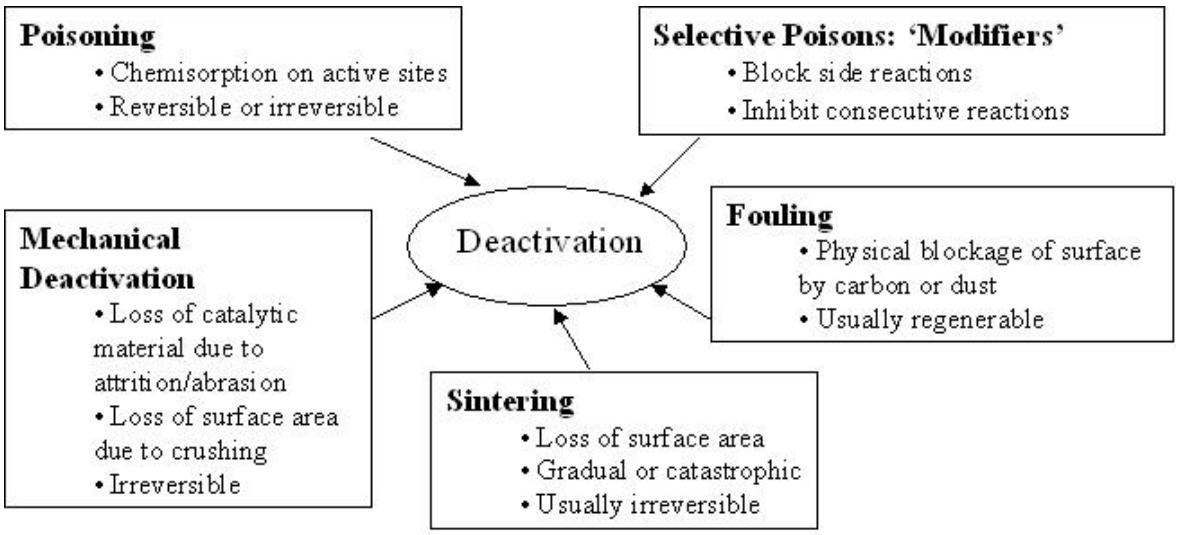

Figure 5 Deactivation phenomena. Causes and effects. (34)

Sintering can be significant in reforming due to the high temperature process conditions but deactivation is primarily due to fouling and poisoning.

Fouling of the catalyst surface with carbon (product of Boudouard) or coke (product of hydrocarbon cracking) blocks active sites and results in a decrease in activity.

Poisons are present in the hydrocarbon feedstock for steam reforming, in particular sulphur compounds, which are still present after desulphurization. Even at very low concentrations (<ppm) their presence significantly reduces catalyst activity. The following sections examine the mechanisms by which sulphur poisons catalysts, factors influencing the degree of poisoning and also advances in catalyst formulations.

1.3.1. Sulphur Poisoning

Poisoning is the strong chemisorption of a species on a site otherwise available for catalysis. Whether a species is a poison depends upon its adsorption strength relative to other species competing for active sites. The mechanisms by which a poison may affect catalytic activity include [35]:

1. Physically blocking at least one 3- of 4- fold active site.

2. Electronically modifying the nearest neighbour metal atoms and possibly the next nearest neighbour; possibly affecting there adsorb reactant molecules.

3. Restructuring of catalyst surface.

4. Poison blocking access of adsorbed reactants to each other.

5. Slows surface diffusion of adsorbed reactants.

Specifically, when considering poisoning by sulphur, it is the first two effects, which are of prime concern.

1.3.1.1. Adsorption

In order to be able to interpret quantitatively the extent and nature of poisoning by sulphur it is essential to know the structure and bonding of sulphur to metal atoms at the surface. Thus, the thermodynamics of adsorption, adsorption mechanisms, stoichometries and competitive adsorption are considered in this section.

1.3.1.1.1. Adsorption Thermodynamics

There are two types of sulphides that form on the catalyst, 2-D surface sulphides and 3-D bulk sulphide.

Bulk sulphide formation requires the metal cation to diffuse through the adsorbed sulphide layer [36]. This forms a new metal sulphide layer on the outer surface, figure 6.

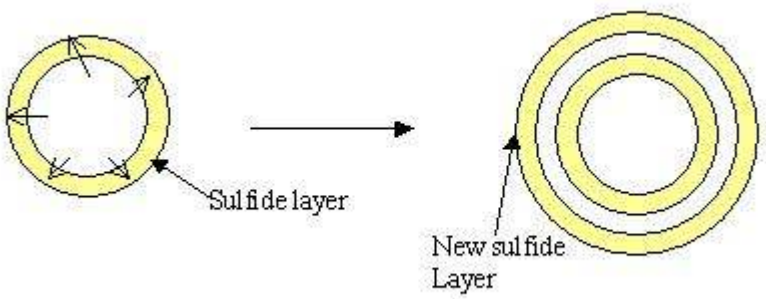

Figure 6 Formation of bulk sulphide

This phenomenon of segregation is strongly exothermic and is therefore favoured by a reduction in temperature. Surface sulphide formation is simply the adsorption of sulphur on the surface of the metal.

It is possible to predict which phase will form at specific conditions, as each phase exists over a limited range of sulphur temperature and concentration. Pt, Ni, Ru and Rh all have lower free energies of formation of their bulk sulphides than their surface sulphides, this suggests that large H_2S concentrations are

required for stable bulk sulphides to exist. Therefore the metals of catalytic interest form surface sulphides under typical reaction conditions.

The surface Ni – S bonds are substantially more stable than bulk Ni – S bonds. This can be seen by comparing the bond lengths:

Bond length for surface Ni – S = 0.218nm
Bond length for bulk Ni – S = 0.238nm

This is also seen on comparison of the relative enthalpies:

$H^{o}ads$~155KJmol^{-1} for dissociative chemisorption of H_2S on Ni surface
$H^{o}f$~75 KJmol^{-1} for bulk Ni_3S_2

Bond strength of M-S decreases in the following order in relation to the type of metal: Cr > Ni > Mo > Co > Ru > Pt > Fe > Cu > Ag.

1.3.1.1.2. Adsorption Mechanisms

Three different mechanisms have been proposed for the adsorption of hydrogen sulfide on Ni surfaces [36]. It is agreed that H_2S chemisorbs dissociatively, the uncertainty is over the number of surface Ni atoms involved per sulfur atom.

Saleh et al. [37] suggested a three-site mechanism in the temperature range of 193-373K:

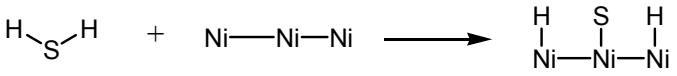

Whilst another mechanism, proposed by Den Beston and Selwood [38], suggests that four Ni atoms are required, from studies conducted between 273-393K:

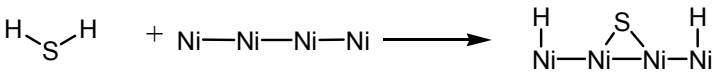

A final one-site mechanism was proposed by Rostrup-Nielsen for adsorption in the range of 823-918K[39]:

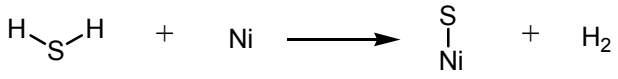

Due to data obtained from desorption isotherms [40], the three-site mechanism is favoured, at least at high temperatures.

Typically, on saturation of the surface, S/Ni_s ratios of 0.7-1 are observed for polycrystalline and supported Ni, the value obtained being dependant on partial pressure of H_2S and temperature.

The adsorption of other sulphur species on Ni have been investigated, their modes of adsorption are summarized in table 2.

Table 2 Adsorption of different sulpur species on Ni

Sulphur species	Adsorption at low temperatures	Adsorption at high temperatures
CS_2	Dissociatively at room temp.	Bulk sulphidation >298K
SO_2	Chemisorbs rapidly and irreversibly at 193K	Extensive incorporation into bulk >373K
Methyl mercaptan	Dissociatively at r.t, accompanied by evolution of H_2, CH_4, $(CH_3)_2S$	
Dimethyl sulphide	Associatively at 298K	Rapid dissociation >500K accompanied by evolution of H_2, CH_4, C_2H_6
Mercaptans with longer chain alkyl groups	Adsorbed as mercaptide structures*	Mercaptan decomposes >350K

Other catalytic metals, Fe, Pt, Pd, W and Cu, adsorb sulphur compounds dissociatively in much the same way as Ni.

It has also been inferred that a SH surface species is present as an intermediate in the dissociation of hydrogen sulphide on Pt/Al_2O_3. It was observed that at increasing sulphur coverages, dissociated hydrogen is gradually desorbed and a percentage spends a significant lifetime on the catalyst [41]. Exchange experiments with deuterium have depicted two types of hydrogen on the surface, figure 7.

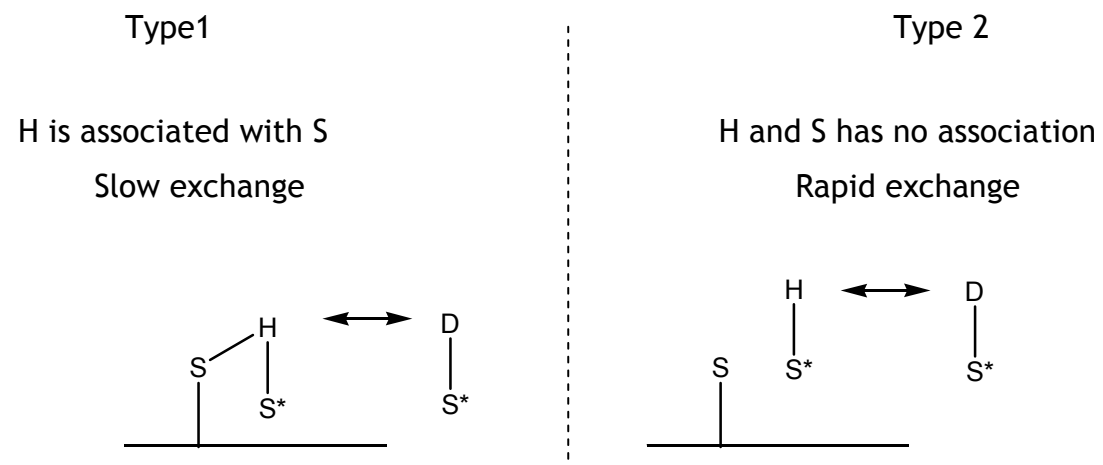

Figure 7 SH species

The retained hydrogen can participate in reactions. It maximises methane production and reduces carbon laydown.

On Pt/alumina there are two types of adsorbed hydrogen sulphide, different due to strengths of adsorption, and three different adsorption sites. These include: a site which bonds sulphur strongly and will not exchange, a site which bonds sulphur weakly and is removed under vacuum and a site which will allow exchange between gas and adsorbed phases. These were determined from radioactive labelling experiments [42], in which it was also found that the S/Pt_S ratio was 1:1 on Pt/SiO_2 but only 0.6:1 on Pt/Al_2O_3.

Sulphur adsorption studies of single crystal faces have provided evidence that the metal surface can reconstruct on adsorption of sulphur, particularly in regard to Pt. It was observed that the Pt (111) surface reorients to the (100) plane in the presence of H_2S [47]. It has also been found that the clean stepped Pt surfaces, Pt(S)-[6(111)X(100)] reconstructs to other stepped faces in the presence on adsorbed sulphur [48]. The reconstruction of the stepped Pt surface would suggest an additional type of sulphur poisoning of a metallic catalyst. In addition to site blocking and electronic effects of sulphur on the metallic surface, adsorbate induced reconstruction could expose or eliminate catalytically active sites on the metallic surface.

There has been limited research on the adsorption of sulphur species on Rh catalysts, however some work has been conducted on Rh single crystal faces. Hedge et al. studied the chemisorption and decomposition of H_2S on Rh(100)[49]. At 100K, AES results they obtained suggested saturation coverage near 0.5 monolayer. However, on heating to 600K sulphur coverage increased. The authors disregarded this was due to migration of sulphur beneath the surface, since saturation was reached quickly. Instead they inferred this was due to physisorbed H_2S, which is consistent with results for H_2S adsorption on Pt and Ni. Moreover, the thermal desorption spectra of molecular H_2S from Rh(100) exhibits low- and high temperature peaks, the authors assigned the low temperature peak as physiorbed H_2S, further supporting their claim.

It was also found that a decreasing fraction of H_2S dissociated as the coverage of H_2S increased. The similarities between H_2S adsorption on Rh(100) and Pt(111), Ru(110) and Ni(100) were noted. In all these cases, there is complete dissociative adsorption at high temperatures and low coverages with hydrogen remaining on the surface. At low temperatures and higher coverages on Pt(111), Ru(110) and Ni(100), first SH and then H_2S were observed.

1.3.1.1.3. Effect of Sulphur on the adsorption of other species

In general it appears that adsorptions of hydrogen, oxygen and CO are prevented by adsorbed sulphur. Bartholomew et al. [43] observed that hydrogen uptakes for Ni bimetallics and Ru decreased proportional to sulphur coverage. Whilst, Bonzel and Ku [44] found that each sulphur atom on partially sulphurized Pt (110) surfaces ($\theta<0.25$) blocked two CO chemisorption sites.

The interaction of CO and H_2S over supported Pt catalysts was studied in detail by Jackson et al [45]. It was found when H_2S was pre-adsorbed on Pt/Silica no subsequent CO adsorption was detected. This is due to the adsorption of H_2S being dissociative, so there is no mechanism by which sulphur can desorb and hence no sites can be liberated for CO adsorption.

CO was preadsorbed on Pt/Silica and the amount of H_2S adsorbed was decreased by 81% in comparison to a fresh surface, though it was suggested that 20% of the H_2S was able to adsorb onto the Silica support, indicating CO had completely suppressed H_2S adsorption on the Pt sites. However, when the same experiment was carried out over Pt/Alumina there was no reduction in adsorptive capacity for H_2S on a CO saturated surface. This indicates that CO does not block H_2S adsorption on the metal sites and must be related to the effect of the support. It has previously been reported that CO_2 is produced from the reaction of adsorbed CO with hydroxyl groups from the alumina support [45], therefore CO may be able to desorb via this route liberating sites for H_2S adsorption.

CO and H_2S were also co-fed over Pt/Silica and whilst the amount of H_2S adsorbed decreased by 78%, the amount of CO adsorbed increased by 67%. The enhancement in CO adsorption was explained by the adsorption of H_2S and its displacement by CO. This caused desorption of residual hydrogen from the reduction procedure, possibly by surface reconstruction, which has been found deleterious effect on CO adsorption [45].

A similar study examining the interaction of CO and H_2S over Rh/silica catalysts was carried out [46].

Unlike with Pt, it was found that CO could adsorb onto samples that had been saturated with sulphur. Displacement of H_2S was also evident but was dependent on the metal precursor used. It was only found to occur on the oxide catalyst and since the desorption of sulphur requires hydrogen, it is proposed that H_2S only partially dissociates on the oxide catalyst to produce an HS-* species, this would provide a source of hydrogen to allow for desorption.

The effect of passing H_2S over CO pre-covered surfaces was the displacement of CO and the adsorption of H_2S, i.e. similar to Pt/Alumina. It was speculated that the CO displaced reflected the different modes of adsorbed CO, and this was also found to be dependant on the metal precursor. For example, the chloride-derived catalyst appeared to displace bridge-bonded Rh_2-CO.

1.3.1.2. Factors influencing extent of catalyst deactivation: Improving sulphur tolerance

The vast majority of sulphur poisoning studies are concerning the deactivation of Ni; there is very little in the literature illustrating the effect of sulphur on precious metal catalysts. The examples depicted below are relevant to precious metal catalysts however it should be noted that the sulphur poisoning experiments have not been performed under steam reforming conditions. In most cases, catalyst deactivation was examined by hydrogenation reactions under milder conditions in comparison to steam reforming.

Factors effecting the deactivation of catalysts by the presence of sulphur compounds are discussed below:

1. Identity of poison

It has been suggested [50] that the degree of toxicity of a sulfur species depends on how shielded the sulphur atom is. For example the sulphate ion is considered non-toxic because the sulphur atom is bonded to four oxygen atoms, thereby stopping the sulphur electrons from interacting with other species.

Alternatively, the sulphur atom in hydrogen sulphide is only bonded to two hydrogen atoms, leaving two lone pairs of electrons.

Molecular size and structure of the poison are also important factors. Generally, the toxicity of sulphur increases with molecular weight of a sulphur compound. If there was a non-toxic structure attached to sulphur, such as an alkyl chain, it would be considered a more toxic poison. This is the result of the sulphur atom anchoring the compound to the catalyst so that the alkyl portion has an obstructive effect due to its proximity to the surface.

However, other studies [51] have reported that the nature of the poison does not have an important effect and the toxicity of a given poison is determined mainly by the $S_{irreversible\ ads}/S_{total\ ads}$ ratio. Therefore, not only the reactivity properties of the poison and the reactant molecule but also the experimental reaction conditions may affect the resistance to sulphur poisoning.

2. Support Effects

When the catalyst is supported on acidic supports the catalyst exhibits a higher resistance to sulphur poisoning. In one study [52] the alumina support was impregnated with chlorine to increase the acidity of the support. It was found the addition of chlorine greatly enhanced the thioresistance of the Platinum catalyst. In the same study potassium was added to alumina to decrease the acidity and this was found to reduce the thioresistance. Similarly, deactivation constants were found to decrease in the order: $Rh/SiO_2 > Rh/TiO_2 > Rh/Al_2O_3$ when sulphur thiotolerance was investigated by thiophene during toluene hydrogenation [53]. The lower surface acidity of the silica support does not allow a strong interaction of the poison and the support and also limiting the adsorption of fragments or organometallic precursor, therefore a high deactivation rate should be expected by this system. Additionally, the acid sites on the support may provide additional sites or the adsorption of thiophene, contributing to an increase in the thiotolerance level.

Another interesting support effect was documented with rhodium catalysts supported on alumina and silica [54]. Deactivation due to thiophene exposure was four times faster when the support was silica rather than alumina (this effect was only seen when the Rh particles are smaller than 40A). The authors suggested this is due to the rhodium particles exhibiting different morphologies depending on the support. Deactivation is faster on silica because the sulfur reacts preferentially at sites with higher electron density i.e. on the icosahedra. The Rh particles on silica would be icosahedra, whilst on alumina the particles are a mixture of icosahedra and cuboctahedra for smaller particles.

The support was found to play a crucial role in sulphur resistance of Rh catalysts during partial oxidation reaction. Torbati et al. [55] found that in the presence of a sulphating support such as La_2O_3-Al_2O_3, the partial oxidation reaction was much less inhibited than a less sulphating support such as SiO_2-Al_2O_3. The sulphating support acts as a sulphur getter and keeps the sulphur away from the active metal sites and this minimizes the build-up sulphur on or close to the active Rh sites where reactions take place.

3. Particle Size Effects

Clear particle size effects have been noted with the deactivation of Rh/alumina catalysts [44]. It was found the rate of deactivation increased with increasing particle size.

However, during poisoning experiments on platinum it was found that smaller particle size catalysts had a faster initial deactivation. This particle size effect was masked by a more important catalysts property (support acidity) and the authors came to the conclusion that metal dispersion is not directly related to thiotolerance [43].

Variation in particle size may also influence the mode of sulfur adsorption [57].

4. Effect of Precursor

In a recent study [56] platinum catalysts were prepared from two different metal salts; Pt $(acac)_2$ and H_2PtCl_6. The catalysts prepared from Pt $(acac)_2$ retained most of their activity in the presence of the poison, thiophene. Whilst, the H_2PtCl_6 catalysts retained less than 50% of their activity. Since the Pt $(acac)_2$ catalysts had a lower particle size in theory they may have deactivated more. Again, it seems that the particle size effects are masked by a more important catalysts property, in this case the nature of the precursor. The precursor effect was attributed to morphological differences in Pt particles. The catalysts from Pt $(acac)_2$ have a higher portion of atoms in unsaturated positions (kinks, edges), which may strongly chemisorb fragments of orgaonometallic residue and avoid the poisoning of theses sites by H_2S.

5. Alloying/ Addition of alkali metals

Bimetallic catalysts have been reported to exhibit higher tolerance levels to sulphur. One example is Ni-Re/Al_2O_3 [58]. It is proposed that the Ni alloys to the Re, followed by the formation of sulphur-rhenium bonds, which make the catalyst more resistant to deactivation.

A decrease in sulphur poisoning has been reported when alkali metals such as Li, K, and Na are added to the catalyst. Rh-K/La-Al_2O_3 showed a higher and more stable H_2 yield than un-promoted Rh/La-Al_2O_3 during ATR of sulphur-containing gasoline [53]. The larger increase in sulphur tolerance of Rh-K/La-Al_2O_3 maybe explained by a blockage of Rh sites preventing H_2S adsorption and coke formation. Alternatively, it may be due to the addition of K producing a higher reaction temperature, which is the result of K blocking active sites that promote endothermic steam reforming.

6. Additives to feed

The aim is to achieve competitive adsorption between sulfur and an electron acceptor molecule, in order to decrease the amount of sulfur adsorbed. In the

case of the addition of CH_2Cl_2 to the feed [43] it had a positive effect on thioresistance because it also increased the acidity of alumina.

7. Reaction conditions

The effect of altering the conditions of steam reforming on the sulphur tolerance of a Rh/La-Al_2O_3 catalyst was recently studied by Kraues et al [65]. The effect of temperature and the steam-to-carbon ratio were examined. A significant improvement in the sulphur tolerance of the catalyst was observed when the furnace temperature was increased from 700 to 800°C. It was expected that the decrease in sulphur coverage with increasing reaction temperature would help improve the sulphur tolerance of the catalyst, however they attributed most of the improvement to the ability of the catalyst to gasify carbon. Increasing the furnace temperature from 700 to 800°C decreased the amount carbon from 44.6 to 4.4wt%.

A beneficial effect was also seen on increasing the H_2O:C ratio on the performance of Rh/La-Al_2O_3 in the reforming of low-sulphur gasoline at 700°C. This has been attributed to steam aiding regeneration of the catalyst, see section 1.3.1.5 on catalyst regeneration.

1.3.1.3. Sulphur poisoning and steam reforming

Sulphur poisoning studies regarding steam reforming have mostly been conducted using Ni catalysts. Rostrup-Nielsen showed the effect of sulphur poisoning on the specific activity of 25wt. % Ni/MgOAl_2O_3 in steam reforming of ethane at 775K[60] and the data is presented in table 3.

Table 3 Infulence of Sulphur Poisoning on Specific Activity in Steam Reforming of Ethane on 25% Ni/Al_2O_3 MgO

Sulphur content (wt.ppm)	Sulphur coverage	Reaction rate (mol/g hr) x10	Reaction rate (mol/m^2 Ni hr) x10^3
80	<0.1	2.41	120
239	0.30	0.66	62
360	0.45	0.53	69
398	0.49	0.59	64
615	0.76	0.38	56
805	1.00	<0.01	-

The specific activities based on remaining Ni surface area are reasonably constant over a wide range of sulphur coverage, providing evidence that chemisorbed sulphur poisons by blocking the metal surface for adsorption of reactants. At a sulphur coverage of 1.0, the rate is lowered by more than two orders of magnitude. Therefore the tolerance of conventional Ni catalysts to sulphur poisoning during steam reforming at 775K is very low.

Rostrup-Neilsen [61] also performed calculations to consider the effects of pore diffusion. He found that equilibrium coverage is attained rapidly at the external surface of the catalyst pellets in the entire bed. This means a large, but short-term, increase in the inlet sulphur concentration in the feed could significantly upset the entire process by causing a large increase in the coverage of the external pellet layer throughout the reactor bed. It also means that accumulation in the interior of the pellet is a slow process.

Duprez at al. corroborated this result by determining the profiles of sulphur in Rh/Al_2O_3 by electron microprobe analysis following poisoning of steam reforming of 1-Methylnapthalene [62]. It was shown that sulphur invaded the bed progressively from inlet to outlet and each pellet from exterior to the interior. This was found to be very similar to the profile of coke; moreover the presence of the sulphur compound considerably increased the coking rate.

With low sulphur content (<5ppm) the coking rate first decreased and as the sulphur content increases the rate of coking began to increase. Therefore, the effect of sulphur on the coking rate appears to be very complex. It has been proposed that sulphur inhibits carbon formation on the metal while increasing

the amount of coke deposited on the support [63]. Accordingly, it seems that whereas at low contents the effect of sulphur on the total coking rate depends on the mechanism of coke formation on the support, on the metal coke formation is inhibited.

For the role of sulphur at higher concentrations, two hypotheses were suggested to explain the definite increase in the coking rate: (i) the coke results from preferential adsorption of the sulphur containing molecules together with cracking of these molecules; or (ii) sulphur inhibits the carbon-steam reaction, which induced a shift of the equilibrium in favour of more carbon. As the amounts of coke deposited were found to be close to the amounts of carbon contained in the sulphur molecules, the authors concluded that the coke results essentially from the preferential cracking of these molecules [51]. Nevertheless, the inhibition by sulphur of the carbon-steam reaction could not be out ruled and the role of sulphur could not be entirely elucidated.

In addition to sulphur chemisorbing onto active metal sites and increasing the formation of coke, sulphation of the support can also occur, which consequently will have an impact on the metal-support interaction. Sulphation of the support is implicated as the main cause of deactivation for steam reforming over supported Rh catalysts [64]. Based on the kinetic model for steam reforming over Rh catalysts, it has been demonstrated that the turnover frequency is proportional to the specific perimeter of the metal particles i.e. the total length of the metal-support interface per unit surface area. The kinetics can be explained by a bi-functional reaction mechanism in which the hydrocarbon is activated by the Rh, while the water adsorbs onto the support to form surface hydroxyl species. Sulphation of the support inhibits steam reforming by preventing (i) the formation of hydroxyl species adjacent to the metal-support interface and (ii) migration of more remote hydroxyl species to the interface where they can interact with the adsorbed hydrocarbon.

1.3.1.4. Sulphur benefits

The formation of a bond between a metal atom in an array and a sulphur atom may affect the ability of neighbouring metal atoms to form bonds of the correct

strength to allow a catalytic reaction to occur. For example, the addition of sulphur results in an eightfold increase in selectivity to methanol in carbon monoxide hydrogenation over Rh/silica [66]. The change in product distribution and yield is believed to be due to an electronic effect of the sulphur on the strength of the C-O bond.

A poison may also preferentially interact with the most active sites, referred to as 'selective poisoning'. In catalytic processes involving more than one reaction, a poison may suppress the activity of one reaction more than another leading to a change in product distribution. Reaction-selective poisoning may be beneficial as in the case of hydrogenolysis reactions in reforming. Somorjai [67] has proposed that facile reactions such as hydrogenation should be less affected by sulphur poisoning than demanding reactions such as hydrogenolysis because the sulphur can, by reconstructing the surface, effect the deactivation of more than one or two surface sites for the structure-sensitive reaction.

1.3.1.5. Catalyst Regeneration

Two types of adsorbed sulphur are thought to exist: 'reversible' and irreversible' [68]. The sulphur that adsorbs on the alumina support is reversible, as is the sulphur that adsorbs on low coordination sites. Whilst the sulphur adsorbed on high coordination sites is considered to be irreversible.

Since the chemisorption of sulphur is an exothermic process, there is an improved rate of sulphur removal with increased temperature. However, there are restrictions imposed because of thermal degradation of the catalyst.

In a study of the regeneration using steam it, was found that up to 80% removal of surface sulphur from Ni steam reforming catalyst could be achieved at 973K[69]. The regeneration by steam has been proposed to occur via the following:

$$Ni - S + H_2O \longrightarrow NiO + H_2S$$

$$H_2S + 2H_2O \longrightarrow SO_2 + 3H_2$$

Treatment with steam and air resulted in the formation of sulphates, which were subsequently reduced back to sulphide upon reduction with hydrogen. Although the steam regeneration above 973K successfully removes adsorbed sulphur, use of such high temperatures results in severe sintering of commercial high surface area catalysts.

Also the regeneration under an atmosphere of carbon monoxide has been studied [70], but has proven to not be a very sufficient method. The carbon monoxide was able to extract sulphur atoms, but as a result formed COS, which in turn adsorbed dissociatvely.

A more useful method of regenerating the catalyst is to heat under hydrogen. It was found that heating to 400°C under hydrogen would regenerate 80% of a poisoned Pt catalyst surface [68]. In a study conducted by Mathieu et al [70] Al_2O_3 supported Pt catalysts were poisoned with H_2S during benzene hydrogenation, after hydrogen treatment the adsorption capacity towards the CO chemisorption in the linear for is almost fully restored. However, all the adsorptions or reactions which are concerned with polyatomic Pt sites are still inhibited i.e. chemisorption of CO in bridged form, hydrogen chemisorption and n-butane hydrogenolysis.

A further treatment involving heating to 300 ^{o}C under oxygen, followed by hydrogen reduction under mild conditions, removed sulphur atoms from Pt with the formation of sulphate groups bonded to the support; fully restoring the chemisorptive and catalytic properties. However, if the reduction conditions became more severe (>200°C), the sulphate groups are reduced to H_2S, which again poisons the metal particles.

1.4. Project Aims

The aim of this project was to examine the nature of sulphur poisoning of precious metal steam reforming catalysts with the view of developing a sulphur tolerant catalyst. Two methods were to be employed to study this. Firstly by examining sulphurs adsorption behaviour on precious metal model catalysts, to include adsorption under steam reforming conditions and competitive adsorption. Secondly, by examining the deactivation of the catalysts during the steam reforming of ethane when sulphur is introduced.

The catalysts were to be prepared on different supports to examine if this was a factor in susceptibility to sulphur poisoning. Two different precious metals were used, rhodium and platinum, to compare the effects. Whether the identity of the poison affected the degree of catalyst deactivation was to be investigated, along with effect of poison concentration.

2. Experimental

2.1. Catalyst Preparation

A series of model precious metal catalysts were prepared for the adsorption study. Four catalysts were prepared, two on silica and two on alumina using two metal precursors. Two Pt catalysts were used in this study, one prepared on alumina, whilst the silica supported catalyst was supplied by Johnson Matthey.

Lower loaded (0.2%) Rh and Pt catalysts supported on alumina and zirconia were supplied by E.Opara for the steam reforming experiments. The preparation of these catalysts is fully detailed by E.Opara [71], but is summarized here. Both the alumina and the zirconia were purchased as fine powders so were first converted to granules before they could be impregnated with the metal precursors. The precursors, H_2PtCl_6 and $Rh(NO_3)_2$, were dissolved in a volume of water equal to the support pore volume and then added to the supports. The catalysts were then dried and calcined.

2.1.1. Properties of Supports

The alumina support used for the catalysts in the adsorption study mainly consisted of theta alumina with small quantities of alpha and delta. Some analysis of the support is provided in table 4.

Table 4 Analysis of alumina support

Surface Area m^2/g	101
Pore Volume ml/g	0.42
Bulk density g/cm^3	0.69

The silica support was provided by Degussa and BET analysis of the support is provided in table 5.

Table 5 Analysis of alumina support

Surface Area m^2/g	220
Pore Volume ml/g	0.87
Average pore diameter (4V/A by BET)/ A	160

2.1.2. Support Impregnation

The catalysts were prepared by impregnating the support to incipient wetness with an aqueous solution containing the precursor salt. The wet catalyst was then oven dried before calcination. The metal precursors of the catalysts are listed in table 6.

Table 6 Metal Precursors

Catalyst	Precursor
Rh	$Rh(OAc)_3$
Rh	$Rh(NO_3)_3$
Pt	$Pt(NH_3)_4(OH)_2$

To ensure uniform metal dispersion throughout the support, the precursor salt was dissolved in a volume of water equal to the support pore volume.

By measuring the volume of water required to fully saturate a 1g sample of each support, the support volumes were determined. The measured pores volumes are given in table 7.

Table 7 Pore volumes of catalyst supports

Support	Pore Volume/(cm^3/g^{-1})
Al_2O_3	0.6
SiO_2	0.9-1

From the values obtained in table 7, it was known that 60ml of water would fully saturate 100g of Al_2O_3 support and 100ml of water would fully saturate 100g of SiO_2 support. Therefore, the metal precursor was dissolved in 60ml of distilled water, for Al_2O_3 catalysts, and 100ml of distilled water, for the SiO_2 catalysts. 100g of the support was weighed into a round bottom flask then the metal precursor solution quickly added and shaken vigorously for approximately 10 seconds. The contents of the flask were transferred to a bowl and dried in the oven overnight, held at 70°C. Each of catalyst had a nominal metal loading of 1%, except Rh/Al_2O_3 nitrate which had a loading of 1.2%.

The final stage of the catalyst preparation was calcination to produce a more thermally stable catalyst and to decompose the various catalyst precursors. This involved heating the catalyst and holding at a specific temperature for a period of time in a furnace as outlined in table 8.

Table 8 Temperature program of furnace during catalyst calcinations

Final Temp/K	Ramp Time/°C/min	Hold Time/hrs
773	10	4

2.2. Catalyst Characterisation

2.2.1. Surface Area Analysis

The total surface area of the each catalyst was determined by Brunauer, Emmett, Teller (BET) analysis. It was determined using a Micromeritics Gemini III 2375 Surface Area Analyser. Approximately 0.04g of the catalyst was weighed into a glass tube and purged in a flow of N_2 overnight at 383K before the measurement was carried out.

2.2.2. Thermo-gravimetric analysis

Thermo-gravimetric analysis was performed on post reaction catalysts using a combined TGA/DSC SDT Q600 thermal analyser coupled to a ESS mass spectrometer for evolved gas analysis. Samples were heated from 30°C to 500°C (800°C on post analysis samples) using a heating ramp of 10°Cmin^{-1}. This temperature profile was employed using O_2/Ar at a flow rate of 40 ml/min. For mass spectrometric analysis, mass fragments with m/z=2, 14, 16, 17, 18, 28, 30, 32, 40, 44 and 46 (amu) were followed. The sample loading was typically 10-15mg.

2.3. Reactions

To investigate different aspects of the effect of sulphur on steam reforming catalysts two different pieces of apparatus were used; a high pressure microreactor and a pulse-flow glass line.

2.3.1. High Pressure Reactor

A diagram of the apparatus is shown in figure 8. It consists of a 3/16“ inside-diameter glass-lined metal reactor tube positioned within a furnace. The catalyst bed within the reactor was carefully positioned so it sat in line with the external thermocouple. On either side of the catalyst bed was fused alumina packing material. The reaction conditions were 873K and 20 barg total pressure.

The flow rates of the gases entering the reactor were controlled using Brooks 5805S mass flow controllers that allowed gas flows between 5 and 250mlmin^{-1}. The three-way tap labelled '1' in figure was in place to avoid mixing of oxidising and reducing gases. The feed gas and steam were mixed in the vaporiser, which was kept at a temperature of 773K. The flow rate of steam was fixed at 460ml/min which was generated by pumping water through a Gilson pump at a rate of 0.369ml/min. The steam was generated from a deionised water reservoir. The ethane flowrate was kept constant at 92ml/min in order to achieve a steam: ethane of 5:1, this was important to limit carbon deposition.

Downstream from the vaporiser all lines were heated to 523K to avoid steam condensing. Gases could be directed through the reactor tube in the direction indicated by the arrow in figure, or three-way taps 2 and 3 could be changed to isolate the reactor and the flow directed through the by-pass. After exiting the reactor the product gases enter the knockout pot where the water was collected allowing the gases to be analysed by on-line G.C.

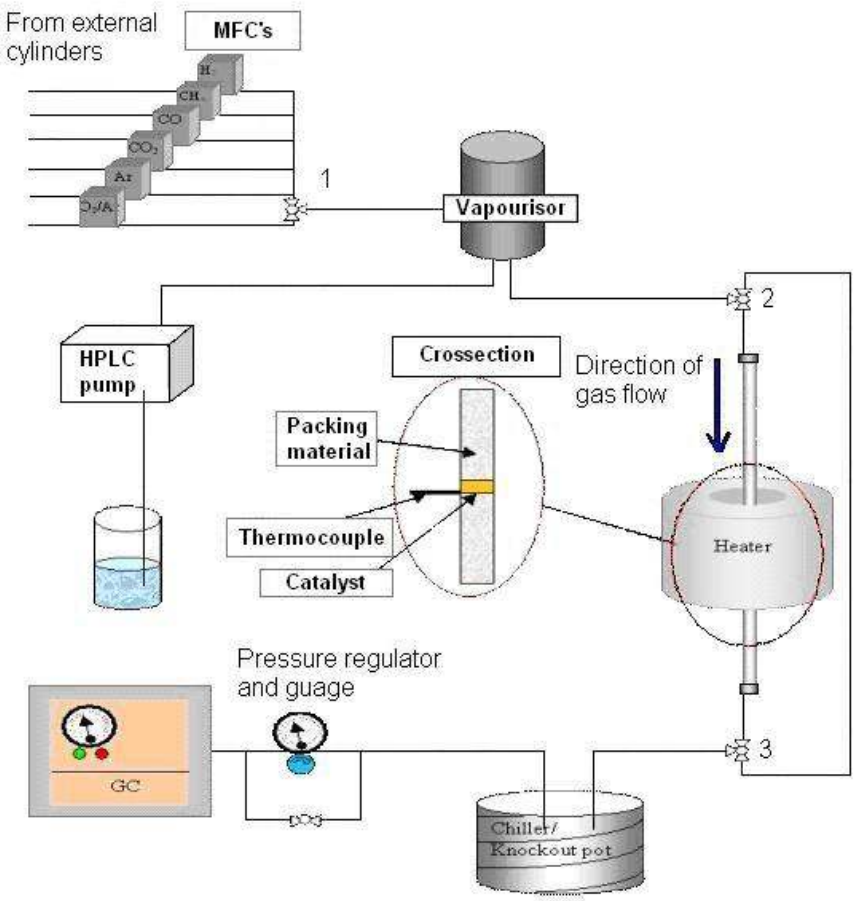

Figure 8 High-pressure apparatus

Initially steam is pumped through the reaction system for a period of an hour, before the ethane is brought in gradually over a period of 15 minutes. After a further 15 minutes of full ethane flow the first injection into the G.C. is taken and at this point the time on stream is 15 minutes. However, despite the flowrate of ethane being at its maximum for 15 minutes this may not be a sufficient enough time for the gas to flow through and establish itself through the whole system, particularly considering the volumes involves in the system e.g. a 2 litre knock out pot. It has been calculated that the knock out pot would take 160 minutes to purge assuming it is completely purged after 8 flushes (8 x 20 minutes).

It is therefore possible that the initial conversion of 100% with respect to the Rh/Al_2O_3 catalyst (fig.43) is incorrect and the reason there is no ethane in the exit flow is because it has yet to make its way through the whole system. As the

conversion appears to decrease to 65% in the first 200 minutes, this is ethane flow fully establishing itself throughout the system.

No diffusional effect of the flow can be evidenced over Rh/ZrO_2 since initially ethane conversion is 100% and is therefore masked. It may appear that the Pt catalysts take longer to establish the ethane flow rate than Rh/Al_2O_3, however deactivation is also occurring over the Pt catalysts from the beginning of the reaction. Therefore, the decrease in conversion over the Pt catalysts at the beginning of the reaction is a combination of the establishment of the gas flow and catalyst deactivation. In order to separate the two effects, catalyst deactivation and the flow not being established a line at 160 minutes on stream will be included on each of the conversion graphs to indicate that the ethane flow is now fully established.

2.3.1.1. Gaseous Materials

Table 9 Gases used, supplier and purity

Gas	Supplier	Purity/ %
H_2	BOC	>99.9
$2\%H_2/N_2$	BOC	>99
Ar	BOC	>99.99
C_2H_6	BOC	>99
H_2S	BOC	>99
CH_3SH	BOC	>99

2.3.1.2. Mass Flow Controllers (MFCs)

In order to calibrate the MFCs, a digital flow meter was attached to the vent of the high pressure rig. For each gas, the MFC was set at a particular flow rate and a reading was taken from a digital flowmeter. The actual flowrate versus the MFC set point is plotted in figure 9. This graph was used to relate set point to actual flow.

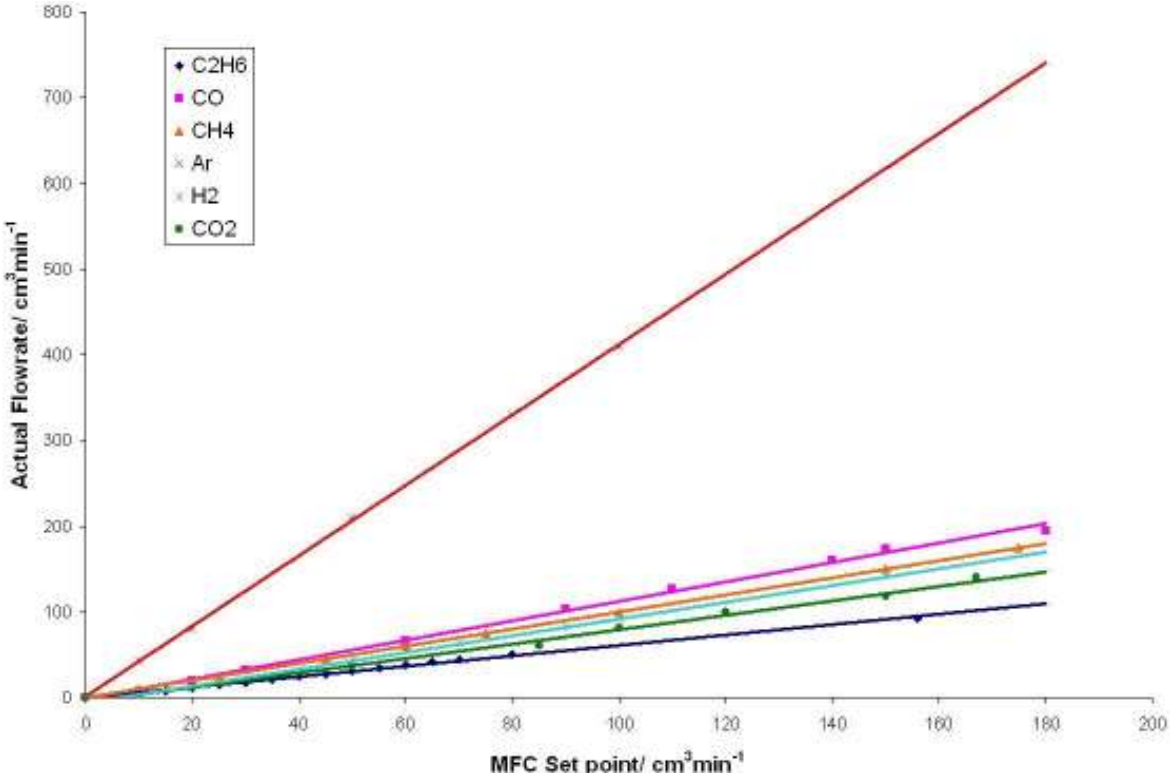

Figure 9 Mass flow controller calibrations

2.3.1.3. Gas Chromatograph

The gases leaving the apparatus were monitored on-line and real-time via a varian gas chromatograph, fitted with a CARBO XEN™ 1010 PLOT column. The computer software used was Star chromatography workstation version 5.5.1.

In order to determine the relationship between peak area and gas concentration, each gas was mixed with inert gas (Ar). Different concentrations were flowed through the G.C. by varying the flowrates of the gas and the inert, whilst ensuring the total flowrate of the gas mixture was kept constant. The number of moles of gas being injected into the G.C was calculated using the following relationship:

$$\text{No. of moles} = PV/RT \times \% \text{ of gas in mixture}$$

Where P = pressure (1atm), V = volume of sample loop ($250 \times 10^{-6} cm^3$), R = gas constant (0.0820578), T=298K

The linear relationship between moles of gas and peak area for each of the gases is shown in figure 10.

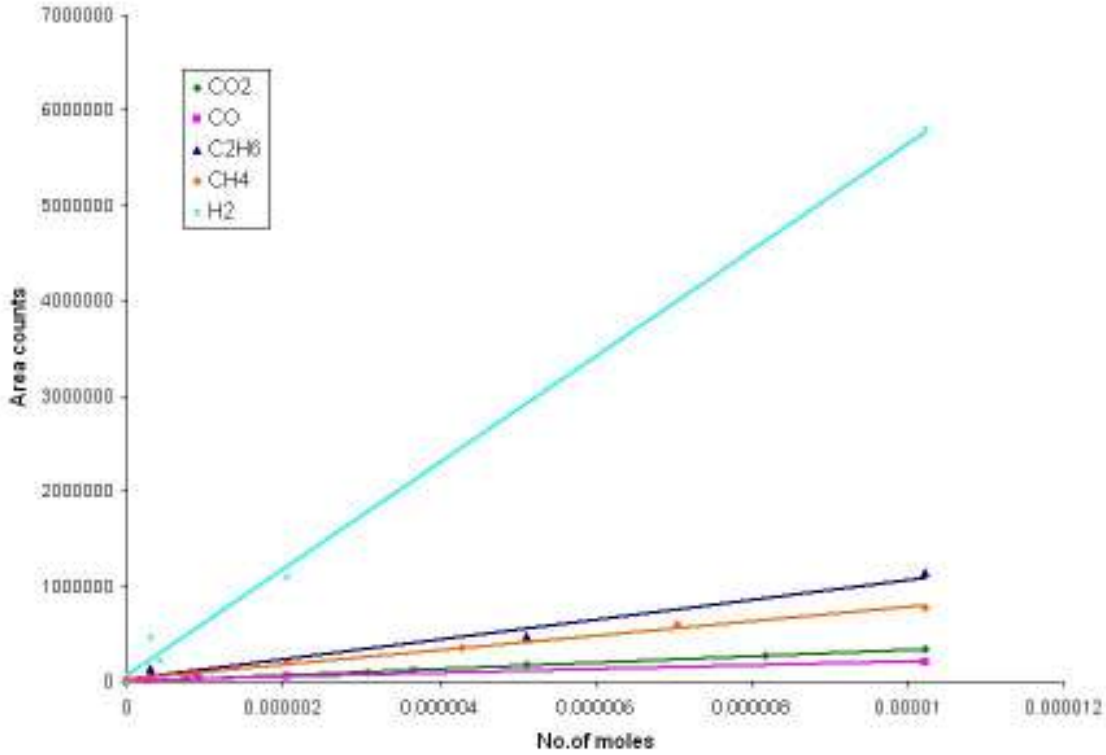

Figure 10 G.C. peak area count vrs no. of moles of gas

2.3.1.4. Steam reforming calculations

The following calculations were used to evaluate the results obtained from the steam reforming rig.

Conversion

Conversion =

(flow of ethane in – flow ethane out)/ flow of ethane in x 100

flowrate of ethane out =

(moles of C_2H_6 out/(moles out of C_2H_6 + H_2 + CO +CO_2 + CH_4)) x total exit flow

Rate of formation of products

e.g. rate of formation of H_2 =

(Moles out of H_2 x 1000)/ residence time/ catalyst weight

Product selectivity

e.g. selectivity towards H_2 =

Moles out of H_2/ (Moles out of H_2 + CO + CO_2 + CH_4) x 100

Carbon mass balance

Carbon mass balance =

(Moles out ethane*2 + CO + CO_2 +CH_4)/ (Moles in ethane *2) x total exit flow

2.3.1.5. High pressure reactions

The reactions carried out on the high pressure apparatus are outlined in tables 10 and 11.

Table 10 Summary of standard reactions carried out on high pressure apparatus

Catalyst	Temperature(K)		
	773	823	873
Rh/Al_2O_3	√	√	√
Pt/Al_2O_3	√	√	√
$Rh/La\text{-}ZrO_2$	√	√	√
$Pt/La\text{-}ZrO_2$	√	√	√

Table 11 Summary of poisoning reactions carried out on the high pressure apparatus

Catalyst	Poisoning conditions (all carried out at 873K)			
	H_2S 11.3ppm	H_2S 5.3ppm	CH_3SH 11.3ppm	CH_3SH 5.3ppm
Rh/Al_2O_3	√	√	√	√
Pt/Al_2O_3	√	√	√	√
$Rh/La\text{-}ZrO_2$	√	√	√	√
$Pt/La\text{-}ZrO_2$				

All reactions carried out on the high-pressure rig followed the same initial procedure. The reactor was filled with fused Al_2O_3 boiling chips to just below the point at which the thermocouple contacts the reactor, followed by 0.5g of catalyst and then the rest of the reactor was filled with more boiling chips. This ensured the thermocouple was in contact with the section of the reactor where the catalyst was situated. Once loaded, the reactor was sealed and the system was purged for an hour in a flow of $50cm^3min^{-1}$ of Ar. The system was then pressurised to 20 barg over a period of two hours, also during this period the catalyst was heated to a reaction temperature of 873 K. Once at temperature and pressure, hydrogen was added to the gas stream until it matched the argon flow. The $50cm^3min^{-1}$ of Ar and $50cm^3min^{-1}$ of H_2 was passed over the catalyst for 2 hours to reduce the catalyst. After reduction, the Ar flow was switched off and steam was introduced, maintaining the H_2 flow to keep the gas mix reducing. This H_2/H_2O feed was maintained for one hour to ensure the steam was well established before introducing the hydrocarbon. Also, any adjustments in temperature were made at this point. Ethane was then introduced over 15 minutes by gradually increasing the flow to 98 cm^3min^{-1}. The H_2 flow was then stopped. The first G.C injection was taken 15 minutes after the full introduction of ethane, hereafter injections were taken every 30 minutes.

After this stage, the reaction mixture flowed until steady state was reached or until no further reaction was observed.

The knockout pot where the water was collected had to be dropped frequently throughout the course of a reaction. There was a valve situated at the bottom of the pot which was opened slowly to release the pot contents into a beaker.

At the end of an experiment, the system would be purged with argon for an hour. The ethane flow was switched off and the $50cm^3min^{-1}$ argon switched on. During this period the heat to the furnace was switched off to allow the catalyst to cool. Once the furnace was at room temperature the system was depressurised by opening the back pressure regulator and venting off the gas. The reactor was now in a safe mode to be opened and the catalyst could be discharged.

For the poisoning experiments, once steady state was reached (normally after 17 hours), the water being pumped into the system was changed for water with dissolved sulphur species. This water was pumped for 7 hours before changing back to the normal distilled water.

2.3.1.6. Preparation of Sulphur solutions

In order to introduce poison to the catalysts hydrogen sulphide and methanthiol were dissolved into distilled water, and the resultant solution was pumped into the system. Four solutions were prepared; 11.2 ppm methanthiol, 5.3 ppm methanthiol, 11.2 ppm hydrogen sulphide and 5.3 ppm hydrogen sulphide.

A glass sample loop with a known volume, 0.0021l, was attached to the methanthiol/hydrogen sulphide cylinder and purged with gas for a few minutes. The taps of the sample loop were then closed to seal in approximately one atmosphere of the gas. The sample loop was immersed in a 900ml of water and the taps were opened. This procedure was repeated until the desired concentration of sulphur in the water had been achieved.

The volume of the sample loop was 0.0021l, this corresponds to $9.37x10^{-5}$ mol H_2S. The sample loop was filled and discharged into 50 moles of water 6 times to produce a solution of 11.2ppm, see below equation.

Moles of solute = (Moles of solvent/1000000) x concentration of solution (ppm)

Concentration of solution (ppm) =

(50 mol H_2O/1000000) x **6** x 9.37×10^{-5} mol H_2S = 11.2ppm

2.3.1.7. Steam Reformer Clean up procedure

The steam reforming unit was put through a clean procedure after each poisoning experiment to remove the sulphur retained by the system. This involved flowing hydrogen through the system for a period of two days, with the unit still at reaction temperature. Following this a catalytic run would be performed and if deactivation of the catalyst was apparent the reaction would be stopped to repeat the hydrogen purge step. The system was deemed acceptably clean when the catalyst exhibited stable conversion and the production of hydrogen was consistent with the non-poisoned rate. Once these two criteria were met the poisoning experiment could be continued.

2.3.2. Pulse Flow Reactor

The glass apparatus consisted of three main parts separated by vacuum taps: gas manifold, sample loop and continuous flow section. A diagram is given figure 11. The gas manifold could be evacuated to a minimum pressure of 1×10^{-1} torr using a vacuum pump. The pressure was monitored with an Edwards Barocel pressure sensor. After evacuation, the manifold was isolated from the vacuum pump and filled with a pressure of reactant gas from a storage bulb.

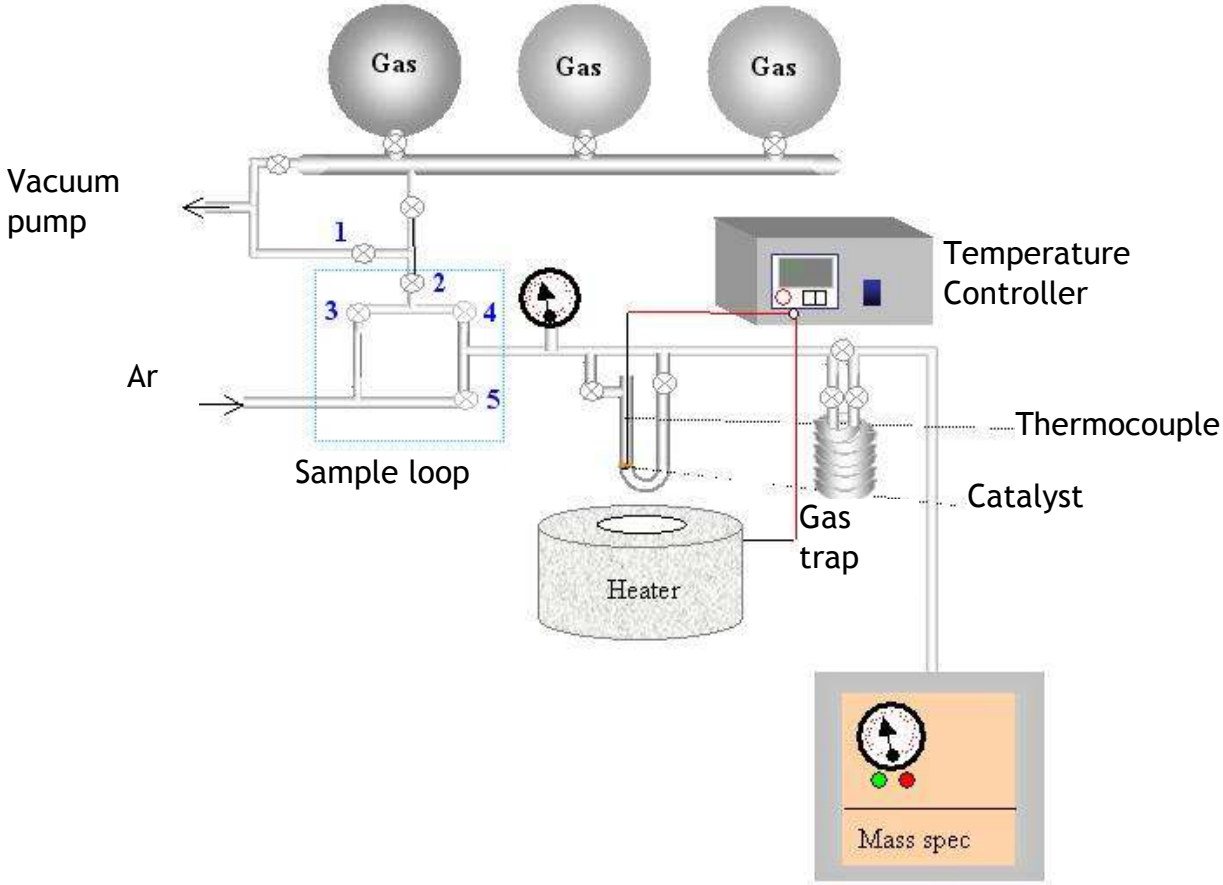

Figure 11 Pulse flow apparatus

The sample loop is labelled in figure 11. It connects the gas manifold to the continuous flow section. The volume of the sample loop between taps 3 and 4 was pre-determined (8.62 cm^3) and a known pressure of gas from the manifold could be stored here. The carrier gas coming in to the apparatus could flow through this section to deliver a pulse to the catalyst. To isolate the pulse from the continuous flow section, tap 5 was initially open to allow the carrier to flow through and taps 3 and 4 were closed.

The continuous flow section consisted of a removable quartz glass u-bend reactor; this contained a sinter upon which the catalyst was placed. A K-type thermocouple was connected to a temperature controller and placed in a quartz glass pocket inside the reactor, which sat on top of the catalyst bed. In order to obtain reference peaks, the reactor could be isolated to allow the gases to bypass the catalyst. Also, in the continuous flow section has a gas trap positioned downstream from the reactor to trap out product gases by freezing. A gauge was also attached to monitor the pressure in this section.

2.3.2.1. Gas Chromatograph

A Shimadzu gas chromatograph connected to a Hewlette Packard integrator was used to analyse the gases emerging from the pulse flow reactor. The G.C. was fitted with a Molecular sieve, 60-80 mesh column and a Poropak Q, 80-100 mesh column.

Calibrations were done by varying the pressure of the pulse to obtain different number of moles of gas and relating this peak area. These were carried beforehand to ensure the peak area were directly proportional to the pulse pressure. Pulses of varying pressure were passed through the reactor bypass and recorded on the G.C.

The Molecular sieve column was used to detect carbon monoxide whilst the Poropak column was used to detect hydrogen sulphide. Both columns were able to detect hydrogen so hydrogen had to be calibrated for each column. Figure 12 shows the linear relationship between pulse pressure and peak area for hydrogen for each column.

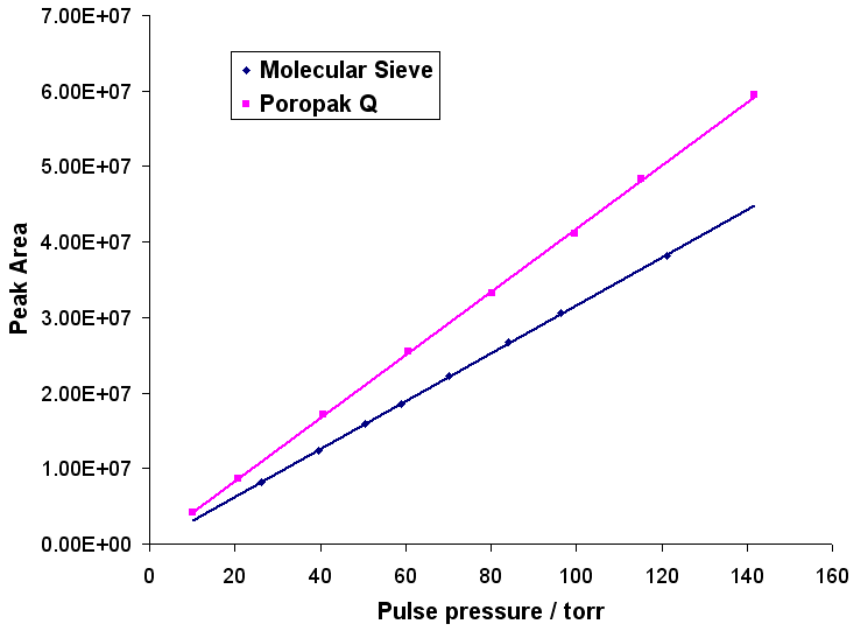

Figure 12 Linear relationship between peak area and pulse pressure

It appears from figure 12 that the GC detector is responding differently to the same amount of hydrogen in the pulse. This is due to the integrator rather than a defect of the G.C. From figure 13 the hydrogen which passes through the

Poropak column produces the greatest response this is because the poropak column gives a very sharp peak for hydrogen, which the integrator is able to integrate more easily as it can detect the start and end of the peak much better. Meanwhile, the molecular sieve column produces a weaker response because it produces a peak that looks like a normal distribution curve making it more difficult for the integrator to identify where the peak begins and ends.

2.3.2.2. Adsorption Calculation

To calculate whether adsorption had taken place the reference pulse was used. The pressure of the CO reference pulse was known and from this the number of molecules of CO could be calculated, using the following equation:

$PV = nRT$

Where: P = pulse pressure, V = volume of sample loop ($8.62cm^3$), R = molar gas constant ($62388\ cm^3torrmol^{-1}K^{-1}$), T = temperature of sample loop (room temperature)

A peak for the CO reference pulse was obtained by flowing a single CO pulse through the reactor by-pass then into the gas chromatograph. The area under the peak was integrated and this represents a known number of moles as shown in table 12. Two references were taken to ensure reproducibility.

Table 12 CO reference peak areas with corresponding pressure and number of moles

Pulse	Pressure/ torr	Molecules	Area
CO Reference 1	100	2.79x1019	2354662
CO Reference 2	97	2.71x1019	2254950

For the subsequent pulses CO was passed over the catalyst and then to the gas chromatograph. For each pulse, the area under the CO peak was obtained and converted to molecules ($CO_{molecules\ out}$) using the reference pulse information in table 12. The results obtained for CO pulses over SiO_2 support are given in table 13.

Table 13 Moles of CO out over SiO_2, calculated peak areas

Pulse	Area	CO molecule out/x10^{18}
1	1938804	2.31
2	1865975	2.24
3	1832974	2.19
4	1735595	2.07
5	1695732	2.02
6	1557779	1.86
7	1558025	1.86

The molecules of CO out can be subtracted from the molecules of CO in to find the amount of CO adsorbed.

2.3.2.3. Pulse Flow Reactions

Prior to a reaction, typically 0.5g of catalyst was reduced in a flow of 30cm^{3}min^{-1} 2%H_2/N_2 at atmospheric pressure for two hours at 673 K. This temperature was reached by heating the catalyst at a rate of 10°C/min and then it was held at 673K for two hours. The catalyst was then purged with 30cm^{3}min^{-1} Ar for 30 minutes while the catalyst cooled back down to room temperature. The adsorptions were carried out at room temperature unless otherwise stated (see below).

The gas manifold was evacuated and filled with approximately 100 torr of adsorption gas. The first few pulses of gas were flowed through the by-pass and used as references. References were obtained until reproducible peak areas were obtained. Then pulses of approximately 100 torr were passed through the catalyst using Ar gas as a carrier until the catalyst was saturated. All pulses were recorded on the gas chromatogrph.

Following reduction, the procedure differed for some of the adsorption studies and this is outlined in the following sub-sections.

2.3.2.3.1. Room Temperature single gas adsorptions; H_2S, CO, CH_3SH, H_2S and H_2 (1:1)

Pulses at room temperature until catalyst saturated.

2.3.2.3.2. High Temperature; H_2S, H_2S and H_2 (1:1)

Following reduction, the catalyst was heated to 873K under a flow of Ar. The catalyst was maintained at this temperature until pulses were complete and the catalyst was saturated.

2.3.2.3.3. Room Temperature; CO adsorption followed by H_2S

The catalyst was saturated with CO, and then purged with Ar for 30 minutes. The manifold was evacuated, filled with H_2S and this was pulsed over the catalyst.

2.3.2.3.4. Room Temperature; H_2S adsorption followed by CO

The catalyst was saturated with H_2S, and then purged with Ar for 30 minutes. The manifold was evacuated, filled with CO and this was pulsed over the catalyst.

All the reactions carried out on the glass-line apparatus are given in tables 14 and 15.

Table 14 Pulse flow adsorptions

Reaction / Catalyst	Room Temperature				High Temperature	
	CO	H_2S	CH_3SH	H_2:H_2S (1:1)	H_2S	H_2:H_2S (1:1)
Al_2O_3	√	√	√	√	√	√
Rh/Al_2O_3 acetate	√	√	√	√	√	√
Rh/Al_2O_3 nitrate	√	√	√	√	√	√
SiO_2	√	√	√	√	√	√
Rh/SiO_2 acetate	√	√	√	√	√	√
Rh/SiO_2 nitrate	√	√	√	√	√	√
Pt/Al_2O_3	√	√	√	√	√	√
Pt/SiO_2	√	√	√	√	√	√

Table 15 Pulse flow competitive adsorptions

Adsorption Catalyst	$CO:H_2S$ (1:1)	CO followed by H_2S	H_2S followed by CO
Rh/Al_2O_3 acetate	√	√	√
Rh/Al_2O_3 nitrate	√	√	√
Rh/SiO_2 acetate	√	√	√
Rh/SiO_2 nitrate	√	√	√
Pt/Al_2O_3		√	√
Pt/SiO_2		√	√

3. Results

3.1. Characterisation

3.1.1. BET

The data obtained from the BET analysis is tabulated below.

Table 16 Determined BET surface area of each catalyst

	Rh/Al_2O_3 acetate	Rh/Al_2O_3 nitrate	Rh/SiO_2 acetate	Rh/SiO_2 nitrate	Pt/Al_2O_3	Pt/SiO_2
BET surface area/(sq.m/g)	102.67	99.80	205.61	237.66	108.11	187.34
Single point surface area at P/Po 0.1995/(sq.m/g)	100.88	97.53	210.36	232.11	110.00	190.03
BJH cumulative adsorption surface area of pores between 17 & 3000A diameter/(sq.m/g)	142.65	124.57		372.48	190.07	

Table 17 Catalyst pore volumes determined by BET analysis

	Rh/Al_2O_3 acetate	Rh/Al_2O_3 nitrate	Rh/SiO_2 acetate	Rh/SiO_2 nitrate	Pt/Al_2O_3	Pt/SiO_2
Single point total pore vol. of pores <3345.8406 A diameter at p/Po 0.9943/(cc/g)	0.509	0.466		0.918	0.536	
BJH cumulative adsorption pore vol. of pores between 17 and 500A diameter/(cc/g)	0.496	0.454	0.848	0.911	0.540	0.847

Table 18 Catalyst pore diameters determined by BET analysis

	Rh/Al_2O_3 acetate	Rh/Al_2O_3 nitrate	Rh/SiO_2 acetate	Rh/SiO_2 nitrate	Pt/Al_2O_3	Pt/SiO_2
Average pore diameter (4V/A by BET)/ A	198.55	186.66	161.04	154.61	194.84	178.64
BJH adsorption average diameter (4V/A)/ A	139.32	145.63	134.67	97.79	113.66	134.02

3.1.2. TGA

3.1.2.1. Calcination

TGA profiles of uncalcined Rh/Al_2O_3 (acetate), Rh/Al_2O_3 (nitrate), Rh/SiO_2 (acetate) and Rh/SiO_2 (nitrate) were collected as described in section 2.2.2, to determine at what temperature the metal precursors decompose. Figures 13 to 16 present curves for TGA, the derivative weight loss and mass spectrometric data for each of the catalysts in oxygen.

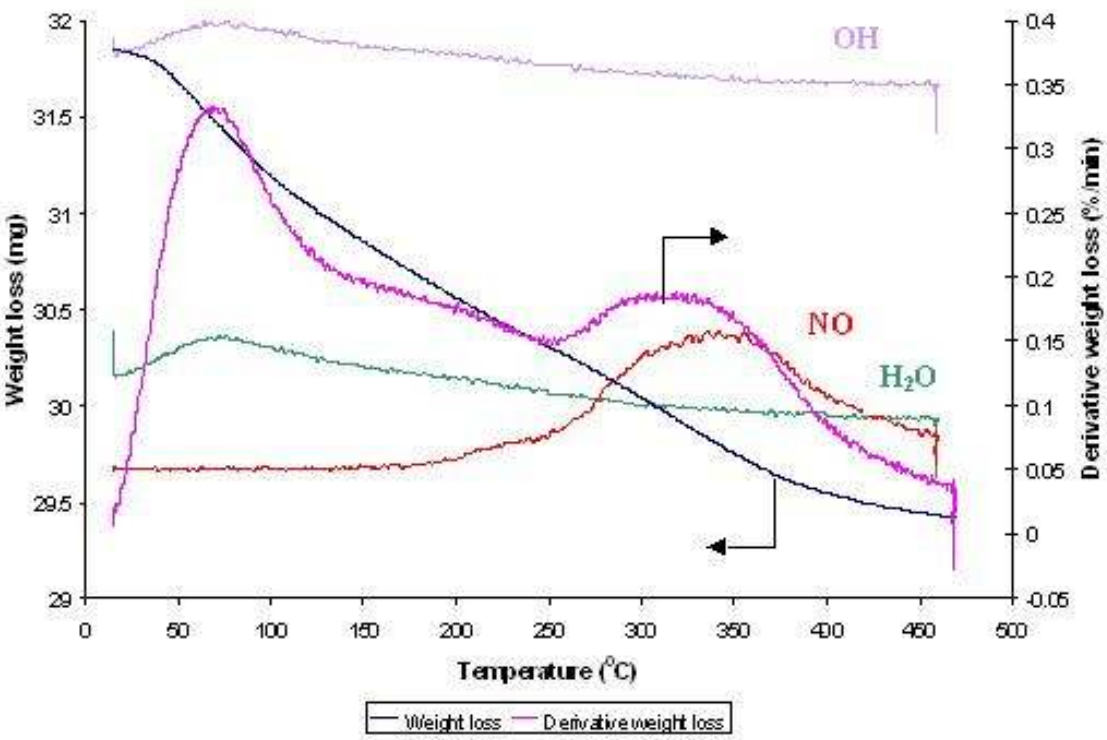

Figure 13 TGA and mass spectrometric data for Rh/Al_2O_3 (nitrate) in O_2/Ar

From the derivative weight loss curve two prominent periods of weight loss are evident. The first event occurring at 80°C can be attributed to water loss, from the mass spectrometric data. The second event occurring at 320°C is accompanied by evolution of NO indicating decomposition of the nitrate precursor.

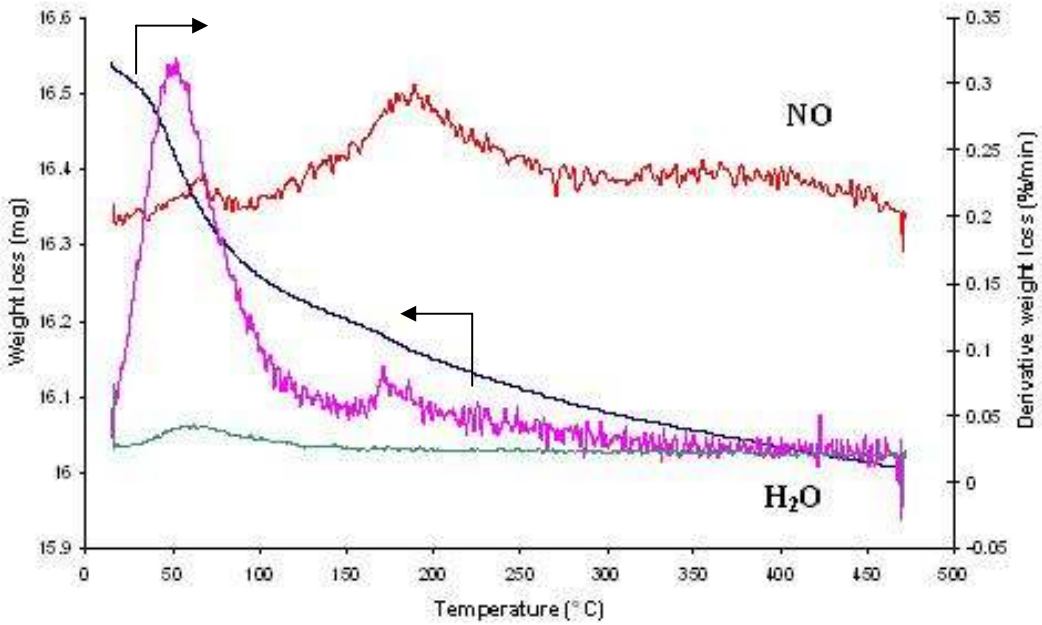

Figure 14 TGA and mass spectrometric data of Rh/SiO_2 (nitrate) in O_2/Ar

Derivative weight loss of Rh/SiO_2 (nitrate) again shows two weight loss events, with the first being attributed to water loss. The second period occurs at a lower temperature than Rh/Al_2O_3 (nitrate), 170°C, and is associated with NO evolution signifying nitrate decomposition is occurring at a lower temperature.

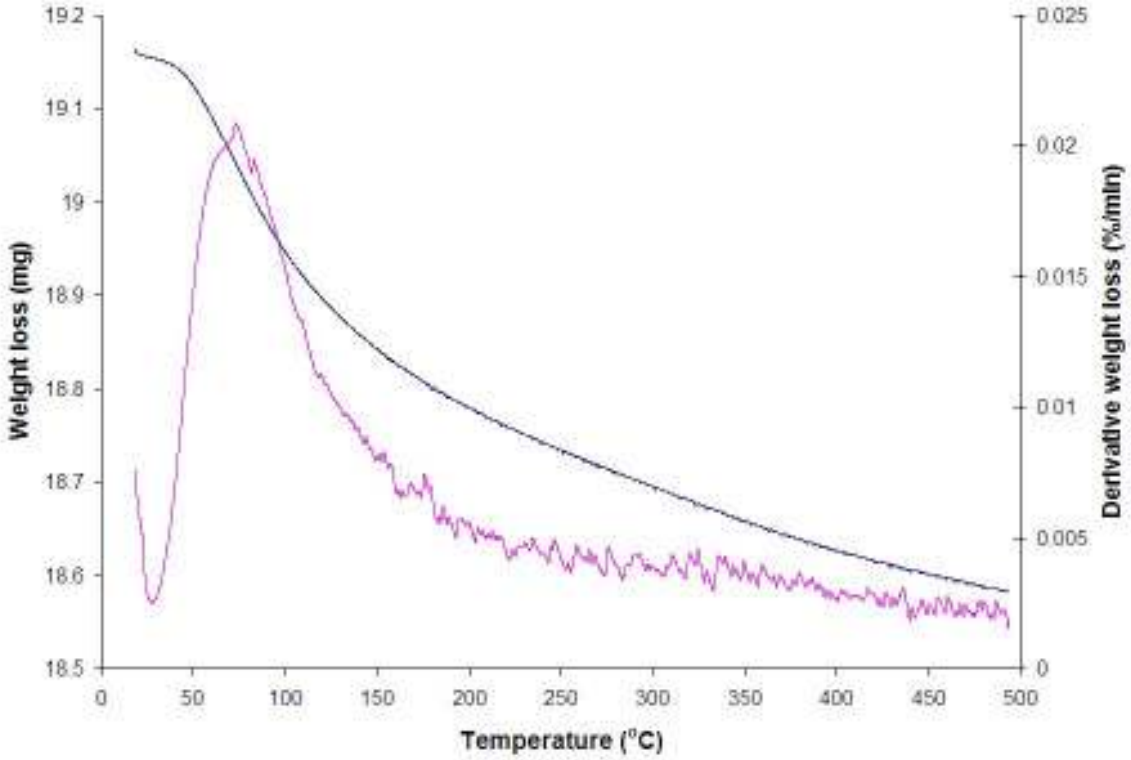

Figure 15 TGA data for Rh/Al_2O_3 (acetate) in O_2/Ar

Only one major weight loss event is initially apparent from the derivative weight of Rh/Al_2O_3 (acetate). The peak is at 80°C which indicates it was due to water loss. The acetate precursor does not appear to be decomposing from the absence of other peaks and there is no evidence of any gas evolutions.

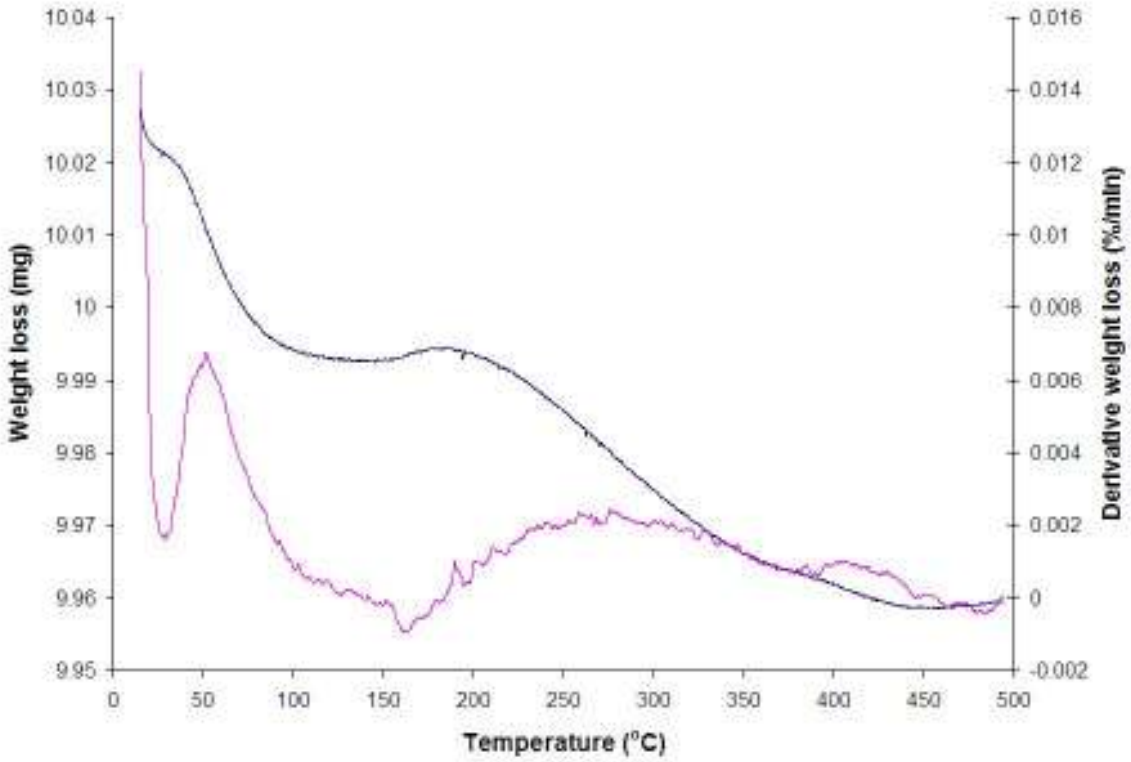

Figure 16 TGA data of Rh/SiO_2 (acetate) in O_2/Ar

There are two weight loss events apparent from the derivative weight; one at 60°C, attributed to water loss, and a broad peak which reaches it's maximum at approximately 270°C. Unfortunately no evolution of gas was detected from the mass spectrometric data, probably due to the small quantity of weight loss, but it is likely this weight loss is due to the decomposition of the metal precursor.

3.1.2.2. Reduction

TGA profiles of calcined Rh/Al_2O_3 (nitrate) and Rh/SiO_2 (nitrate) were collected in hydrogen to examine the effect reduction has on the catalysts, figures 17 and 18.

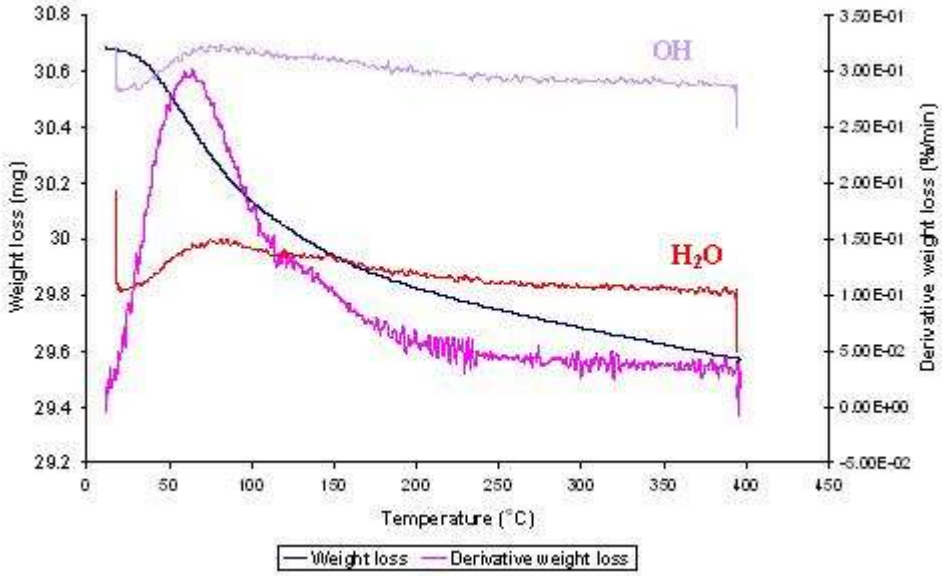

Figure 17 TGA and mass spectrometric data for Rh/Al_2O_3 (nitrate) in H_2

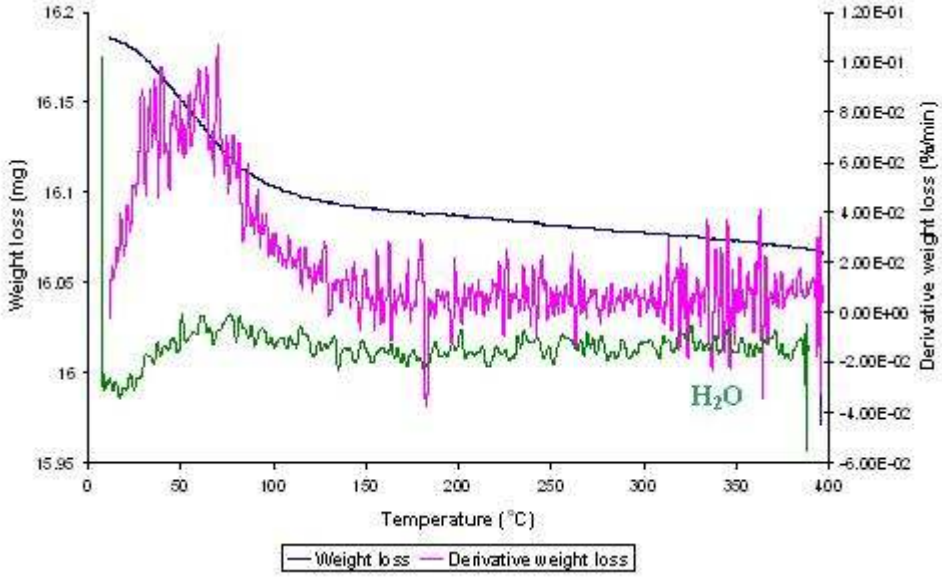

Figure 18 TGA and mass spectrometric data for Rh/SiO_2 (nitrate) in H_2

For both catalysts tested there is a weight loss peak around 60°C, which can be ascribed to the evolution of water. This indicates that that the only process occurring during reduction of the catalyst is dehydration.

3.1.2.3. Post Analysis

3.1.2.3.1. Rh/ZrO_2: Influence of Poison on Carbon Laydown

TGA profiles, along with mass spectrometric data, were collected for Rh/ZrO_2 samples which had been poisoned during steam reforming. Figure 19 is a sample of Rh/ZrO_2 which has been poisoned with 11.2ppm methanthiol and figure 20 has been poisoned with 11.2ppm hydrogen sulphide, they were both carried out in O_2/Ar.

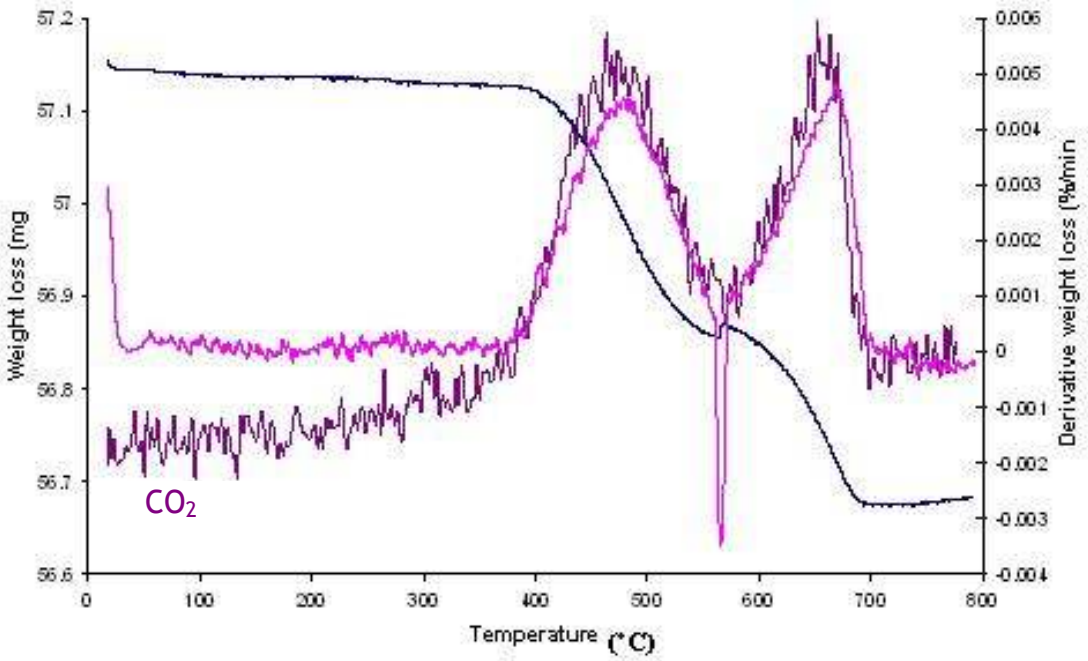

Figure 19 TPO of methanthiol poisoned Rh/ZrO_2

Two weight loss events are apparent from the derivative weight loss, which are both the result of CO_2 evolution. This suggests carbon has been deposited on the catalyst surface from steam reforming and has reacted with oxygen to produce CO_2. The CO_2 has evolved at two different temperatures, 470 °C and 670°C, indicating two different forms of carbon on the catalyst.

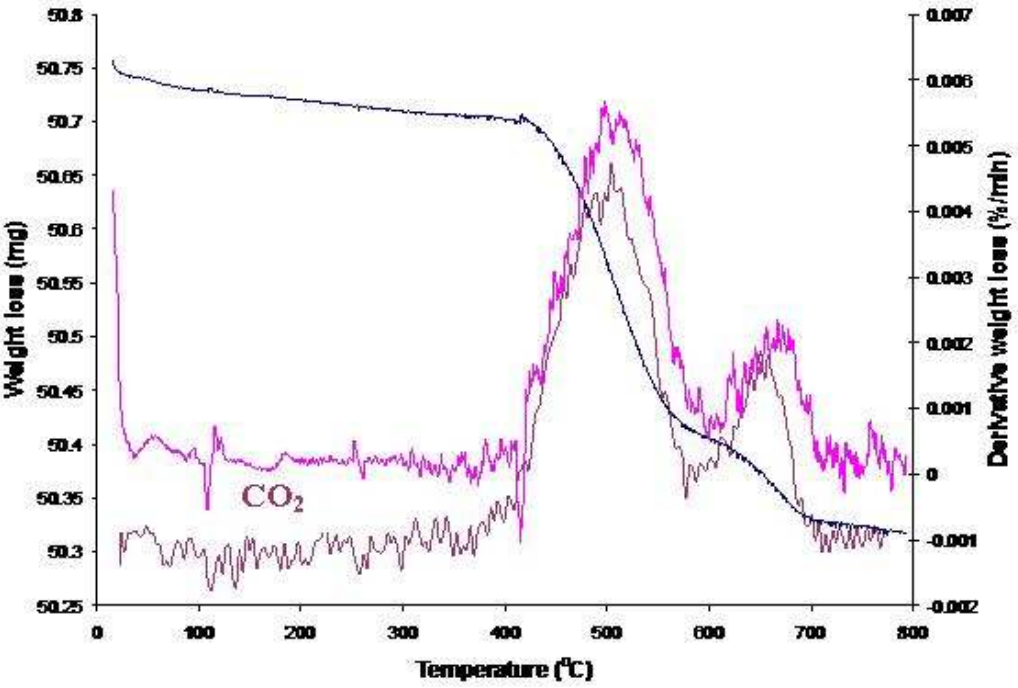

Figure 20 TPO of hydrogen sulphide poisoned Rh/ZrO_2

Again, there are two major weight loss events due to CO_2 evolution which now occur at 500°C and 650°C. In this case, where H_2S has been used to poison the catalyst rather than CH_3SH, the higher temperature peak is significantly smaller then the lower temperature peak. The carbon that requires a higher temperature to be removed, presumably because it is more strongly bound, does not form to the same extent compared to when CH_3SH poisons the catalyst.

From the weight loss the amount of carbon deposited on the catalysts can be deduced, table 19.

Table 19 Mass of carbon produced per 0.5 g Rh/ZrO_2 from a steam reforming reaction poisoned with methanthiol and another reaction poisoned with hydrogen sulphide

Poison	Mass of C at low temp(g)	Mass of C at high temp(g)	Total mass of C (g)
Methanthiol	0.3	0.2	0.5
Hydrogen Sulphide	0.3	0.1	0.4

3.1.2.3.2. Effect of H_2S on Carbon Laydown over Rh/Al_2O_3 and Comparison with Rh/ZrO_2

A TPO profile was collected for Rh/Al_2O_3, which had been poisoned using a 11.2ppm H_2S solution during steam reforming, and is presented in figure 21.

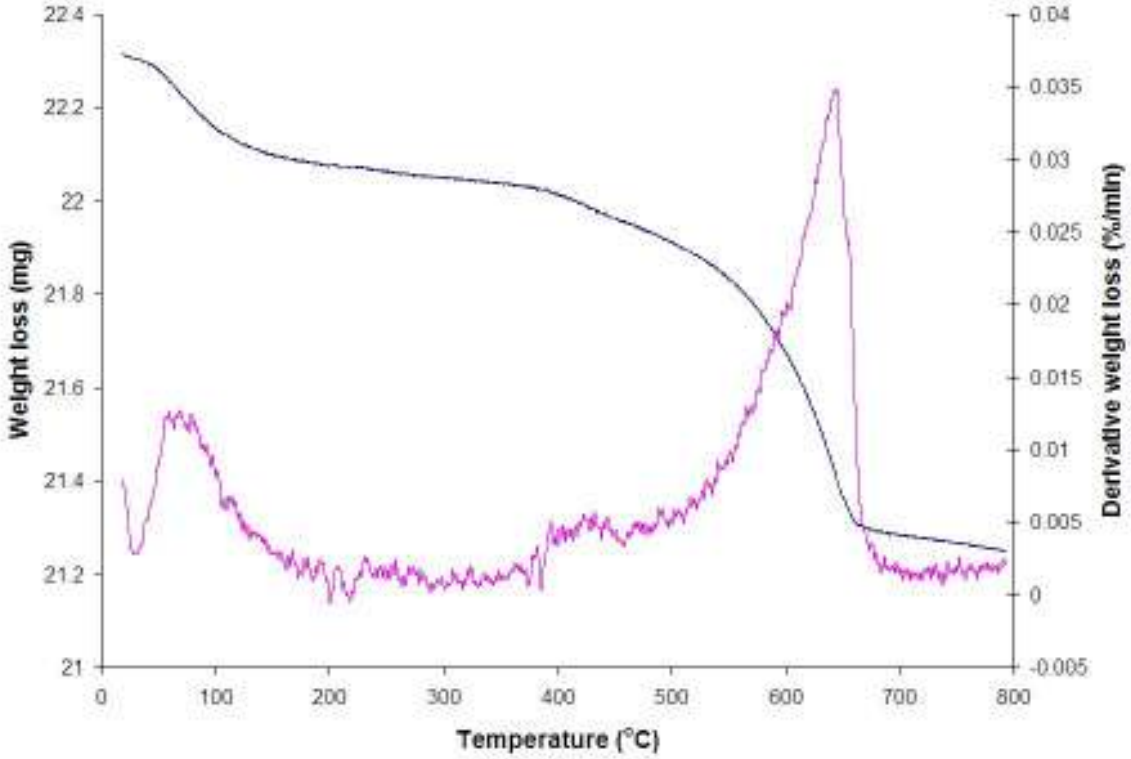

Figure 21 TPO of hydrogen sulphide poisoned Rh/Al_2O_3

Only one major weight loss event is evident, occurring at 650°C, though there appears to be some minor weight loss at 420°C. CO_2 evolution at 650°C also occurred over Rh/ZrO_2 but to a lesser extent. Table 20 compares the weight loss at 650°C for Rh/ZrO_2 and Rh/Al_2O_3.

Table 20 Weight loss (mg) during TPO at 650°C

Catalyst	Rh/ZrO_2	Rh/Al_2O_3
% Weight loss (mg) at 650°C	0.1	3

When H_2S poisons the catalysts during steam reforming carbon laydown occurs. Two forms of carbon have been identified; over Rh/ZrO_2 the carbon which is removed at lower temperature is more prominent, whilst the carbon removed at higher temperature constitutes the bulk of the carbon on the Rh/Al_2O_3 surface.

3.1.2.3.3. Effect of CH_3SH on Carbon Laydown over Pt/Al_2O_3 and comparison with Rh/ZrO_2

Figure 22 shows a TPO profile and mass spectrometric data which was collected for Pt/Al_2O_3, it had been poisoned using a 11.2ppm CH_3SH solution during steam reforming.

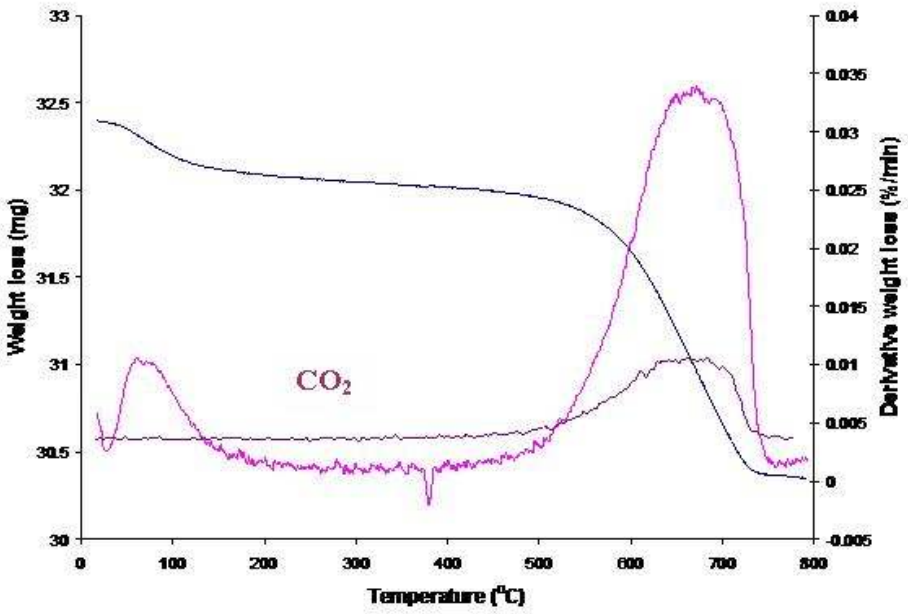

Figure 22 TPO of methanthiol poisoned Pt/Al_2O_3

From the derivative weight loss there is a broad weight loss peak at 670°C, which was accompanied by evolution of CO_2. Similarly, when a TPO was carried out over CH_3SH poisoned Rh/ZrO_2 a weight loss peak at 670°C was evident. However, there was also a lower temperature peak which is absent here. Table 21 compares the weight loss at 670°C for Rh/ZrO_2 and Pt/Al_2O_3.

Table 21 Weight loss (mg) during TPO at 670°C

Catalyst	Rh/ZrO_2	Pt/Al_2O_3
Weight loss (mg) at 670°C	0.3	4.6

Considerably more carbon is deposited on Pt/Al_2O_3 than on Rh/ZrO_2. Also, Rh/ZrO_2 has the ability to form a carbon species, which is more easily removed

3.2. Single Gas Adsorptions

Pulses of CO, H_2S and CH_3SH were passed over the catalysts at room temperature and atmospheric pressure until the catalysts were saturated.

3.2.1. CO Adsorption

3.2.1.1. CO pulses over SiO_2 support

Pulses of CO were passed over the SiO_2 support to determine if any adsorption took place. No adsorption was observed on the SiO_2 support.

3.2.1.2. CO Pulses over SiO_2 Supported catalysts

CO pulses were passed over Rh/SiO_2 (acetate), Rh/SiO_2 (nitrate) and Pt/SiO_2 catalysts at room temperature. Prior to this reference peaks were obtained by passing pulses through the reactor by-pass. The results from each series of pulses were treated in the same way as the peaks obtained from the SiO_2 support, as described in section 2.3.2.2. The results are given in tables 22 to 24; they include amount of CO adsorbed per pulse/gram of catalyst and the cumulative amount of CO adsorbed/gram of catalyst.

Table 22 Data obtained from CO pulses over Rh/SiO_2 acetate

Pulse	CO in/ $x10^{19}$ molecules	CO out/ $x10^{19}$ molecules	CO adsorbed/ $x10^{19}$ molecules/g of catalyst	Cumulative CO adsorbed/ $x10^{19}$ molecules
1	2.97	0.43	5.09	5.09
2	2.88	2.88	0	5.09

Table 23 Data obtained from CO pulses over Rh/SiO_2 nitrate

Pulse	CO in/ $x10^{19}$ molecules	CO out/ $x10^{19}$ molecules	CO adsorbed/ $x10^{19}$ molecules/g of catalyst	Cumulative CO adsorbed/ $x10^{19}$ molecules
1	2.85	1.45	2.79	2.79
2	2.77	2.71	0.11	2.91
3	2.70	2.64	0.11	3.02
4	2.63	2.70	-0.15	2.87
5	2.55	2.55	0	2.87

Table 24 Data obtained from CO pulses over Pt/SiO_2

Pulse	CO in/ $x10^{19}$ molecules	CO out/ $x10^{19}$ molecules	CO adsorbed/ $x10^{19}$ molecules/g of catalyst	Cumulative CO adsorbed/ $x10^{19}$ molecules
1	1.65	0.51	2.27	2.27
2	1.64	1.52	0.24	2.52
3	1.63	1.48	0.29	2.81
4	1.62	1.61	0.02	2.83

All the catalysts adsorbed CO during the first pulse; hereafter there was no significant adsorption, suggesting the catalysts were virtually saturated with the first pulse. Since the SiO_2 support did not adsorb any CO, all the CO is being adsorbed onto the metal.

3.2.1.3. CO : M ratios - SiO_2 Catalysts

The ratio of CO molecules adsorbed : Metal atom can be obtained by dividing the total number of CO molecules adsorbed by the number of metal atoms present. The table below compares theses values for the three SiO_2 supported catalysts. The error values displayed are produced from repeat experiments.

Table 25 CO:M ratios for SiO_2 supported catalysts

Catalyst	Rh/SiO_2 acetate	Rh/SiO_2 nitrate	Pt/SiO_2
CO:M	0.9 +/- 0.11	0.6 +/- 0.14	0.8 +/- 0.17

These values are fairly high suggesting the metal particles are well dispersed on the SiO_2 support.

3.2.1.4. CO Pulses over Al_2O_3 support

To determine if the Al_2O_3 support adsorbed CO a sample of the support was subjected to pulses of CO. The results obtained were treated in the same manner as described in section 2.3.2.2. There was negligible CO adsorption on the Al_2O_3 support.

3.2.1.5. CO Pulses over Al_2O_3 supported catalysts

CO pulses were passed over Rh/Al_2O_3 (acetate), Rh/Al_2O_3 (nitrate) and Pt/Al_2O_3 catalysts. The results for the catalysts are given in tables 26 to 28.

Table 26 Data obtained from CO pulses over Rh/Al_2O_3 acetate

Pulse	CO in/ $x10^{19}$ molecules	CO out/ $x10^{19}$ molecules	CO adsorbed/ $x10^{19}$ molecules/g of catalyst	Cumulative CO adsorbed/ $x10^{19}$ molecules
1	3.00	0.15	5.70	5.70
2	2.91	1.67	2.48	8.18
3	2.82	2.63	0.37	8.55
4	2.73	2.73	0	8.55

Table 27 Data obtained from CO pulses over Rh/Al_2O_3 nitrate

Pulse	CO in/ $x10^{19}$ molecules	CO out/ $x10^{19}$ molecules	CO adsorbed/ $x10^{19}$ molecules/g of catalyst	Cumulative CO adsorbed/ $x10^{19}$ molecules
1	2.66	0	5.31	5.31
2	2.57	1.17	2.81	8.12
3	2.49	2.49	0	8.12

Table 28 Data obtained from CO pulses over Pt/Al_2O_3

Pulse	CO in/ $x10^{19}$ molecules	CO out/ $x10^{19}$ molecules	CO adsorbed/ $x10^{19}$ molecules/g of catalyst	Cumulative CO adsorbed/ $x10^{19}$ molecules
1	1.73	0.63	2.20	2.20
2	1.72	1.72	0	2.20

All the catalysts adsorbed CO from the first pulse; the Rh catalysts also adsorbed a portion of the second pulse. Since the Al_2O_3 support adsorbed a negligible amount of CO, it is assumed all the CO is going onto the metal.

3.2.1.6. CO : M ratios – Al_2O_3 catalysts

The table below compares the CO:M for the three Al_2O_3 supported catalysts.

Table 29 CO:M ratios for Al_2O_3 supprted catalysts

Catalyst	Rh/Al_2O_3 acetate	Rh/Al_2O_3 nitrate	Pt/Al_2O_3
CO:M	1.5 +/- 0.16	1.4 +/-0.14	0.7 +/- 0.04

The values obtained for CO:Rh are significantly higher than CO:Pt, which is a reflection on differences in dispersion and the mode of CO adsorption.

3.2.2. H_2S Adsorption

3.2.2.1. H_2S pulses over SiO_2 support

Pulses of H_2S were passed over the SiO_2 support to determine if any adsorption took place. The results obtained were treated in the same manner as described in section 2.3.2.2. There is no detectable adsorption of H_2S on the SiO_2 support.

3.2.2.2. H_2S pulses over SiO_2 supported catalysts

H_2S pulses were passed over Rh/SiO_2 (acetate), Rh/SiO_2 (nitrate) and Pt/SiO_2 catalysts. The results for the catalysts are given in tables 30 to 32.

Table 30 Data obtained from H_2S adsorption over Rh/SiO_2 acetate

Pulse	H_2S in/ $x10^{19}$ molecules	H_2S out/ $x10^{19}$ molecules	H_2S adsorbed/ $x10^{19}$ molecules/g of catalyst	Cumulative H_2S adsorbed/ $x10^{19}$ molecules
1	1.85	0	3.66	3.66
2	1.79	1.09	1.38	5.05
3	1.73	1.51	0.44	5.48
4	1.67	1.67	0	5.48

Table 31 Data obtained from H_2S adsorption over Rh/SiO_2 nitrate

Pulse	H_2S in/ $x10^{19}$ molecules	H_2S out/ $x10^{19}$ molecules	H_2S adsorbed/ $x10^{19}$ molecules/g of catalyst	Cumulative H_2S adsorbed/ $x10^{19}$ molecules
1	1.64	0	3.28	3.28
2	1.58	1.58	0	3.28

Table 32 Data obtained from H_2S adsorption over Pt/SiO_2

Pulse	H_2S in/ $x10^{19}$ molecules	H_2S out/ $x10^{19}$ molecules	H_2S adsorbed/ $x10^{19}$ molecules/g of catalyst	Cumulative H_2S adsorbed/ $x10^{19}$ molecules
1	1.65	0.26	2.76	2.76
2	1.59	1.50	0	2.76

The Rh/SiO_2 catalysts adsorb all of the first pulse. Thereafter adsorption slowly dropped off for Rh/SiO_2 acetate and ceased at pulse 4, whilst for Rh/SiO_2 nitrate no adsorption is apparent after the first pulse. Pt/SiO_2 only adsorbed a portion of the first pulse.

Since there was no H_2S being adsorbed onto the SiO_2 support, it is assumed the metal takes up the entire H_2S.

3.2.2.3. S:M ratios

As described in section 3.2.1.1.3 the CO:M was calculated from the amount of CO adsorbed, the same approach can also be adopted using H_2S adsorption data to obtain S:M. The table below compares the ratios obtained from the H_2S pulses for the three SiO_2 supported catalysts.

Table 33 S:M ratios for SiO_2 supported catalysts

Catalyst	Rh/SiO_2 acetate	Rh/SiO_2 nitrate	Pt/SiO_2
S:M	0.9 +/- 0.05	0.6 +/- 0.07	0.9

3.2.2.4. Hydrogen evolution: SiO_2 supported catalysts

As hydrogen sulphide adsorbed onto the catalysts it evolved hydrogen suggesting that the molecule dissociated to form a metal-sulphide bond and hydrogen gas:

$$H_2S(g) \longrightarrow S_{(adsorbed)} + H_2(g)$$

With all the catalysts studied hydrogen evolution accompanied adsorption. Using the hydrogen calibration detailed in the experimental section, the hydrogen evolved could be quantified with respect to the amount of sulphur adsorbed. These results for the three SiO_2 supported catalysts are given in table 34.

Table 34 H_2 evolution for SiO_2 supported catalysts

Catalyst	Total molecules of H_2 evolved / $x10^{19}$	H_2 evolved : S adsorbed
Rh/SiO_2 acetate	4.83	0.9
Rh/SiO_2 nitrate	2.08	0.6
Pt/SiO_2	1.59	0.6

The ratio of H_2 evolved : S adsorbed gives an indication of the degree of dissociation the molecule is undergoing i.e. if this value was 1 there would be full dissociation. As hydrogen sulphide adsorbs over the SiO_2 supported catalysts it appears to only partially dissociate, with most dissociation occurring over Rh/SiO_2 acetate.

3.2.2.5. H_2S Pulses over Al_2O_3 support

Pulses of H_2S were passed over the Al_2O_3 support to determine if any adsorption took place. The results obtained were treated in the same manner as described in section 2.3.2.2 and the data is presented in table 35.

Table 35 Data obtained from H_2S adsorption over Al_2O_3 support

Pulse	H_2S in/ $x10^{19}$ molecules	H_2S out/ $x10^{19}$ molecules	H_2S adsorbed/ $x10^{19}$ molecules/g of catalyst	Cumulative H_2S adsorbed/ $x10^{19}$ molecules	**Repeat** Cumulative H_2S adsorbed/ $x10^{19}$ molecules
1	1.53	0	1.53	1.53	1.61
2	1.49	0.60	0.89	2.41	2.41
3	1.45	0.99	0.46	2.88	3.32
4	1.41	1.15	0.26	3.13	3.32
5	1.38	1.34	0.04	3.17	3.32

From the results, it is clear that there is substantial adsorption on the alumina support. The adsorption was not accompanied with hydrogen evolution suggesting the adsorption on the Al_2O_3 support is associative. This adsorption has to be considered when hydrogen sulphide is pulsed over the Al_2O_3 supported catalysts.

3.2.2.6. H_2S Pulses over Al_2O_3 supported catalysts

H_2S pulses were passed over Rh/Al_2O_3 (acetate), Rh/Al_2O_3 (nitrate) and $PtAl_2O_3$ catalysts. The results are presented as adsorption isotherms, in figures 23 to 25. The total amount of H_2S adsorbed is plotted alongside the amount of H_2S adsorbed onto the support, with the shaded area indicating the amount of H_2S that must be adsorbing onto the metal.

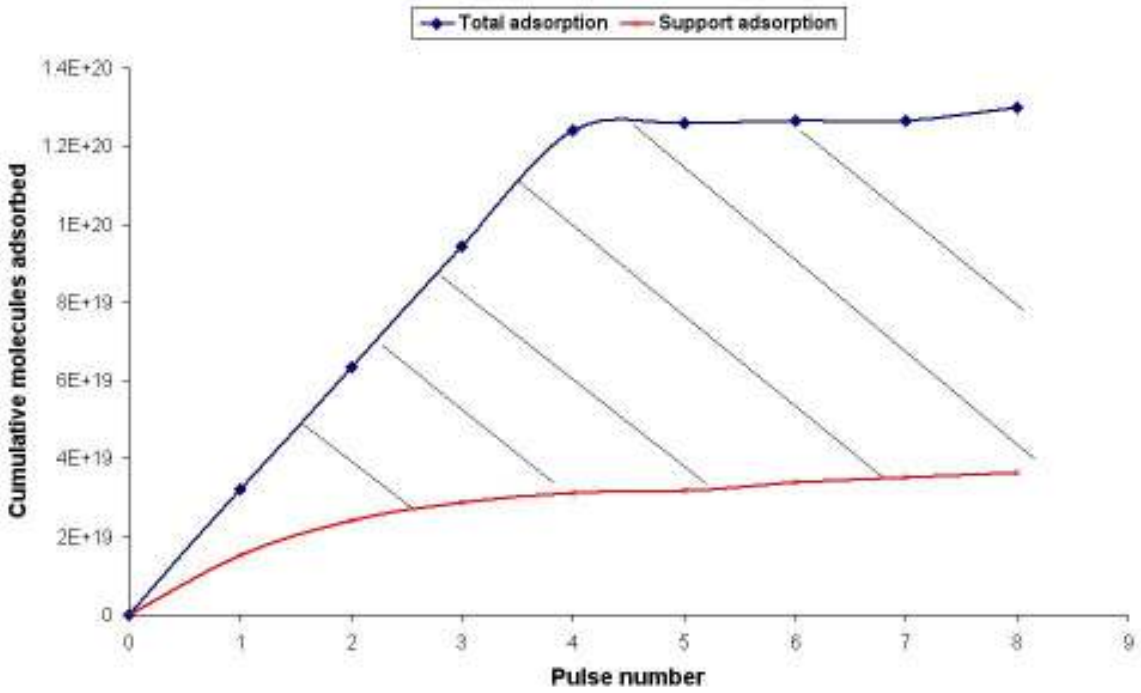

Figure 23 Adsorption isotherms for H_2S over Rh/Al_2O_3 (acetate)

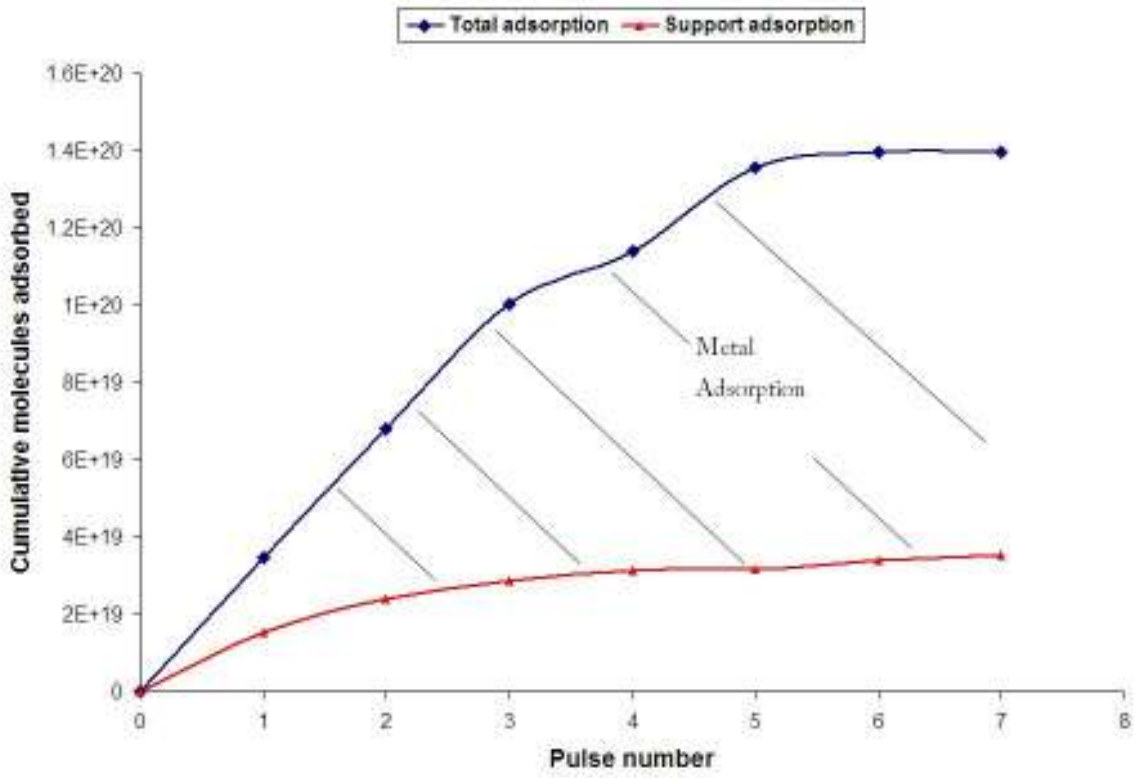

Figure 24 Adsorption isotherms for H_2S over Rh/Al_2O_3 (nitrate)

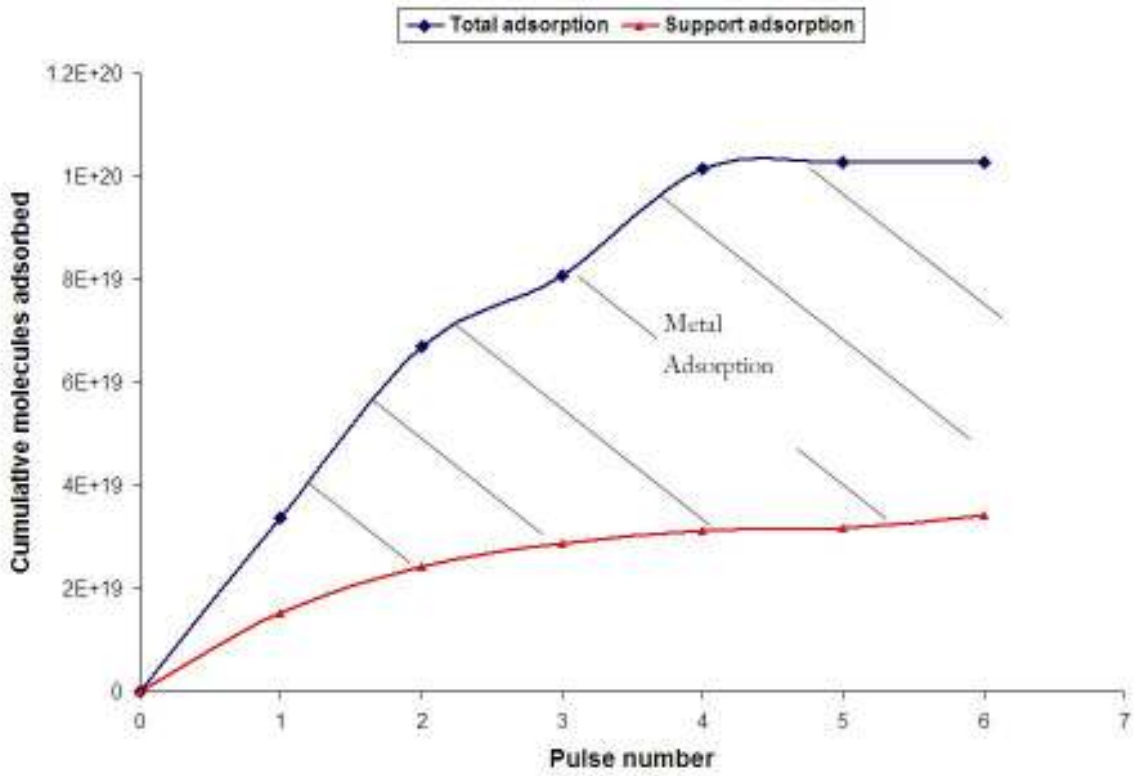

Figure 25 Adsorption isotherms for H_2S over Pt/Al_2O_3

During the first three pulses H_2S appeared to be adsorb on both the metal and the support. After pulse three, the adsorption onto the support began to cease, suggesting H_2S from subsequent pulses was being adsorbed entirely by the metal.

3.2.2.7. S:M ratios

The table below compares the S:M ratios obtained from the H_2S pulses for the three Al_2O_3 supported catalysts. To obtain the ratios the support adsorption was subtracted.

Table 36 S:M ratios for Al_2O_3 supported catalysts

Catalyst	Rh/Al_2O_3 acetate	Rh/Al_2O_3 nitrate	Pt/Al_2O_3
S:M	1.1 +/- 0.01	0.9 +/- 0.06	1.2

3.2.2.8. Hydrogen Evolution: Al_2O_3 supported catalysts

As described in section 3.2.1.2.4 the hydrogen produced during adsorption can be quantified and used to determine the dissociation of H_2S. Since no hydrogen was evolved during the pulses over Al_2O_3 support, no subtraction is needed. The data obtained is presented in table 37.

Table 37 Hydrogen evolution for Al_2O_3 supported catalysts

Catalyst	Total molecules of H_2 evolved / $x10^{19}$	H_2 evolved : S adsorbed
Rh/Al_2O_3 acetate	3.15	0.5
Rh/Al_2O_3 nitrate	7.10	1.0
Pt/Al_2O_3	0.89	0.2

There was a large degree in variation for the Al_2O_3 supported catalysts, with respect to H_2S dissociation. The value obtained for Rh/Al_2O_3 nitrate suggests H_2S fully dissociates, whilst over Pt/Al_2O_3 relatively less dissociation occurs.

3.2.3. CH_3SH Adsorption

CH_3SH could not be detected through the Poropak Q column. From the literature CH_3SH can adsorb in these ways:

$$CH_3SH(g) \longrightarrow CH_4(g) + S_{(adsorbed)} \quad (1)$$

$$2CH_3SH(g) \longrightarrow 2CH_3S_{(adsorbed)} + H_2(g) \quad (2)$$

$$2CH_3SH(g) \longrightarrow 2CH_3SH_{(adsorbed)} \quad (3)$$

During the CH_3SH adsorption pulses neither CH_4 nor H_2S were produced, however hydrogen gas was detected, suggesting that CH_3SH adsorbs and dissociates via route 2.

For every one mole of H_2 produced, 2 moles of CH_3S are adsorbed; therefore to calculate the amount of CH_3SH adsorbed the moles of H_2 produced is multiplied by two.

3.2.3.1. CH_3SH Pulses over SiO_2 supported catalysts

CH_3SH pulses were passed over Rh/ SiO_2 (acetate), Rh/ SiO_2 (nitrate) and Pt/SiO_2. The results for the catalysts are given in tables 38 to 40.

Table 38 Data obtained from CH_3SH over Rh/SiO_2 acetate

Pulse	molecules of H_2 evolved / x10^{19}	CH_3SH adsorbed/ x10^{19} molecules	Cumulative CH_3SH adsorbed/ x10^{19} molecules
1	2.86	5.72	5.72
2	0.03	0.06	5.78
3	0.04	0.07	5.85
4	0.03	0.06	5.91
5	0.02	0.05	5.96

Table 39 Data obtained from CH_3SH over Rh/SiO_2 nitrate

Pulse	molecules of H_2 evolved / x10^{19}	CH_3SH adsorbed/ x10^{19} molecules	Cumulative CH_3SH adsorbed/ x10^{19} molecules
1	2.48	4.96	4.96
2	0.06	0.13	5.09
3	0.05	0.10	5.19

Table 40 Data obtained from CH_3SH over Pt/SiO_2

Pulse	molecules of H_2 evolved / x10^{19}	CH_3SH adsorbed/ x10^{19} molecules	Cumulative CH_3SH adsorbed/ x10^{19} molecules
1	1.60	3.21	3.21
2	0.07	0.14	3.34
3	0.06	0.12	3.46
4	0.05	0.10	3.56
5	0.05	0.10	3.66

For the SiO_2 supported catalysts dissociative adsorption only occurs during the first pulse, hereafter adsorption ceases.

3.2.3.2. S:M ratios

The S:M ratios were calculated using the CH_3SH adsorption data, and are presented in the table below.

Table 41 S:M ratios for SiO_2 supported catalysts

Catalyst	Rh/SiO_2 acetate	Rh/SiO_2 nitrate	Pt/SiO_2
S:M	1.0	0.9	1.2

3.2.3.3. CH_3SH Pulses over Al_2O_3 supported catalysts

CH_3SH pulses were passed over Rh/Al_2O_3 (acetate), Rh/Al_2O_3 (nitrate) and Pt/Al_2O_3. The results for the catalysts are given in tables 42 to 44.

Table 42 Data obtained from CH_3SH over Rh/Al_2O_3 acetate

Pulse	molecules of H_2 evolved / $x10^{19}$	CH_3SH adsorbed/ $x10^{19}$ molecules	Cumulative CH_3SH adsorbed/ $x10^{19}$ molecules
1	1.71	3.42	3.42
2	0.36	0.72	4.14
3	0.21	0.43	4.56
4	0.21	0.43	4.99
5	0.17	0.33	5.32
6	0.22	0.43	5.76

Table 43 Data obtained from CH_3SH over Rh/Al_2O_3 nitrate

Pulse	molecules of H_2 evolved / $x10^{19}$	CH_3SH adsorbed/ $x10^{19}$ molecules	Cumulative CH_3SH adsorbed/ $x10^{19}$ molecules
1	2.30	4.60	4.60
2	0.44	0.88	5.48
3	0.19	0.39	5.87
4	0.04	0.07	5.95

Table 44 Data obtained from CH_3SH over Pt/Al_2O_3

Pulse	molecules of H_2 evolved / $x10^{19}$	CH_3SH adsorbed/ $x10^{19}$ molecules	Cumulative CH_3SH adsorbed/ $x10^{19}$ molecules
1	1.01	2.02	2.02
2	0.03	0.07	2.10

Dissociative adsorption of CH_3SH continues after the first pulse over the Rh/Al_2O_3 catalysts. Whilst, over Pt/Al_2O_3 dissociative adsorption only occurs during the first pulse, similar to the SiO_2 supported catalysts.

3.2.3.4. S:M ratios

The S:M ratios for the Al_2O_3 supported catalysts are presented in table 45.

Table 45 CH_3SH dispersions for Al_2O_3 supported catalysts

Catalyst	Rh/Al_2O_3 acetate	Rh/Al_2O_3 nitrate	Pt/Al_2O_3
S:M	0.9 +/- 0.05	0.9	0.7

3.2.4. Adsorptions under Steam Reforming Conditions

H_2S was combined with H_2 and pulsed over the catalysts at room temperature. This was to determine the effect of H_2 on adsorption, since during steam reforming H_2 is present in large quantities.

Another important consideration was temperature. Steam reforming is typically carried out at 600°C, so pulses of H_2S over the catalyst at 600°C were carried out. Finally, these conditions were combined and pulses of H_2:H_2S in a 1:1 over the catalysts at 600°C were conducted.

3.2.4.1. H_2:H_2S Pulses

3.2.4.1.1. H_2:H_2S Pulses over SiO_2 supported catalysts

Pulses of a 1:1 mixture of H_2 and H_2S were passed over Rh/Al_2O_3 (acetate), Rh/Al_2O_3 (nitrate) and Pt/Al_2O_3 at room temperature, using the same procedure detailed in the single gas adsorptions. The results are given in tables 46 to 48.

Table 46 Data obtained from H_2:H_2S pulses over Rh/SiO_2 acetate

Pulse	H_2S in/ $x10^{19}$ molecules	H_2S out/ $x10^{19}$ molecules	H_2S adsorbed/ $x10^{19}$ molecules/g of catalyst	Cumulative H_2S adsorbed/ $x10^{19}$ molecules
1	1.68	0	3.36	3.36
2	1.68	0.99	1.36	4.72
3	1.67	1.58	0.17	4.89
4	1.67	1.56	0.22	5.11
5	1.67	1.61	0.10	5.21
6	1.66	1.64	0.03	5.25

Table 47 Data obtained from H_2:H_2S pulses over Rh/SiO_2 nitrate

Pulse	H_2S in/ $x10^{19}$ molecules	H_2S out/ $x10^{19}$ molecules	H_2S adsorbed/ $x10^{19}$ molecules/g of catalyst	Cumulative H_2S adsorbed/ $x10^{19}$ molecules
1	1.69	0.43	2.51	2.51
2	1.68	1.55	0.27	2.78
3	1.68	1.51	0.35	3.13
4	1.67	1.67	0	3.13

Table 48 Data obtained from H_2:H_2S pulses over Pt/SiO_2

Pulse	H_2S in/ $x10^{19}$ molecules	H_2S out/ $x10^{19}$ molecules	H_2S adsorbed/ $x10^{19}$ molecules/g of catalyst	Cumulative H_2S adsorbed/ $x10^{19}$ molecules
1	1.67	0.79	1.74	1.74
2	1.66	1.66	0	1.74

The Rh/SiO_2 catalysts adsorbed similar quantities of H_2S in the presence of H_2 compared to H_2S in the absence of H_2. It did, however take slightly longer for the catalysts to reach saturation e.g. when H_2S was pulsed over Rh/SiO_2 acetate

it was saturated at pulse 4; whilst when H_2:H_2S was pulsed the catalyst was not saturated until pulse 6.

Pt/SiO_2 catalyst only adsorbs a fraction of the first pulse and the overall adsorption of H_2S is considerably lower in the presence of H_2.

3.2.4.1.2. S:M ratios

Table 49 S:M ratios for SiO_2 supported catalysts in a H_2 atmosphere

Catalyst	Rh/SiO_2 acetate	Rh/SiO_2 nitrate	Pt/SiO_2
S:M	0.9	0.5	0.6

3.2.4.1.3. Hydrogen Evolution

As described in section 3.2.1.2.4, H_2 is evolved on adsorption of H_2S. This was quantified and the results are tabulated below.

Table 50 Hydrogen evolution for SiO_2 supported catalysts

Catalyst	Total molecules of H_2 evolved / $x10^{19}$	H_2 evolved : S adsorbed
Rh/SiO_2 acetate	3.16	0.6
Rh/SiO_2 nitrate	1.67	0.5
Pt/SiO_2	2.18	1.2

Both the Rh/SiO_2 catalysts have lower values H_2 evolved : S adsorbed indicating less dissociation of H_2S occurs in the presence of H_2. Whilst the value obtained for Pt/SiO_2 suggests more dissociation occurs when H_2 is present.

3.2.4.1.4. H_2:H_2S Pulses over Al_2O_3 support

Since H_2S adsorbs onto the alumina support and this amount has to be subtracted to determine the actual adsorption onto the metal, it was necessary to establish if the presence of H_2 affected the adsorption on the support. Therefore, pulses of H_2:H_2S were passed over just the alumina support. Figure 26 compares the adsorption isotherms of H_2S over alumina, with and without H_2.

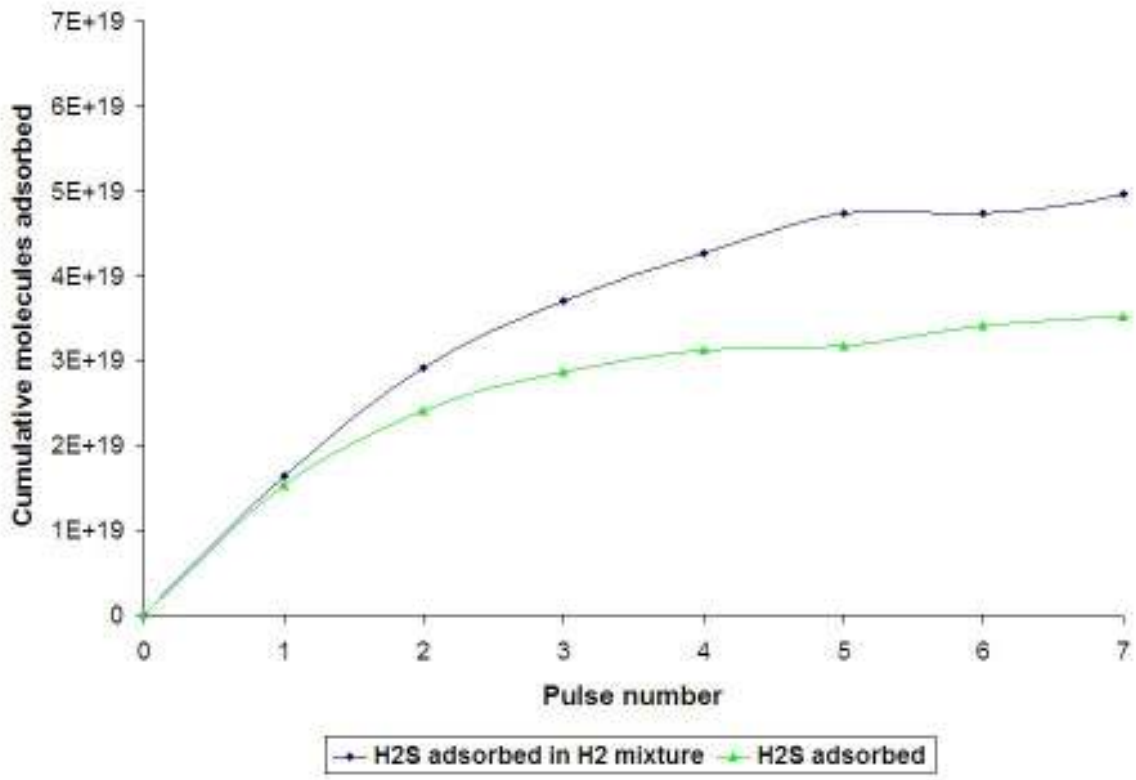

Figure 26 Adsorption isotherms of H_2S over alumina support

In the presence of H_2 more H_2S adsorbed onto the support. This adsorption was subtracted from the H_2:H_2S pulse over the Al_2O_3 supported catalysts to obtain the metal dispersions.

3.2.4.1.5. H_2:H_2S Pulses over Al_2O_3 supported catalysts

Pulses of a 1:1 mixture of H_2 and H_2S were passed over Rh/Al_2O_3 (acetate), Rh/Al_2O_3 (nitrate) and Pt/Al_2O_3 at room temperature. The results are given in figures 27 to 29.

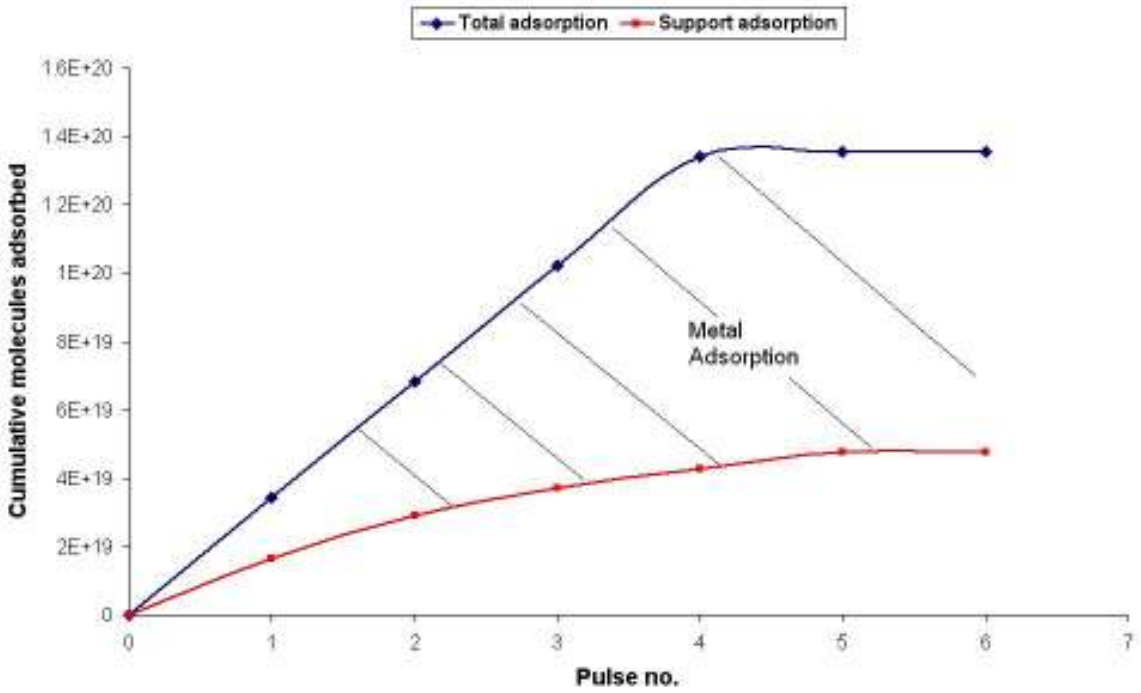

Figure 27 Adsorption isotherms for H_2:H_2S over Rh/Al_2O_3 (acetate)

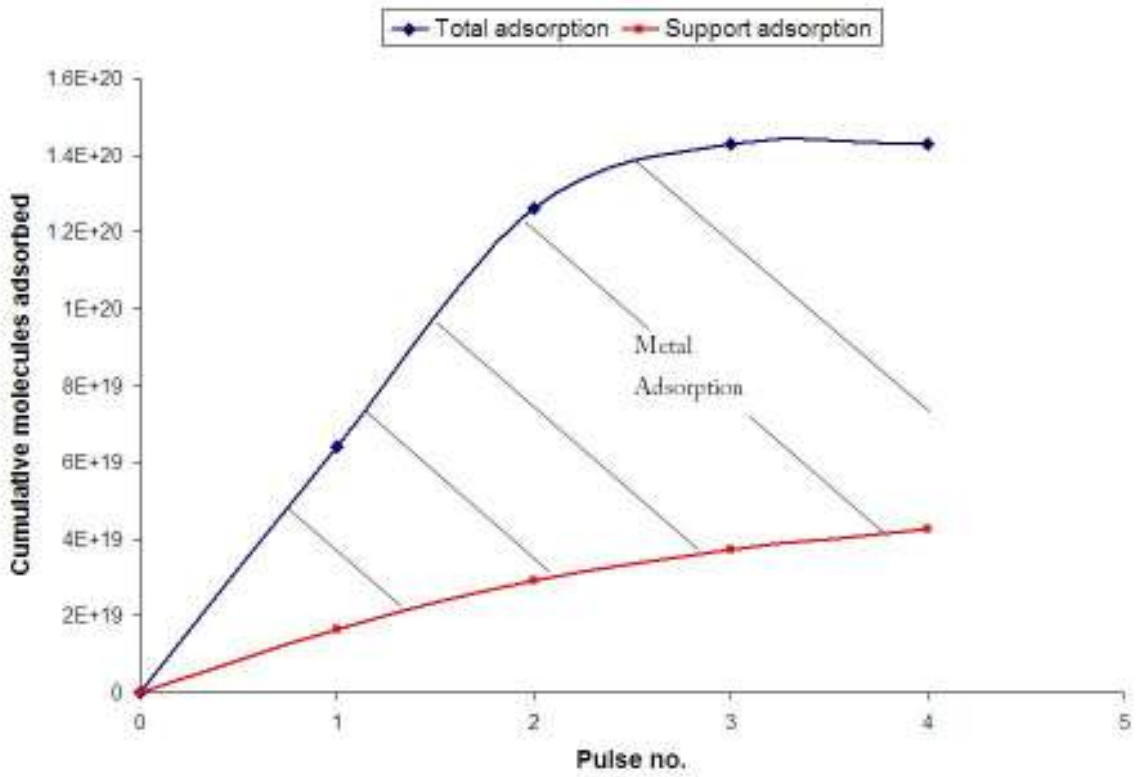

Figure 28 Adsorption isotherms for H_2/H_2S pulses over Rh/Al_2O_3 nitrate

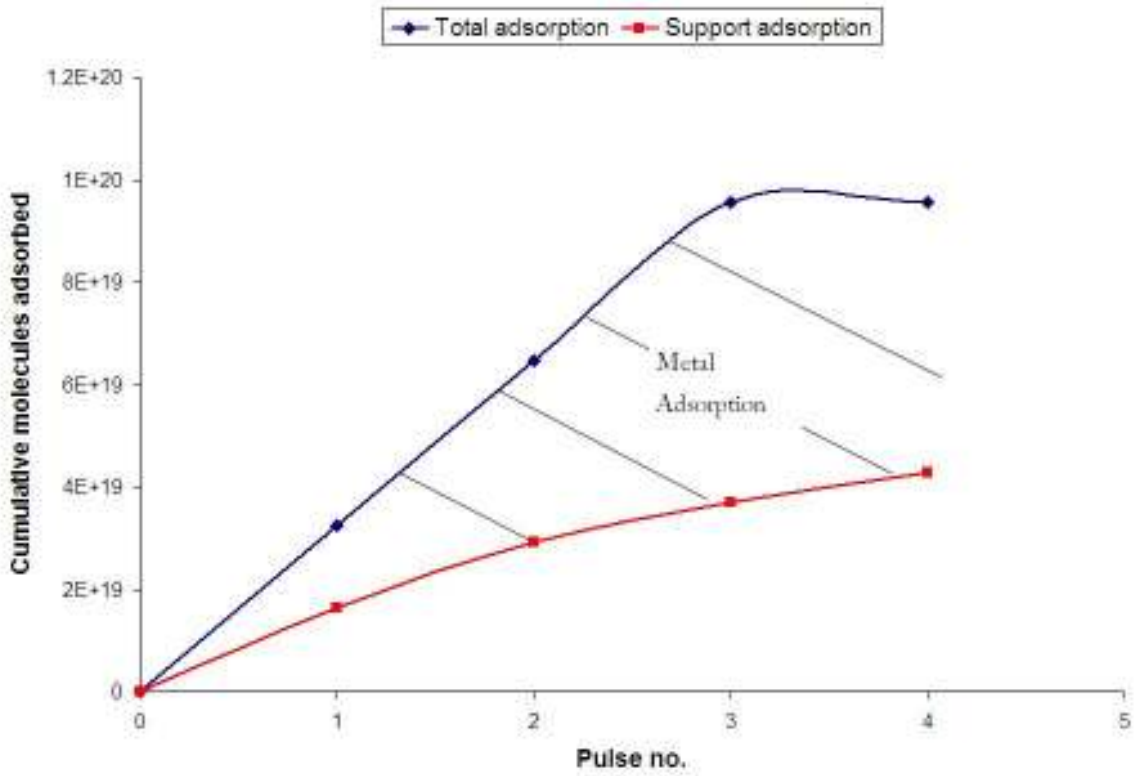

Figure 29 Adsorption isotherms for H_2/H_2S pulses over Pt/Al_2O_3

Rh/Al_2O_3 acetate and Pt/Al_2O_3 both adsorb less H_2S in a H_2 atmosphere, whilst Rh/Al_2O_3 nitrate adsorbs more.

3.2.4.1.6. S:M ratios

Table 51 S:M ratios for Al_2O_3 supported catalysts in a H_2 atmosphere

Catalyst	Rh/Al_2O_3 acetate	Rh/Al_2O_3 nitrate	Pt/Al_2O_3
S:M	0.7	1.2	0.7

Both Rh/Al_2O_3 actetate and Pt/Al_2O_3 have lower S:M ratios in the presence of H_2, whilst Rh/Al_2O_3 nitrate has a higher dispersion.

3.2.4.1.7. Hydrogen Evolution

Table 52 Hydrogen evolution for Al_2O_3 supported catalysts in a H_2 atmosphere

Catalyst	Total molecules of H_2 evolved / $x10^{19}$	H_2 evolved : S adsorbed
Rh/Al_2O_3 acetate	2.81	0.7
Rh/Al_2O_3 nitrate	2.37	0.5
Pt/Al_2O_3	0.72	0.3

The dissociation of H_2S has been significantly lowered, by 50%, in the presence of hydrogen over Rh/Al_2O_3 (nitrate). Over Rh/Al_2O_3 (acetate) and Pt/Al_2O_3, H_2S appears to dissociate slightly more in the presence of hydrogen.

3.2.4.2. High Temperature H_2S Pulses

H_2S was pulsed over the catalysts at 600°C. Following reduction of the catalysts the furnace was programmed to 600°C, when this temperature was reached pulses of H_2S were passed over the catalysts.

3.2.4.2.1. High Temperature H_2S Pulses over SiO_2 supported catalysts

The results for the adsorption of H_2S at 600°C over the SiO_2 supported catalysts are provided in tables 53 to 55.

Table 53 Data obtained from high temp H_2S pulses over Rh/SiO_2 acetate

Pulse	H_2S in/ $x10^{19}$ molecules	H_2S out/ $x10^{19}$ molecules	H_2S adsorbed/ $x10^{19}$ molecules/g of catalyst	Cumulative H_2S adsorbed/ $x10^{19}$ molecules
1	1.78	0	3.54	3.54
2	1.72	0.29	2.82	6.36
3	1.66	1.16	0.99	7.36
4	1.60	1.60	0	7.36

Table 54 Data obtained from high temp. H_2S pulses over Rh/SiO_2 nitrate

Pulse	H_2S in/ $x10^{19}$ molecules	H_2S out/ $x10^{19}$ molecules	H_2S adsorbed/ $x10^{19}$ molecules/g of catalyst	Cumulative H_2S adsorbed/ $x10^{19}$ molecules
1	1.63	0	3.25	3.25
2	1.58	0	3.15	6.40
3	1.52	1.12	0.81	7.21
4	1.47	0.99	0.96	8.17
5	1.42	1.01	0.83	8.99
6	1.37	1.04	0.67	9.66
7	1.33	1.18	0.29	9.95
8	1.28	1.28	0	9.95

Table 55 Data obtained from high temp H_2S pulses over Pt/SiO_2

Pulse	H_2S in/ $x10^{19}$ molecules	H_2S out/ $x10^{19}$ molecules	H_2S adsorbed/ $x10^{19}$ molecules/g of catalyst	Cumulative H_2S adsorbed/ $x10^{19}$ molecules
1	1.64	0	3.24	3.24
2	1.58	1.14	0.88	4.12
3	1.53	0.89	1.25	5.37
4	1.47	1.47	0	5.37

There is considerably more adsorption of H_2S over all the SiO_2 supported catalysts at 600°C compared with room temperature.

3.2.4.2.2. S:M ratios

Table 56 S:M ratios for SiO_2 supported catalysts at 600°C

Catalyst	Rh/SiO_2 acetate	Rh/SiO_2 nitrate	Pt/SiO_2
S:M	1.3	1.7 +/- 0.13	1.7 +/-0.04

3.2.4.2.3. Hydrogen Evolution

Table 57 Hydrogen evolution for SiO_2 supported catalysts at 600°C

Catalyst	Total molecules of H_2 evolved / $x10^{19}$	H_2 evolved : S adsorbed
Rh/SiO_2 acetate	8.39	1.1
Rh/SiO_2 nitrate	7.39	0.7
Pt/SiO_2	5.42	1.0

The dissociation of H_2S increased over the SiO_2 supported catalysts when H_2S adsorbed at 600°C.

3.2.4.2.4. High Temperature H_2S Pulses over Al_2O_3 support

To determine if the adsorption of H_2S on the alumina support changed at high temperatures, pulses were carried out at 600°C. The graph below is an adsorption isotherm comparing the adsorption at 600 °C to the room temperature adsorption.

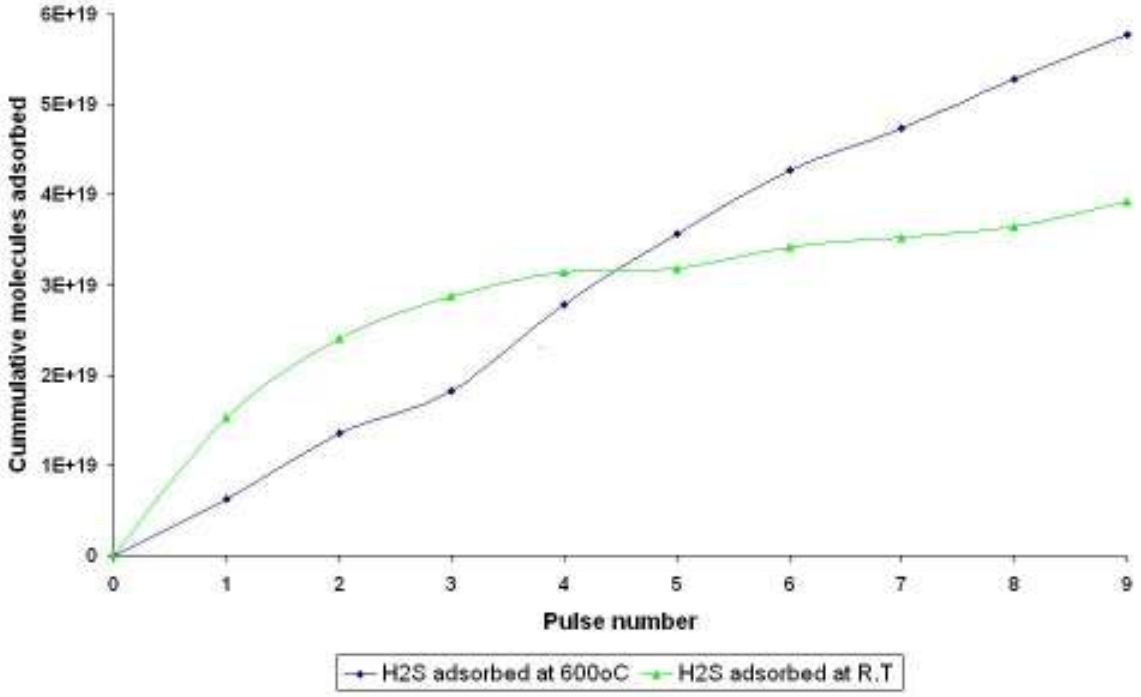

Figure 30 Adsorption isotherms of H_2S over alumina support

From the isotherm, it appears the Al_2O_3 support continually adsorbed H_2S at high temperature, which differs from room temperature where adsorption began to level off at pulse 4.

3.2.4.2.5. High Temperature H_2S Pulses over Al_2O_3 supported catalysts

The results for the adsorption of H_2S at 600°C over the Al_2O_3 supported catalysts are provided in figures 31 to 33.

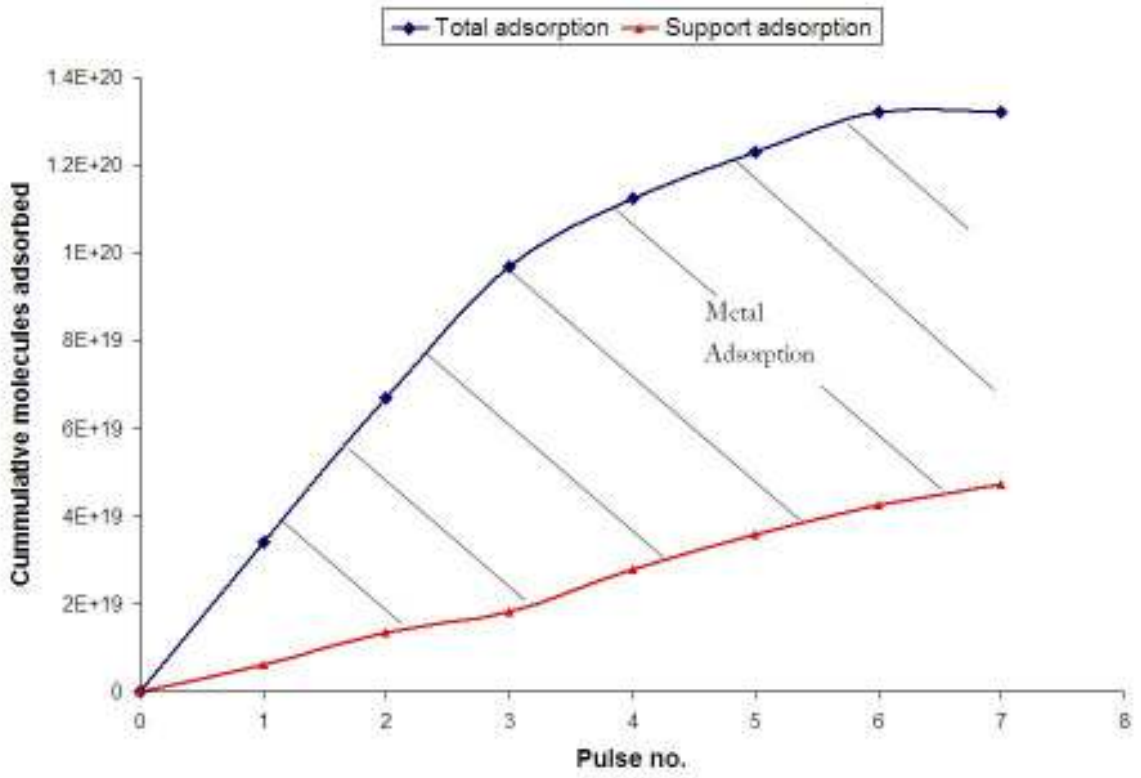

Figure 31 Adsorption isotherms for H_2S pulses over Rh/Al_2O_3 acetate at 600°C

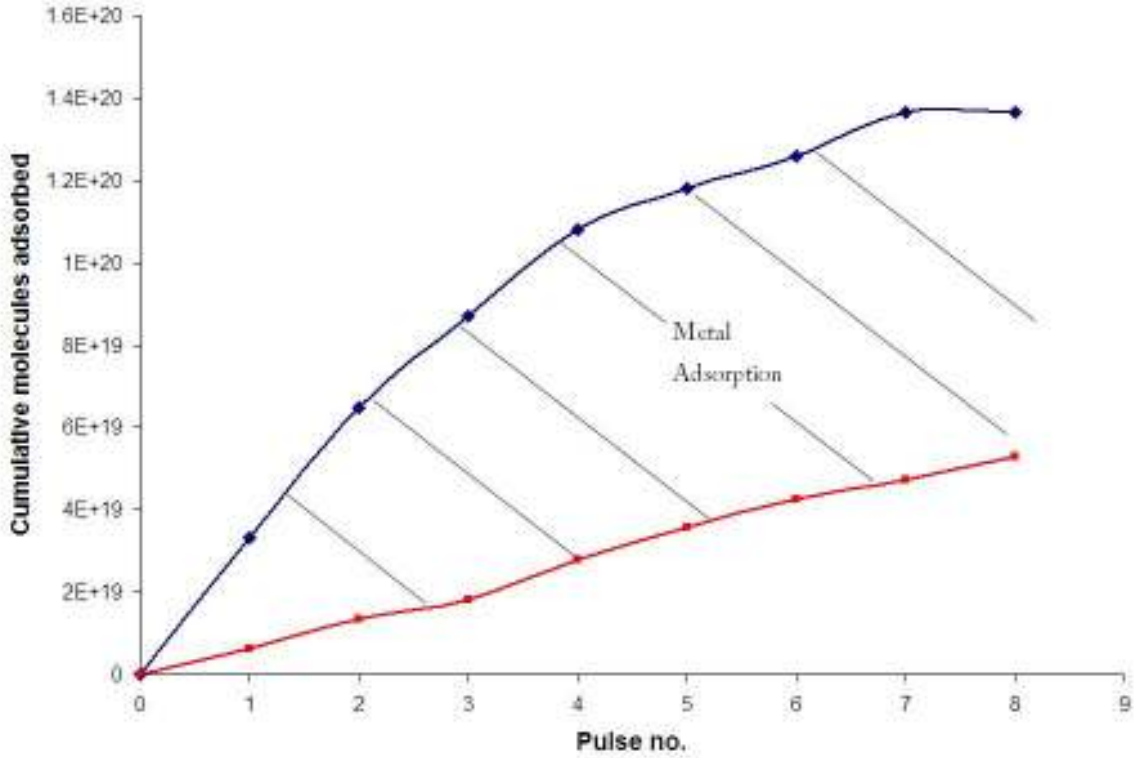

Figure 32 Adsorption isotherms for H_2S pulses over Rh/Al_2O_3 nitrate at 600°C

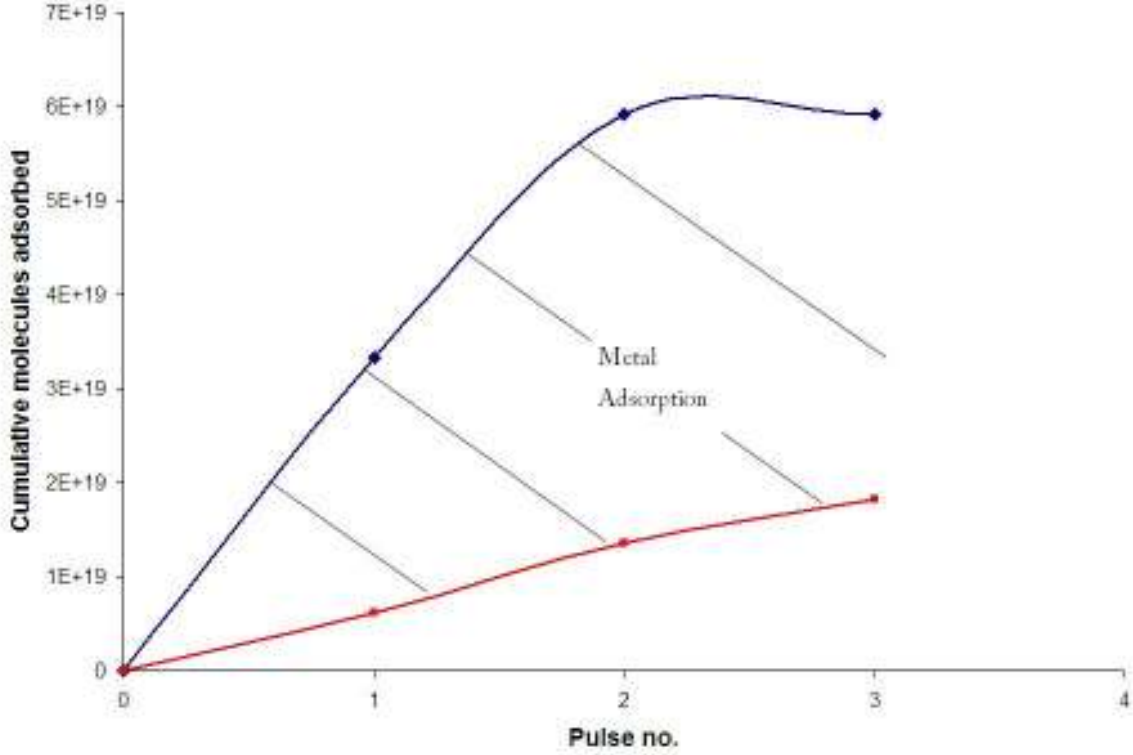

Figure 33 Adsorption isotherms for H_2S pulses over Pt/Al_2O_3 at 600°C

3.2.4.2.6. S:M ratios

Table 58 S:M ratios for Al_2O_3 supported catalyst at 600°C

Catalyst	Rh/Al_2O_3 acetate	Rh/Al_2O_3 nitrate	Pt/Al_2O_3
S:M	1.0	0.9	1.1

The S:M ratios obtained at high temperature are very similar to those obtained from the room temperature H_2S pulses.

3.2.4.2.7. Hydrogen Evolution

Table 59 Hydrogen evolution for Al_2O_3 supported catalysts at 600°C

Catalyst	Total molecules of H_2 evolved / $x10^{19}$	H_2 evolved : S adsorbed
Rh/Al_2O_3 acetate	6.49	1.1
Rh/Al_2O_3 nitrate	8.91	1.7
Pt/Al_2O_3	2.73	0.8

Hydrogen evolution increased significantly at 600°C, indicating more dissociative adsorption occurred.

3.2.4.3. High Temperature H_2:H_2S Pulses

The above two conditions were combined and a 1:1 mixture of H_2:H_2S was pulsed over the catalysts at 600°C.

3.2.4.3.1. High Temperature H_2:H_2S pulse over SiO_2 supported catalysts

Table 60 Data obtained from H_2:H_2S pulses over Rh/SiO_2 acetate at 600°C

Pulse	H_2S in/ $x10^{19}$ molecules	H_2S out/ $x10^{19}$ molecules	H_2S adsorbed/ $x10^{19}$ molecules/g of catalyst	Cumulative H_2S adsorbed/ $x10^{19}$ molecules
1	1.81	0	3.63	3.63
2	1.75	0.66	2.17	5.81
3	1.69	1.52	3.58	6.16
4	1.63	1.63	0	6.16

Table 61 Data obtained from H_2:H_2S pulses over Rh/SiO_2 nitrate at 600°C

Pulse	H_2S in/ $x10^{19}$ molecules	H_2S out/ $x10^{19}$ molecules	H_2S adsorbed/ $x10^{19}$ molecules/g of catalyst	Cumulative H_2S adsorbed/ $x10^{19}$ molecules
1	1.73	0	3.45	3.45
2	1.72	0.78	1.87	5.32
3	1.71	1.42	0.59	5.91
4	1.71	1.71	0	5.91

Table 62 Data obtained from H_2:H_2S pulses over Pt/SiO_2 at 600°C

Pulse	H_2S in/ $x10^{19}$ molecules	H_2S out/ $x10^{19}$ molecules	H_2S adsorbed/ $x10^{19}$ molecules/g of catalyst	Cumulative H_2S adsorbed/ $x10^{19}$ molecules
1	1.64	0.08	3.11	3.11
2	1.64	1.64	0	3.11

The total number of H_2S molecules adsorbed for the Rh/SiO_2 catalysts lies between the values obtained for the separate conditions, suggesting both these conditions are affecting adsorption.

3.2.4.3.2. S:M ratios

Table 63 S:M ratios for SiO_2 supported catalysts at 600°C in a H_2 atmosphere

Catalyst	Rh/SiO_2 acetate	Rh/SiO_2 nitrate	Pt/SiO_2
S:M	1.1	1.0	1.0

3.2.4.3.3. Hydrogen Evolution

Table 64 Hydrogen evolution for SiO_2 supported catalysts at 600°C in a H_2 atmosphere

Catalyst	Total molecules of H_2 evolved / $x10^{19}$	H_2 evolved : S adsorbed
Rh/SiO_2 acetate	3.61	0.6
Rh/SiO_2 nitrate	6.92	1.2
Pt/SiO_2	0.78	0.25

3.2.4.3.4. High Temperature H_2:H_2S Pulses over Al_2O_3 support

To determine if the adsorption of H_2S on the alumina support changed at high temperatures and in a hydrogen atmosphere, H_2:H_2S pulses were carried out at 600°C. The graph below is an adsorption isotherm comparing the adsorption at 600°C in hydrogen to the room temperature adsorption.

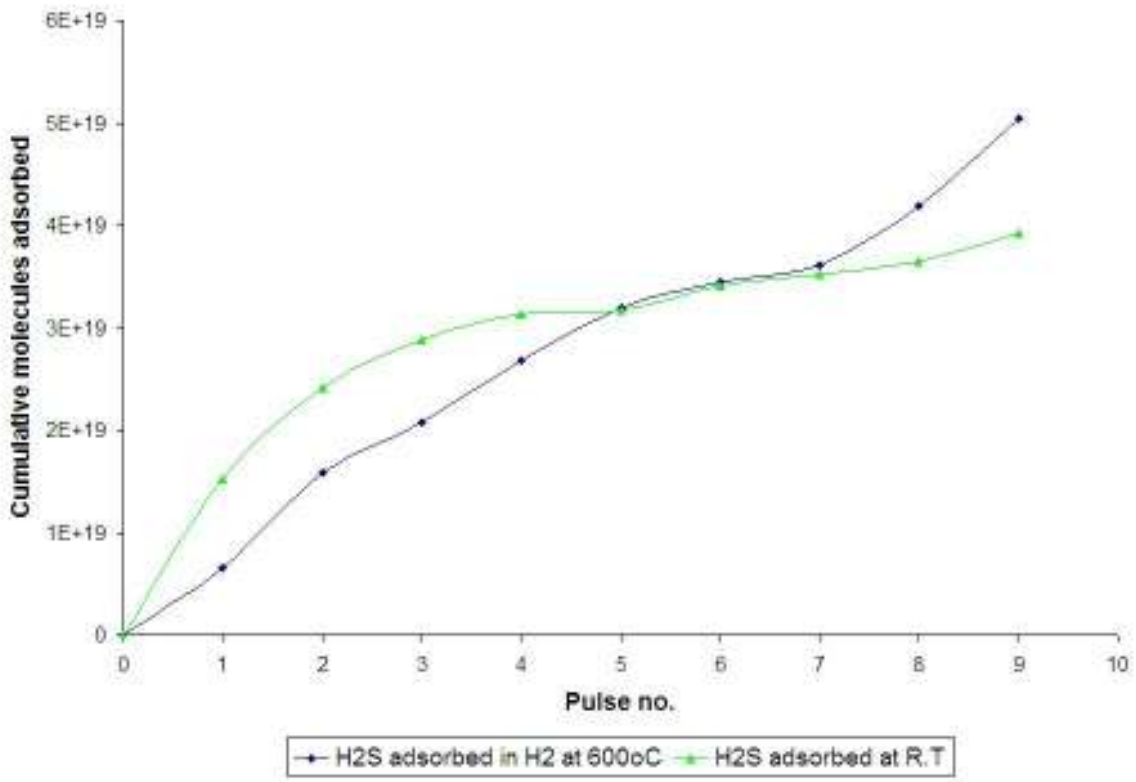

Figure 34 Adsorption isotherms of H_2S pulses over alumina support

Initially it appears the combined effect of H_2 and high temperature slows the rate of adsorption onto the support, however by pulse 7 H_2S adsorption increases again.

3.2.4.3.5. High Temperature H_2:H_2S pulse over Al_2O_3 supported catalysts

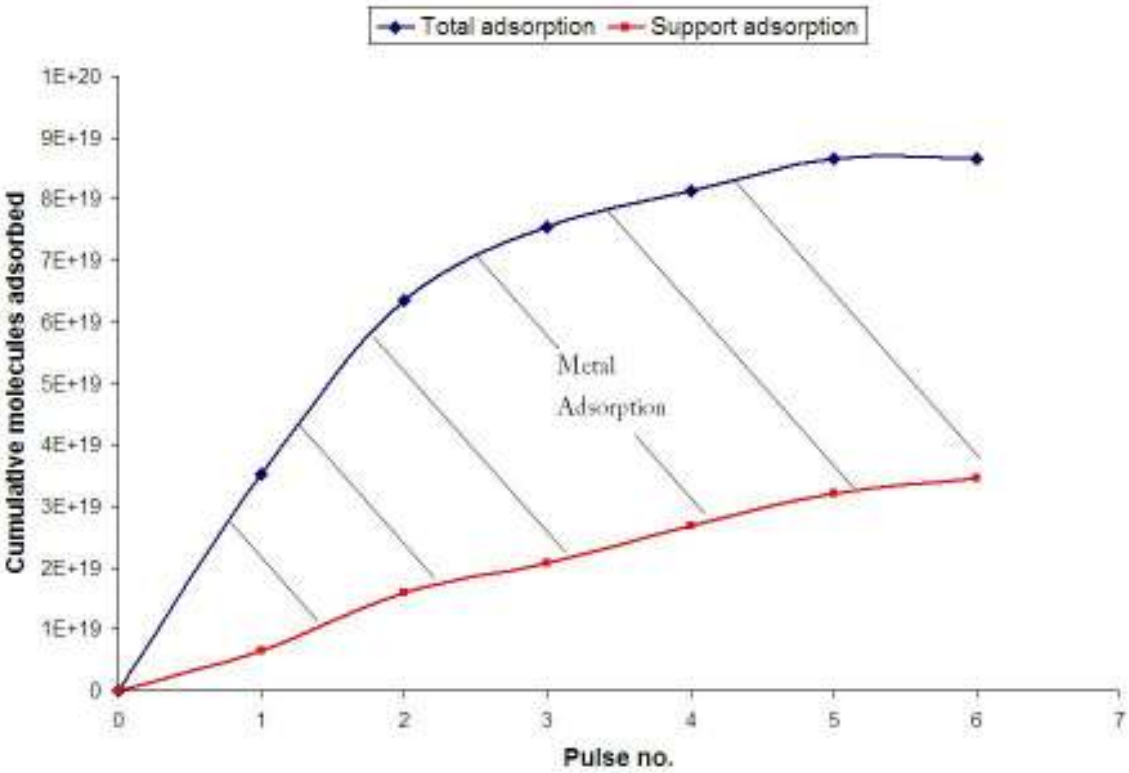

Figure 35 Adsorption isotherms for H_2/H_2S pulses over Rh/Al_2O_3 acetate at 600°C

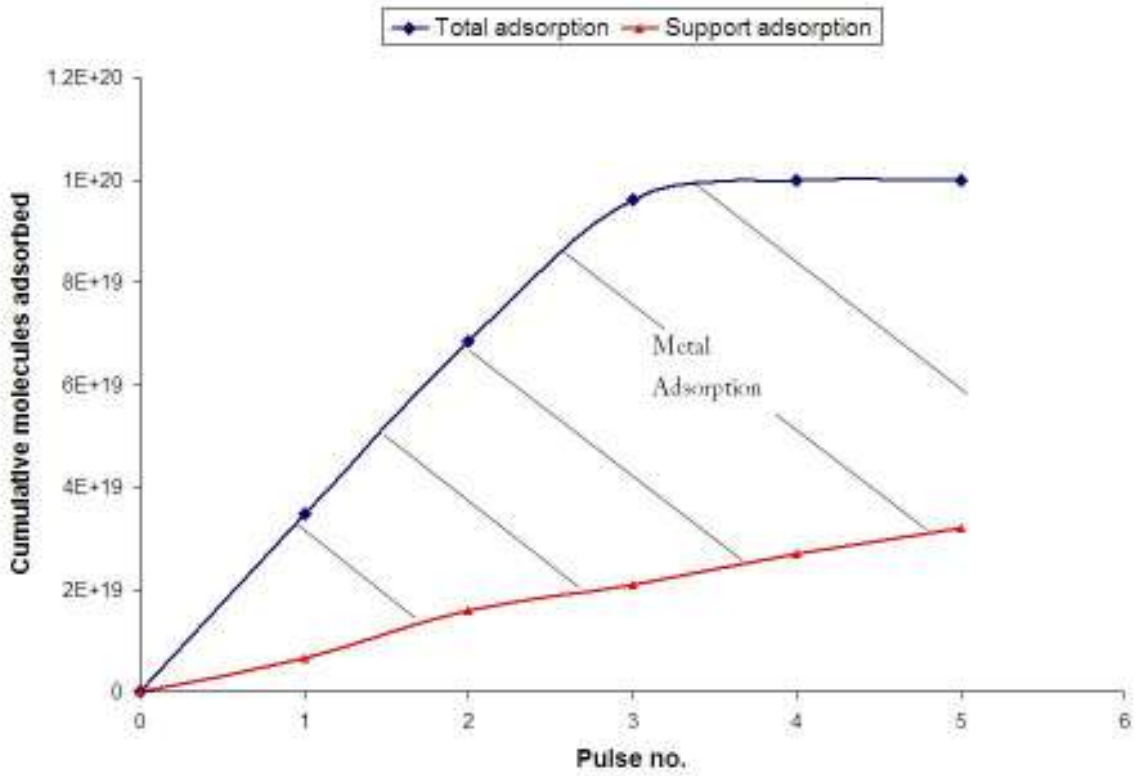

Figure 36 Adsorption isotherms for H_2/H_2S pulses over Rh/Al_2O_3 nitrate at 600°C

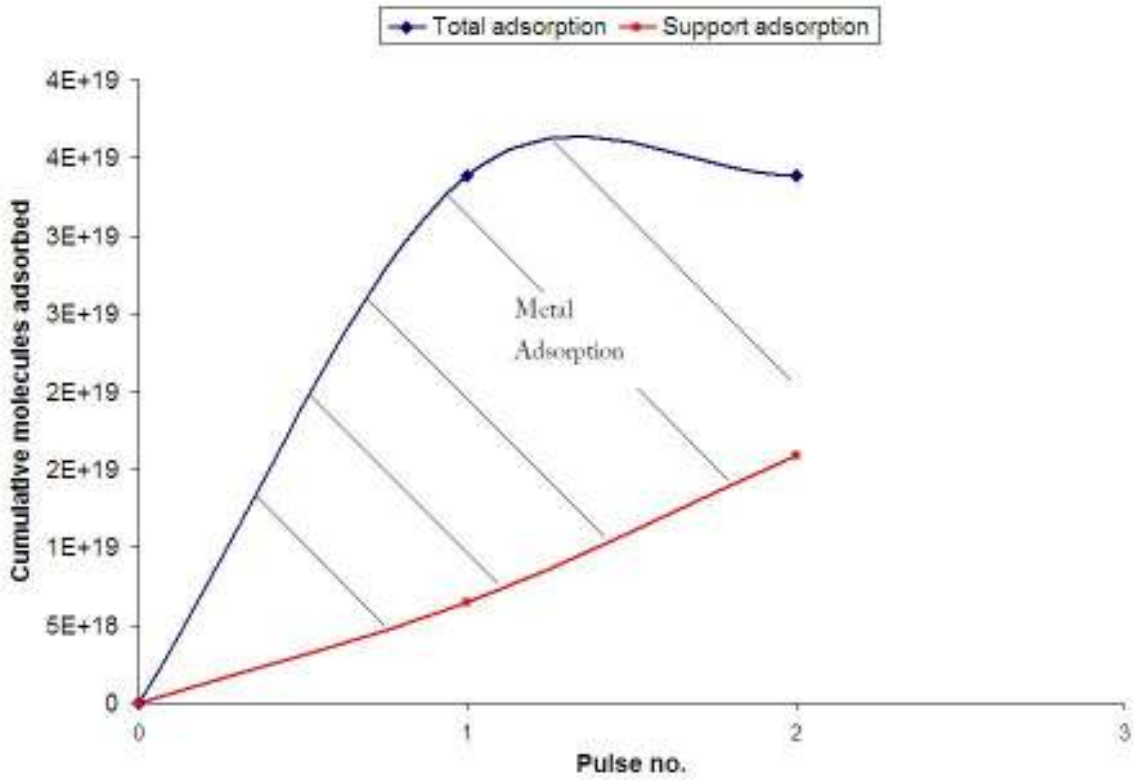

Figure 37 Adsorption isotherms for H_2/H_2S pulses over Pt/Al_2O_3 at 600°C

3.2.4.3.6. S:M ratios

Table 65 S:M ratios for Al_2O_3 supported catalysts at 600°C in a H_2 atmosphere

Catalyst	Rh/Al_2O_3 acetate	Rh/Al_2O_3 nitrate	Pt/Al_2O_3
S:M	0.5	0.8	0.7

3.2.4.3.7. Hydrogen Evolution

Table 66 Hydrogen evolution for Al_2O_3 supported catalysts at 600°C in a H_2 atmosphere

Catalyst	Total molecules of H_2 evolved / $x10^{19}$	H_2 evolved : S adsorbed
Rh/Al_2O_3 acetate	3.22	0.95
Rh/Al_2O_3 nitrate	3.67	0.7
Pt/Al_2O_3	1.50	0.7

3.2.5. Competitive Adsorption

Competitive adsorption over was probed by carrying out sequential adsorptions and co-adsorptions. The sequential adsorptions first involved the saturation of the catalysts with CO, followed by pulses of H_2S, to determine if sulphur could adsorb onto a saturated catalyst. Then to examine how sulphur affects the adsorption of molecules, the catalysts were saturated with H_2S followed by pulses of CO.

Also, CO and H_2S were co-adsorbed over the catalysts in a 1:1 mixture.

3.2.5.1. Sequential Adsorption: CO adsorption followed by H_2S

3.2.5.1.1. H_2S pulses over CO saturated Rh catalysts

The Rh catalysts were saturated with CO before pulsing over H_2S. The total amount of H_2S that was able to adsorb onto the saturated catalyst and the amount of hydrogen evolved is given in table 67.

Table 67 H_2S adsorbed and H_2 evolution over CO saturated Rh catalysts

Catalyst	Total molecules of H_2S adsorbed/ $x10^{19}$ molecules/g of catalyst	Total molecules of H_2 evolved / $x10^{19}$	H_2 evolved : S adsorbed
Rh/SiO_2 acetate	0.42	0.43	1.0
Rh/SiO_2 nitrate	0.54	0.32	0.6
Rh/Al_2O_3 acetate	0.55	0.26	0.5
Rh/Al_2O_3 nitrate	1.51	0.41	0.3

The amount of sulphur adsorbing onto the catalysts has been greatly reduced by saturation with CO. A very small amount of H_2S to is able to adsorb onto the catalysts and dissociate.

3.2.5.2. Sequential Adsorption: H_2S adsorption followed by CO

3.2.5.2.1. CO pulses over H_2S saturated Rh catalysts

The catalysts were saturated with H_2S and purged with Ar prior to the pulses of CO. The values obtained for the amount of CO adsorbed are giving below, along with amount of CO adsorbed on fresh catalysts for comparison.

Table 68 CO adsorption on sulphided Rh catalysts

Catalyst	Total molecules of CO adsorbed/ $x10^{19}$ molecules/g of catalyst	Total molecules of CO adsorbed on Sulphided catalyst / $x10^{19}$ molecules	% Adsorbed
Rh/SiO_2 acetate	5.09	0.19	4
Rh/SiO_2 nitrate	2.87	0.42	15
Rh/Al_2O_3 acetate	8.55	0.34	4
Rh/Al_2O_3 nitrate	8.12	0.57	7

It is apparent that very little adsorption of CO can occur on sulphided Rh catalysts.

3.2.5.3. Co-adsorption (1:1) H_2S and CO

3.2.5.3.1. H_2S:CO pulses over SiO_2 supported catalysts: CO adsorption

The affect of co-adsorbing H_2S with CO can be examined by comparing the single gas CO adsorption to the co-adsorbed CO. Figure 38 compares these two adsorptions over Rh/SiO_2 acetate.

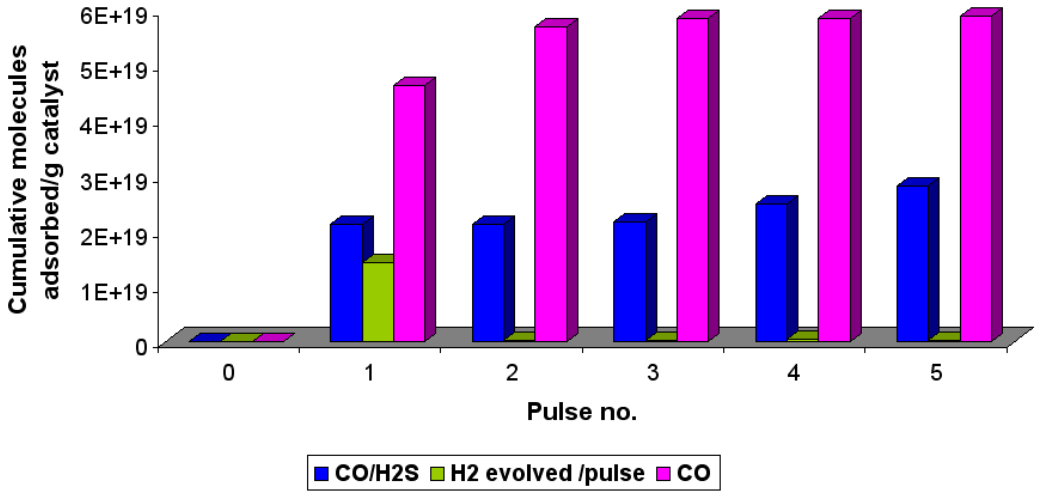

Figure 38 Adsorption of CO with (blue) and without (pink) H_2S over Rh/SiO_2 nitrate

When H_2S is co-adsorbed with CO it dramatically reduces the amount of CO adsorbed onto the catalyst. H_2 is also evolved indicating dissociative adsorption of H_2S is still occurring.

The results from the co-adsorption over Rh/SiO_2 nitrate are shown in fig 39.

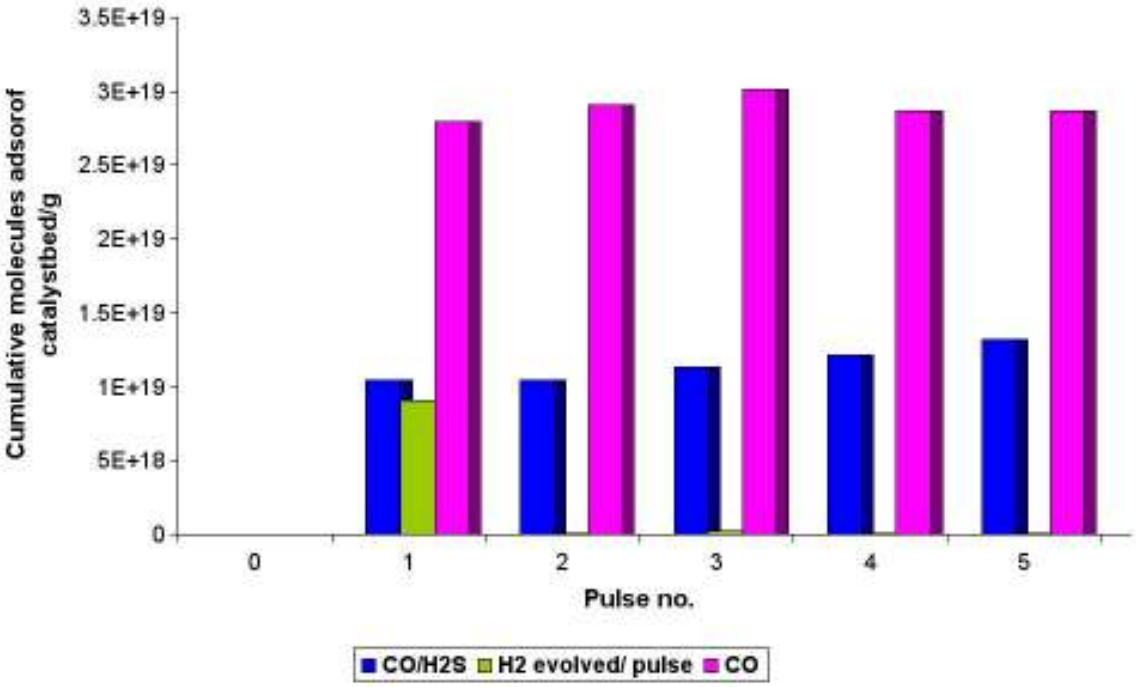

Figure 39 Adsorption of CO with (blue) and without (pink) H_2S over Rh/SiO_2 nitrate

The adsorption of CO has again been significantly reduced by H_2S, and dissociative adsorption of H_2S occurs during the first pulse.

3.2.5.3.2. H_2S:CO pulses over SiO_2 supported catalysts: H_2S adsorption

The dissociative adsorption of H_2S, gauged by the quantity of hydrogen evolved, onto the Rh/SiO_2 catalysts has been significantly reduced by the presence of CO.

Table 69 Hydrogen evolution over SiO_2 supported catalysts

Catalyst	Total molecules of H_2 evolved during single adsorption/ $x10^{19}$	Total molecules of H_2 evolved during co-adsorption / $x10^{19}$
Rh/SiO_2 acetate	4.83	1.52
Rh/SiO_2 nitrate	2.08	0.91

3.2.5.3.3. H_2S:CO pulses over Al_2O_3 supported catalysts: CO adsorption

The H_2S and CO mixture was also pulsed over the alumina supported catalysts. These results obtained for Rh/Al_2O_3 acetate are presented in figure 40, alongside CO single gas adsorption for comparison.

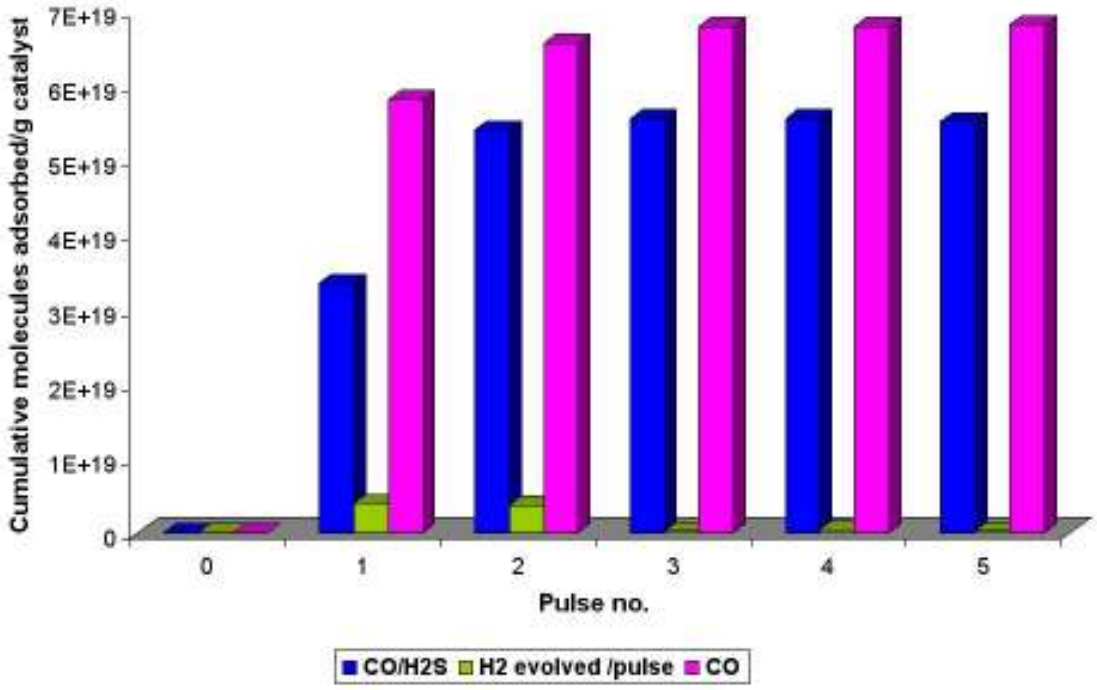

Figure 40 CO adsorption with (blue) and without (pink) H_2S over Rh/Al_2O_3 acetate

The CO adsorption is affected to a much lesser degree by the presence of H_2S over Rh/Al_2O_3 acetate. The evolution of H_2 is more gradual, over 2 pulses, indicating that dissociative adsorption of H_2S has been retarded.

The results from the co-adsorption over Rh/Al_2O_3 nitrate are shown in fig 41.

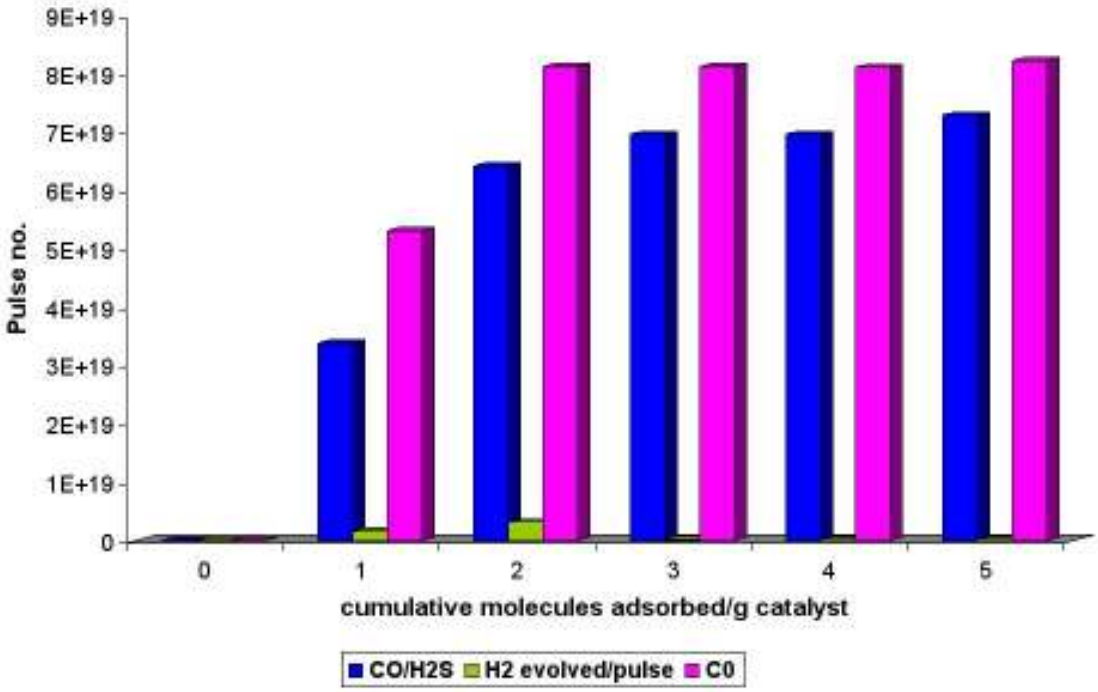

Figure 41 CO adsorption with (blue) and without (pink) H_2S over Rh/Al_2O_3 nitrate

Similarly, over Rh/Al_2O_3 nitrate the adsorption of CO is barely affected by H_2S, and dissociative adsorption of H_2S occurs more gradually.

3.2.5.3.4. H_2S:CO pulses over Al_2O_3 supported catalysts: H_2S adsorption

It is apparent that as well as the dissociative adsorption of H_2S being a more gradual process than seen with SiO_2 supported catalysts, there is also a lot less total dissociative adsorption occurring, table 70.

Table 70 Hydrogen evolution over Al_2O_3 supported catalysts

Catalyst	Total molecules of H_2 evolved during single adsorption/ $x10^{19}$	Total molecules of H_2 evolved during co-adsorption / $x10^{19}$
Rh/Al_2O_3 acetate	3.15	0.87
Rh/Al_2O_3 nitrate	7.10	0.39

3.3. Steam Reforming Experiments

3.3.1. Temperature Effects

Steam reforming experiments were conducted over Rh/Al_2O_3, Pt/Al_2O_3, Rh/ZrO_2 and Pt/ZrO_2 at 20 bar pressure. The temperature was varied to deduce what affect this had on catalyst activity and selectivity.

3.3.1.1. Rh/Al_2O_3

3.3.1.1.1. Conversion

The conversion of ethane was calculated as described in section 2.3.1.4, and plotted against time on stream. The conversion of ethane over Rh/Al_2O_3 at 600°C, 550°C and 500°C are shown in figures 42 to 44. As afore mentioned in the experimental section 2.3.1 a line at 160 minutes on stream has been included in all the conversion graphs to indicate where flow restraints are no longer an issue.

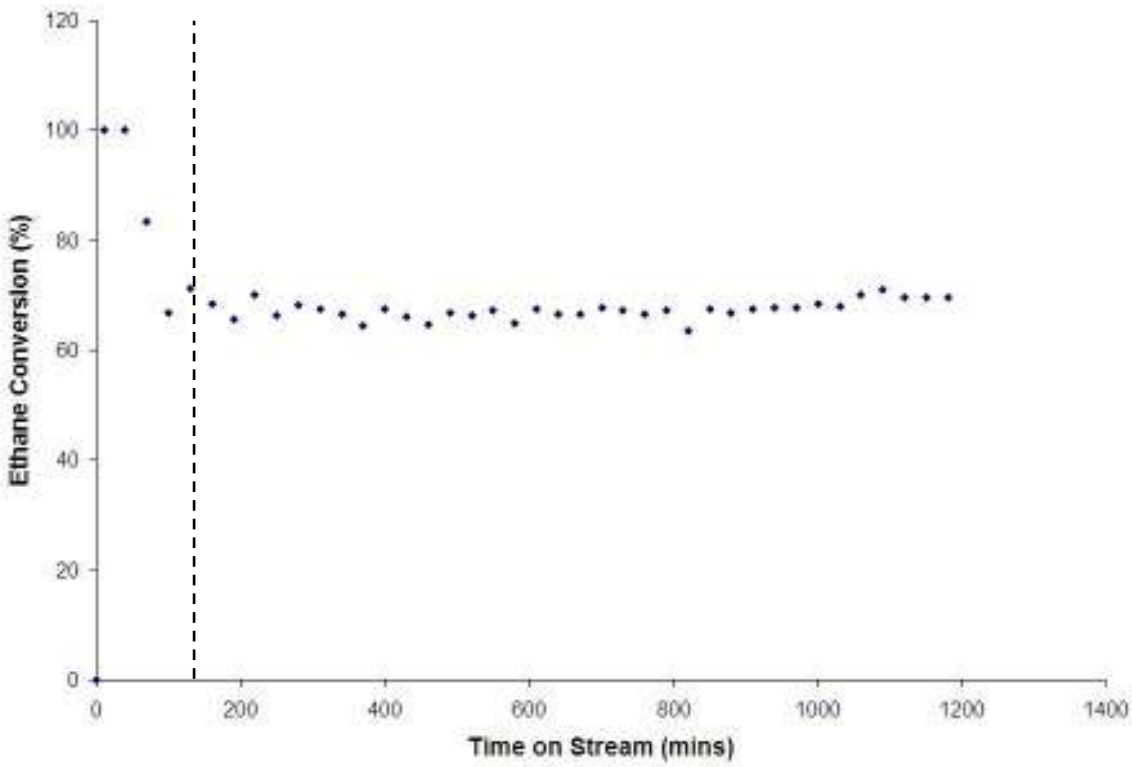

Figure 42 Ethane conversion at 600°C

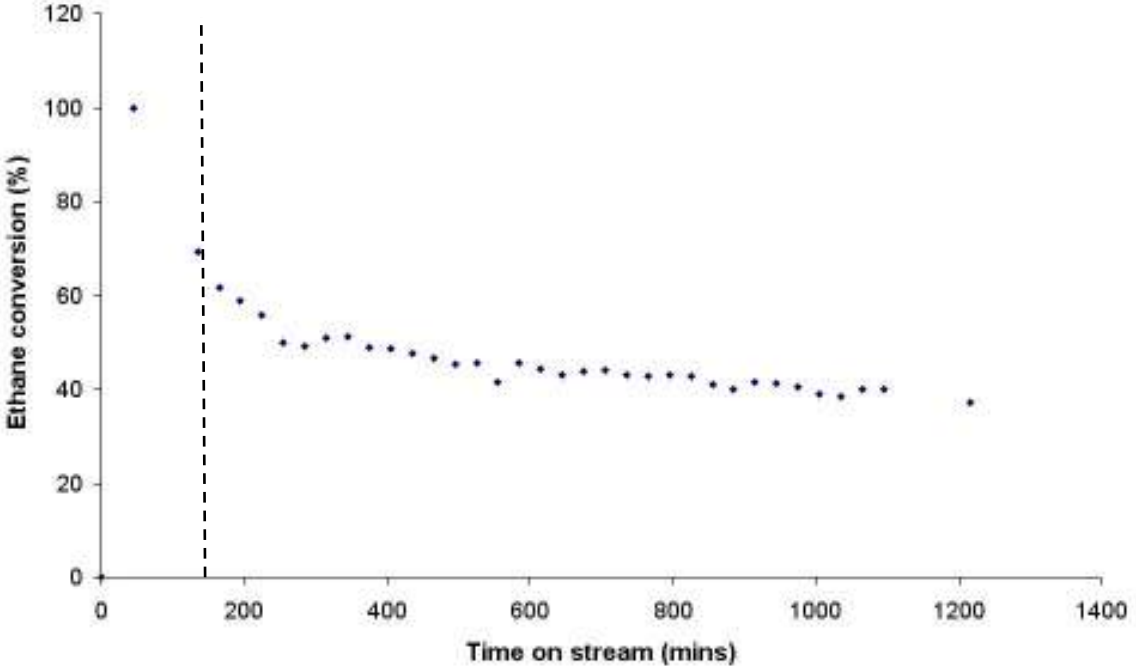

Figure 43 Ethane conversion at 550°C

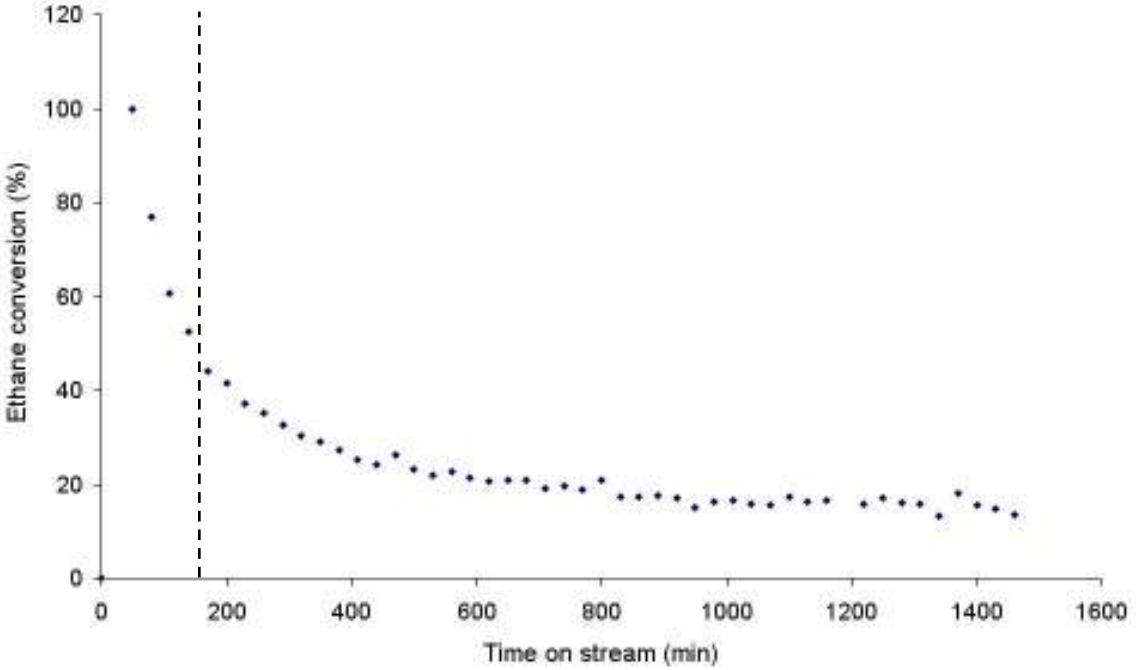

Figure 44 Ethane conversion at 500°C

At 600°C the conversion of ethane is approximately 70% and is stable. As the reaction temperature is lowered to 550°C the conversion is no longer stable; in the first 300 minutes conversion decreases to 50%, hereafter deactivation continues with conversion falling below 40% at 1200 minutes on stream. When

the reaction is conducted at 500°C conversion is reduced further to below 20% and deactivation of the catalyst is more significant.

3.3.1.1.2. Rate of Deactivation

When steam reforming of ethane was conducted at temperatures below 600°C, deactivation of Rh/Al_2O_3 was apparent. Assuming first order deactivation, Ln (ethane conversion) was plotted against time on stream to obtain deactivation rate constants. These graphs are shown in figures 45 and 46. The deactivation rate constant is obtained from the data plotted after 200 minutes on stream to ensure that the establishment of the ethane flow has not influenced the deactivation constant.

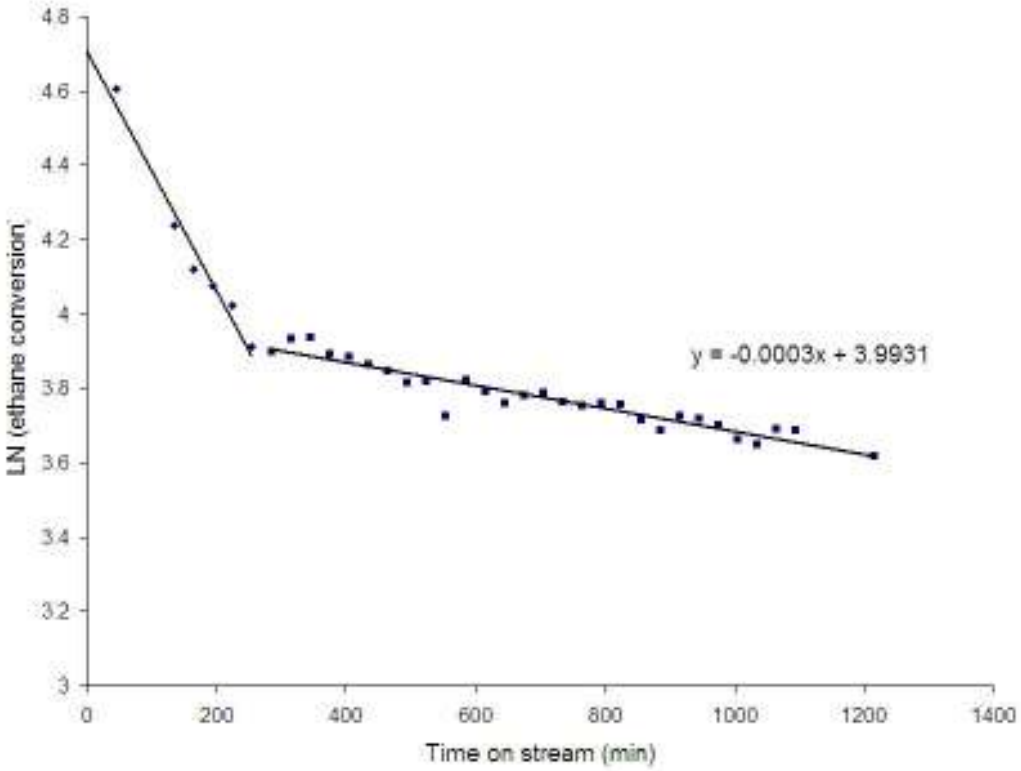

Figure 45 Rh/Al_2O_3 deactivation at 550 °C

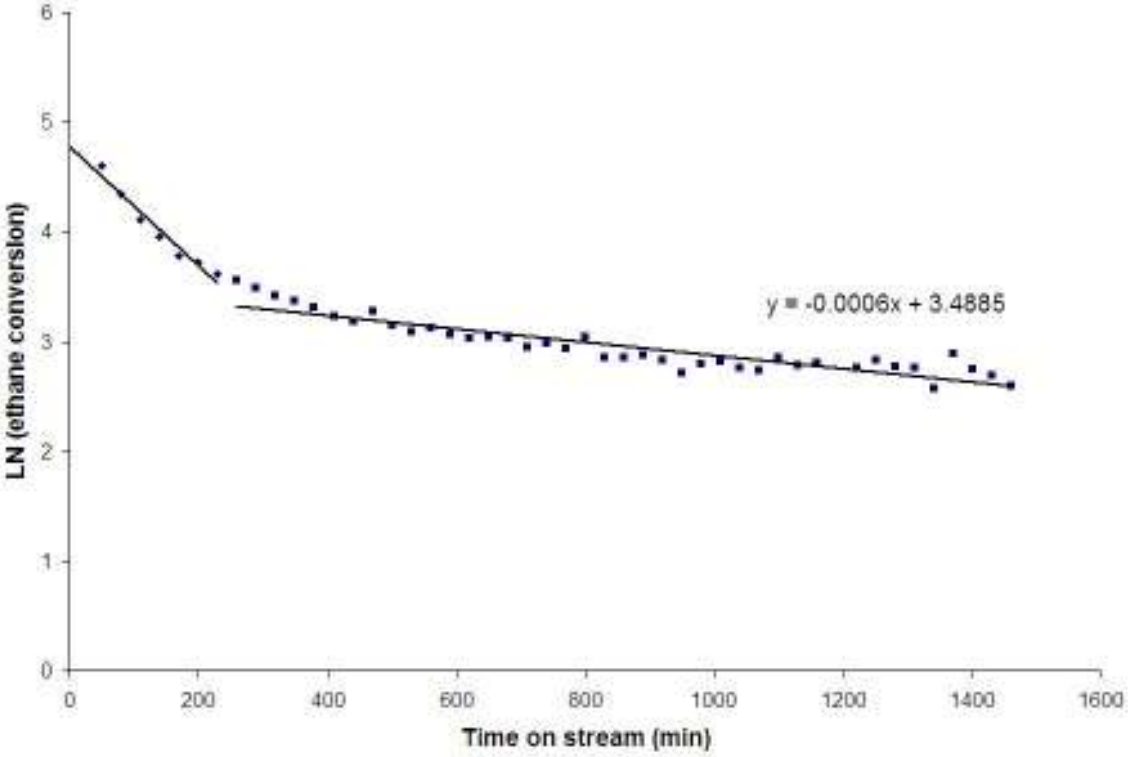

Figure 46 Rh/Al_2O_3 deactivation at 500°C

There is a good straight line fit with the data, indicating the deactivation is first order. It is apparent that when the reaction temperature was reduced from 550°C to 500°C the rates of deactivation have increased.

3.3.1.1.3. Rates of Formation of Products

Four gaseous products were formed during the reaction: H_2, CO, CO_2 and CH_4. Through the course of the reaction, every 30 minutes, the relative concentrations of each product were obtained, allowing the rate of formation of each gaseous product to be plotted against time on stream, figures 47 to 49.

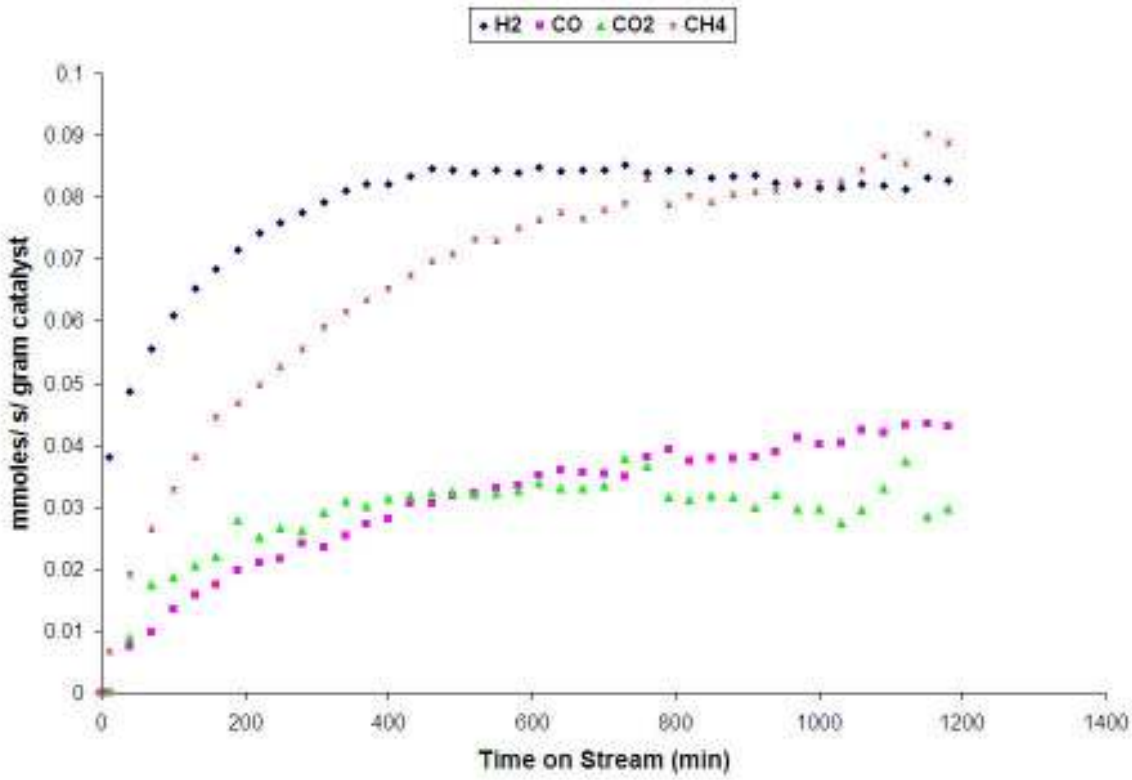

Figure 47 Rate of formation of products over Rh/Al_2O_3 at 600°C

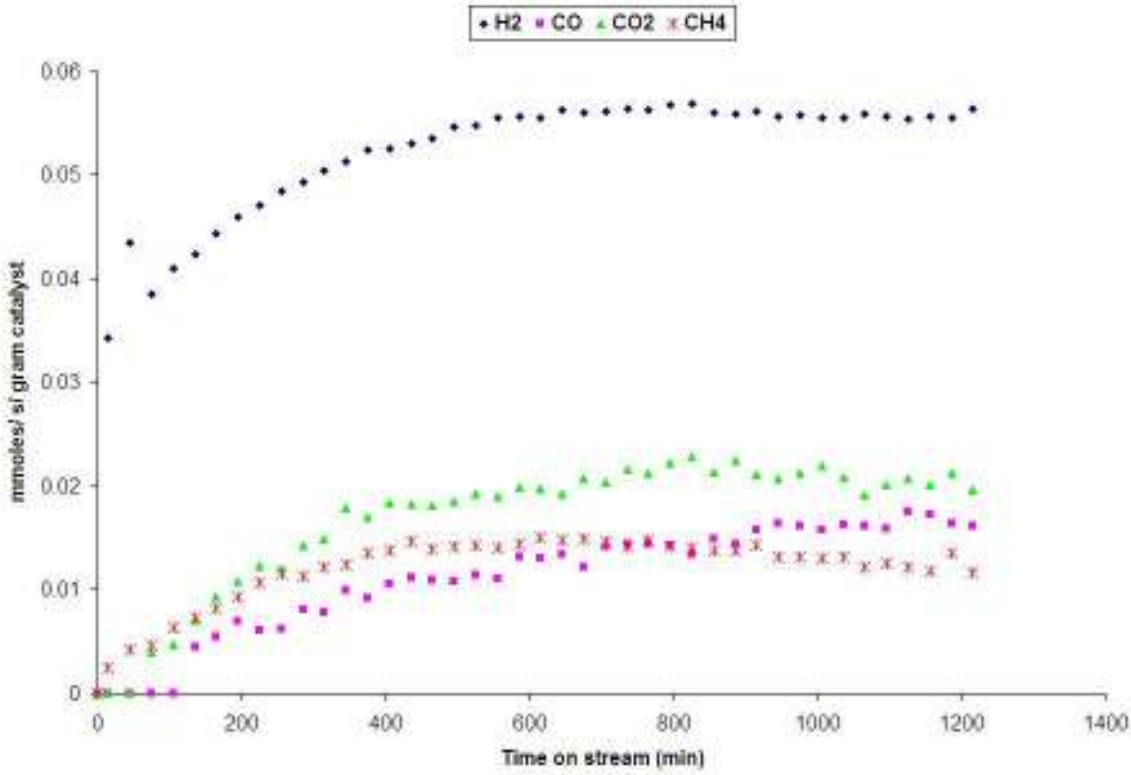

Figure 48 Rate of formation of products over Rh/Al_2O_3 at 550°C

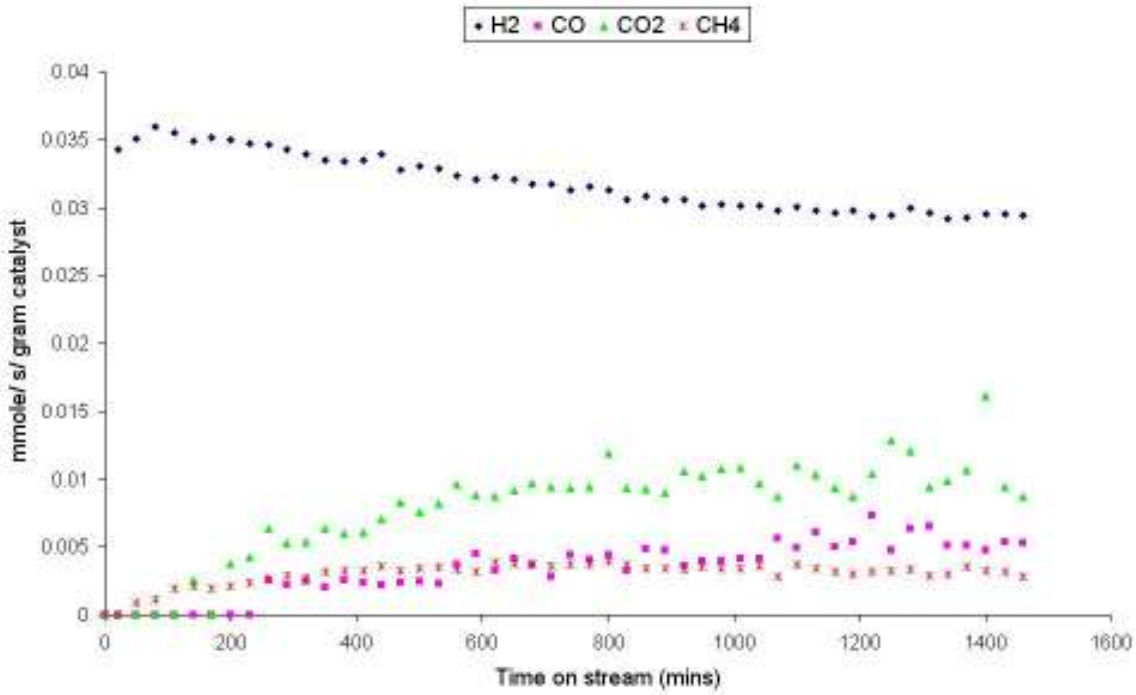

Figure 49 Rate of formation of products over Rh/Al_2O_3 at 500°C

At 600°C the rate of formation of H_2 and CH_4 are the most significant reaching approximately 0.09 mmoles/s/g. The other products, CO and CO_2, form at half this rate, approximately 0.04 mmoles/s/g.

At lower temperatures H_2 is still the major product, however the rate has dropped to 0.06 mmoles/s/g at 550°C and approximately (there is significant deactivation throughout this reaction with regard to hydrogen) 0.03 mmoles/s/g at 500°C.

CH_4 formation has dropped off significantly at temperatures below 600°C. From being a major product at 600°C, the rate of formation of CH_4 is comparable to that of CO and CO_2 at lower temperatures.

3.3.1.1.4. Product Selectivity

The selectivity of the products was calculated as described in section 2.3.1.4, and plotted against time on stream. The selectivity of products over Rh/Al_2O_3 at 600°C, 550°C and 500°C are shown in figures 50 to 52.

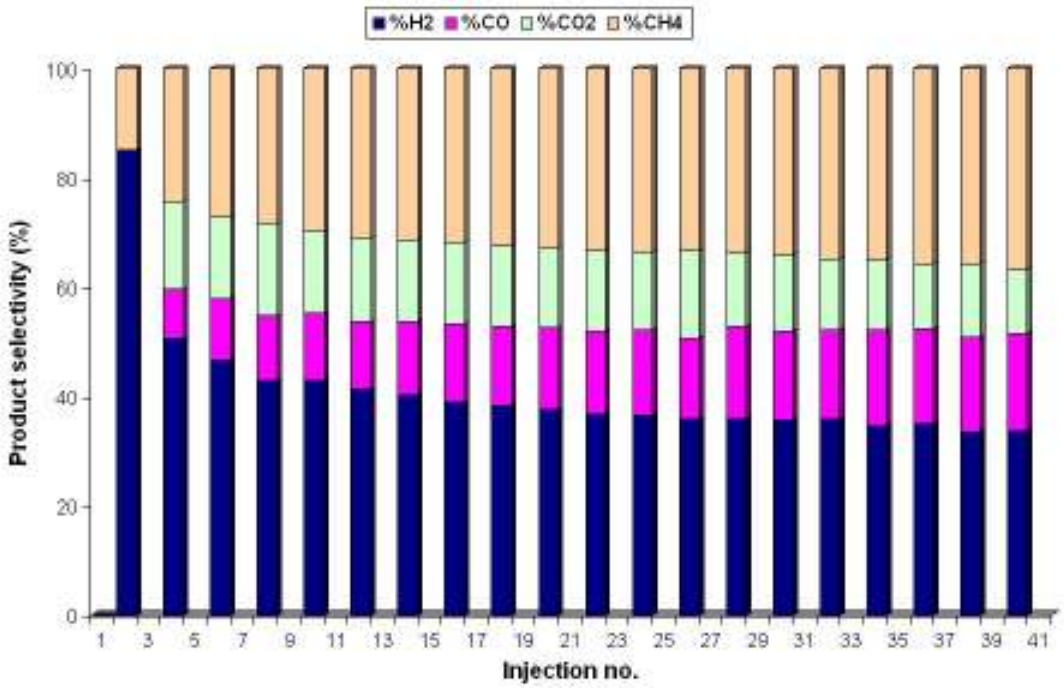

Figure 50 Product selectivity at 600°C

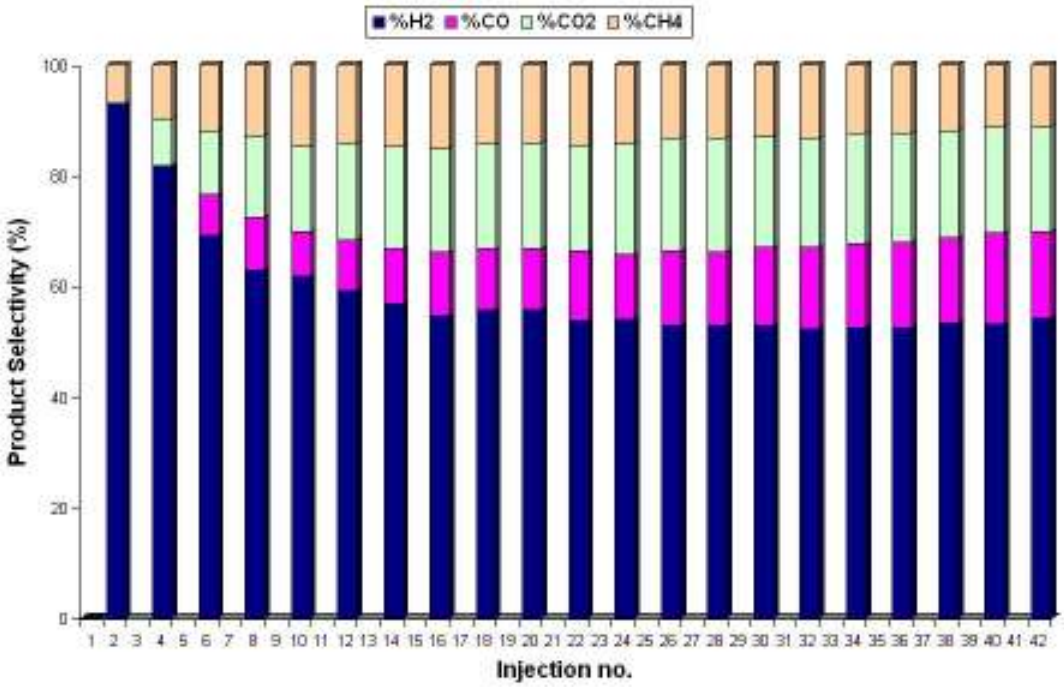

Figure 51 Product selectivity at 550°C

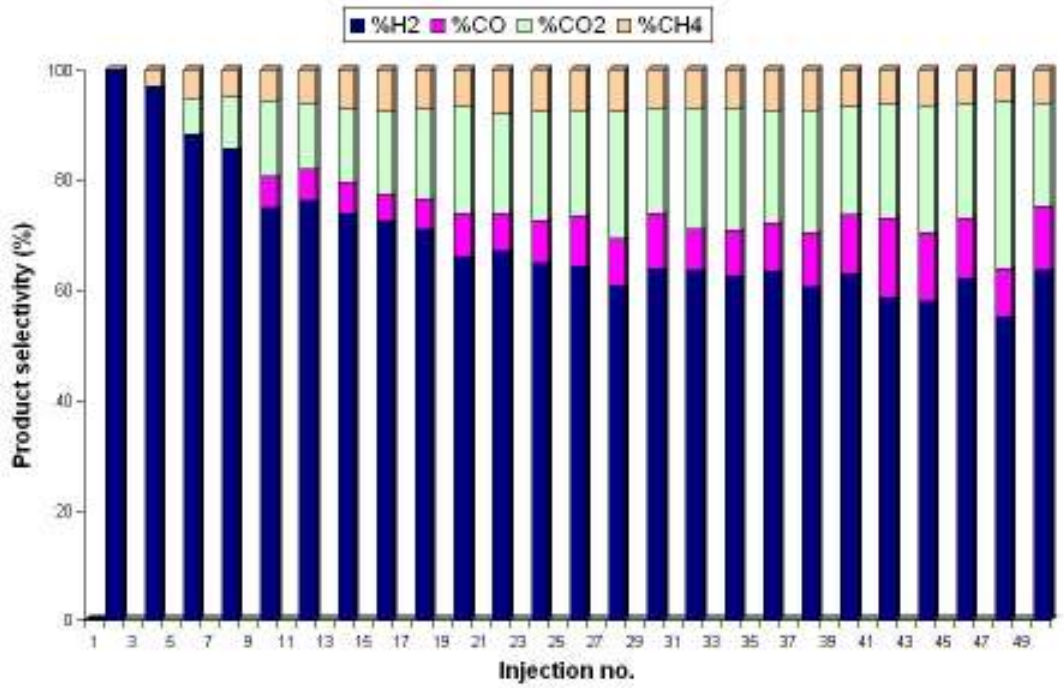

Figure 52 Product selectivity at 500 °C

As the reaction temperature decreases, the selectivity towards H_2 increases, whilst the selectivity towards CH_4 significantly decreases.

3.3.1.1.5. Carbon Mass balance

The carbon mass balance was calculated as described in section 2.3.1.4, and plotted against time on stream. The carbon mass balance of Rh/Al_2O_3 at 600°C, is shown in figure 53.

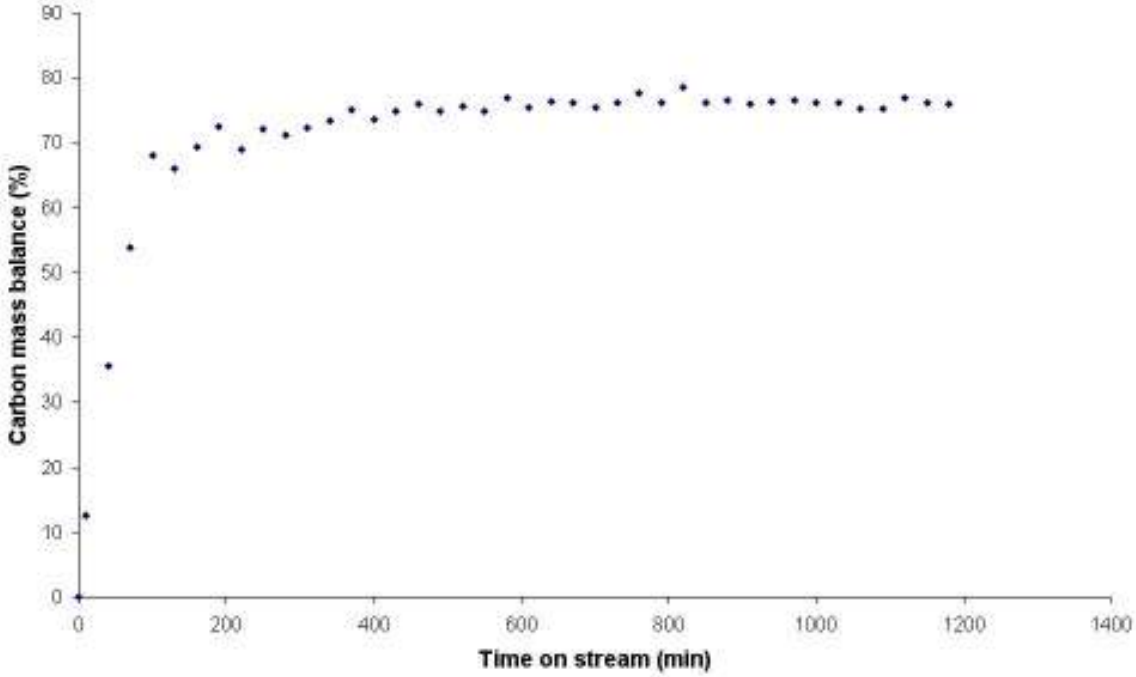

Figure 53 Carbon mass balance for Rh/Al_2O_3 at 600°C

3.3.1.2. Pt/Al_2O_3

3.3.1.2.1. Conversion

The conversion of ethane over Pt/Al_2O_3 at 600°C, 550°C and 500°C are shown in figures 54 to 56. At the three reaction temperatures examined, ethane conversion was not stable over Pt/Al_2O_3. The catalyst performed best at 600°C, with conversion just beginning to level off at 45% at 1400 minutes on stream. At lower temperatures ethane conversion falls to less than 10%.

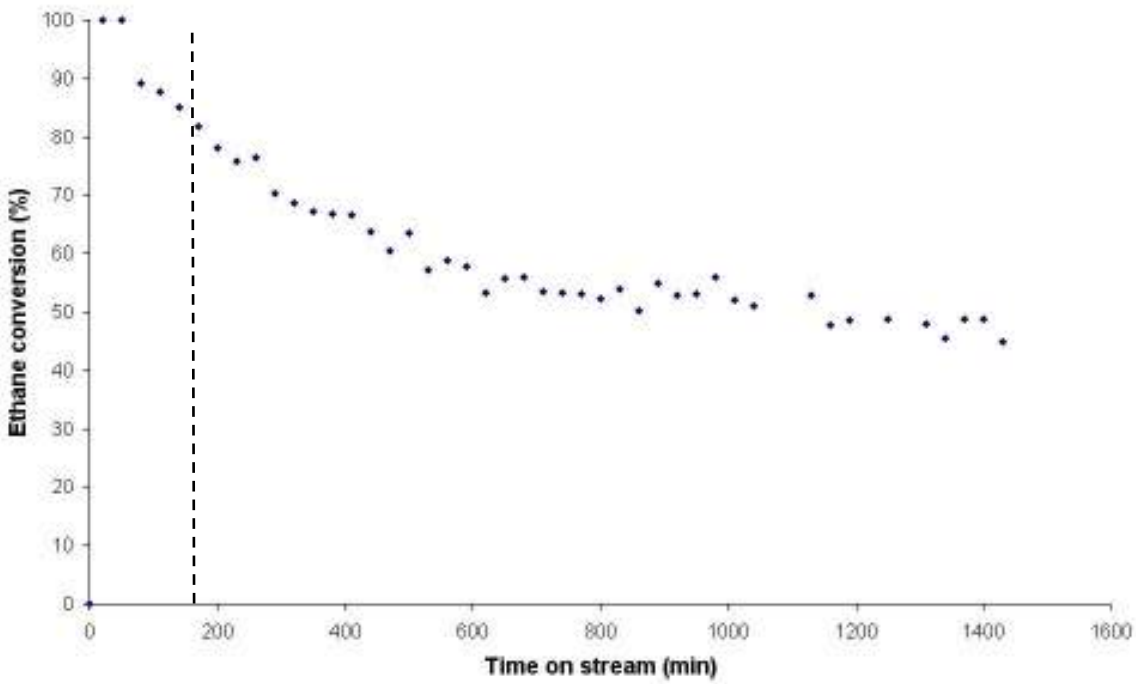

Figure 54 Ethane conversion over Pt/Al_2O_3 at 600°C

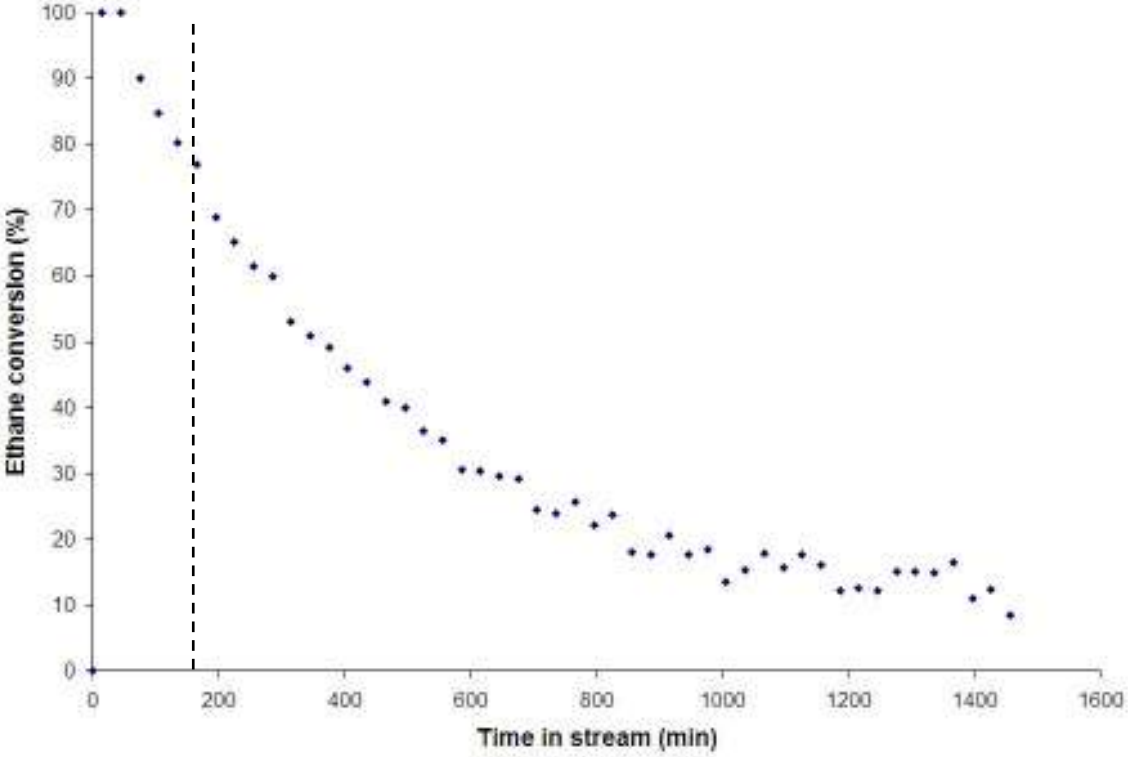

Figure 55 Ethane conversion over Pt/Al_2O_3 at 550°C

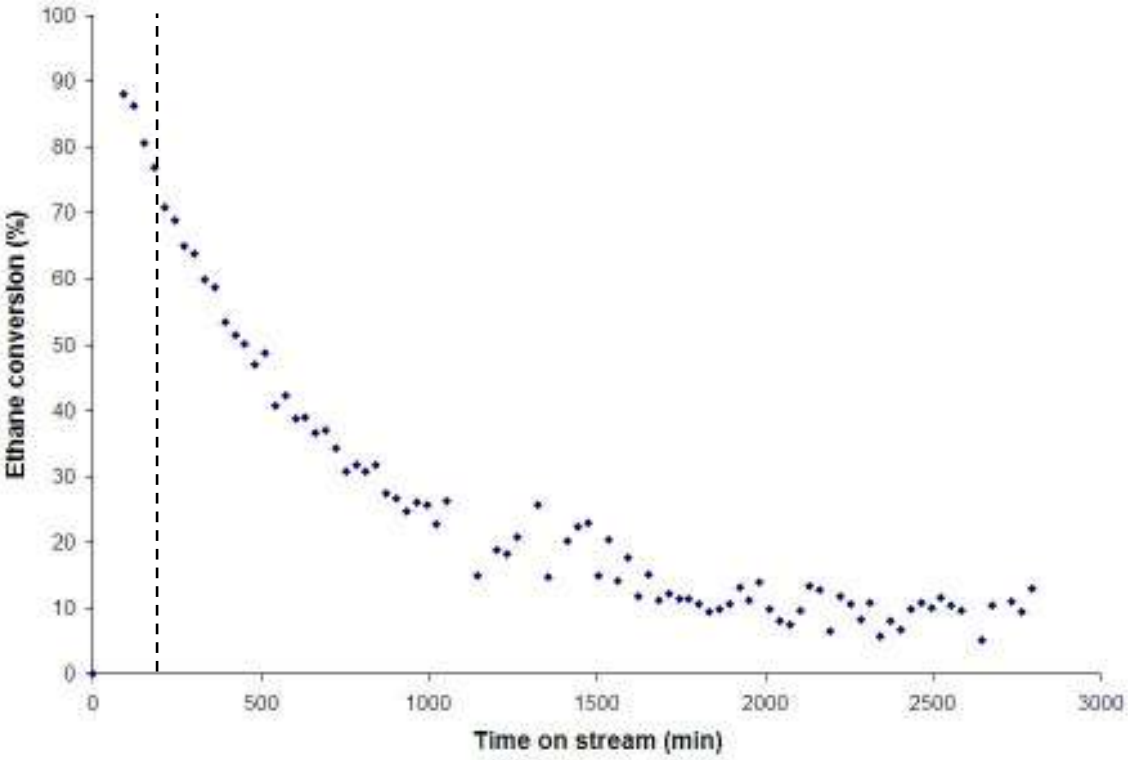

Figure 56 Ethane conversion over Pt/Al_2O_3 at 500°C

3.3.1.2.2. Rate of Deactivation

Deactivation of Pt/Al_2O_3 occurred at all three temperatures during the steam reforming of ethane, figures 57 to 59.

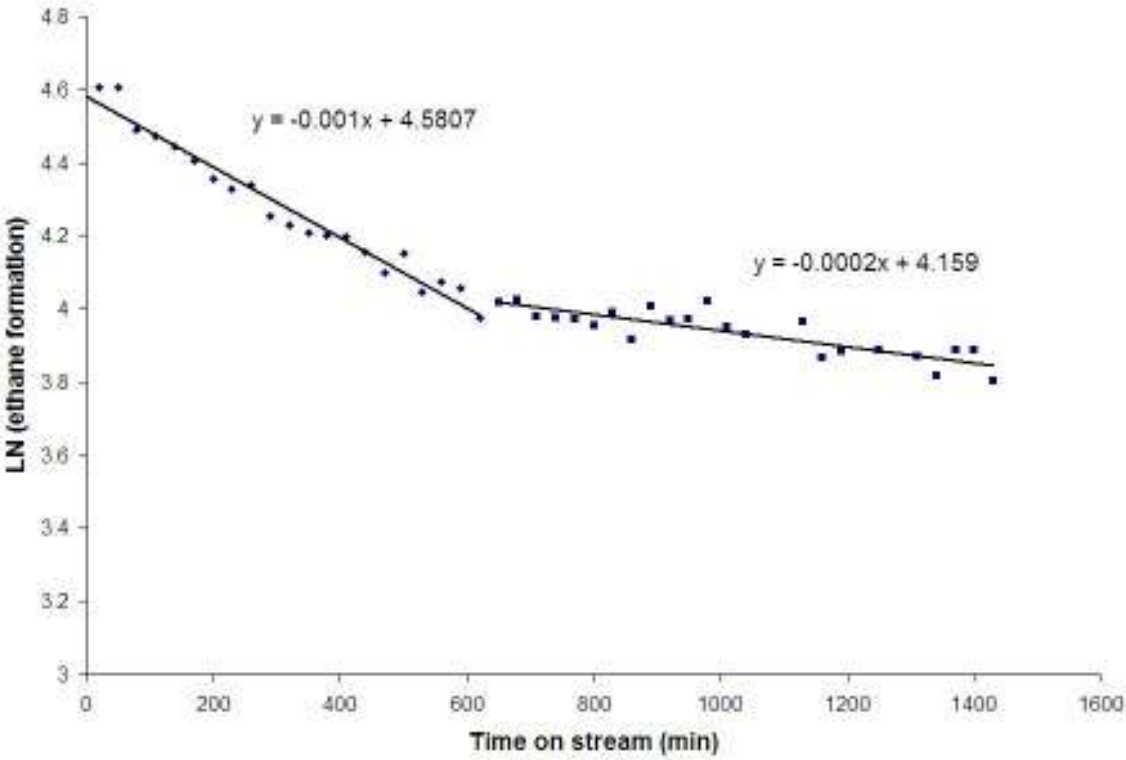

Figure 57 Pt/ Al_2O_3 deactivation at 600°C

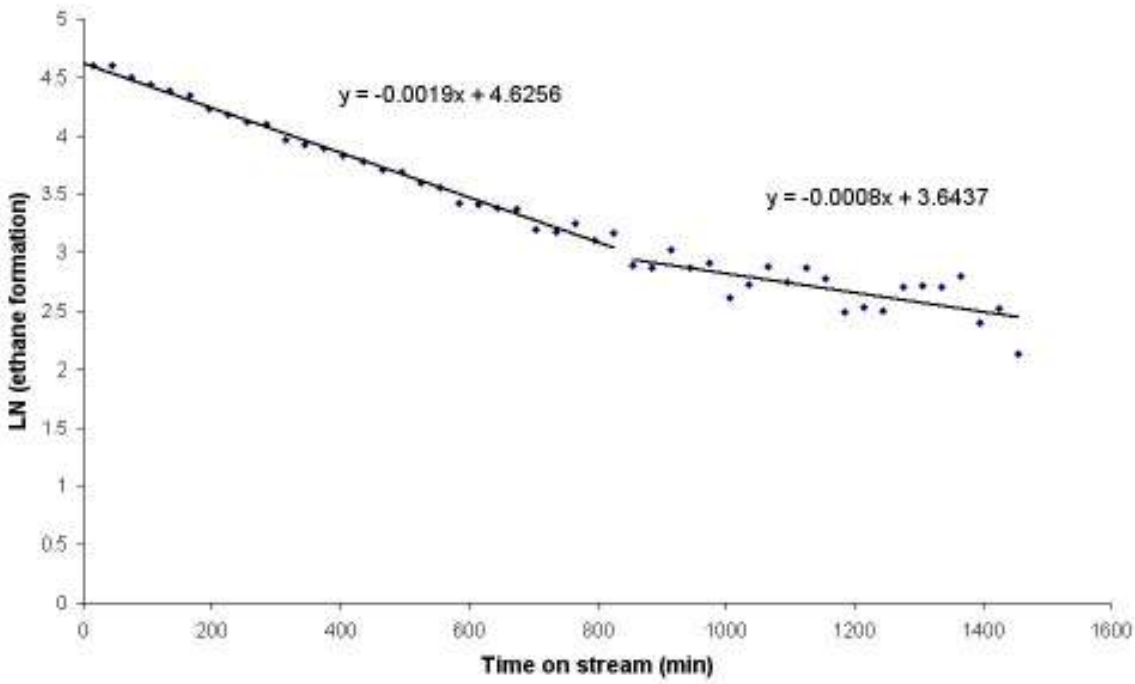

Figure 58 Pt/Al_2O_3 deactivation at 550°C

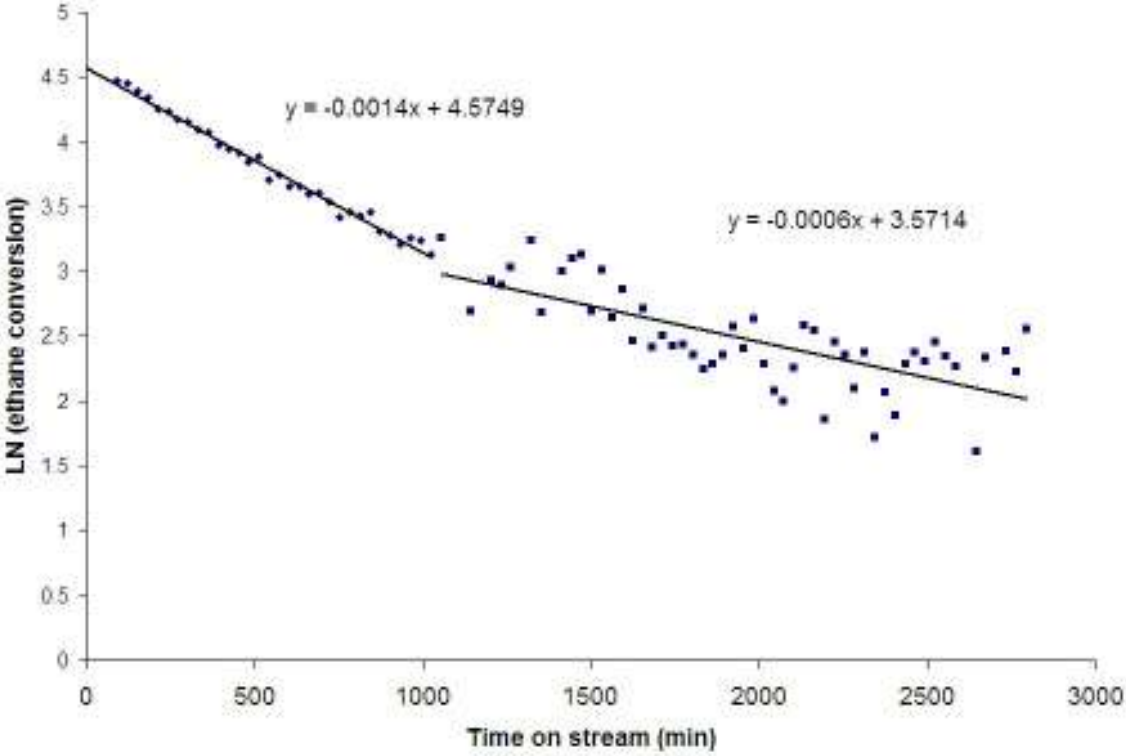

Figure 59 Pt/Al_2O_3 deactivation at 500°C

The deactivation of Pt/Al_2O_3 occurs in two stages, with the first stage of deactivation occurring at a faster rate than the latter. Also, the initial period of deactivation becomes extended as the reaction temperature decreases, ending at 600 minutes on stream at 600°C to 1000 minutes on stream at 500°C.

Decreasing the reaction temperature from 600°C to 550°C increases the rates of deactivation. However, a further decrease in reaction temperature to 500°C *decreases* the rates of deactivation, i.e. Pt/Al_2O_3 deactivation is most significant at 550°C.

3.3.1.2.3. Rates of formation of Products

Hydrogen is the major product formed at all reaction temperatures over Pt/Al_2O_3. Deactivation of hydrogen formation is evident even at 600°C and gets more significant as the reaction temperature is lowered, particularly at 500°C, figures 60 to 62.

The formation of CH_4 and CO_2 are the next most significant products, with their formation appearing relatively stable at 600°C and 550°C. Deactivation of CO_2 only becomes evident at 500°C.

CO is only a minor product over Pt/Al_2O_3, with its formation decreasing with reaction temperature. No CO was detected at 500°C.

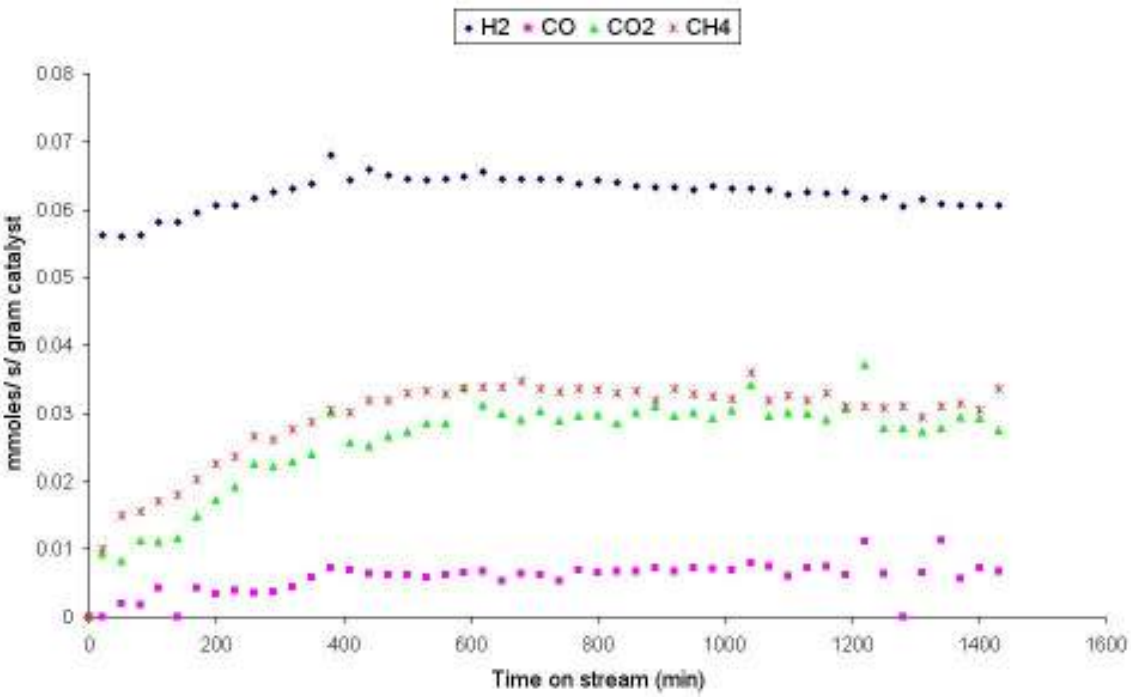

Figure 60 Rate of formation of products over Pt/Al_2O_3 at 600°C

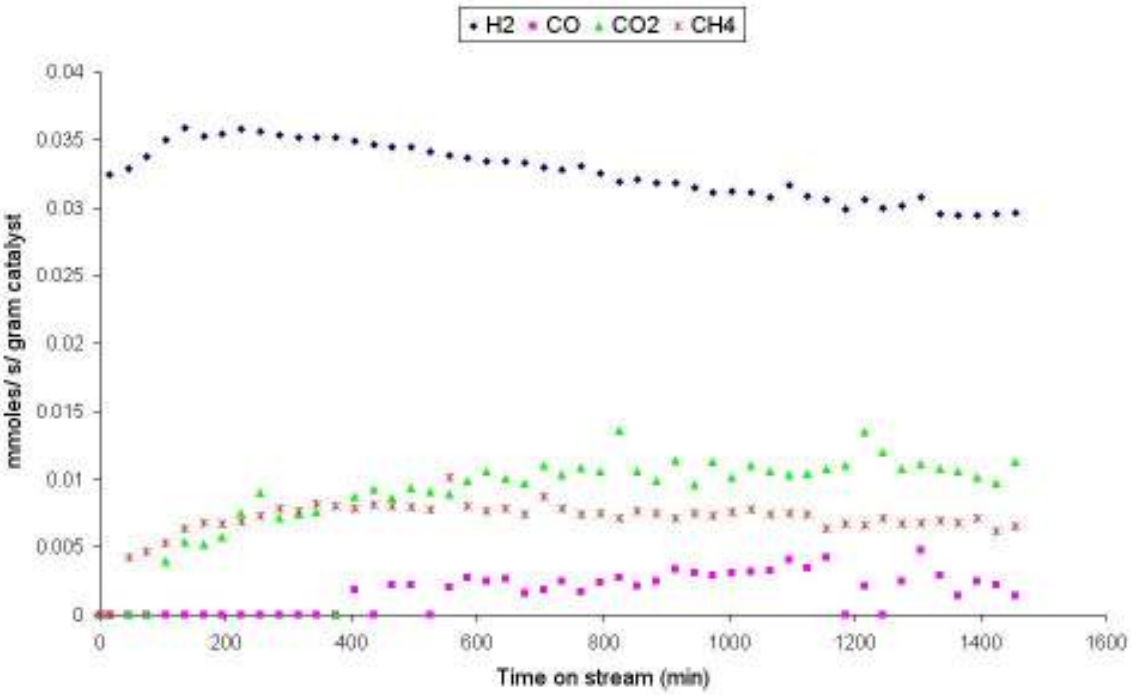

Figure 61 Rate of formation of products over Pt/Al_2O_3 at 550°C

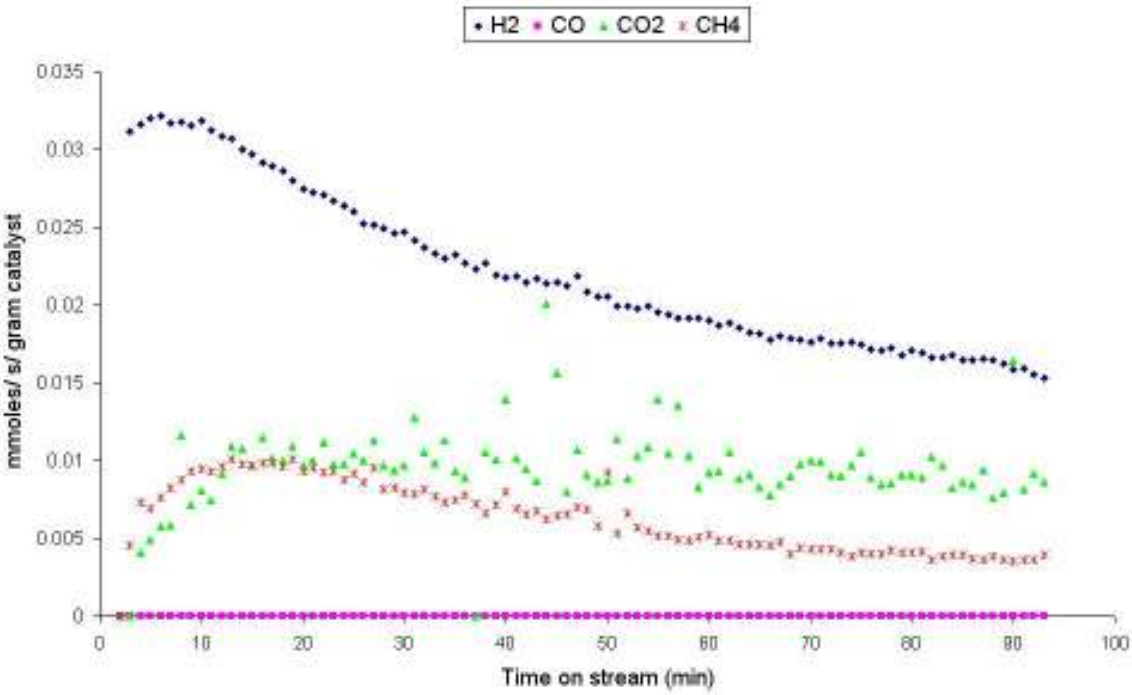

Figure 62 Rate of formation of products over Pt/Al_2O_3 at 500°C

3.3.1.2.4. Product Selectivity

Decreasing the reaction temperature appears to have slightly increased the selectivity towards H_2, whist the selectivity towards CH_4 has decreased, figures 63 to 65. There is also a higher selectivity towards CO_2 over Pt/Al_2O_3 than found over Rh/Al_2O_3, particularly a 600°C.

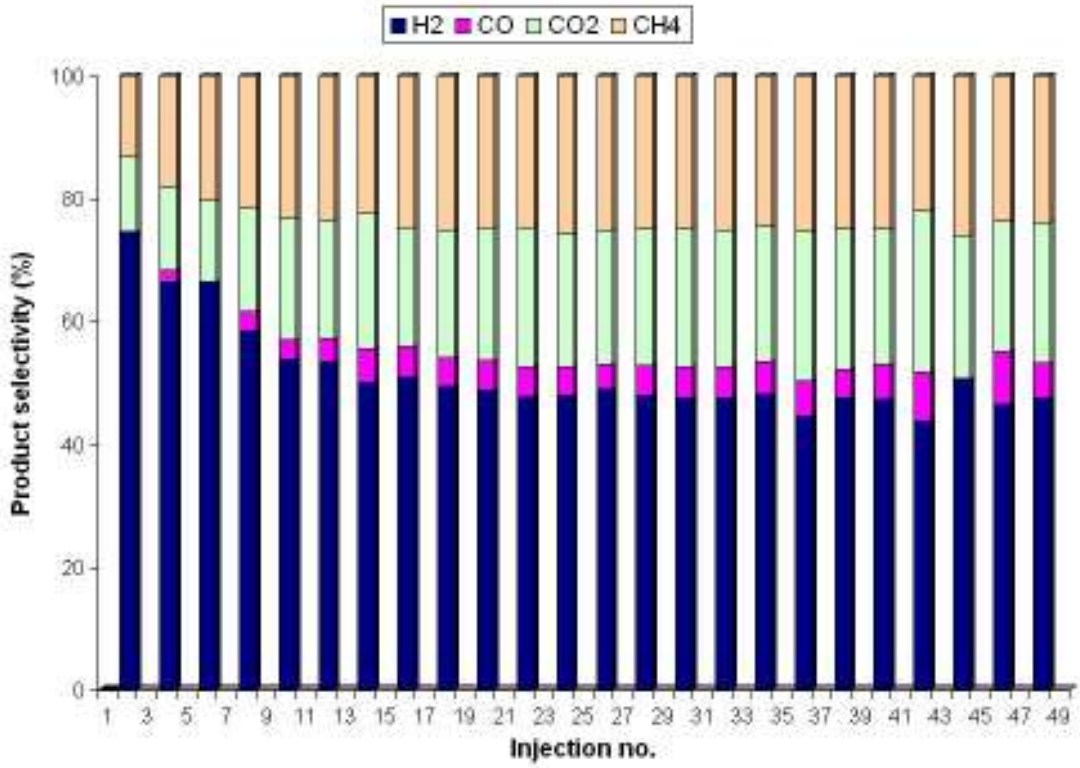

Figure 63 Product selectivity over Pt/Al_2O_3 at 600°C

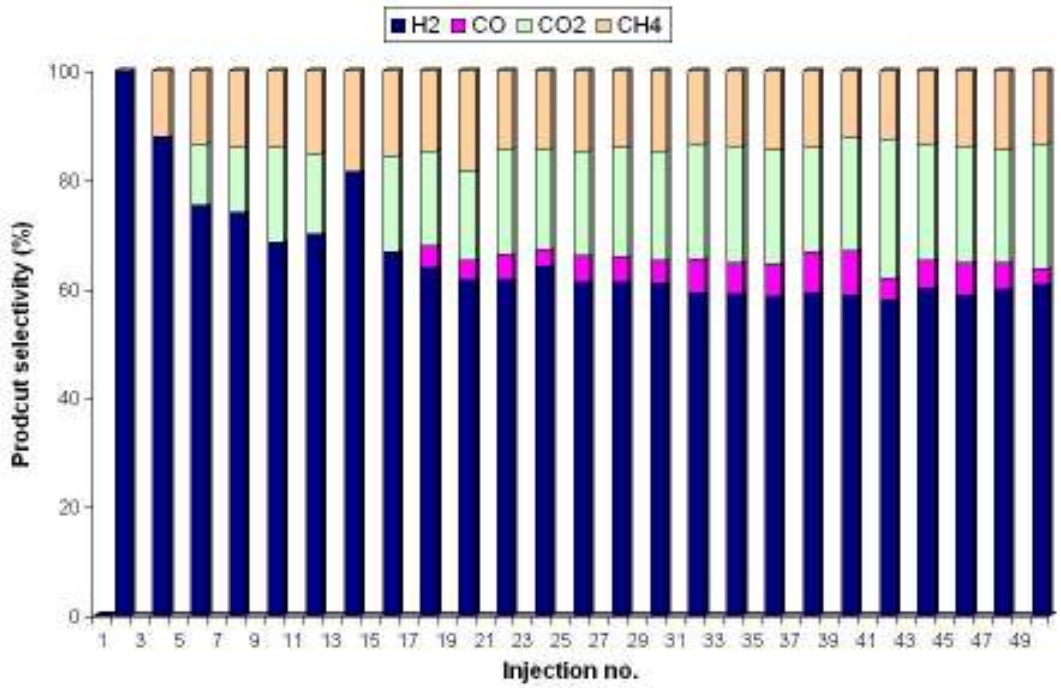

Figure 64 Product selectivity over Pt/Al_2O_3 at 550°C

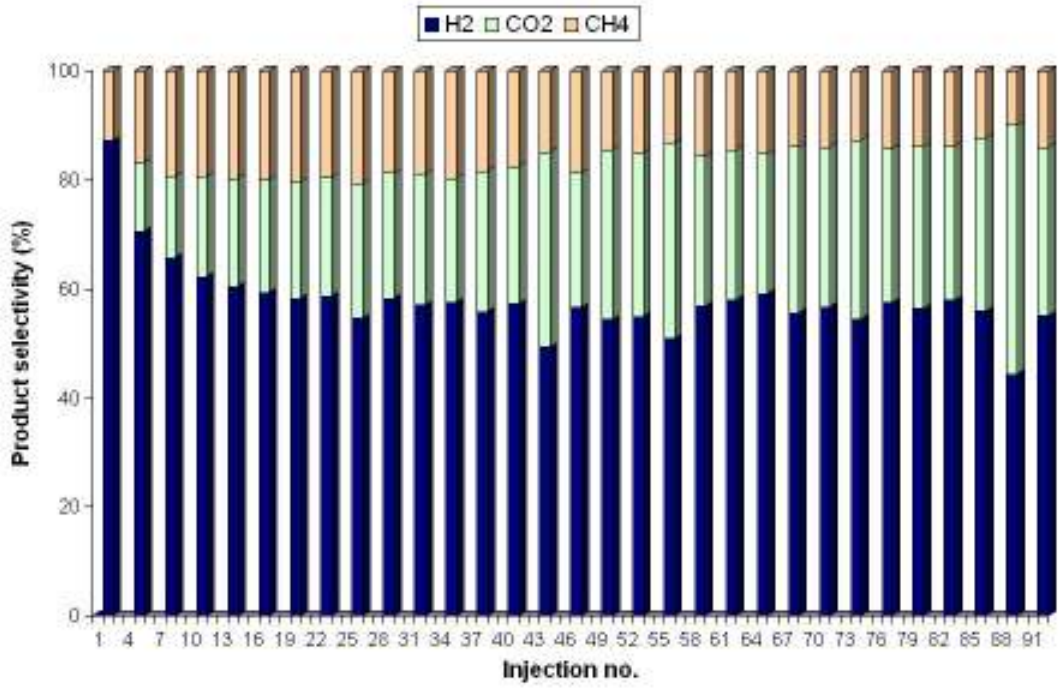

Figure 65 Product selectivity over Pt/Al_2O_3 at 500°C

3.3.1.2.5. Carbon mass balance

The carbon mass balances for Pt/Al_2O_3 at 600°C, 550°C and 500°C, are shown in figures 66 to 68.

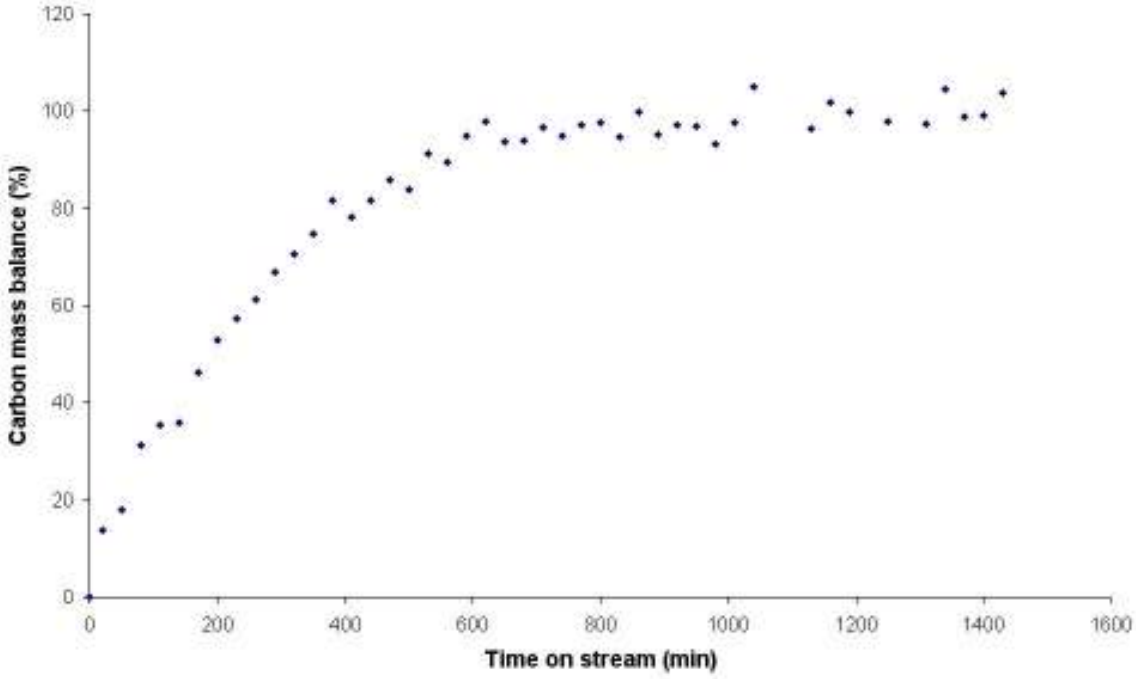

Figure 66 Carbon balance for Pt/Al_2O_3 at 600°C

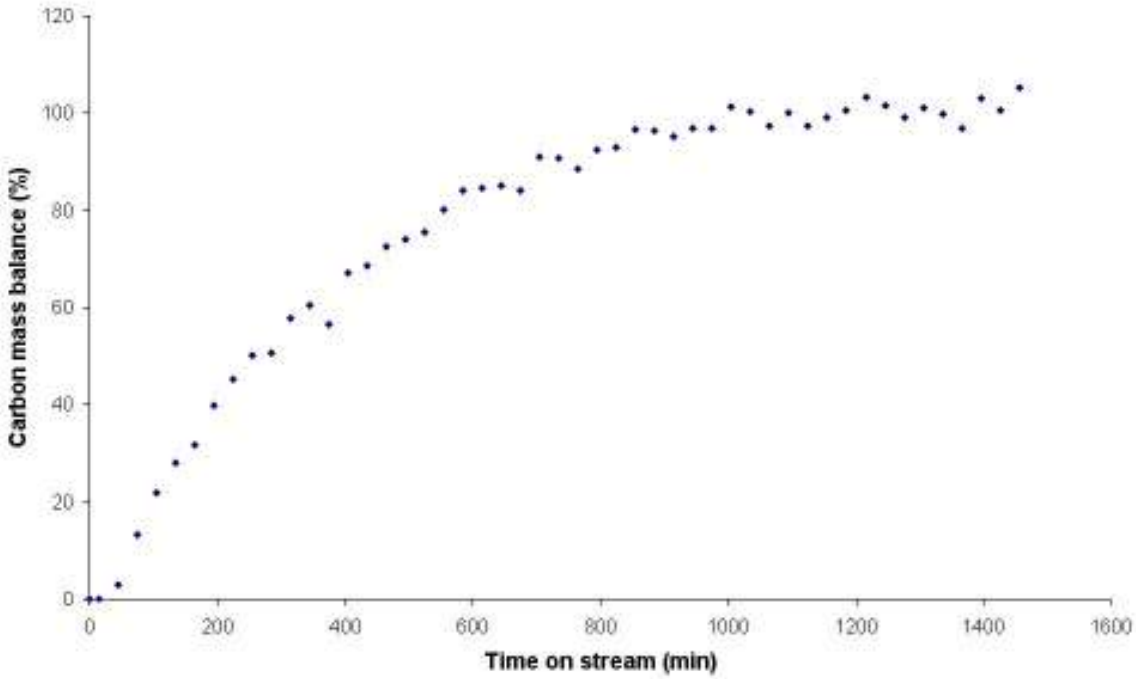

Figure 67 Carbon balance for Pt/Al_2O_3 at 550°C

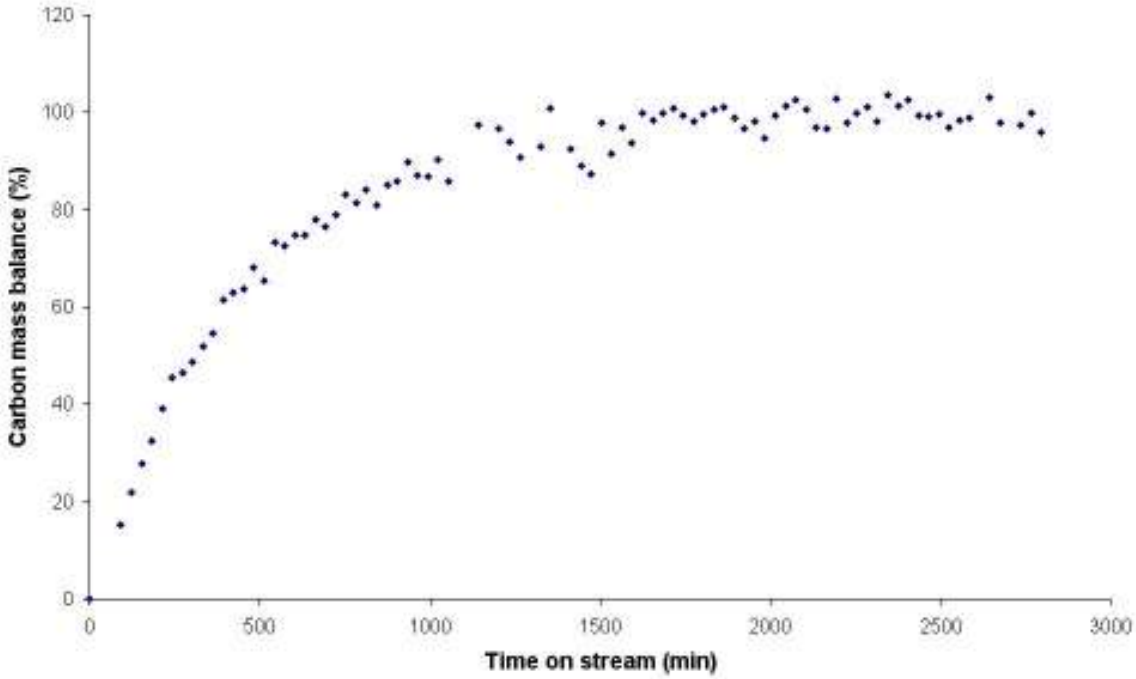

Figure 68 Carbon balance for Pt/Al_2O_3 at 500°C

3.3.1.3. Rh/ZrO_2

3.3.1.3.1. Conversion

The conversion of ethane was calculated as described in section 2.3.1.4, and plotted against time on stream. The conversion of ethane over Rh/Al_2O_3 at 600°C, 550°C and 500°C are shown in figures 69 to 71.

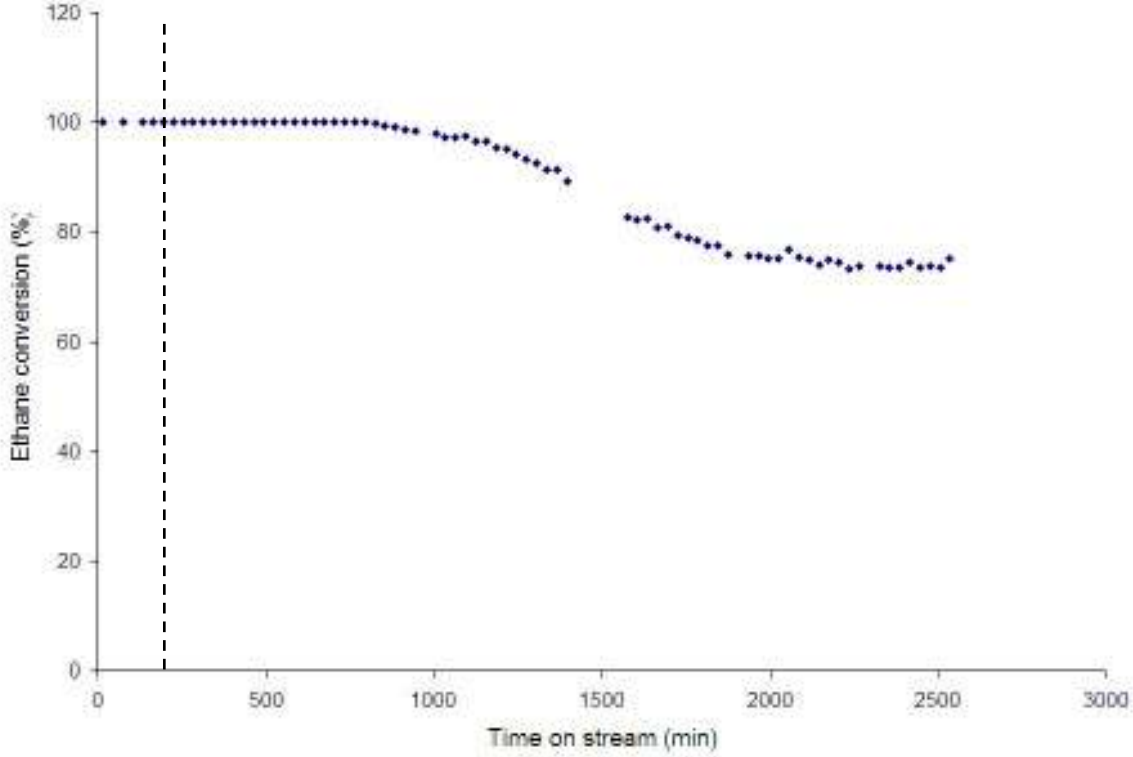

Figure 69 Ethane conversion over Rh/ZrO_2 at 600°C

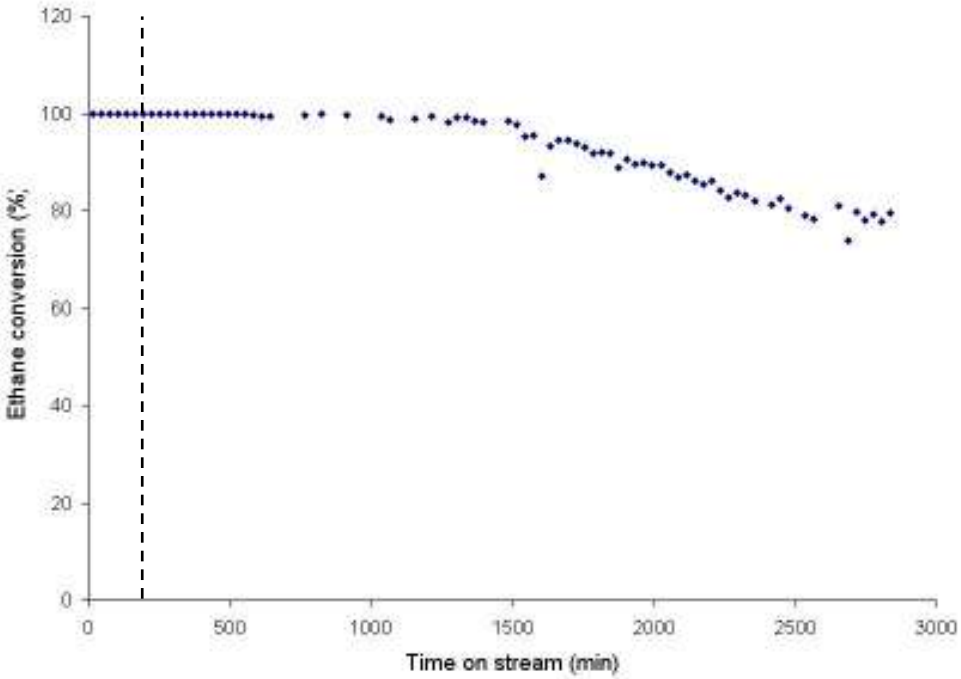

Figure 70 Ethane conversion over Rh/ZrO_2 at 550°C

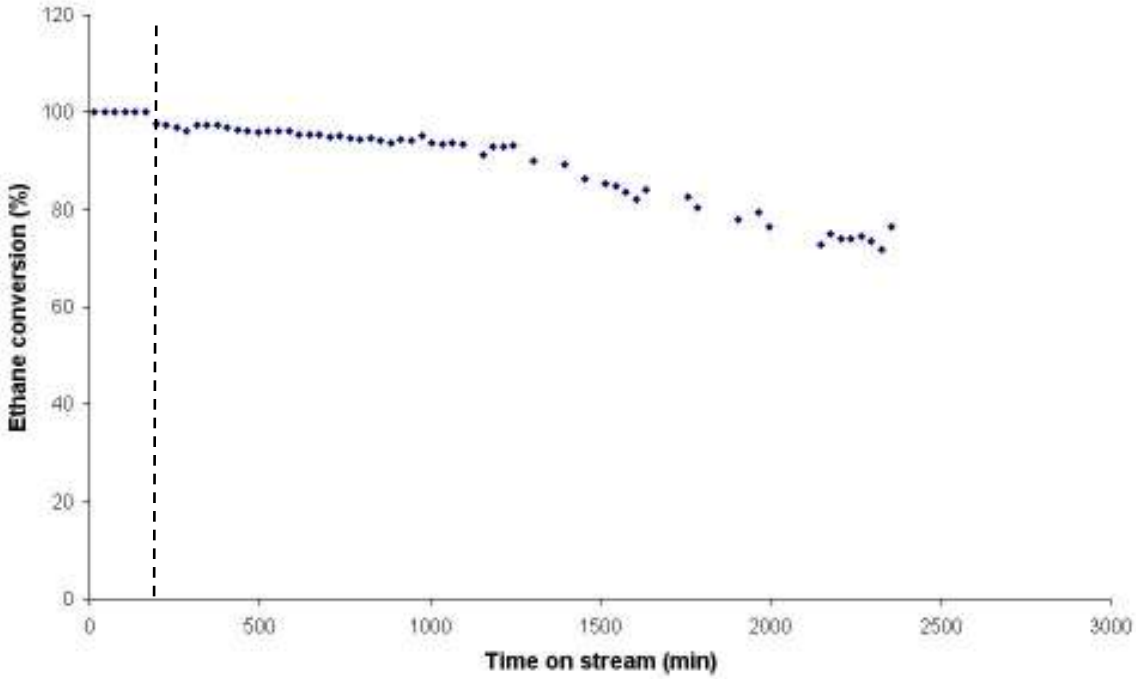

Figure 71 Ethane conversion over Rh/ZrO_2 at 500°C

At 600°C ethane is fully converted until approximately 1000 minutes on stream, hereafter deactivation occurs until 2000 minutes on stream where ethane conversion begins to stabilise again at about 75%.

A similar profile is obtained at 550°C, however the catalysts initially stability appears to have extended, with deactivation not significantly occurring until 1500 minutes on stream. After deactivation, the catalyst starts to re-stabilise ethane conversion at about 80%.

When the reaction temperature is reduced further to 500°C, the conversion of ethane is more significantly effected. The catalyst begins to slowly deactivate after only 100 minutes. At approximately 1200 minutes on stream deactivation continues but at a faster rate. The conversion of ethane does not stabilise within 2500 minutes on stream.

3.3.1.3.2. Rate of Deactivation

Deactivation of Rh/ZrO_2 was apparent at all reaction temperatures. Therefore the rates of deactivation have been plotted and are provided in figures 72 to 74.

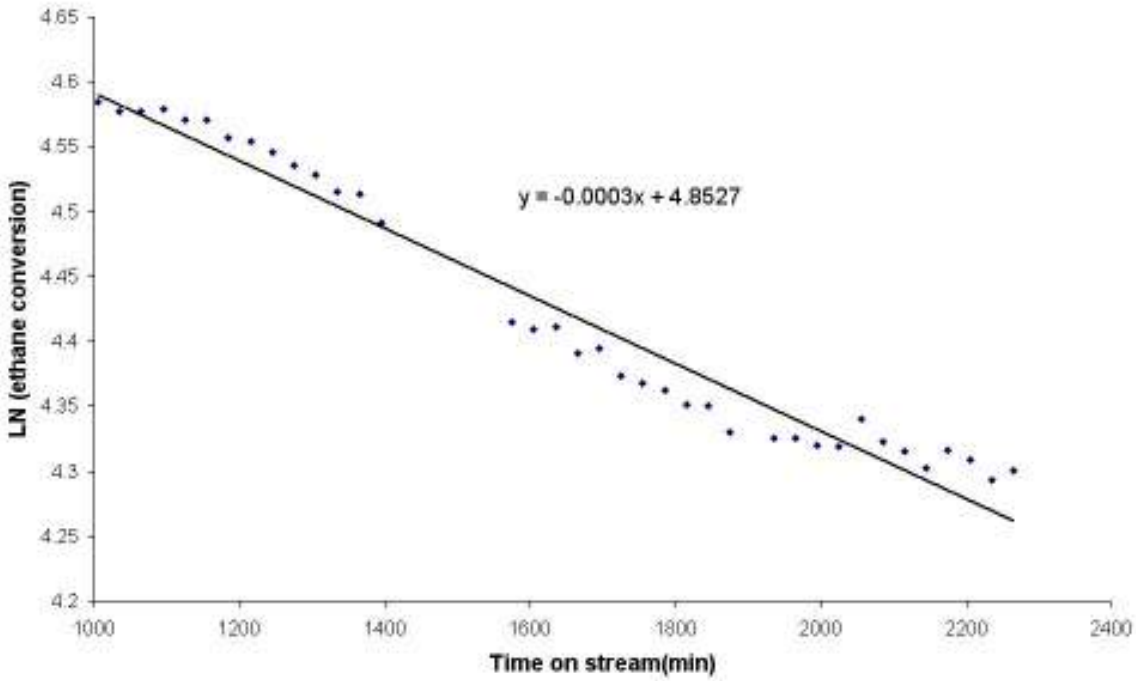

Figure 72 Rh/ZrO_2 deactivation at 600°C

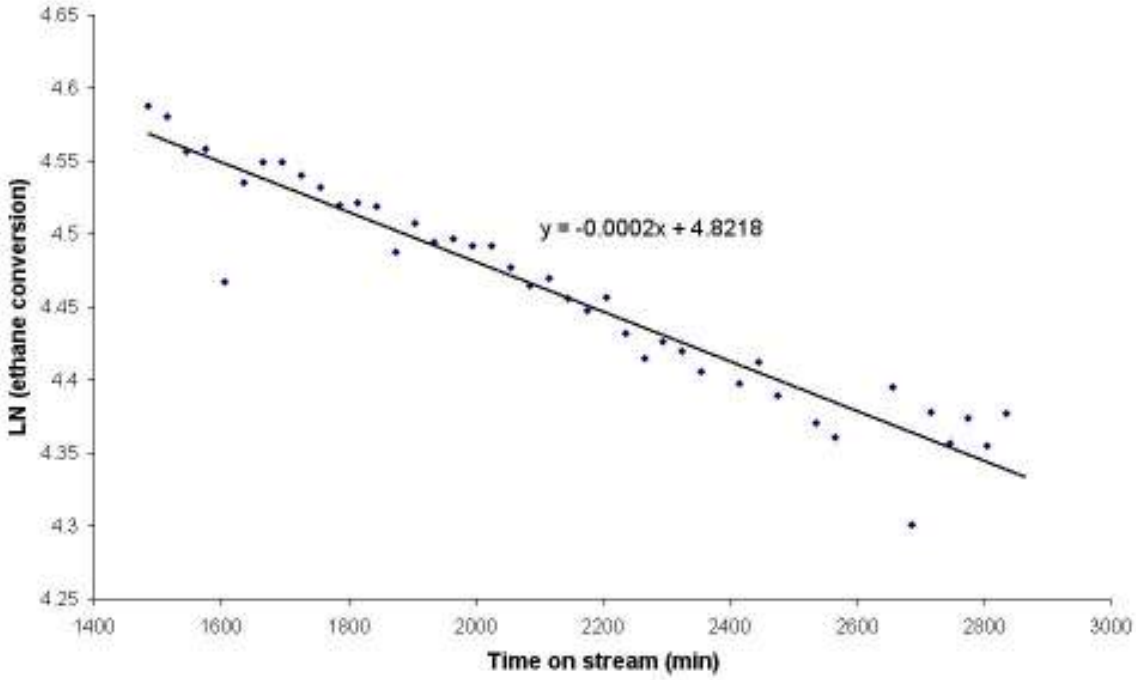

Figure 73 Rh/ZrO_2 deactivation at 600°C

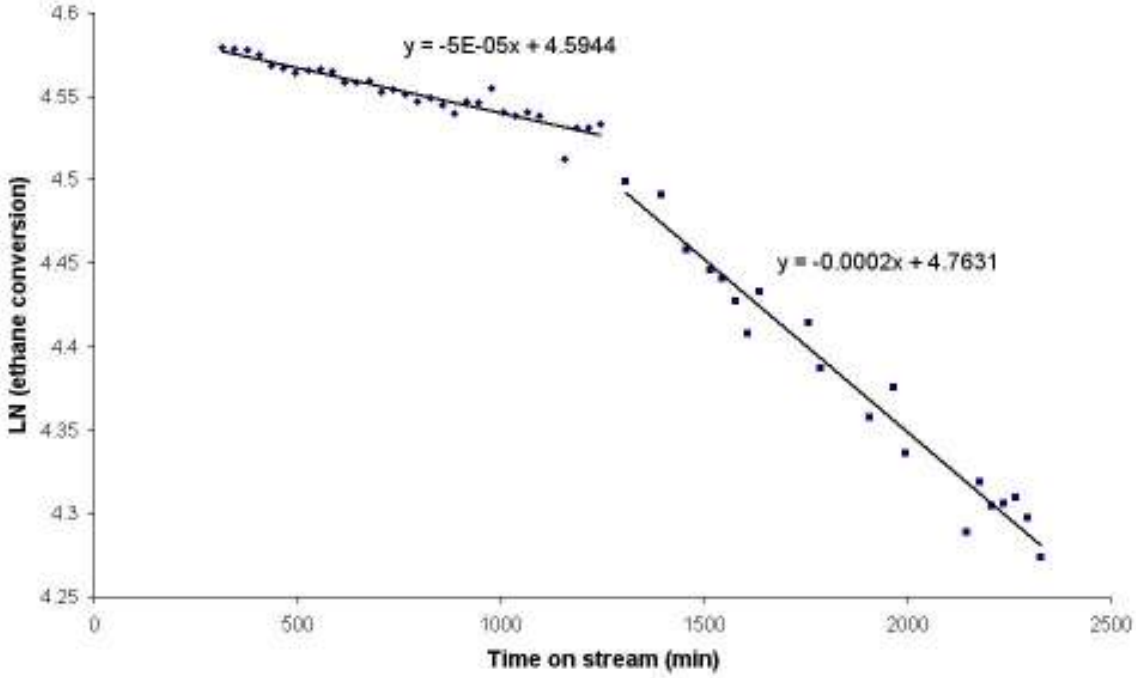

Figure 74 Rh/ZrO_2 deactivation at 500°C

It appears that Rh/ZrO_2 only has one period of deactivation at 600°C and 550°C, with the catalyst deactivating faster at 600°C. At 500°C, Rh/ZrO_2 deactivates in two stages. Initially deactivating slowly, then after 1500 minutes on stream it deactivates at the same rate as Rh/ZrO_2 at 550°C.

3.3.1.3.3. Rates of Formation of Products

For the three reaction temperatures, figures 75 to 77, CH_4 is the major product over Rh/ZrO_2, however its formation drops off extensively after 1000 minutes on stream.

Hydrogen appears to be the next major product, closely followed by CO_2 formation. The formation of CO is minimal over Rh/ZrO_2.

The formation of H_2 is relatively stable at the three temperatures, though deactivation starts to become evident at 550°C, which was the longest run. CO_2 formation deactivates slowly from about 1000 minutes on stream, with less deactivation appearing to occur at 500°C.

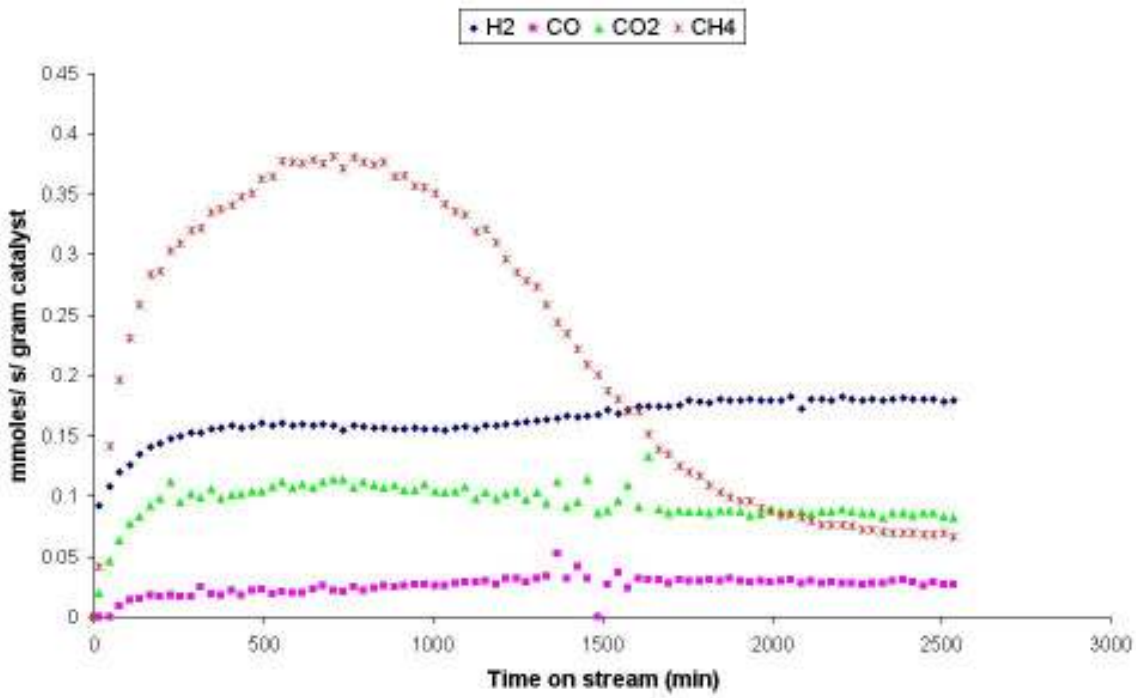

Figure 75 Rate of formation of products over Rh/ZrO_2 at 600°C

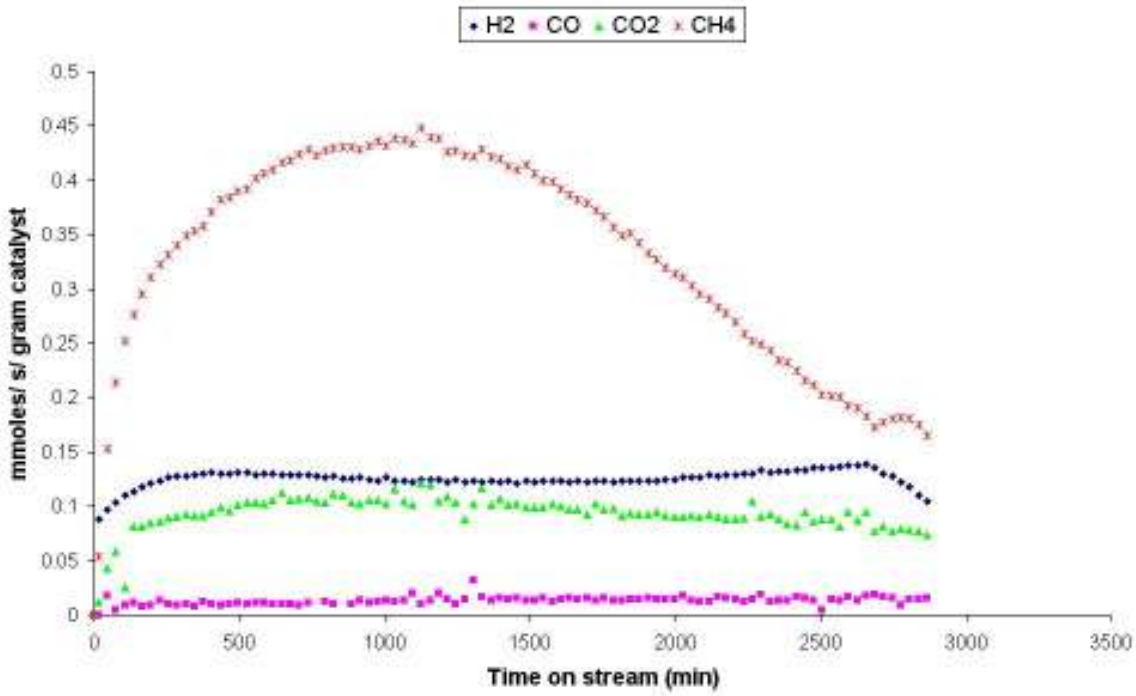

Figure 76 Rate of formation of products over Rh/ZrO_2 at 550°C

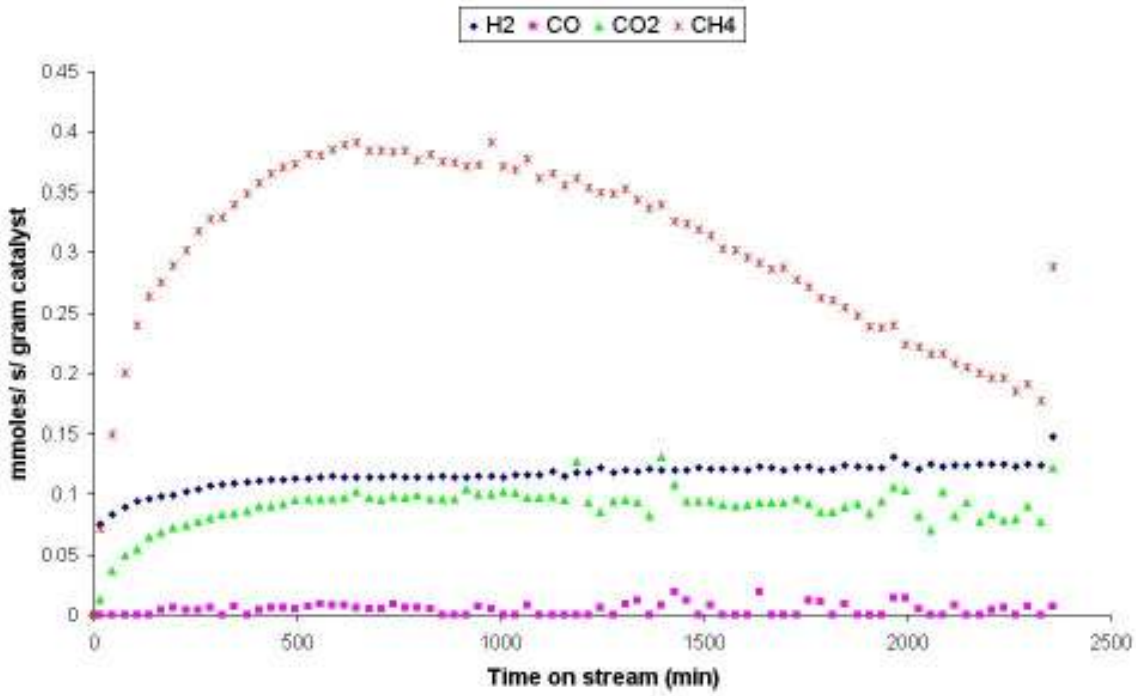

Figure 77 Rate of formation of products over Rh/ZrO_2 at 500°C

3.3.1.3.4. Product Selectivity

The selectivity graphs for Rh/ZrO_2, figures 78 to 80, are dominated by the formation and deactivation of CH_4. The selectivity towards hydrogen is highest at 600°C.

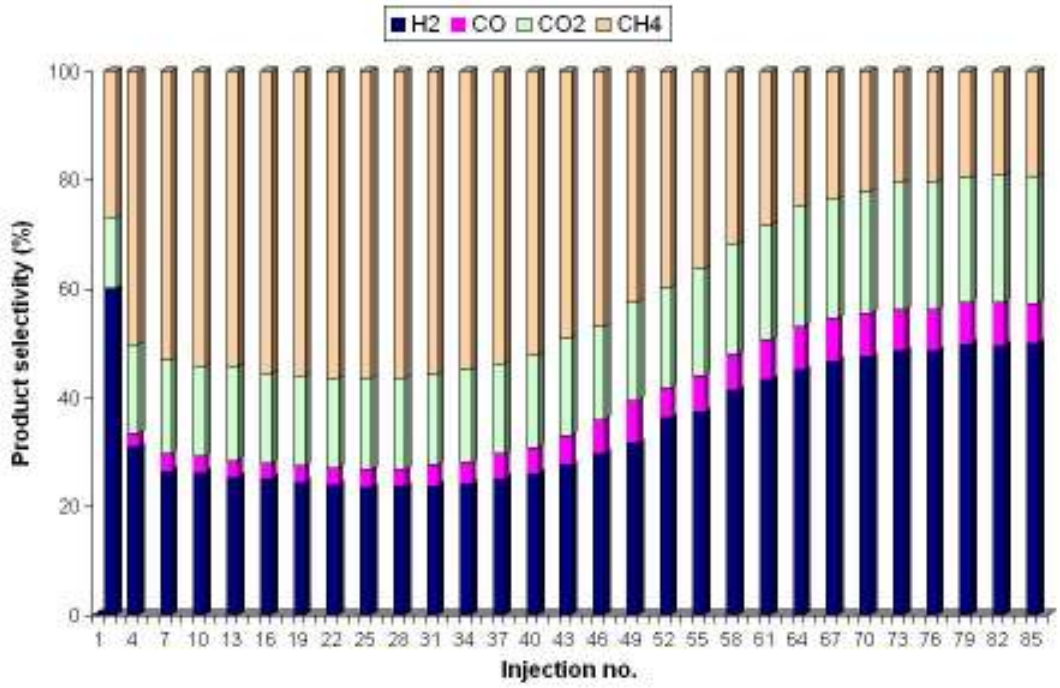

Figure 78 Product selectivity over Rh/ZrO_2 at 600°C

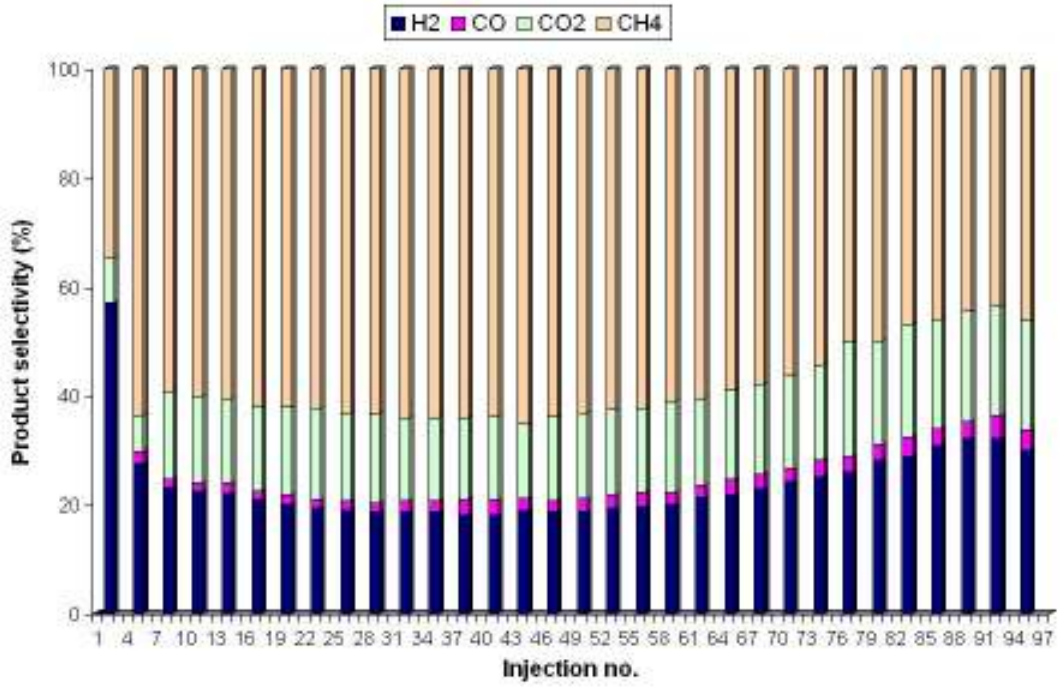

Figure 79 Product selectivity over Rh/ZrO_2 at 550°C

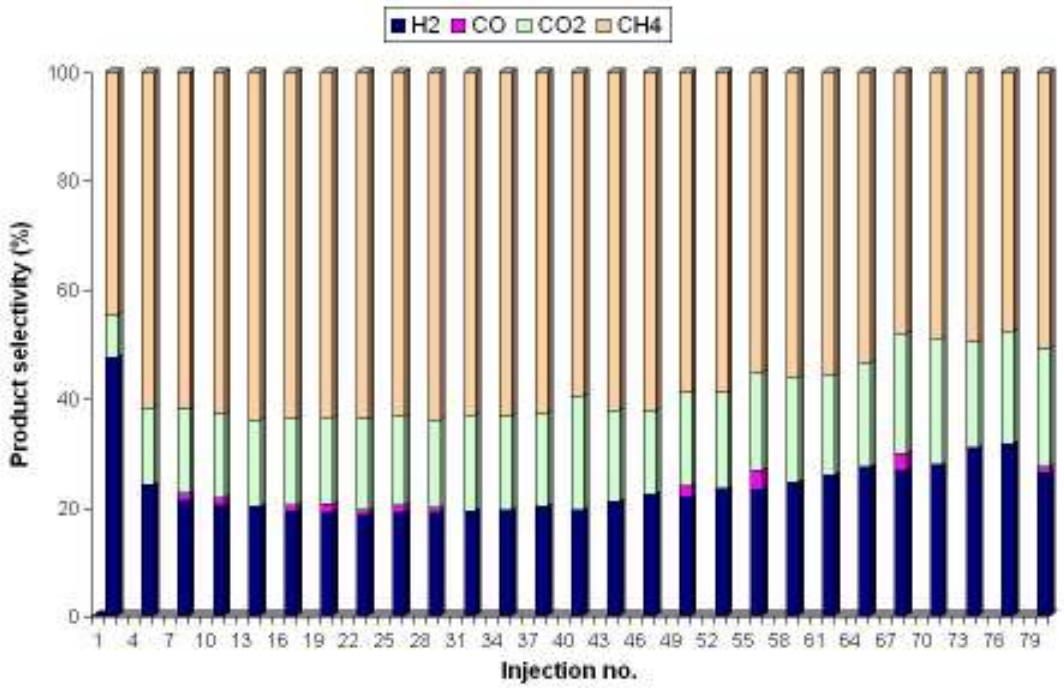

Figure 80 Product selectivity over Rh/ZrO_2at 500°C

3.3.1.3.5. Carbon mass balance

The carbon mass balance for Rh/ZrO_2 at 600°C is shown in figure 81.

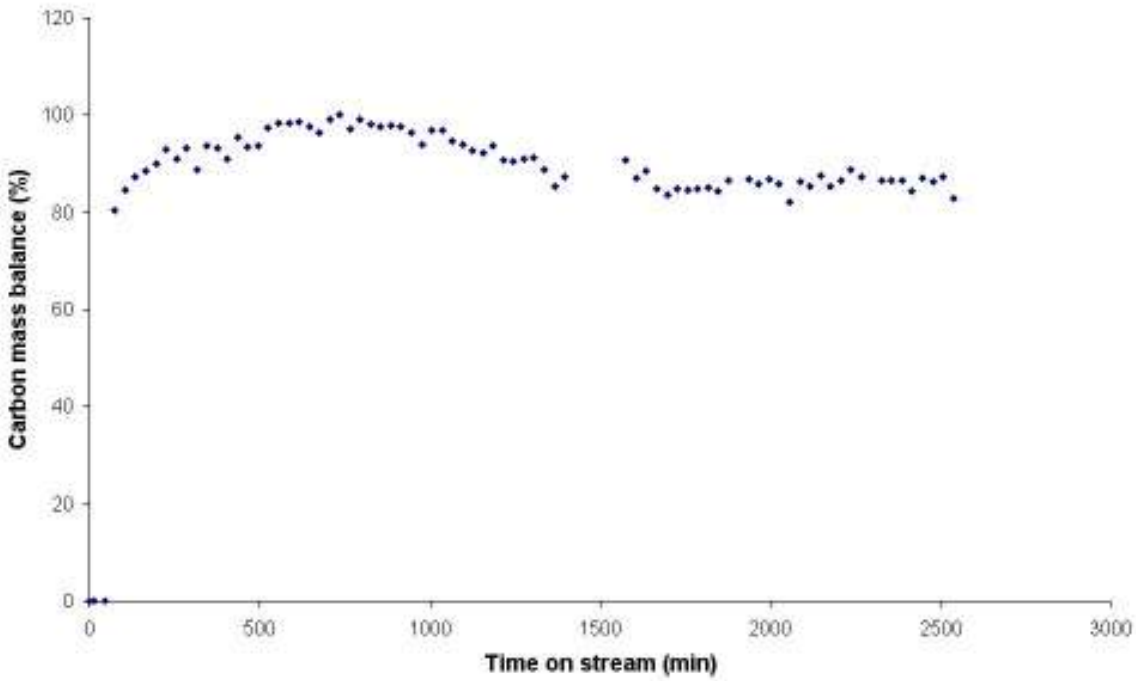

Figure 81 Carbon balance for Rh/ZrO_2 at 600°C

3.3.1.4. Pt/ZrO_2

3.3.1.4.1. Ethane conversion

The conversion of ethane over Pt/ZrO_2 showed extensive deactivation at all three reaction temperatures, figures 82 to 84. Conversion was highest at 600°C, where it plateaus at approximately 10%. At lower reaction temperatures conversion falls below 10%.

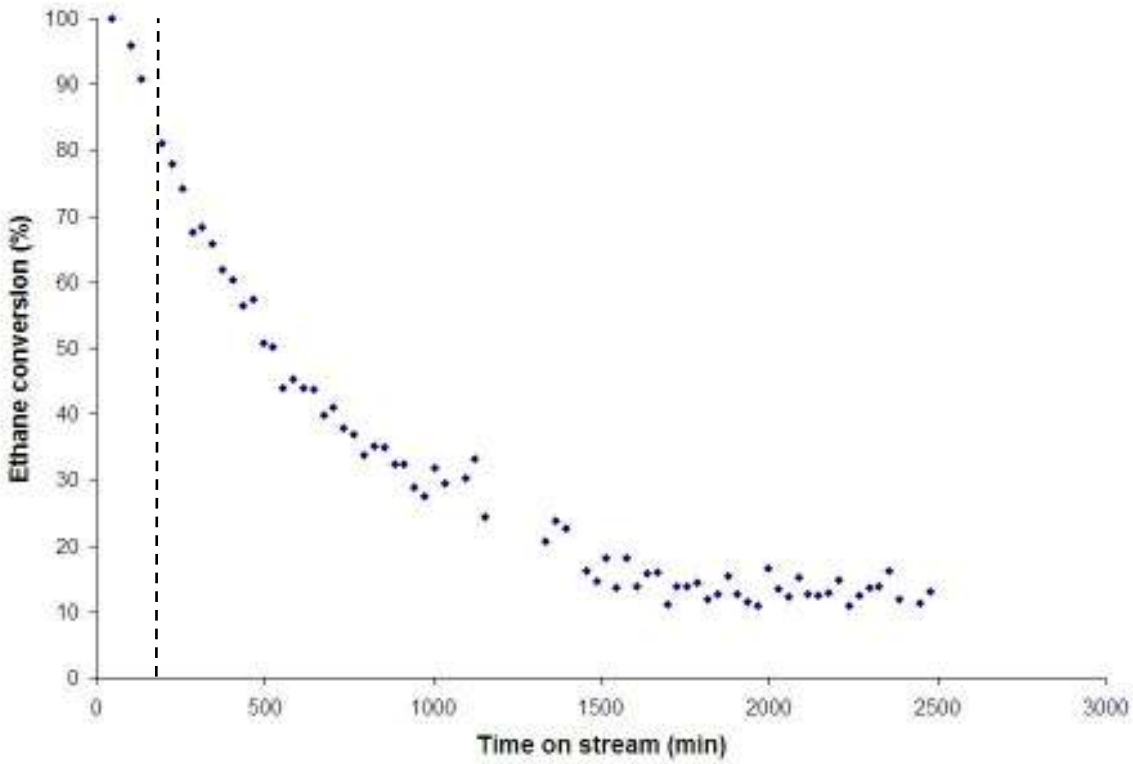

Figure 82 Ethane conversion over Pt/ZrO_2 at 600°C

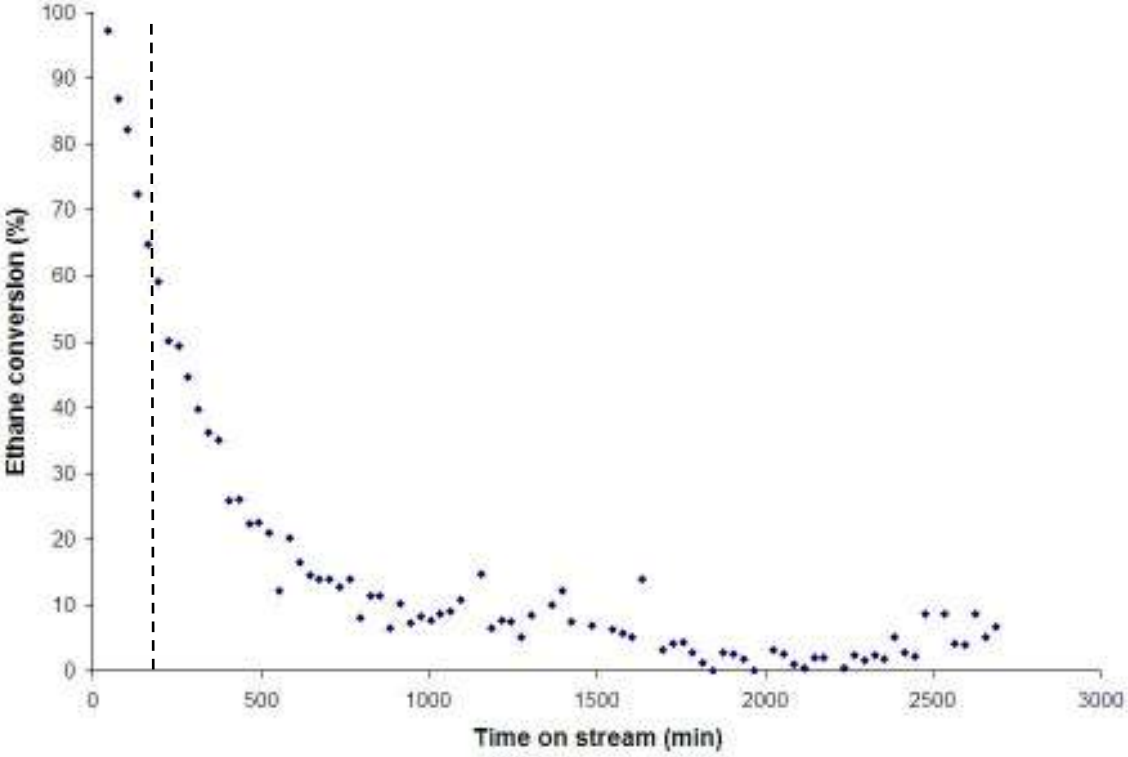

Figure 83 Ethane conversion over Pt/ZrO_2 at 550°C

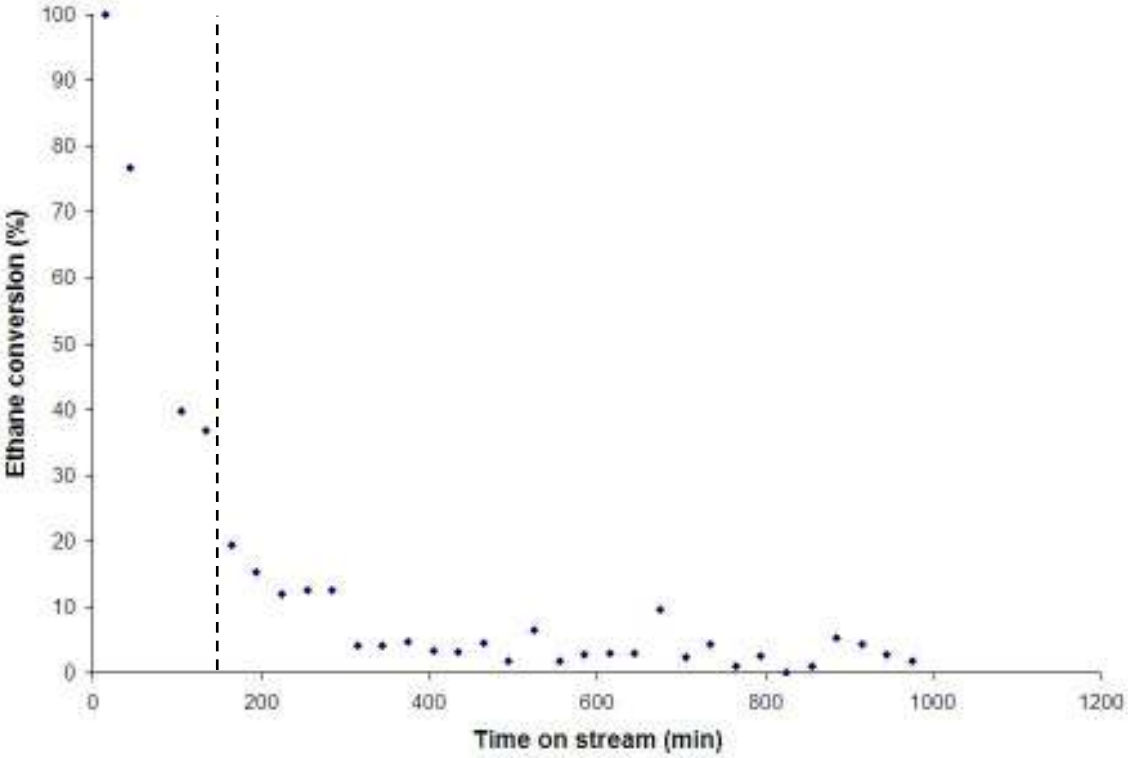

Figure 84 Ethane conversion over Pt/ZrO_2 at 500°C

3.3.1.4.2. Rate of Deactivation

Deactivation of Pt/ZrO_2 was apparent at all reaction temperatures, the rates of deactivation have been plotted and are provided in figures 85 to 87.

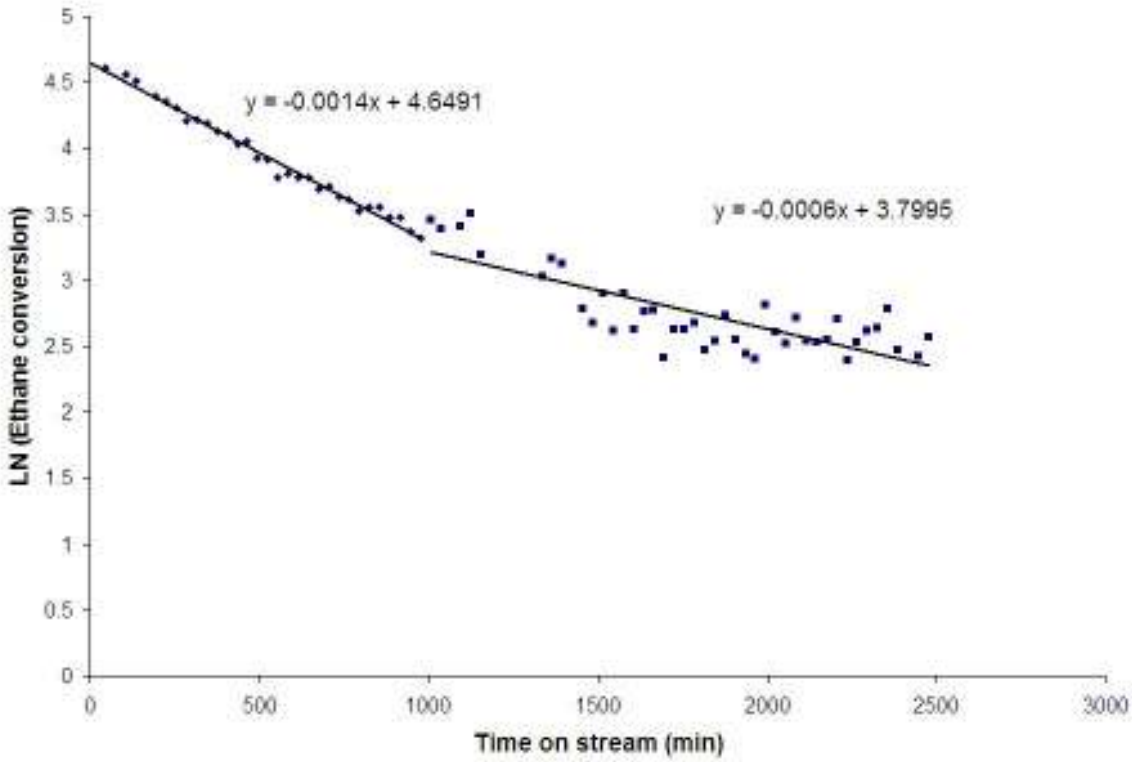

Figure 85 Pt/ZrO_2 deactivation at 600°C

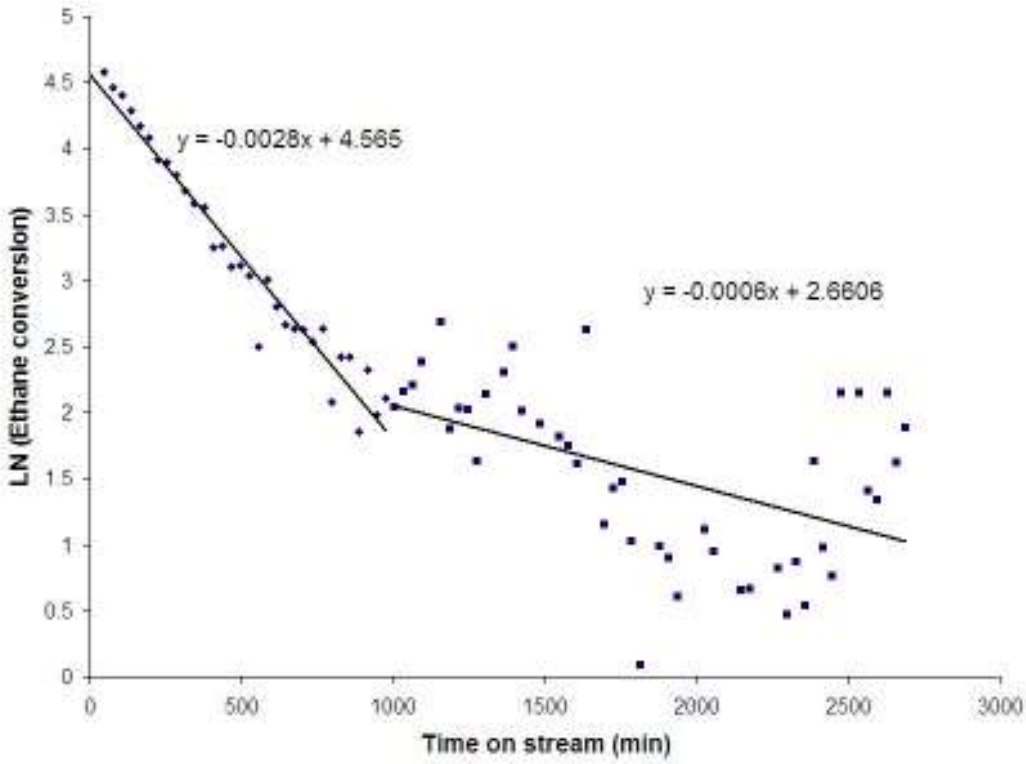

Figure 86 Pt/ZrO_2 deactivation at 550°C

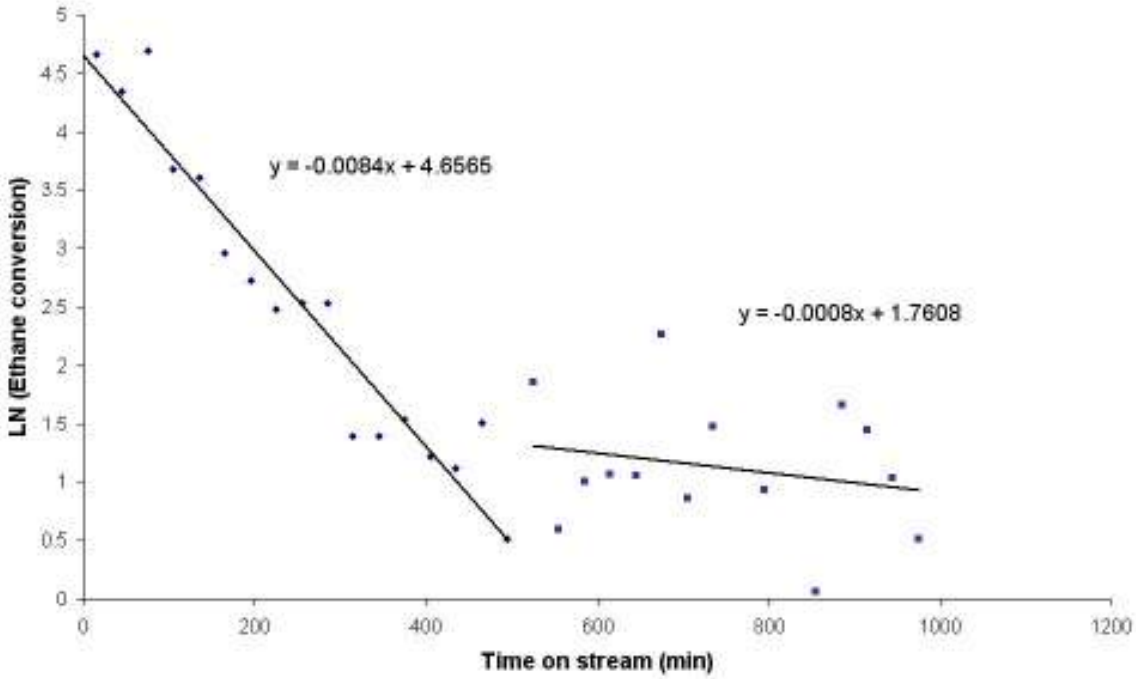

Figure 87 Pt/ZrO_2 deactivation at 500°C

Similar to the deactivation of Rh/Al_2O_3 and Pt/Al_2O_3, the deactivation of Rh/ZrO_2 occurs in two stages: (i) initial rapid deactivation in the first 1000 minutes on stream followed by (ii) a second period of slower deactivation. From the deactivation rate constants it is evident that the rate of deactivation increased when the reaction temperature was lowered.

3.3.1.4.3. Rate of Formation of Products

Over Pt/ZrO_2 the formation H_2 is most significant; however its formation fell considerably at all temperatures, figures 88 to 90. At 600°C it began to decline at approximately 600 minutes on stream, whilst at lower temperatures deactivation was apparent from the beginning of the reaction.

CO_2 was also formed over Pt/ZrO_2. This was most pronounced at 600°C, though its formation also began to decline at 600 minutes on stream.

CH_4 was a minor product of this reaction over Pt/ZrO_2 at 600°C and 550°C, with no CH_4 detected at 500°C.

At reaction temperatures studied, no CO was detected over Pt/ZrO_2.

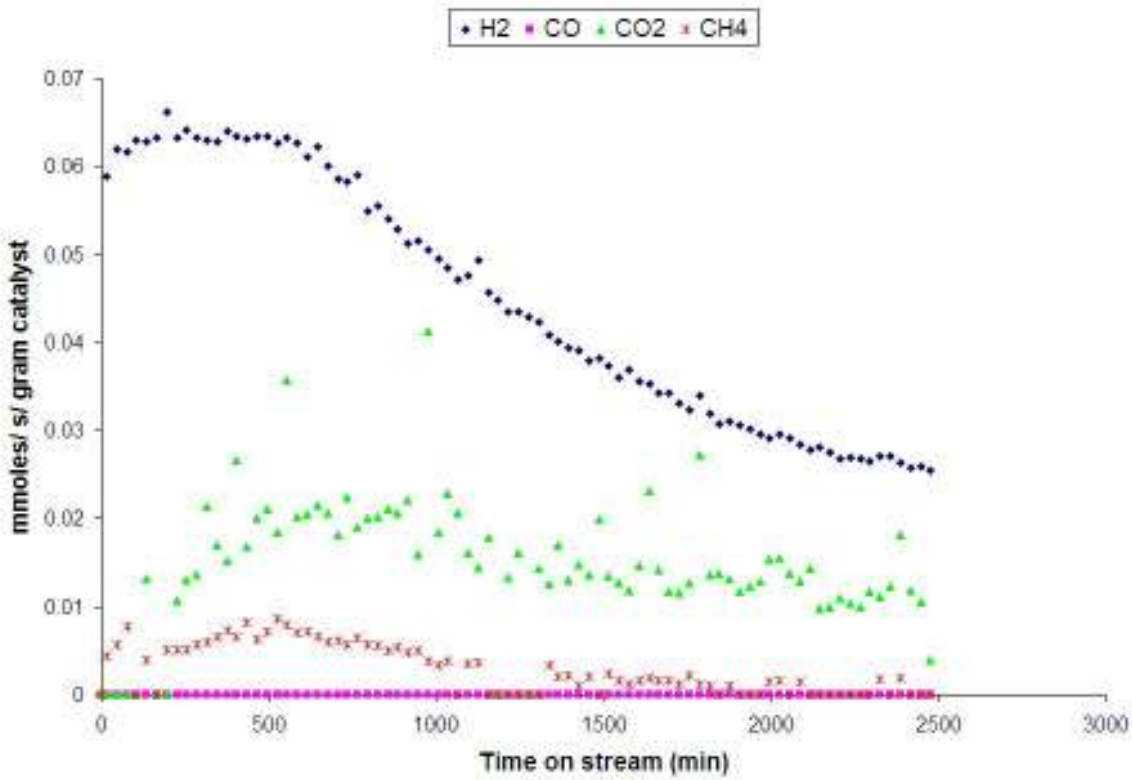

Figure 88 Rate of formation of products over Pt/ZrO_2 at 600°C

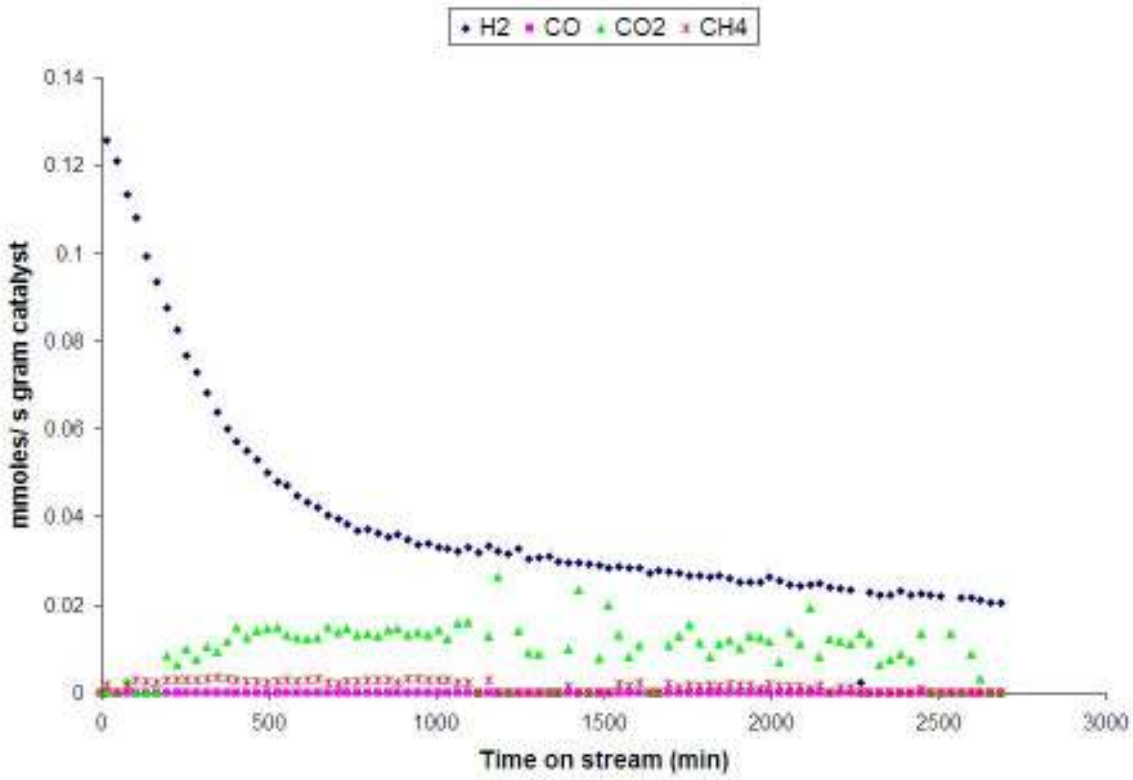

Figure 89 Rate of formation of products over Pt/ZrO_2 at 550°C

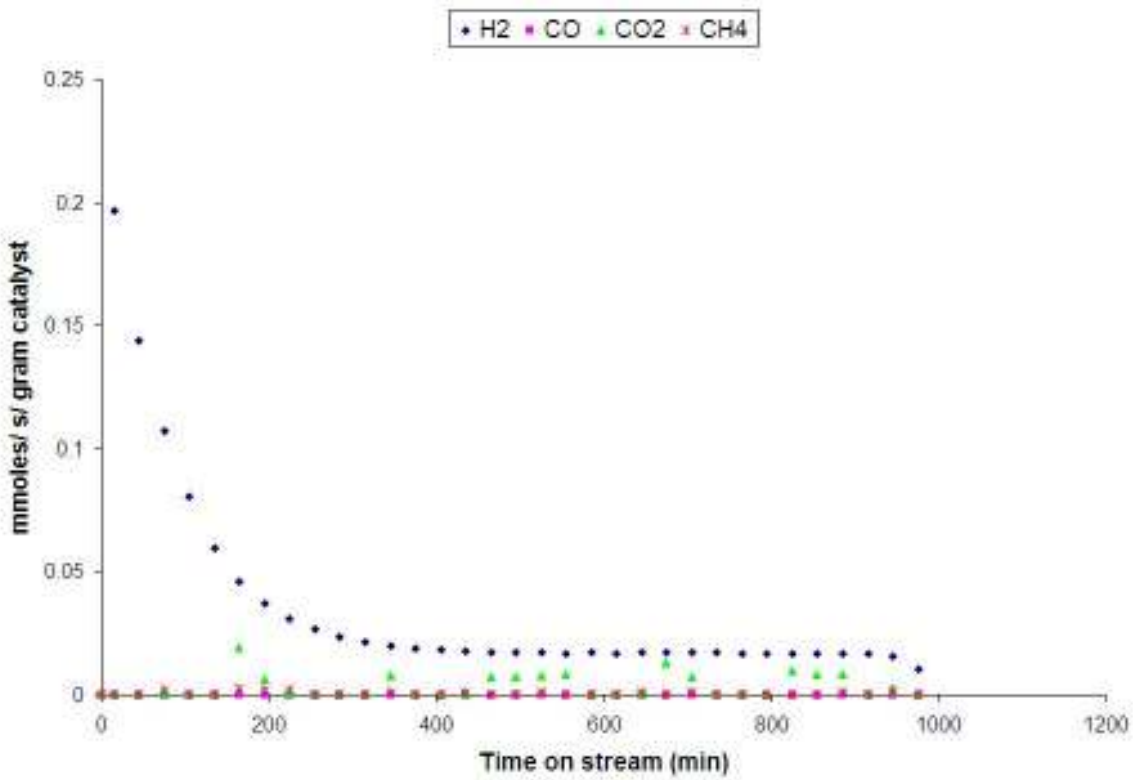

Figure 90 Rate of formation of products over Pt/ZrO_2 at 500°C

3.3.1.4.4. Product Selectivity

The low conversion over Pt/ZrO_2 has resulted in a high selectivity towards H_2 at all three temperatures, figures 91 to 93.

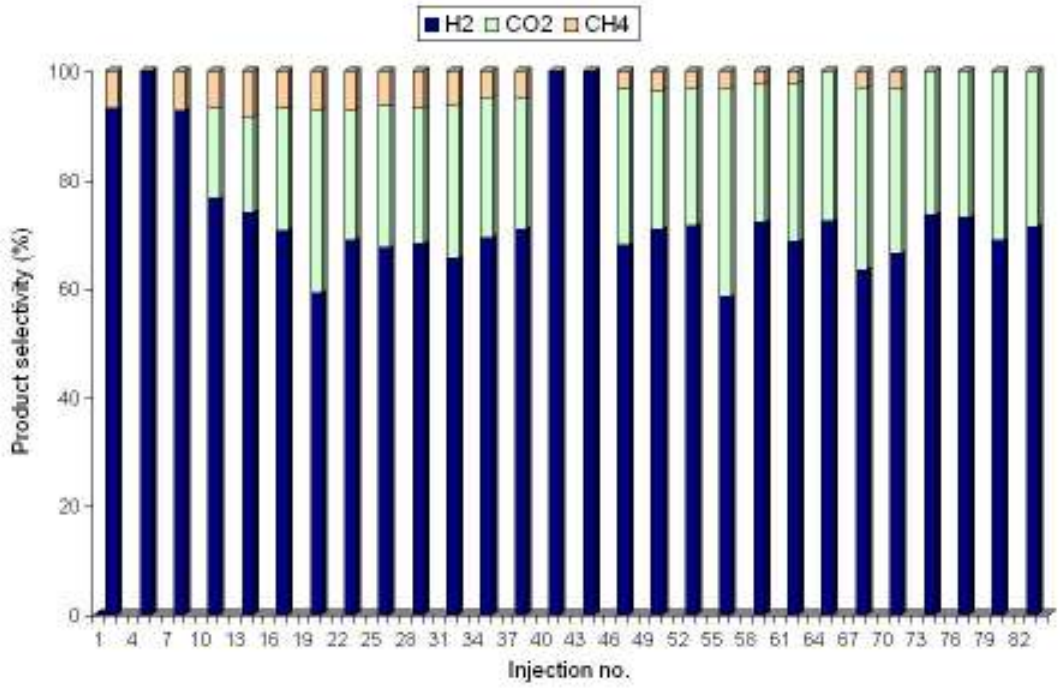

Figure 91 Product selectivity over Pt/ZrO_2 at 600°C

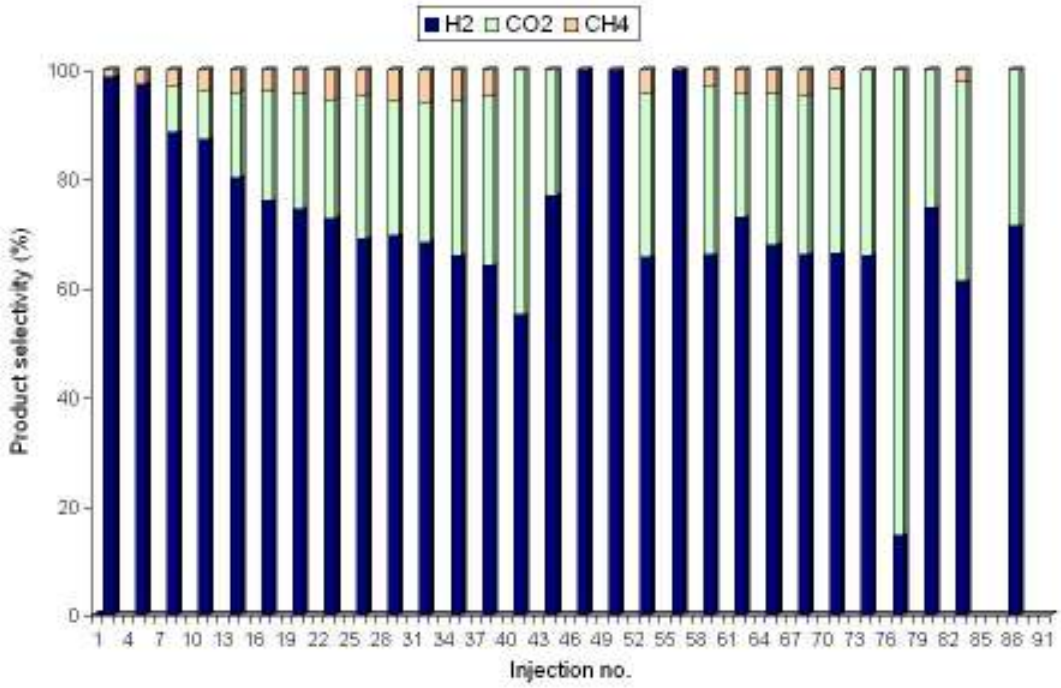

Figure 92 Product selectivity over Pt/ZrO_2 at 550°C

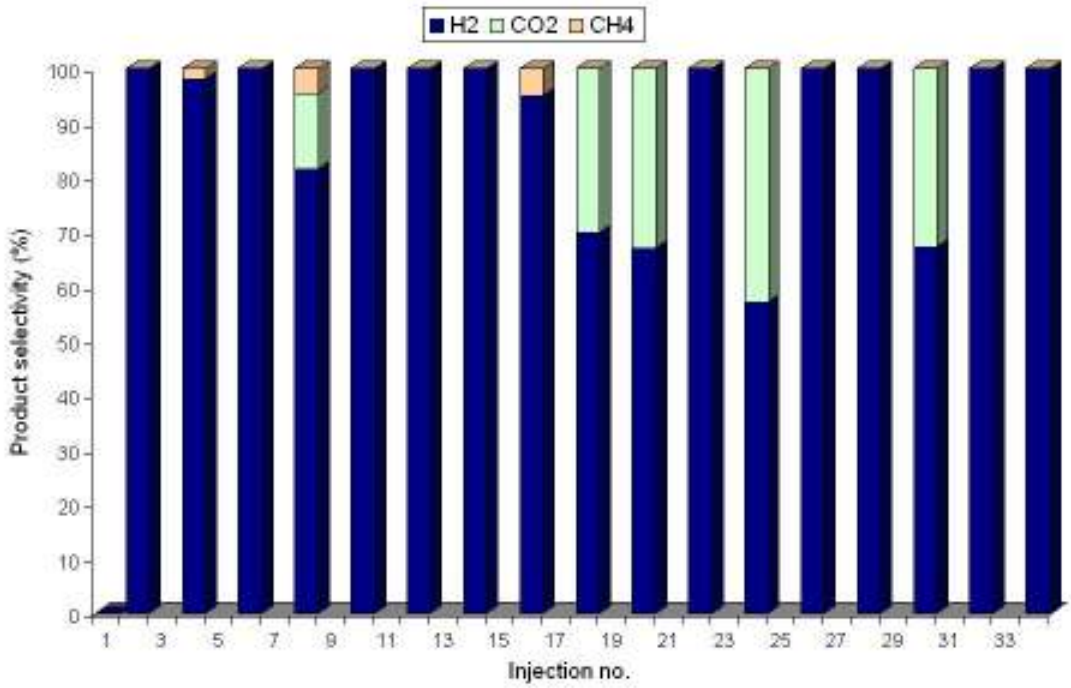

Figure 93 Product selectivity over Pt/ZrO_2 at 500°C

3.3.1.4.5. Carbon Mass Balance

The carbon mass balances for Pt/ZrO_2 at 600°C, 550°C and 500°C, are shown in figures 94 to 96.

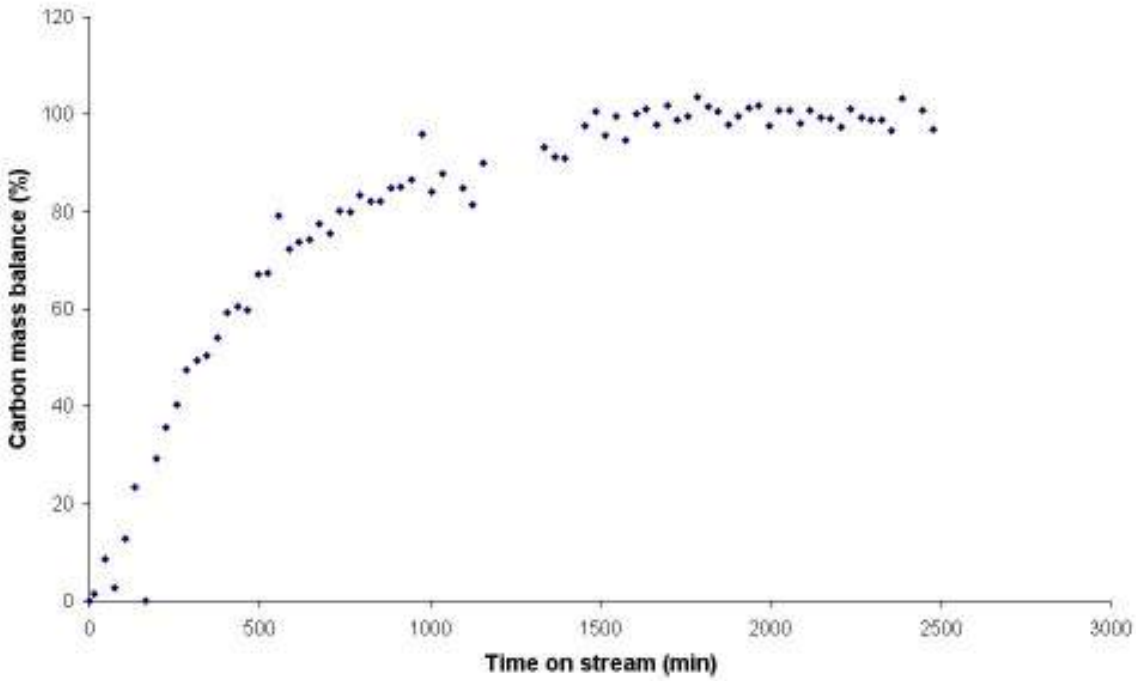

Figure 94 Carbon mass balance for Pt/ZrO_2 at 600°C

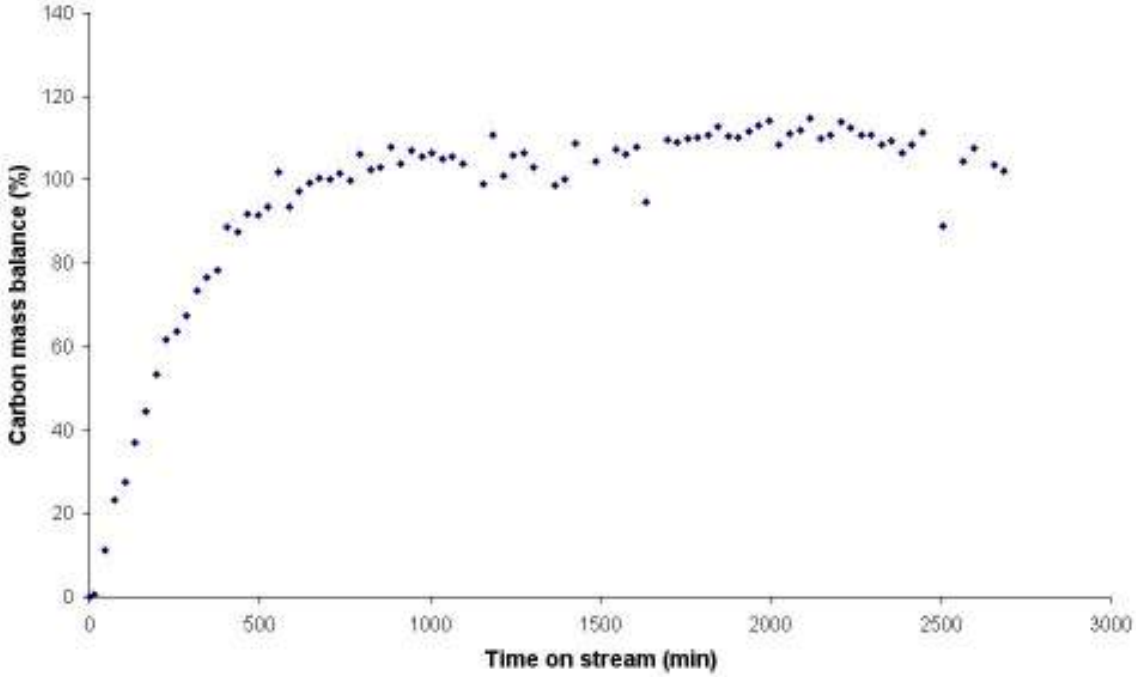

Figure 95 Carbon mass balance for Pt/ZrO_2 at 550°C

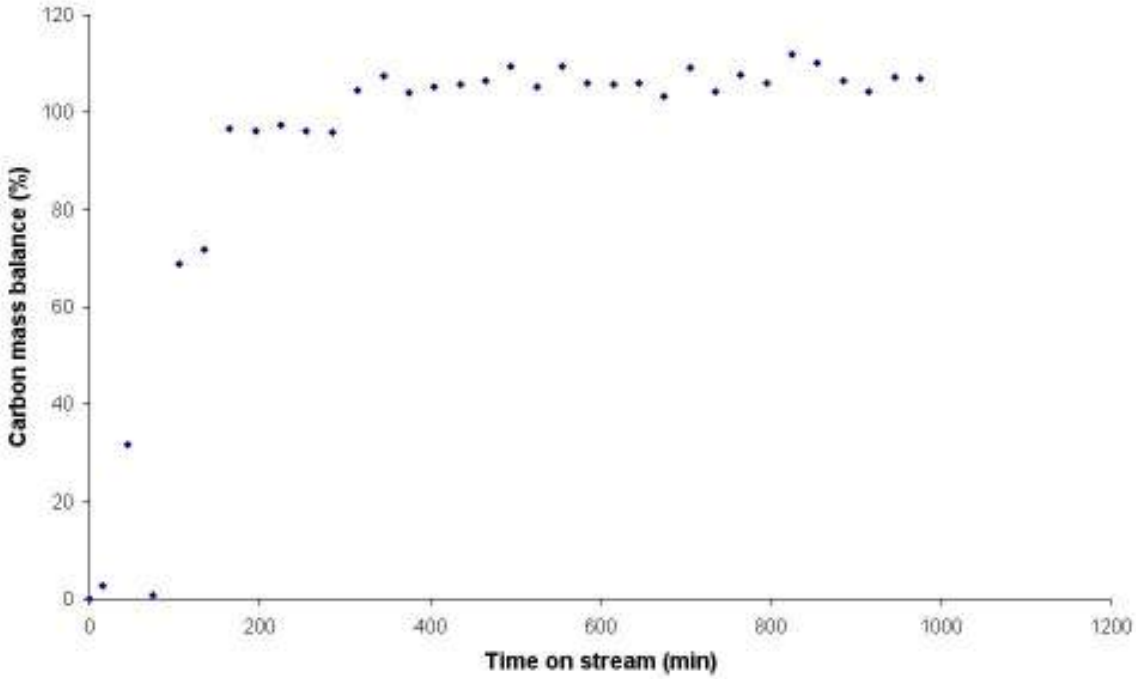

Figure 96 Carbon mass balance for Pt/ZrO_2 at 500°C

3.4. Hydrogen sulphide poisoning

The poisoning experiments were conducted at 600°C, as at this temperature all the catalysts exhibited the highest and most stable conversion of ethane. The catalysts poisoned were Rh/Al_2O_3, Rh/ZrO_2 and Pt/Al_2O_3. Poisoning experiments were not conducted over Pt/ZrO_2, since even at 600°C ethane conversion was not stable.

All the catalysts detailed in this section were poisoned with a hydrogen sulphide solution with a concentration of 11.2ppm. During the testing of the catalysts under poisoning conditions it was found that sulphur was retained by the test unit and could poison a subsequent run. Before each new test the unit was put through the clean up procedure as outlined in the experimental section. Although this did not necessarily bring the catalyst back to non-poisoned activity, overall the production of hydrogen was consistent with non-poisoned rates. As the production of hydrogen is the principle role for steam reforming units this was considered acceptable for comparable purposes.

3.4.1. Rh/Al_2O_3

The feed water was exchanged for a pre-prepared hydrogen sulphide solution at 1365 minutes on stream, to introduce sulphur into the system. At 1725 minutes on stream, after 6 hours of poisoning, the feed was changed back to pure water.

3.4.1.1. Ethane conversion

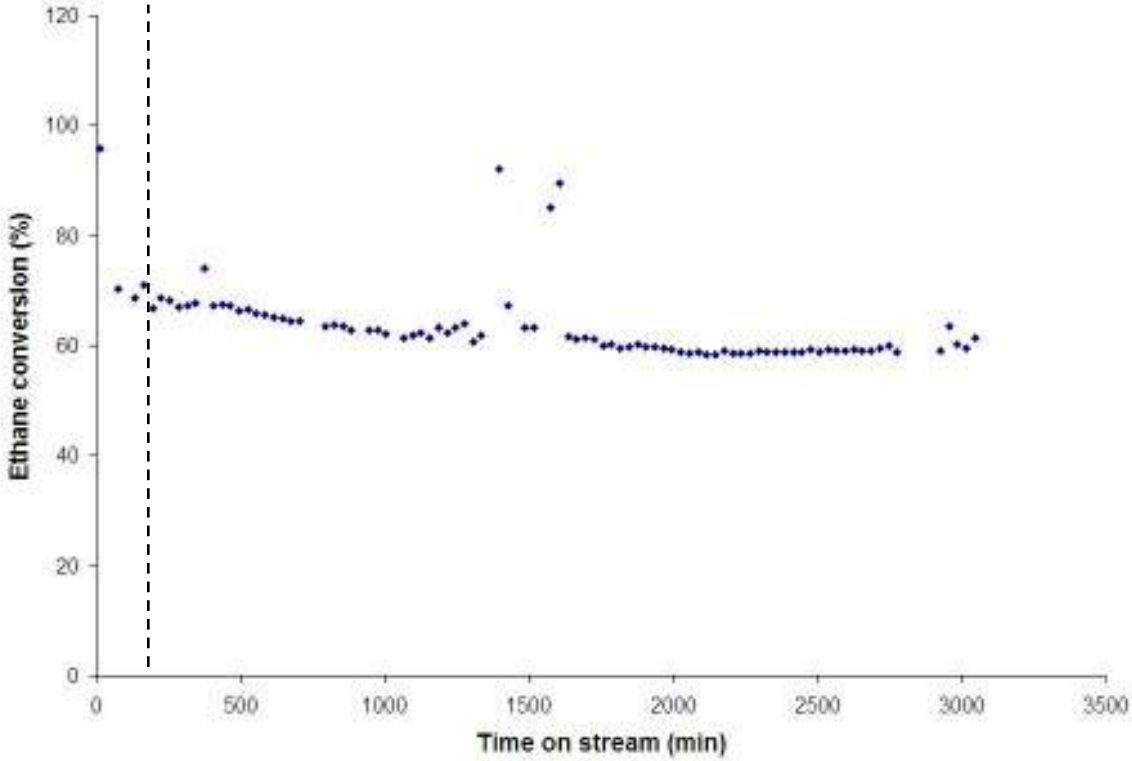

Figure 97 Ethane conversion over Rh/Al_2O_3 at 600°C

The conversion of ethane was stable and met the criteria for test. At the point when sulphur is introduced, the system appears to de-stabilise, evident from the outliers in figure 97. However it quickly stabilises and the recent influx of sulphur seems to have had very little effect on the conversion of ethane.

3.4.1.2. Rate of Deactivation

From the conversion graph two periods of deactivation were identified, one occurred prior to the introduction of the sulphur solution (Pre-poison) and the other after (Post poison). Assuming first order, the deactivation rates are plotted below.

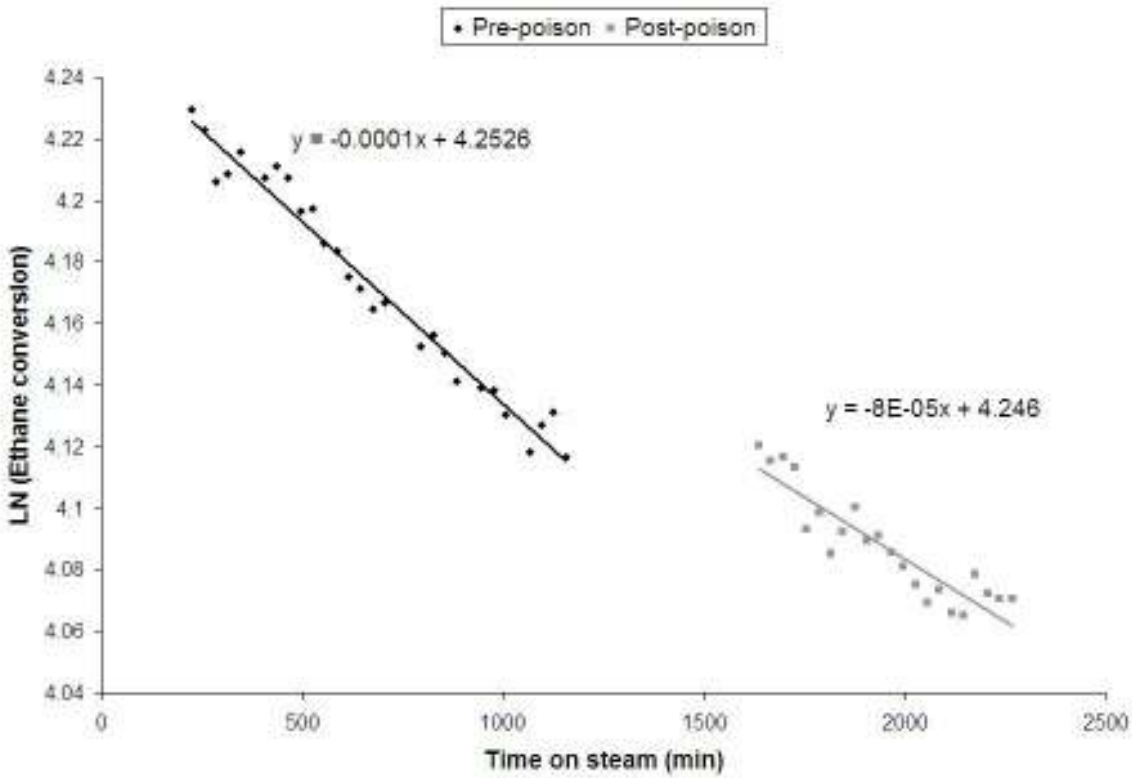

Figure 98 Rh/Al_2O_3 deactivation

3.4.1.3. Rate of formation of products

The rate of formation of H_2, CO and CO_2, figure 100, are all relatively stable prior to poisoning, in accordance with the results obtained from section 3.3.1.1.3. However the formation of CH_4 has clearly been lowered. In the previous standard run, before any sulphur had been in the reactor, CH_4 was forming at similar levels to H_2. Also CH_4 formation begins to deactivate at 500 minutes on stream, no deactivation was evident on the standard run.

It is therefore likely that the deactivation of the rate of formation of CH_4 is responsible for the deactivation of ethane conversion prior to poisoning.

Once the poison is introduced, deactivation of the formation of all the products occurs. On removal of the poison, deactivation ceases and H_2, CO and CO_2 begin to recover. CH_4 formation continues to deactivate.

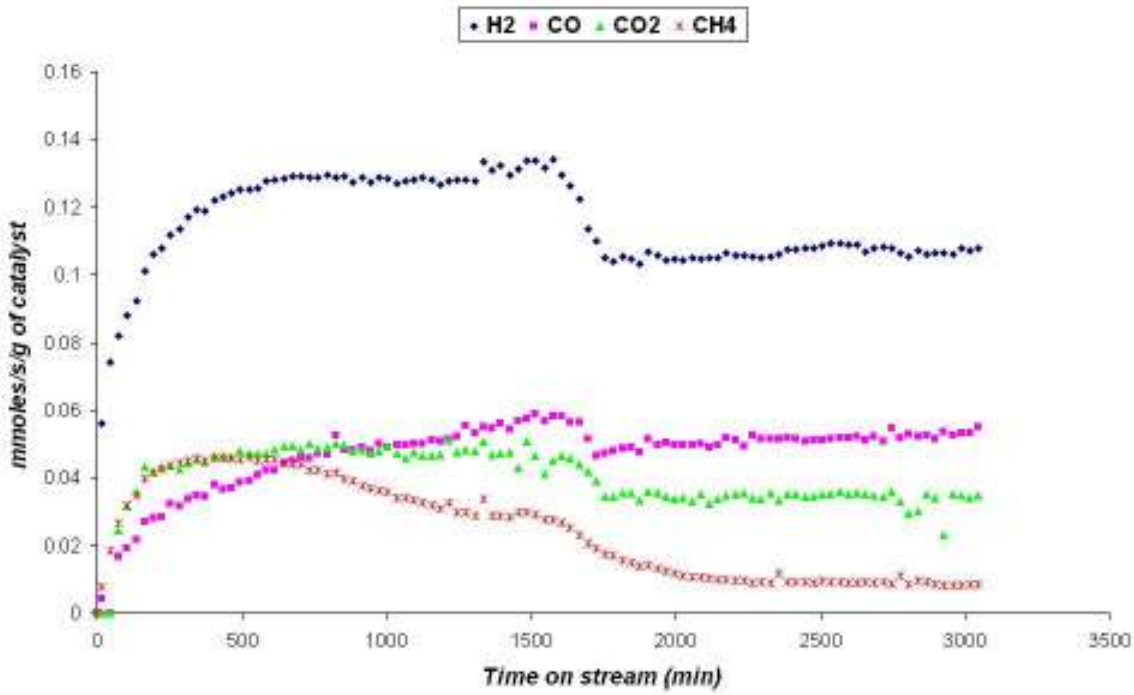

Figure 99 Rate of formation of products over Rh/Al_2O_3

3.4.1.3.1. Deactivation of Products

The rates of deactivation of the four gaseous products were plotted, assuming first order, and the deactivation rate constants obtained. These are tabulated below, table 71.

Table 71 Deactivation rate constants for the formation of gaseous products

Product	H_2	CO	CO_2	CH_4
Deactivation rate constant ($-1x10^{-4}$)	13	12	16	26

H_2, CO and CO_2 all deactivate at comparable rates, whilst CH_4 deactivates at approximately double the rate.

3.4.1.4. Product selectivity

H_2S was introduced between injections 46 and 59, see figure 100. Selectivity towards H_2 and CO_2 remains fairly constant throughout the reaction. Selectivity

towards CH_4 decreases significantly from the beginning of the reaction, in accordance with the deactivation occurring pre-poison. Whilst there is a marked increase in selectivity towards CO during the reaction.

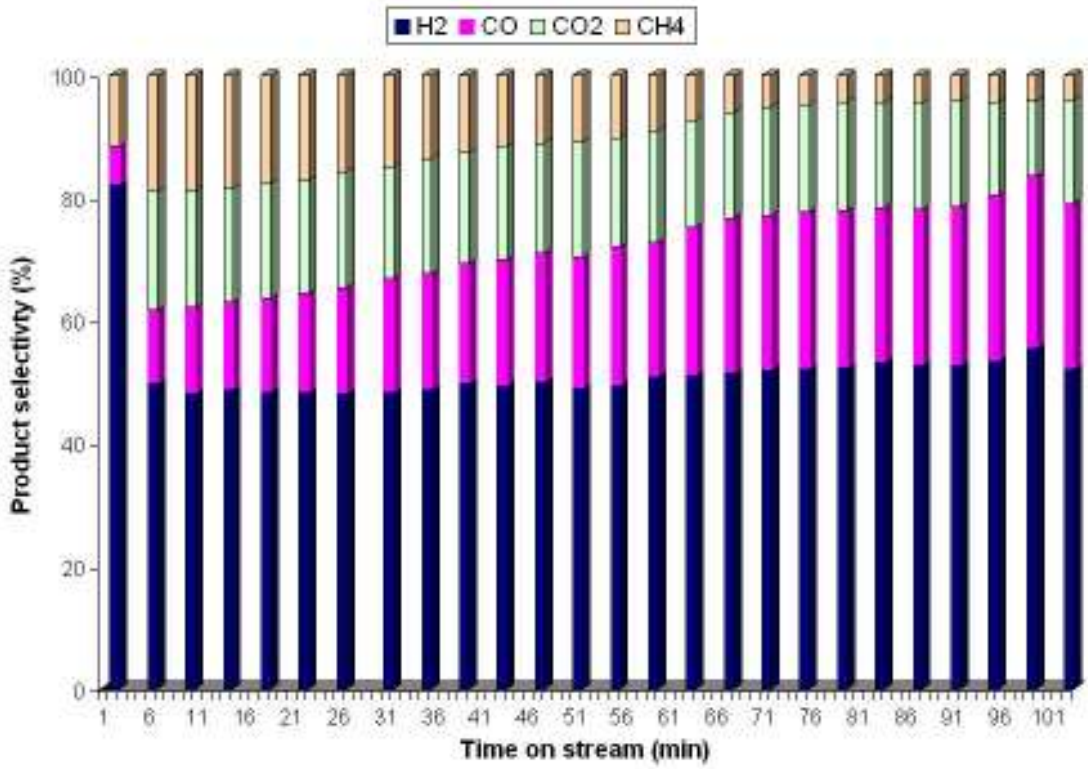

Figure 100 Product selectivity over Rh/Al_2O_3

3.4.1.5. Carbon Mass Balance

The carbon mass balance, figure 101, shows that poisoning has increased the percentage of carbon unaccounted for, which is presumably being deposited on the catalyst. This also accounts for the appearance of the ethane conversion, where it appeared sulphur had very little effect, despite there being clear deactivation of the rate of formation of products. Ethane is still being converted but rather than being converted to desirable products, it is being converted surface carbon.

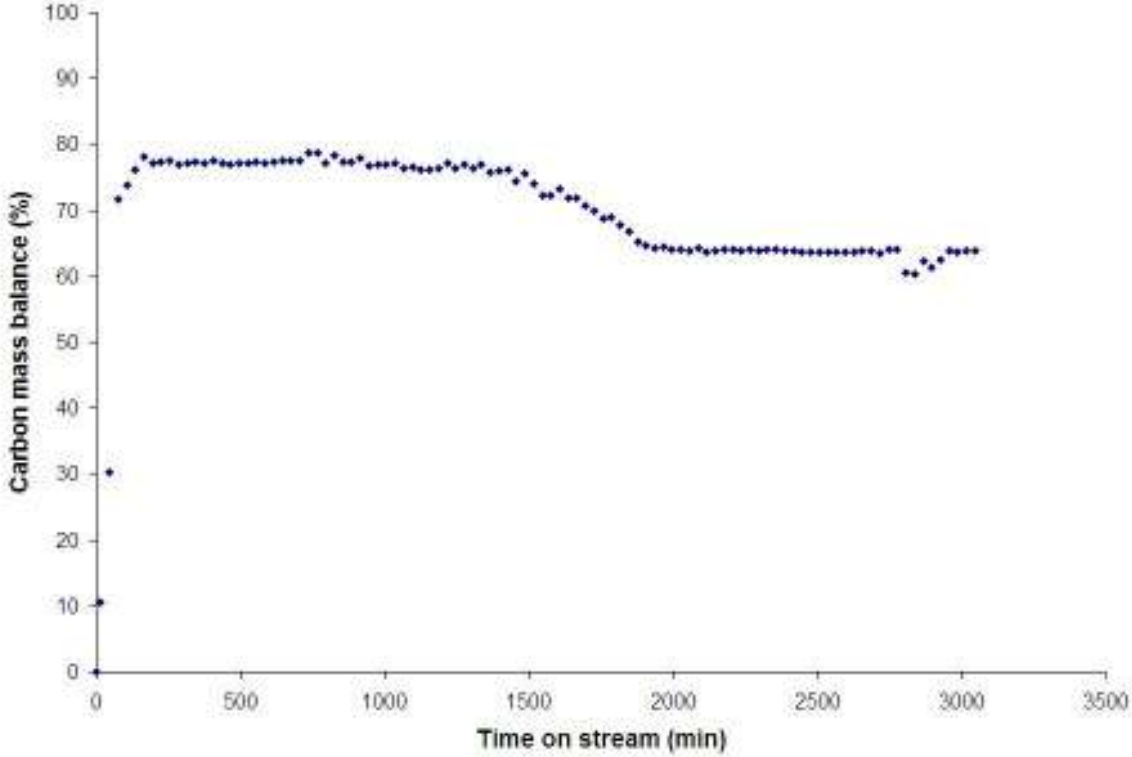

Figure 101 Carbon mass balance for Rh/Al_2O_3 where reaction was poisoned at 1365 minutes on stream

3.4.2. Pt/Al_2O_3

The feed water was exchanged for a pre-prepared hydrogen sulphide solution at 1215 minutes on stream, to introduce sulphur into the system. At 1635 minutes on stream, after 7 hours of poisoning, the feed was changed back to pure water.

3.4.2.1. Ethane Conversion

Deactivation of the catalyst occurred immediately from the beginning of the reaction, and started to slow down at 1300 minutes on stream, figure 102. This is comparable to the conversion of ethane in the standard run which fell to 40% in the first 1300 minutes on stream. The rates of production of all products were also comparable to our standard run at 600°C.

A second period of deactivation occurred from 1500 minutes on stream, at which point the poison had been introduced.

On removal of the poison from feed, deactivation continues but at a slower rate, with conversion ultimately decreasing to approximately 10%.

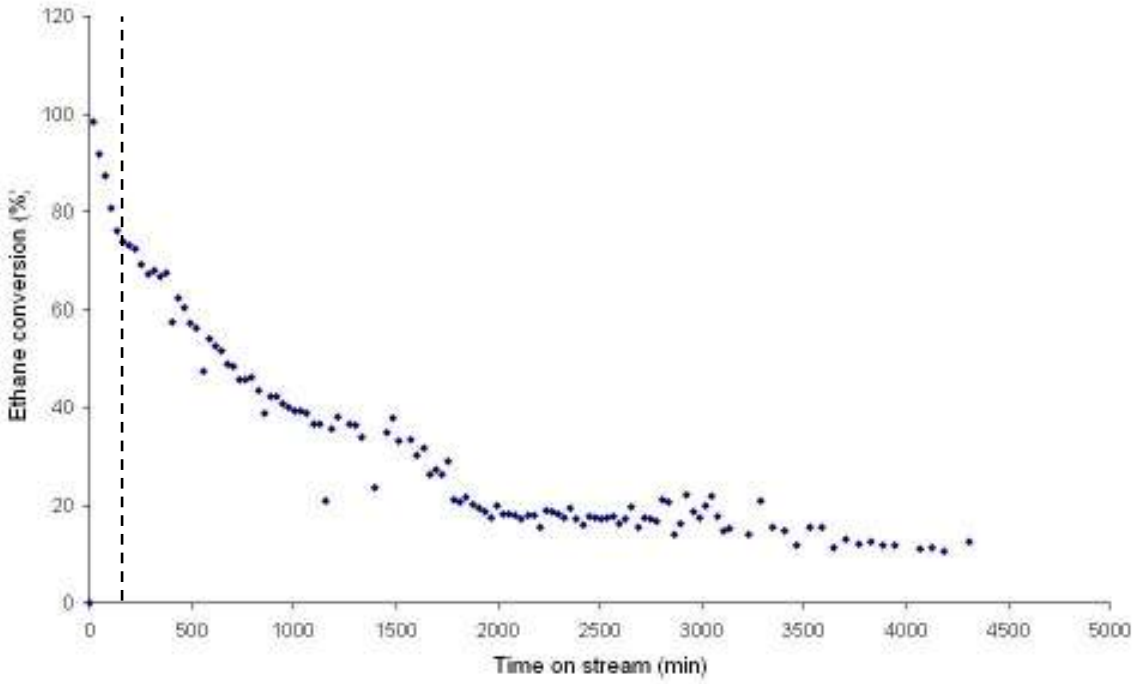

Figure 102 Ethane conversion over Pt/Al_2O_3 at 600°C

3.4.2.2. Rates of Deactivation

During poisoning the rate of deactivation increased to double that prior to poisoning, figure 103. On removal of H_2S the deactivation rate is reduced considerably.

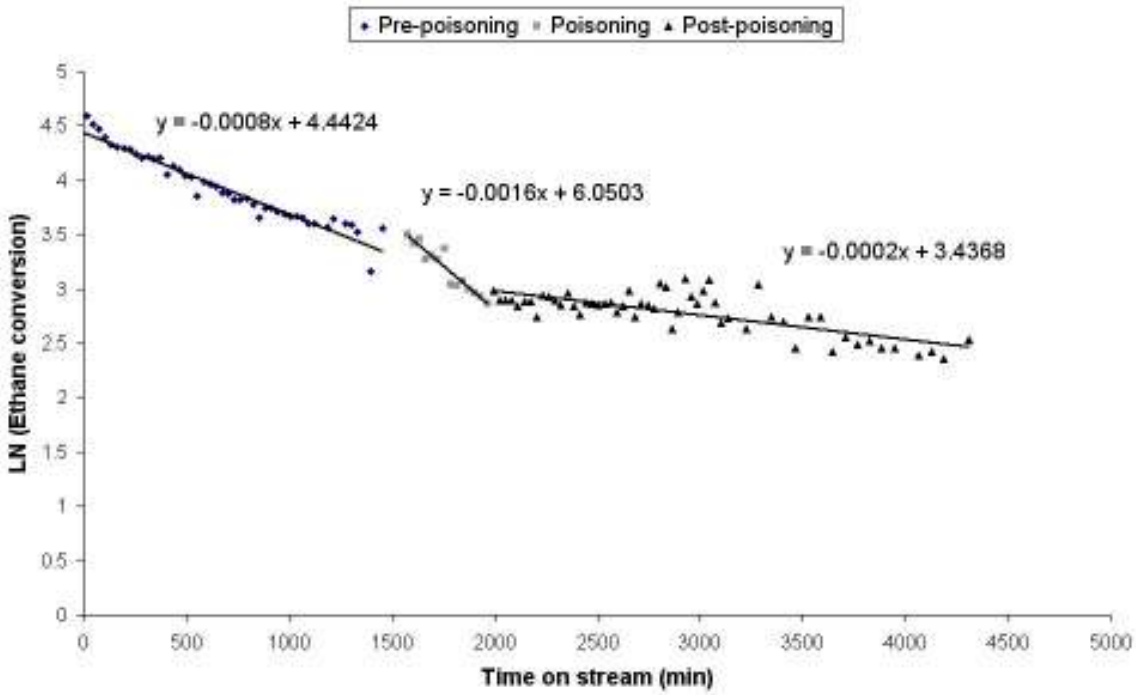

Figure 103 Catalyst deactivation of Pt/Al_2O_3 at 600°C

3.4.2.3. Rate of formation of Products

Prior to poisoning H_2, CO, CO_2 and CH_4 all form at similar levels to the standard run at 600°C in section 3.3.1.2.3.

During poisoning deactivation of H_2, CH_4 and CO_2 is clearly evident, whilst the formation of CO appears unaffected, figure 104.

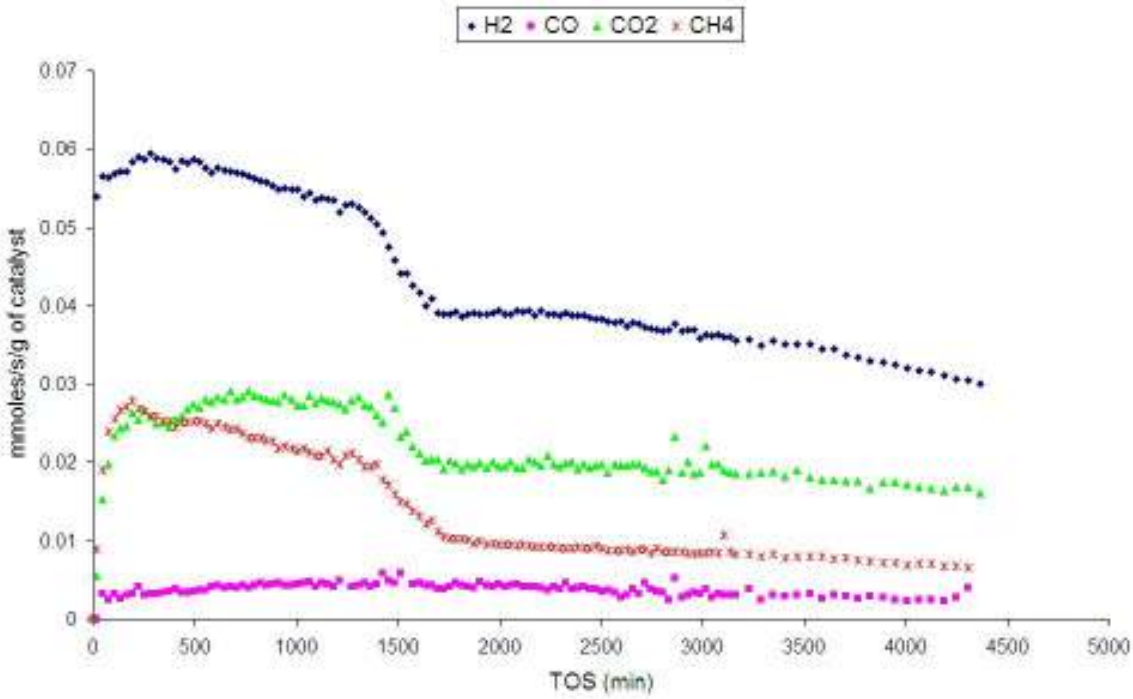

Figure 104 Rate of formation of products over Pt/Al_2O_3

3.4.2.4. Deactivation of Products

The rates of deactivation of the four gaseous products were plotted, assuming first order, and the deactivation rate constants obtained. These are tabulated below, table 72.

Table 72 Deactivation rate constants for the formation of gaseous products

Product	H_2	CO	CO_2	CH_4
Deactivation rate constant ($-1x10^{-4}$)	8	2	9	16

The formation of H_2 and CO_2 deactivate at similar rates. CH_4 formation deactivates at double this rate, as seen over Rh/Al_2O_3. However, different from Rh/Al_2O_3, over Pt/Al_2O_3 there is very little deactivation of CO formation.

3.4.2.5. Product Selectivity

H_2S was introduced between injections 41 and 55, see figure 105. From the beginning of the reaction, selectivity towards CH_4 decreases and selectivity towards CO_2 increases slightly. Product selectivity stabilises from injection 66. Selectivity towards H_2 remained relatively constant throughout the reaction.

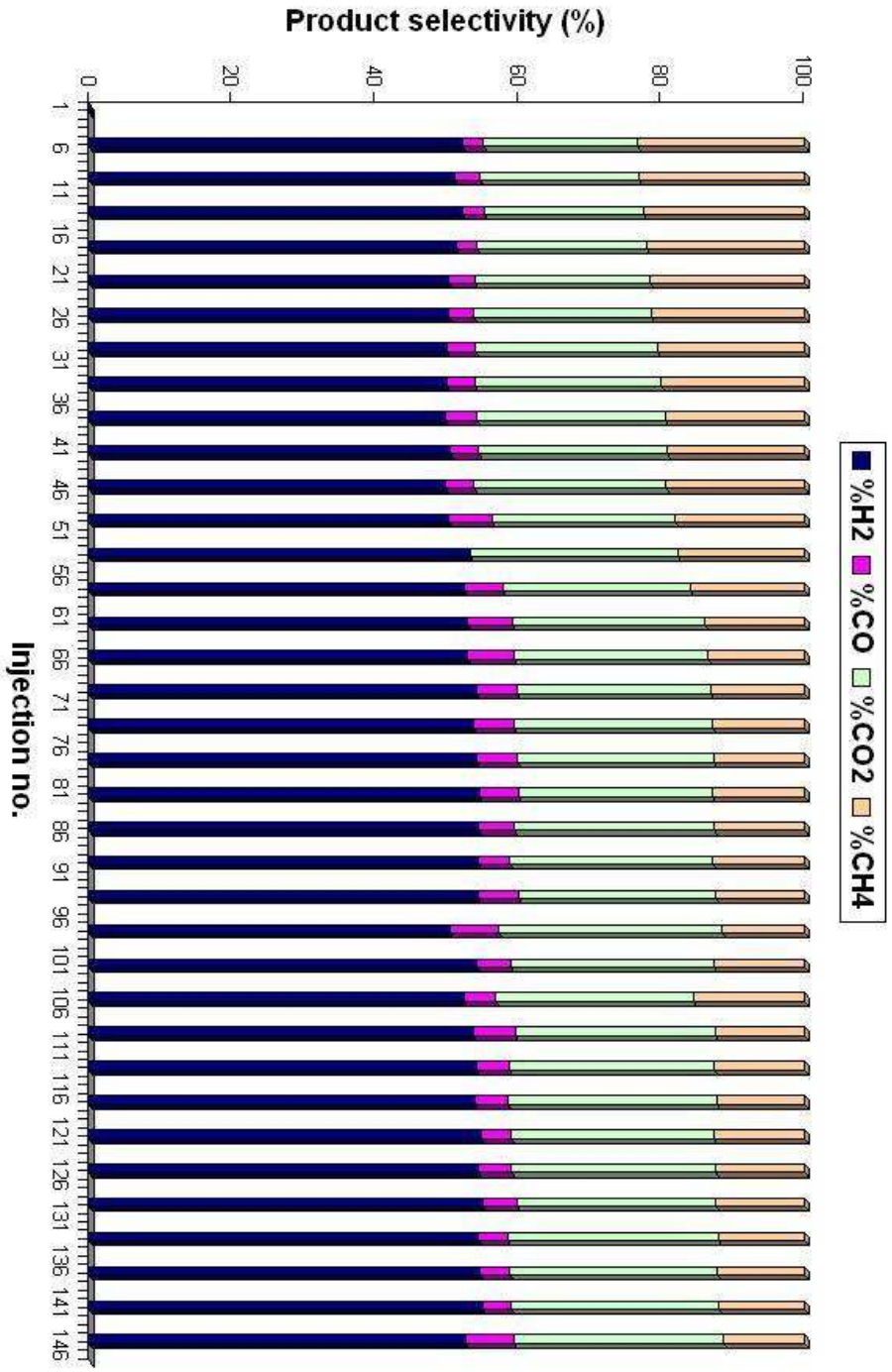

Figure 105 Product selectivity over Pt/Al_2O_3

3.4.2.6. Carbon Mass Balance

The carbon mass balance for poisoned Pt/Al_2O_3 is shown in figure 106.

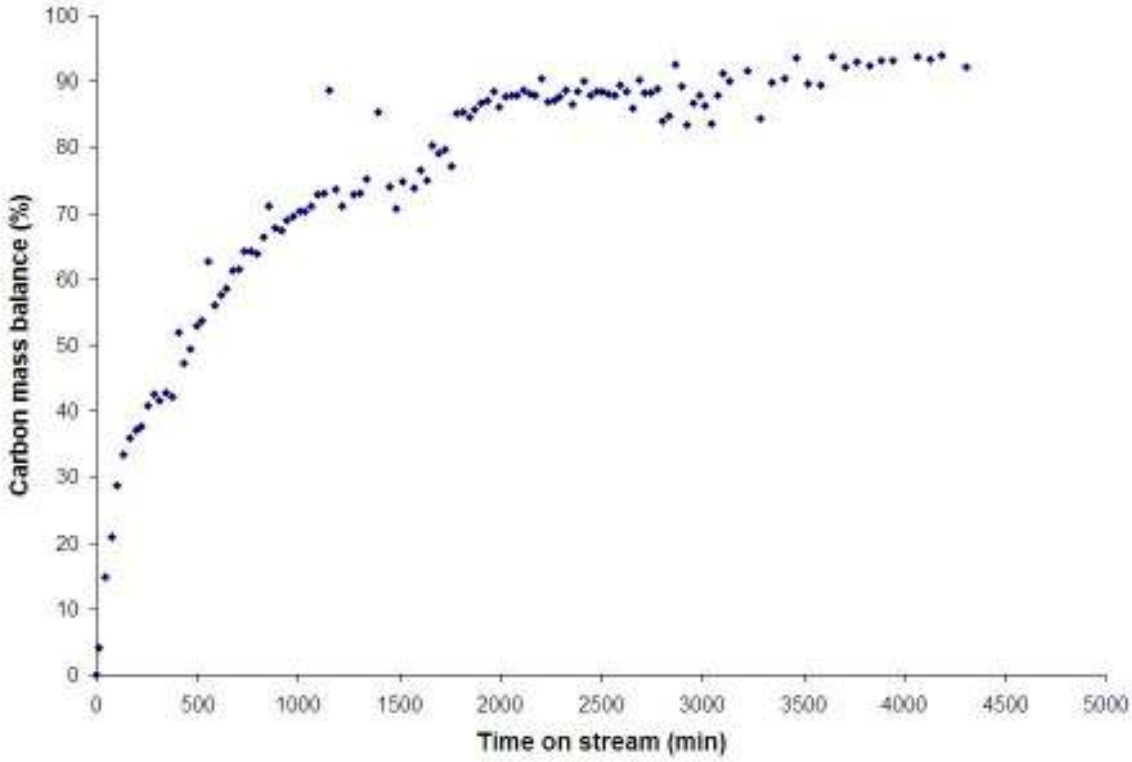

Figure 106 Carbon mass balance for Pt/Al_2O_3 where reaction was poisoned at 1215 minutes on stream.

3.4.3. Rh/ZrO_2

The feed water was exchanged for a pre-prepared hydrogen sulphide solution at 2745 minutes on stream, to introduce sulphur into the system. At 3105 minutes on stream, after 6 hours of poisoning, the feed was changed back to pure water.

3.4.3.1. Ethane Conversion

Within the first 1000 minutes on stream the catalyst deactivates and conversion stabilises out at 75%, figure 107. At approximately 1200 minutes on stream a second period of deactivation takes place, which correlates with a period of deactivation in the standard run in section 3.3.1.3.1.

The standard run does differ somewhat: no deactivation occurred at the beginning; conversion remained at 100% for the first 1000 minutes on stream. Also, the period of deactivation at 1200 minutes is more extensive in the standard run. Ultimately, conversion stabilised at 70%, whilst in the standard run conversion stabilised at 75%; however the conversion is stable when the poison is introduced.

The initial deactivation and lowered conversion are mostly likely the result of residual sulphur in the reactor system from a prior poisoning experiment.

It appears that the conversion of ethane is largely unaffected by the introduction of H_2S at 2745 minutes on stream.

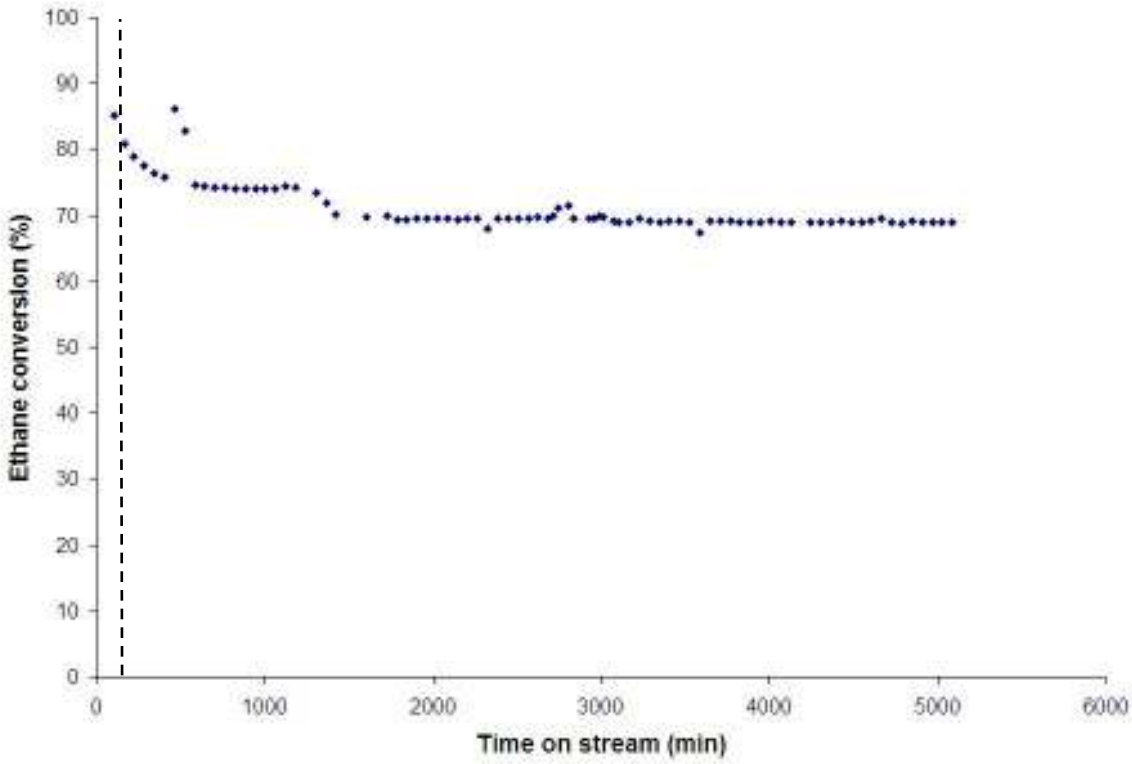

Figure 107 Ethane conversion over Rh/ZrO_2

3.4.3.2. Rate of Deactivation

Two periods of deactivation were identified, both occurred prior to the introduction of H_2S, figure 108. The first period, thought to be the result of left-over sulphur in the rig, is termed residual sulphur deactivation. The second period occurred at approximately the same time on stream as in the standard run and is termed 'normal' deactivation period.

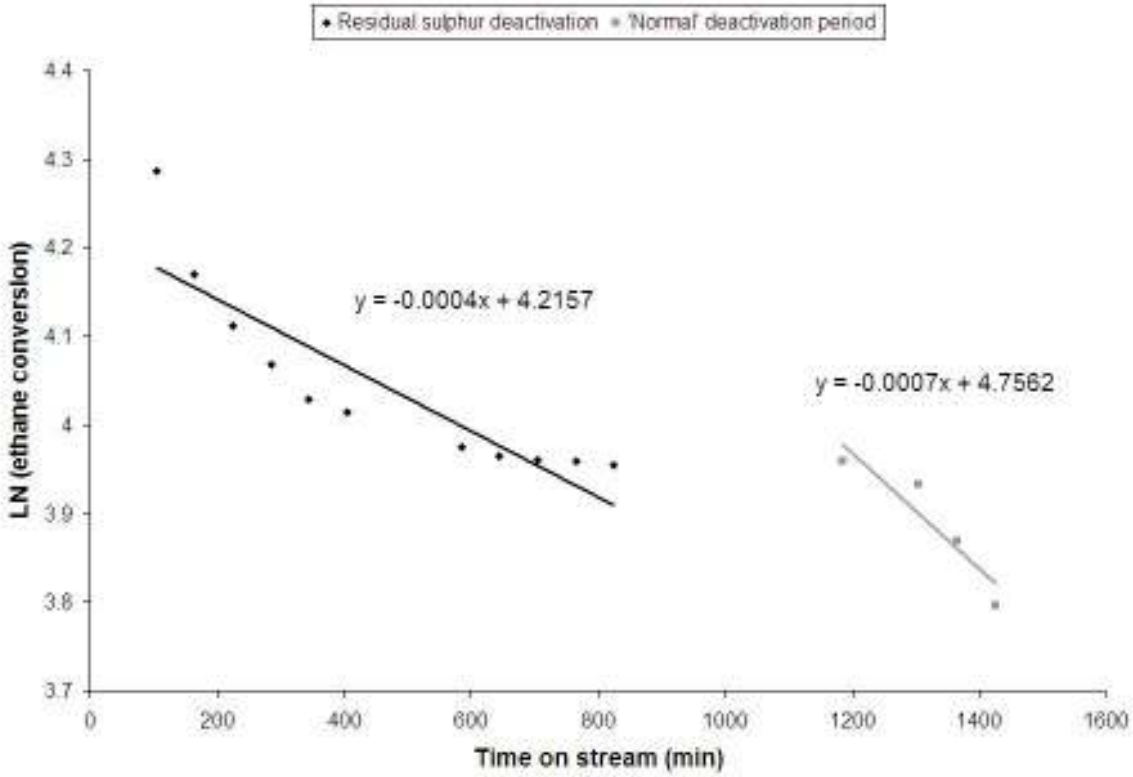

Figure 108 Rh/ZrO_2 deactivation

The deactivation due to residual sulphur is clearly a curve as opposed to a straight line, therefore is not a first order deactivation.

3.4.3.3. Rate of Formation of Products

The rate of formation of H_2 levelled off at 0.18, seen in figure 109, the same result was obtained in the standard run, indicating the residual sulphur had not affected H_2 formation. However, when H_2S was introduced deactivation was apparent and on removal of the poison the catalyst recovered somewhat.

The rate of formation of CH_4 showed great differences from the standard reaction. In the standard reaction CH_4 formation reached 0.4 before deactivating and levelling off 0.1. Here, formation of CH_4 was very low, stabilising at only 0.01. The retarded CH_4 formation, probably due to residual sulphur, has most likely resulted in the lower ethane conversion.

CO_2 formed at a similar rate as in the standard reaction. No deactivation was detected as a result of poisoning.

The formation of CO reached a higher rated than detected in the standard reaction. In the standard run the rate reached a maximum of ~0.03 at 1500 minutes on stream, whilst here the rate reached ~0.05 at 1000 minutes. Deactivation of CO formation began from 1000 minutes on stream, before the introduction of H_2S, and continued to deactivate throughout the reaction.

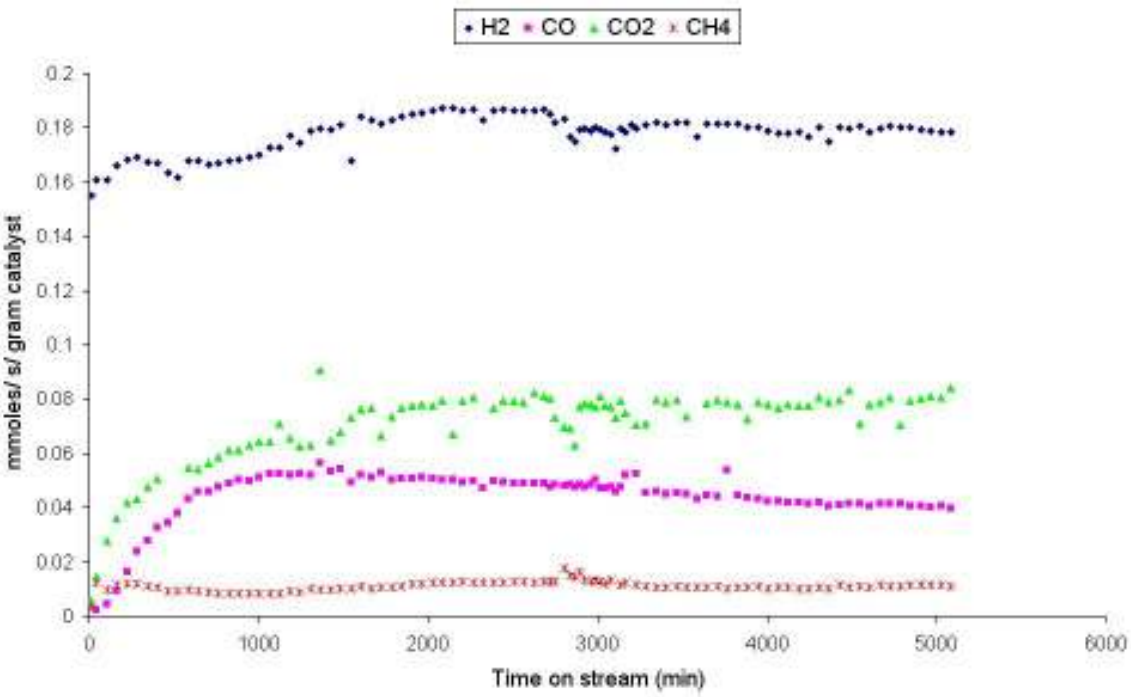

Figure 109 Rate of formation of products over Rh/ZrO_2

3.4.3.4. Deactivation of Products

The rates of deactivation of the four gaseous products were plotted, assuming first order, and the deactivation rate constants obtained. These are tabulated below, table 73.

Table 73Deactivation rate constants for the formation of gaseous products

Product	H_2	CO	CO_2	CH_4
Deactivation rate constant ($-1x10^{-4}$)	3	0	0	9

Both the formation of H_2 and CH_4 deactivate, with CH_4 deactivating at a faster rate. Although the formation of CO deactivates, the deactivation begins before H_2S is introduced and therefore is not attributed to poisoning. No deactivation was detected with respect to CO_2.

3.4.3.5. Product Selectivity

H_2S was introduced between injections 92 and 104, see figure 110. Very little change occurs with regard to product selectivity during the course of the reaction.

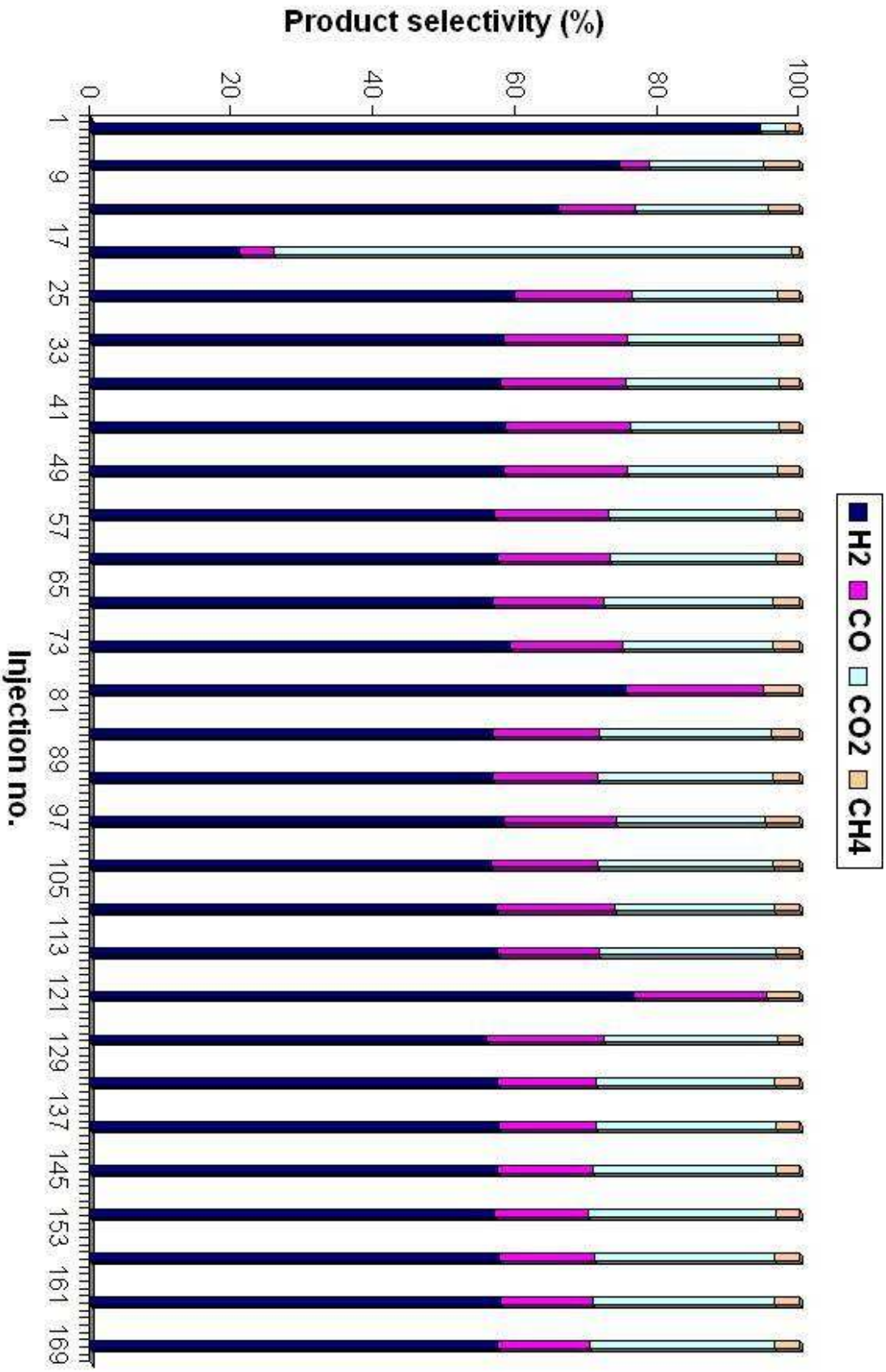

Figure 110 Product selectivity over Rh/ZrO_2

3.4.3.6. Carbon Mass balance

The carbon mass balance for poisoned Rh/ZrO_2 is shown in figure 111.

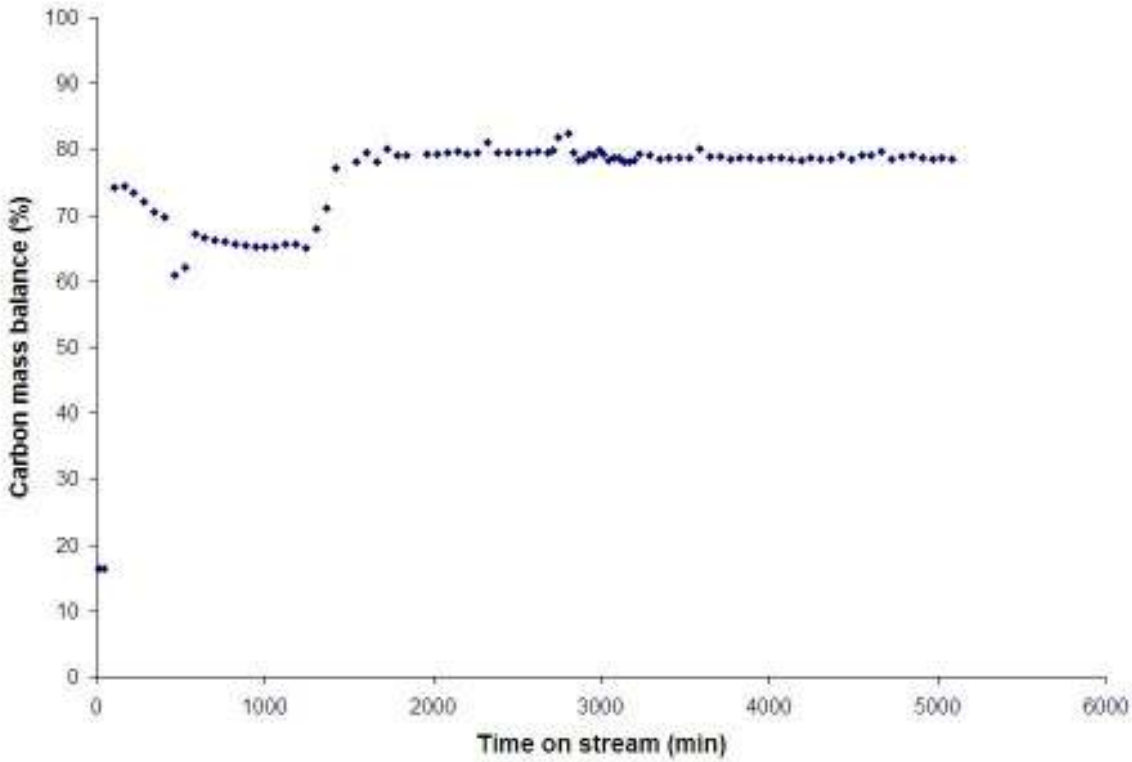

Figure 111 Carbon mass balance for Rh/ZrO_2 where reaction was poisoned at 2745 minutes on stream

3.5. Methanthiol Poisoning

3.5.1. Rh/Al_2O_3

The feed water was exchanged for a pre-prepared hydrogen sulphide solution at 1113 minutes on stream, to introduce sulphur into the system. At 1473 minutes on stream, after 6 hours of poisoning, the feed was changed back to pure water.

3.5.1.1. Ethane Conversion

In the first 1200 minutes on stream Rh/Al_2O_3 exhibits high and relatively stable conversion, figure 112. Once methanethiol is introduced deactivation proceeds, at a fast rate, until the catalyst appears to be fully deactivated. When the feed is switched back to pure water the catalyst regains some activity, with conversion levelling off at ~30%.

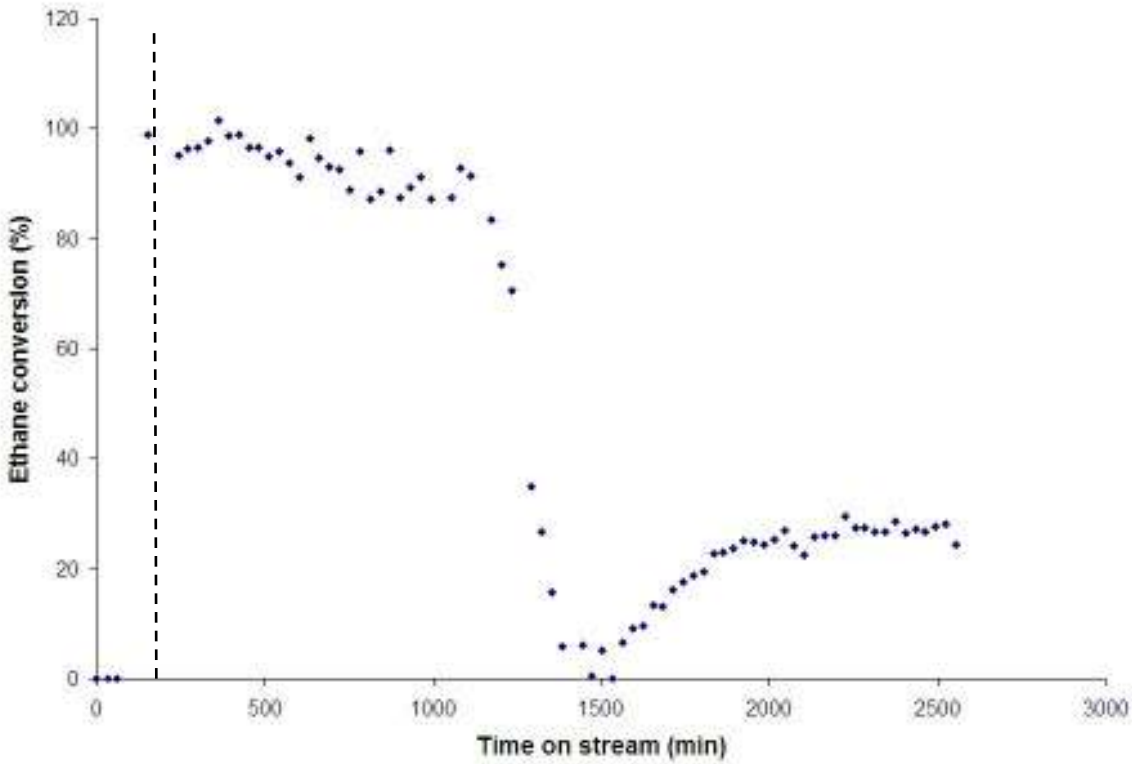

Figure 112 Ethane conversion over Rh/Al_2O_3

3.5.1.2. Rate of Deactivation

Rh/Al_2O_3 deactivates slowly before methanethiol is introduced, but once the poison is introduced deactivation proceeds rapidly. These two periods of deactivation are plotted in figure 113, assuming first order deactivation.

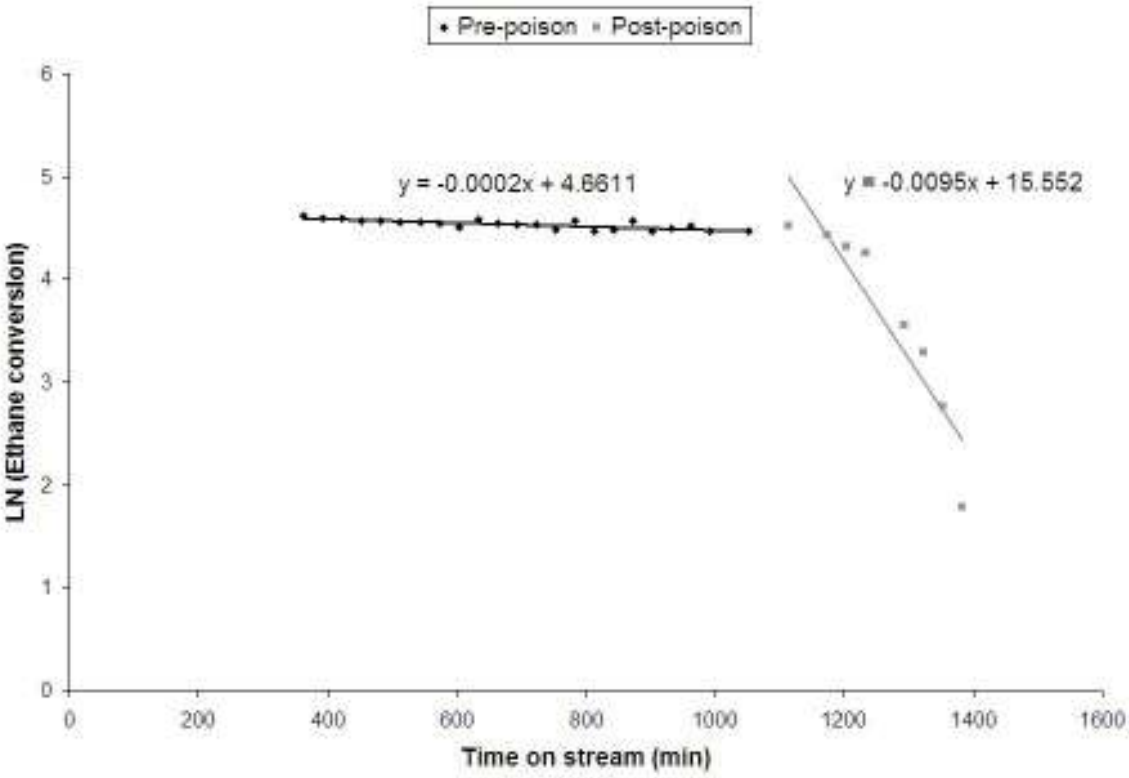

Figure 113 Rh/Al_2O_3 deactivation

It can be seen that although deactivation is occurring prior to methanthiol, it occurs at very slow rate compared to the post poison.

3.5.1.3. Rate of formation of products

Prior to poisoning H_2, CO_2 and CH_4 are all deactivating, figure 114, particularly CH_4 where in the initial standard run (section 3.3.1.1.3) its formation was more comparable with H_2. Although the rate of hydrogen formation is deactivating, the rate is still comparable to the standard run at 600°C. The only gas product not deactivating at this stage is CO.

On poisoning, all product gases show considerable deactivation, the rate at which is provided in the next section.

Once the poison is removed from the feed the product gases show some degree of recovery, except for CH_4, which continues to deactivate.

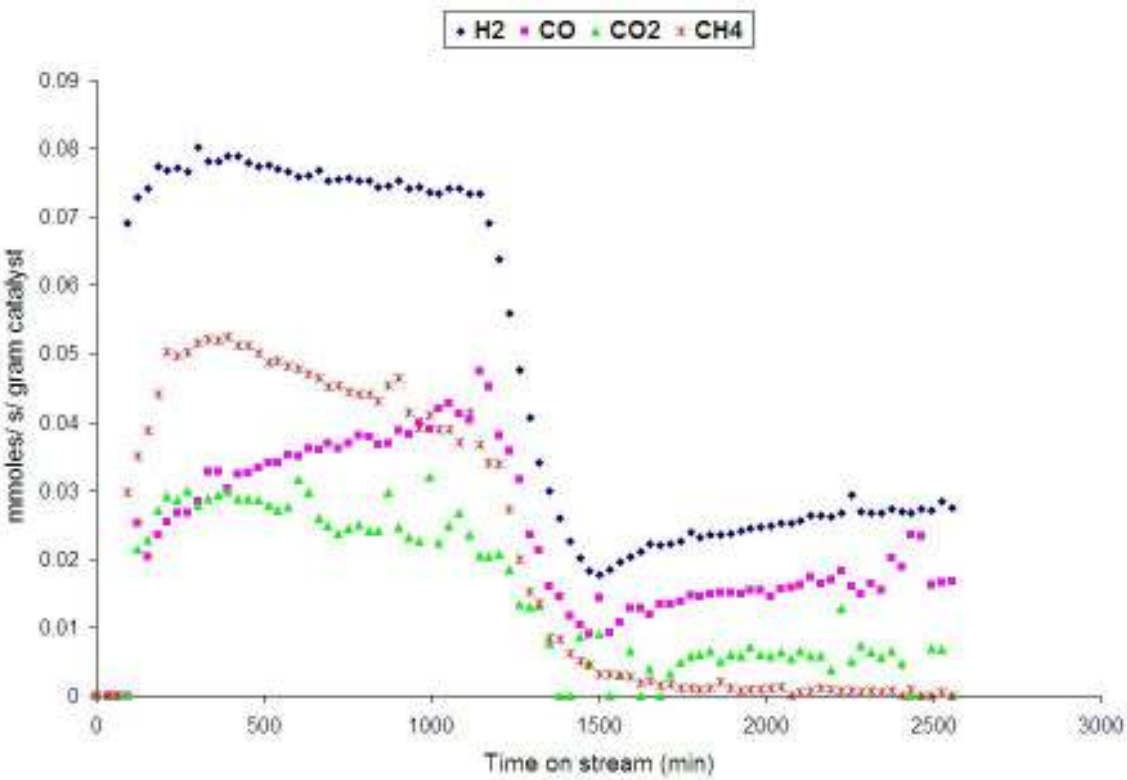

Figure 114 Rate of formation of products over Rh/Al_2O_3

3.5.1.4. Deactivation of Products

The rates of deactivation of the four gaseous products were plotted, assuming first order, and the deactivation rate constants obtained. These are tabulated below, table 74.

Table 74 Deactivation rate constants for the formation of gaseous products

Product	H_2	CO	CO_2	CH_4
Deactivation rate constant ($-1x10^{-4}$)	46	54	36	71

It is evident that formation of CH_4 is the most retarded by the presence of methanethiol.

3.5.1.5. Product selectivity

Poisoning took place between injections 37 and 49, see figure 115. Poisoning appears to improve the catalysts selectivity towards H_2 and CO, whilst selectivity towards CH_4 was significantly reduced.

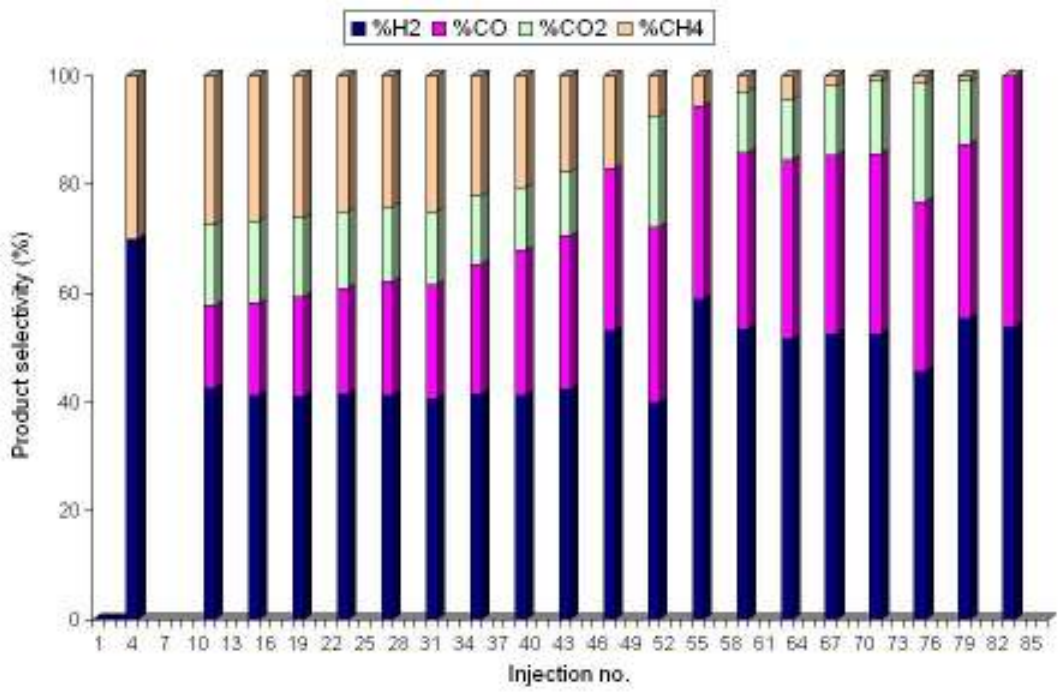

Figure 115 Product selectivity over Rh/Al_2O_3

3.5.2. Pt/Al_2O_3

3.5.2.1. Ethane conversion

Pt/Al_2O_3 deactivates at the beginning of the reaction, before methanthiol is introduced, with deactivation beginning to slow down at 40% conversion, figure 116. This was seen previously in the standard run where conversion was beginning to level off at 45% at 1400 minutes on stream.

On poisoning deactivation of the catalyst recommences and conversion is minimal. Once the poison is removed there appears to be a slight recovery in activity.

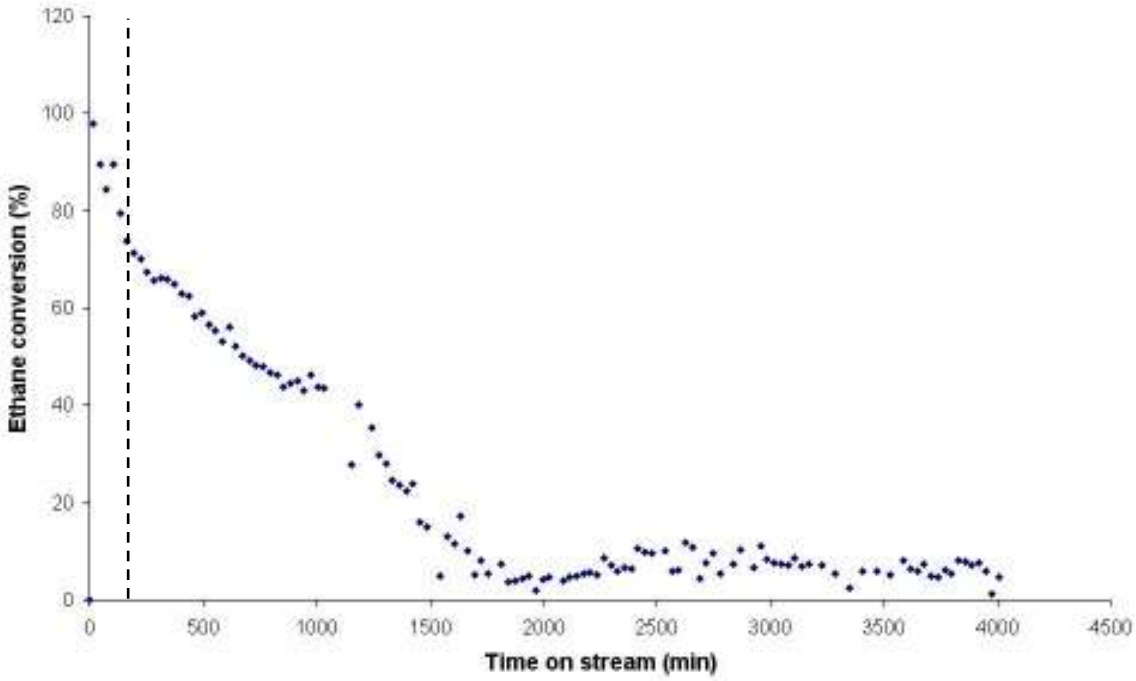

Figure 116 Ethane conversion over Pt/Al_2O_3

3.5.2.2. Rate of Deactivation

The two periods of deactivation are compared in figure 117.

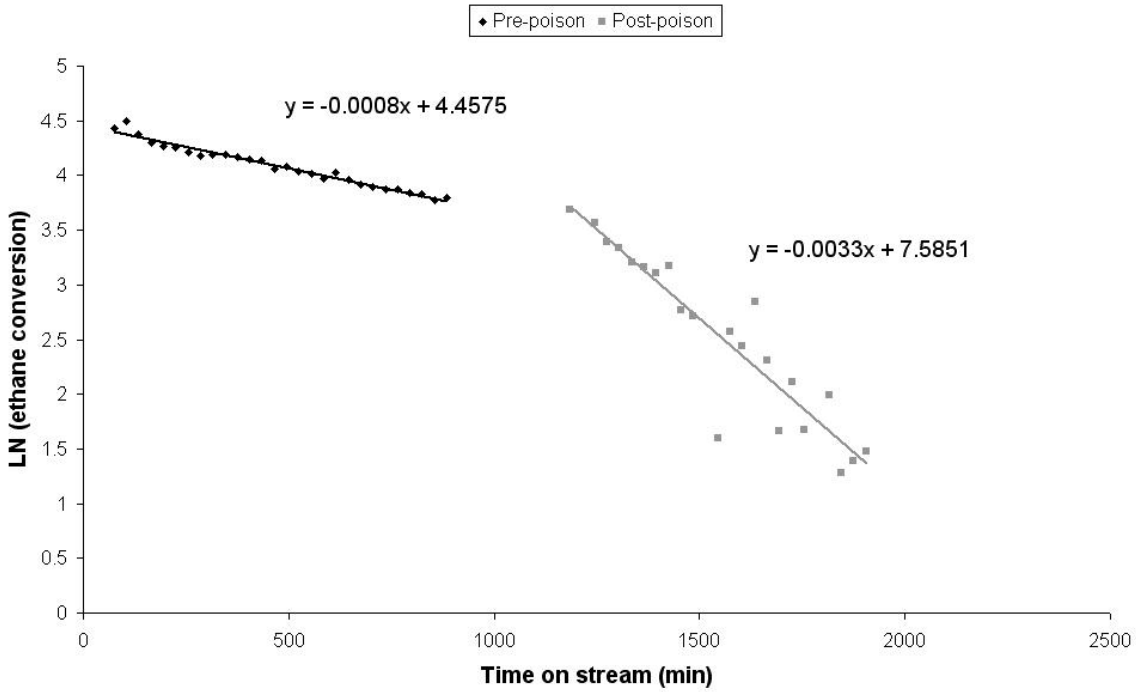

Figure 117 Pt/Al_2O_3 deactivation

The rate of deactivation prior to the poison is very similar to the rate constant obtained from the deactivation of Pt/Al_2O_3 in the standard run.

The rate of deactivation after the poison has been introduced is considerably smaller than that obtained from Rh/Al_2O_3, indicating Pt/Al_2O_3 deactivates slower than Rh/Al_2O_3 as the result of poisoning.

3.5.2.3. Rate of formation of Products

Prior to the introduction of methanthiol all gaseous product are forming at rate comparable to that seen in the standard run at 600°C.

On poisoning, rapid deactivation of H_2, CO_2 and CH_4 is clearly evident. The formation of CO deactivates but at a much slower rate, figure 118.

When the poison was removed the formation of H_2, CO_2 and CH_4 began to increase, however at 2800 minutes on stream they all started to deactivate again. No recovery was evident of CO formation; it continued to deactivate.

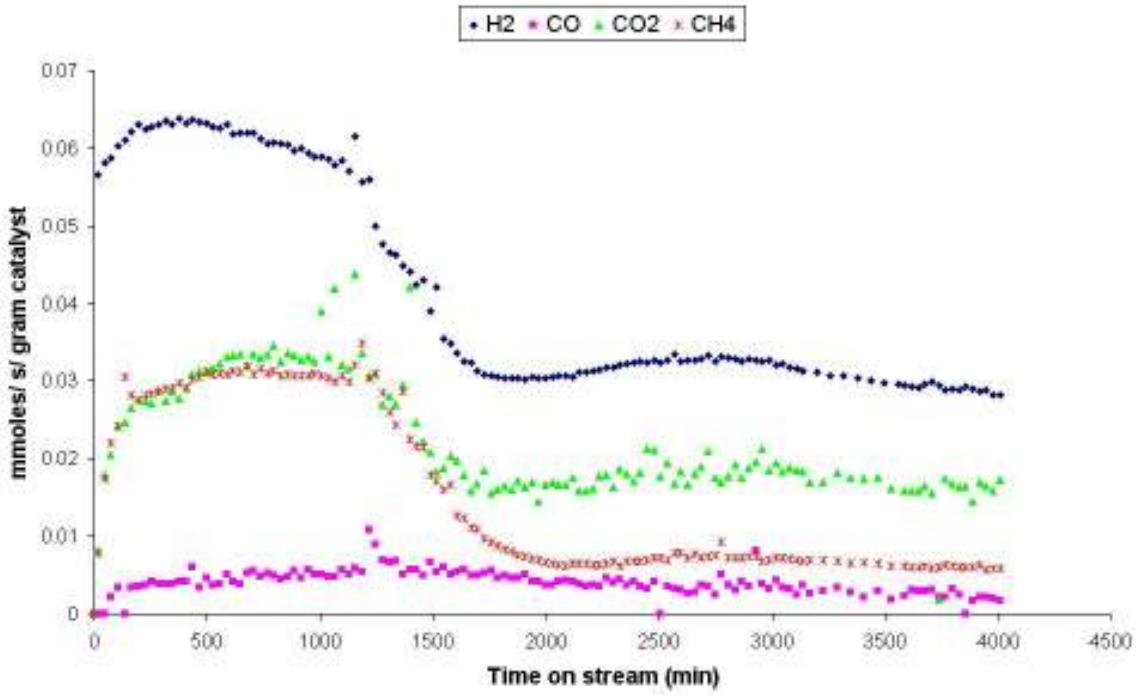

Figure 118 Rate of formation of products over Pt/Al_2O_3

3.5.2.4. Deactivation of Products

The rates of deactivation of the four gaseous products were plotted, assuming first order, and the deactivation rate constants obtained. These are tabulated below, table 75.

Table 75 Deactivation rate constants for the formation of gaseous products

Product	H_2	CO	CO_2	CH_4
Deactivation rate constant ($-1x10^{-4}$)	11	9	14	24

The formation of CH_4 deactivates the fastest, whilst CO formation deactivates the slowest.

3.5.2.5. Product Selectivity

Selectivity has again slightly increased in favour of H_2 during poisoning, with a decrease in selectivity toward CH_4, figure 119.

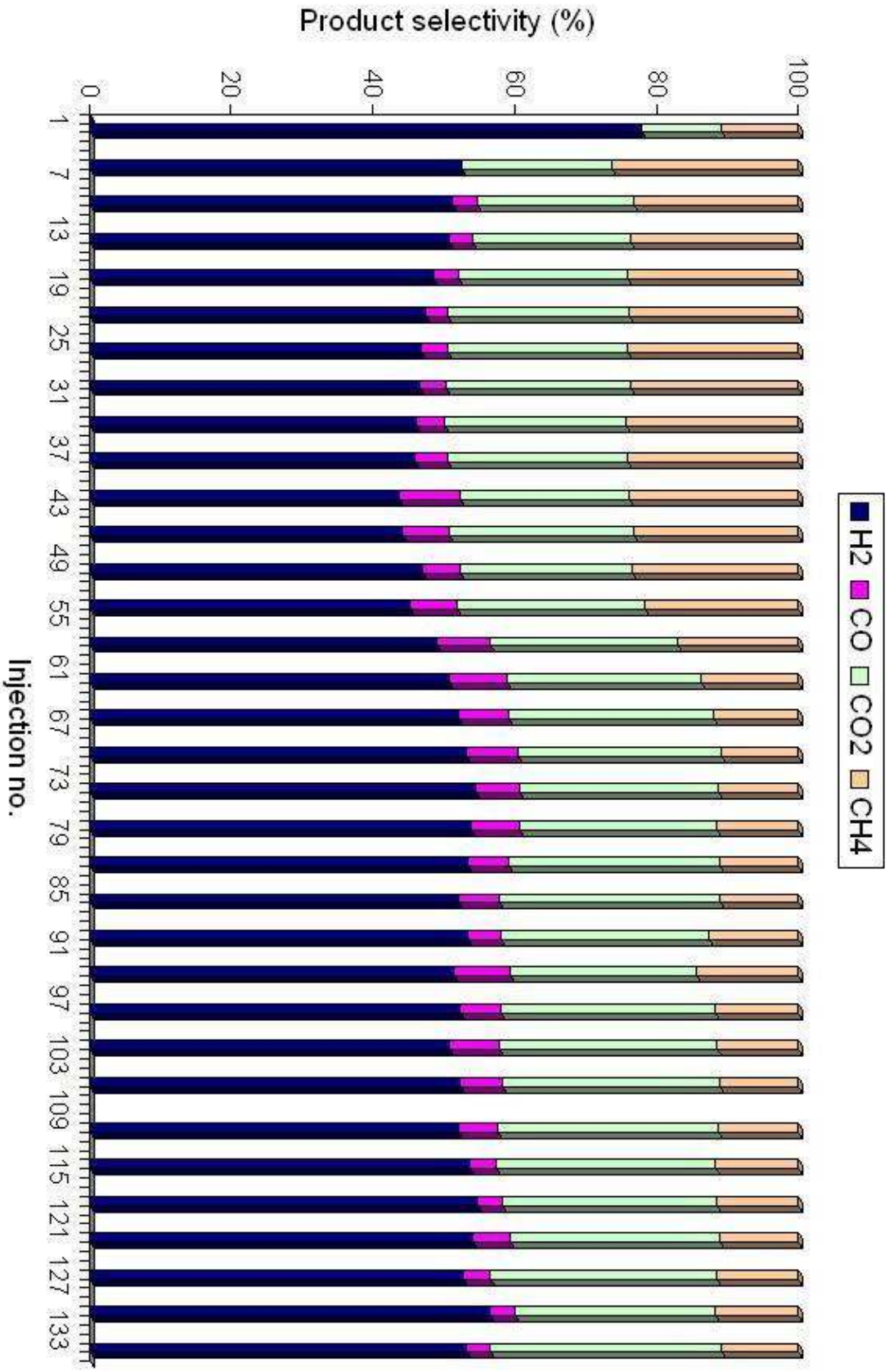

Figure 119 Product selectivity over Pt/Al_2O_3

3.5.3. Rh/ZrO_2

The feed water was exchanged for a pre-prepared methanthiol solution at 2317 minutes on stream, to introduce sulphur into the system. The sulphur was introduced after a longer period of time on stream than the Al_2O_3 catalysts, as from the standard reaction conducted at 600°C, the activity of Rh/ZrO_2 took longer to stabilize out. At 2677 minutes on stream, after 6 hours of poisoning, the feed was changed back to pure water.

3.5.3.1. Ethane conversion

Initially ethane conversion was 100% over Rh/ZrO_2 and fell to 60% at 1000 minutes on stream, figure 120. Unfortunately, the data between this period of time was lost due malfunction with the G.C. Again, further data was lost between 1870 minutes and 2220 minutes on stream due to a re-occurrence of the same problem. However, from the standard reaction, conversion was also seen to fall from 100% to 70%, though this occurred over a longer period of time 2500 minutes.

Once the poison is introduced the catalyst begins to deactivate almost immediately, with conversion reaching zero. On removal of the poison conversion increases to 40%, at which point it plateaus out.

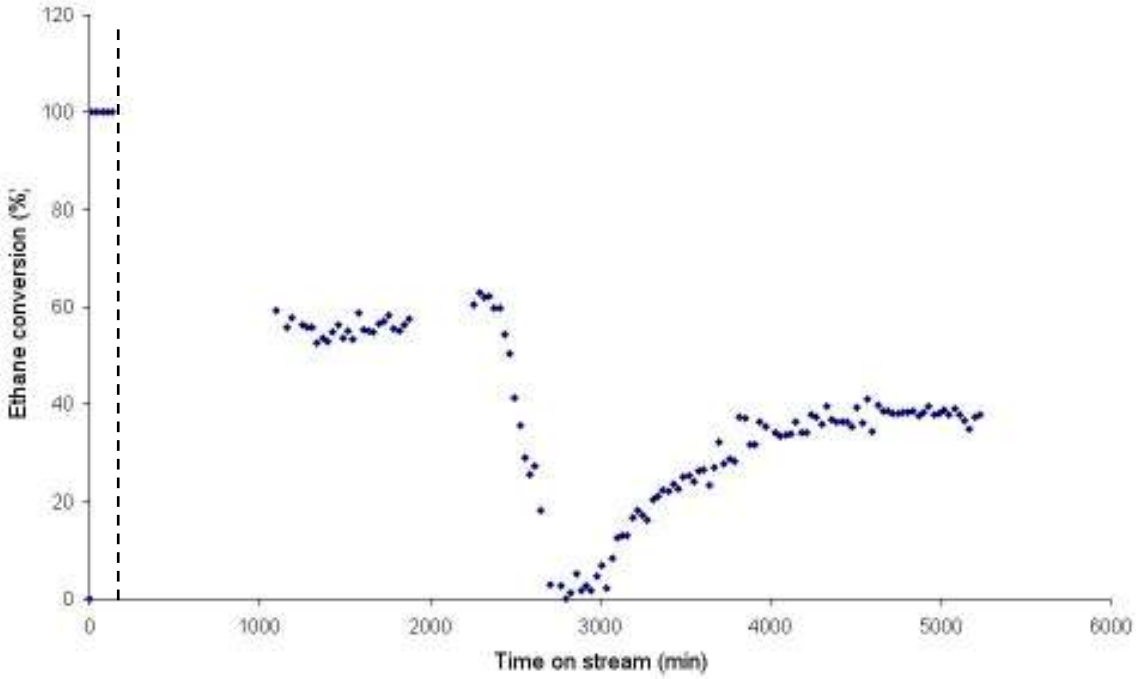

Figure 120 Ethane conversion over Rh/ZrO_2

3.5.3.2. Rate of Deactivation

The deactivation of Rh/ZrO_2 once methanthiol was introduced has been examined by plotting LN (Ethane conversion) vrs time to obtain a deactvation rate constant, figure 121.

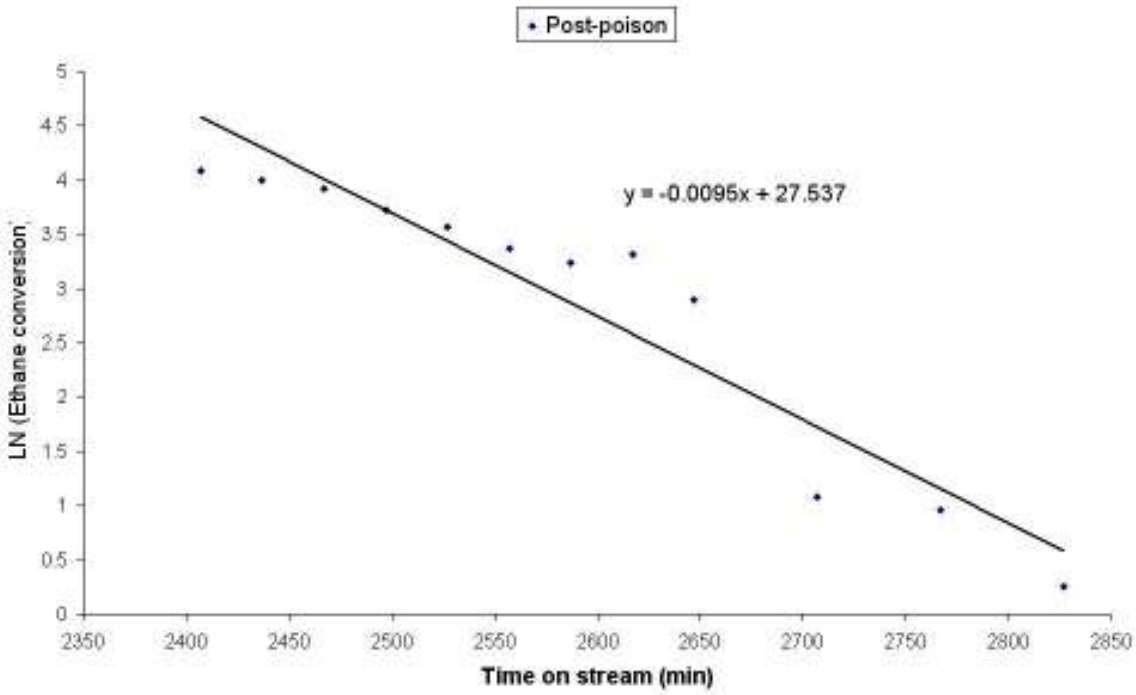

Figure 121 $RhZrO_2$ deactivation

It appears that the deactivation of Rh/ZrO_2 occurs at the same rate as over Rh/Al_2O_3.

3.5.3.3. Rate of Formation of Products

From figure 122, in the first 130 minutes of the reaction the formation of the product gases are increasing, particularly CH_4 formation, which was also seen to form the fastest in the standard reaction. After 1000 minutes on stream the formation of all the products gases have stabilised and at a similar level to that obtained in the standard run, note that a large deactivation occurred with respect to CH_4 formation which was documented in the standard run.

When methanthiol was introduced into the system, the formation of the product gases deactivate extensively. Then, on removal of the poison from the feed the formation of H_2, CO and CO_2 recover somewhat. The formation of CH_4 also begins to recover but at a slower rate.

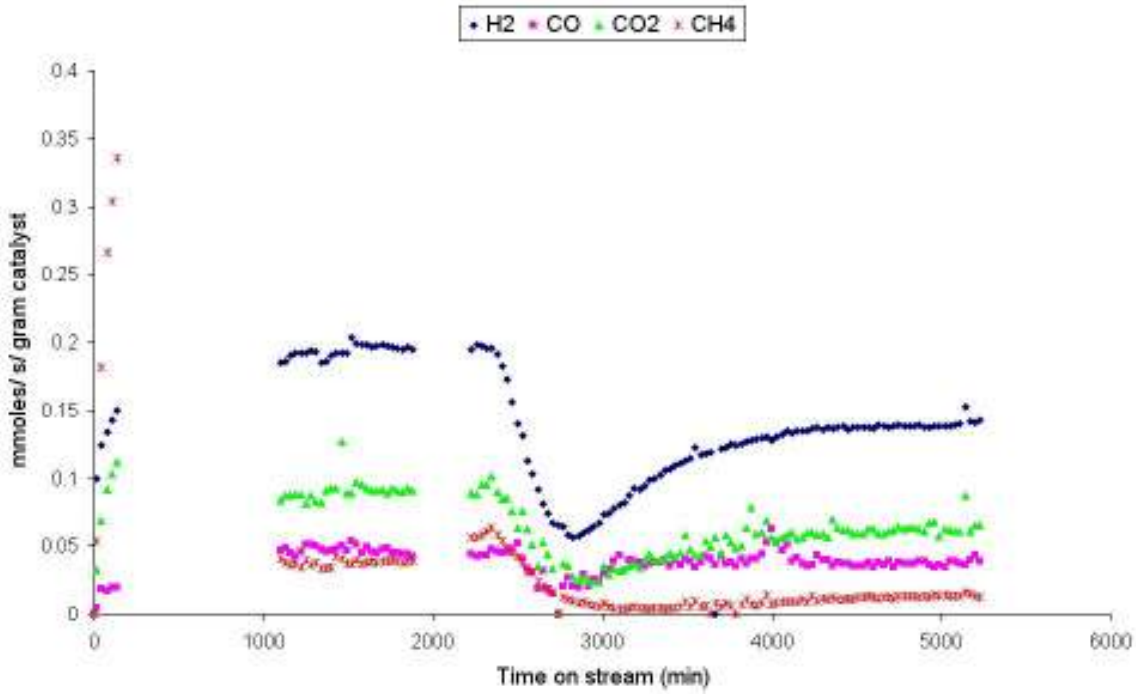

Figure 122 Rate of formation of products over Rh/ZrO_2

3.5.3.4. Deactivation of Products

Table 76 Deactivation rate constants for the formation of gaseous products

Product	H_2	CO	CO_2	CH_4
Deactivation rate constant ($-1x10^{-4}$)	29	22	25	39

CH_4 formation deactivate at the fastest rate. The formation of H_2, CO and CO_2 deactivate at similar rates.

3.5.3.5. Product Selectivity

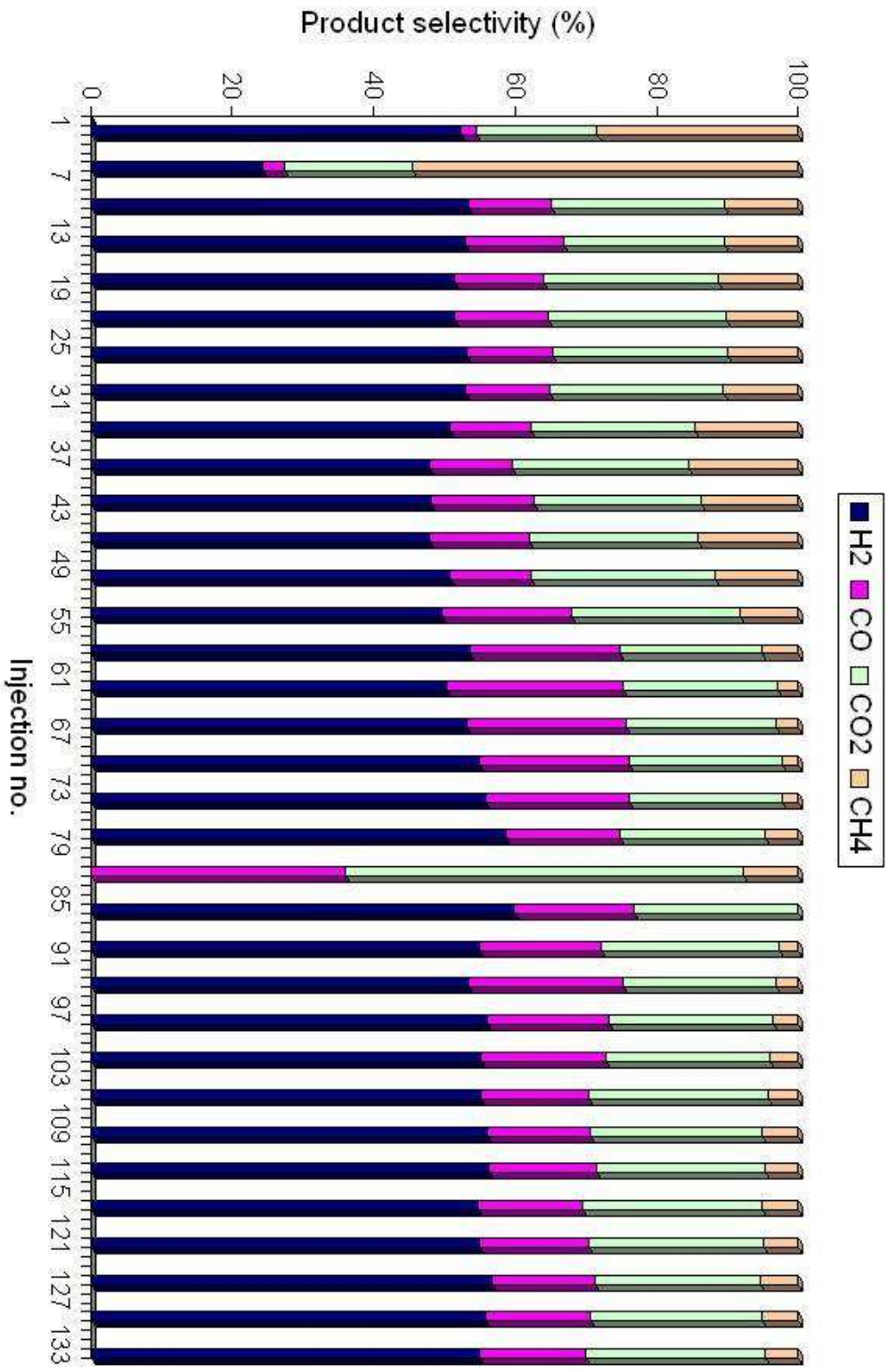

Figure 123 Product selectivity over Rh/ZrO_2

3.6. Effect of Concentration

In the results presented in the previous poisoning chapters the catalysts were poisoned using sulphur solutions with a concentration of 11.2ppm. To examine the effect poison concentration has on catalyst deactivation solutions with a sulphur concentration of 5.6ppm were prepared and introduced by replacing the water feed, as previously described. These experiments were only carried out using methanthiol, as it resulted in greater catalyst deactivation, therefore any changes in deactivation would be more clearly evident. Rh/Al_2O_3 and Rh/ZrO_2 were the catalysts chosen to study concentration effects.

3.6.1. Rh/Al_2O_3

The feed water was exchanged for a pre-prepared hydrogen sulphide solution at 1083 minutes on stream, to introduce sulphur into the system. At 1443 minutes on stream, after 6 hours of poisoning, the feed was changed back to pure water.

3.6.1.1. Rate of Formation of Products

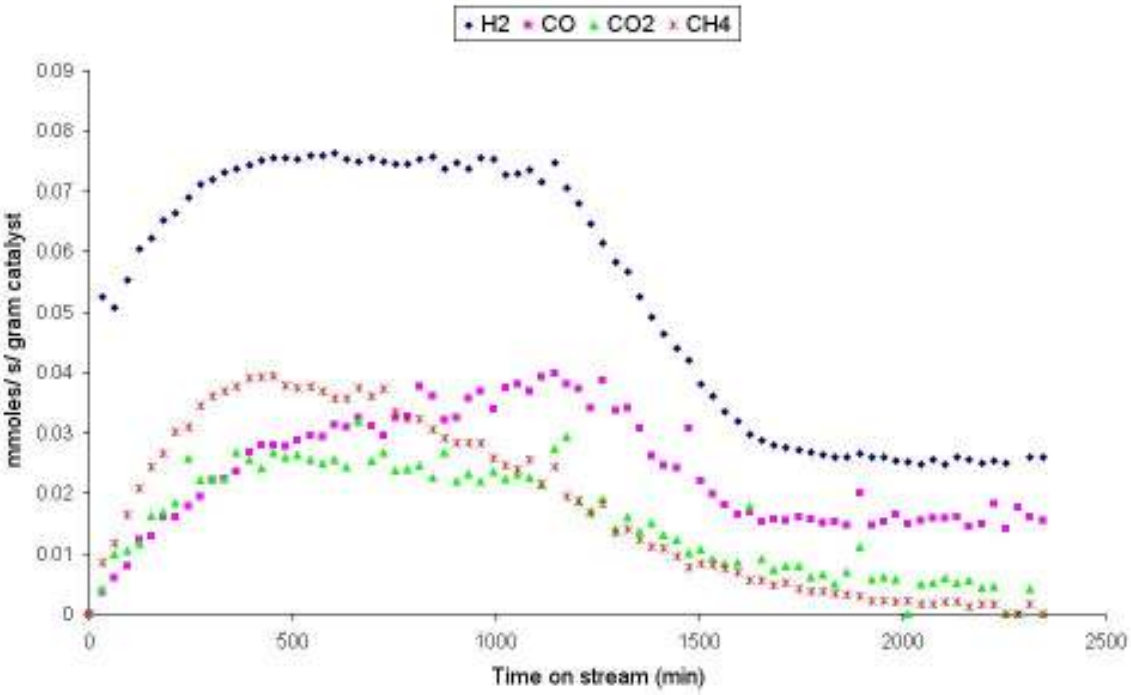

Figure 124 Rate of formation of products over Rh/Al_2O_3

Prior to introducing methanthiol CH_4 formation is deactivating significantly. This was also the case in previous poisoning experiments and indicates there was residual sulphur present in the rig before the beginning of the reaction. However the rate of formation of hydrogen is stable and comparable with the rate obtained from the standard run.

All gaseous products were seen to deactivate when 5.6ppm methanthiol was introduced into the system, with deactivation ceasing on removal of the poison from the feed.

No recovery is apparent in the formation of any of the product gases. This differs from the result obtained from the 11.2ppm methanthiol poisoning experiment, in which the formation of H_2, CO_2 and CO begin to increase on removal of the poison.

3.6.1.2. Deactivation of Products

The rates of deactivation of the four gaseous products were plotted, assuming first order, and the deactivation rate constants obtained. These are tabulated below, table 77.

Table 77 Deactivation rate constants for the formation of gaseous products

Product	H_2	CO	CO_2	CH_4
Deactivation rate constant ($-1x10^{-4}$)	19	19	19	28

The rate of deactivation of all the product gases are approximately half the rate when the poison concentration was 11.2ppm, i.e. halving the poisoning concentration has halved the deactivation rate.

3.6.2. Rh/ZrO_2

The feed water was exchanged for a pre-prepared methanthiol solution at 2745 minutes on stream, to introduce sulphur into the system. At 3105 minutes on stream, after 6 hours of poisoning, the feed was changed back to pure water.

3.6.2.1. Rate of formation of products

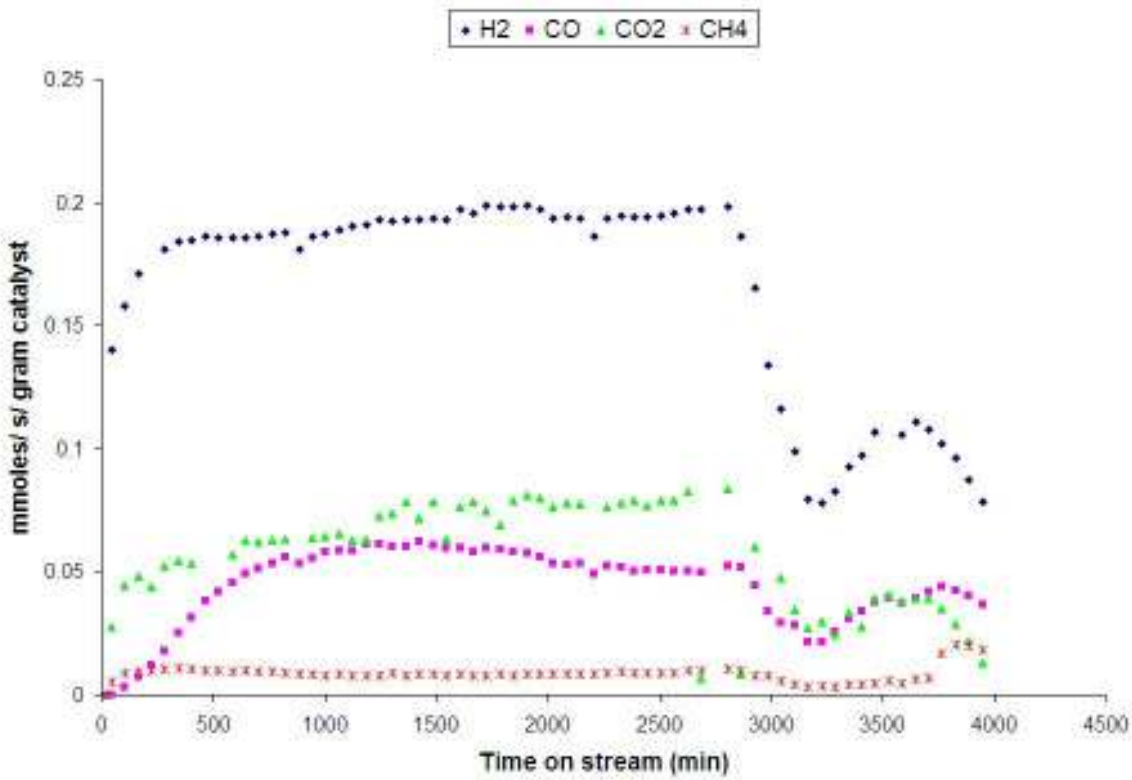

Figure 125 Rate of formation of products over Rh/ZrO_2

In the first 2500 minutes on stream, prior to poisoning, the formation of H_2, CO_2 and CO all form at similar levels as seen in previous runs. However CH_4 formation has been greatly retarded from the beginning of the reaction. This was also seen in the Rh/ZrO_2 hydrogen sulphide poisoning experiment, section 3.3.2.3.3, and is thought to be an effect of residual sulphur in the system.

Deactivation of all the product gases occurred on the introduction of 5.6ppm methanthiol, and on its removal recovery is evident.

At the end of this run a second deactivation is evident. This was due to the water pump failing, resulting in a drop in steam levels and coking of the catalyst.

3.6.2.2. Deactivation of Products

The rates of deactivation of the four gaseous products were plotted, assuming first order, and the deactivation rate constants obtained. These are tabulated below, table 78.

Table 78 Deactivation rate constants for the formation of gaseous products

Product	H_2	CO	CO_2	CH_4
Deactivation rate constant ($-1x10^{-4}$)	26	26	30	33

The deactivation are all very similar to the rates obtained when the poison concentration was 11.2ppm i.e. over Rh/ZrO_2 poison concentration appears to being having little affect. The only difference is here the deactivation rate of CH_4 is lower, presumably due to formation having been already retarded.

4. Discussion

4.1. Pulse Flow Adsorptions

4.1.1. Single Gas Adsorptions

4.1.1.1. CO Adsorption

4.1.1.1.1. CO Pulses over Pt catalysts

Adsorption of CO on metal catalysts has been thoroughly studied in the literature using spectroscopic methods, which has allowed the identification of three adsorbed states corresponding to [81]:

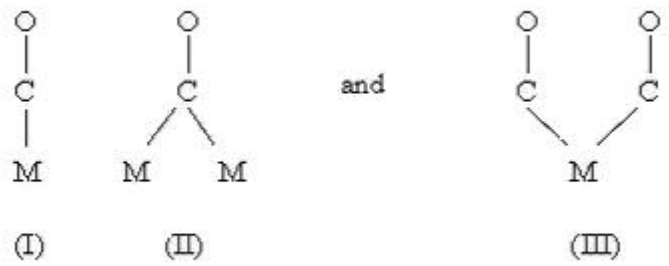

Figure 126 CO adsorption states

The linear form (I) predominates with Cu, Fe and Pt; the bridge form (II) is more common with Ni and Pd, while with Rh all three forms are observed [81]. However, the di-geminal form (III) is only seen at very high dispersions.

In the case of Pt/SiO_2 the CO:Pt ratio of 0.8 indicates CO is adsorbing linearly (I), this is in keeping with the literature and also indicates small Pt crystallites. Dorling and Moss [72] studied the platinum-silica system and obtained a CO/Pt value of about 0.87 on samples containing small crystallites, but this value decreased significantly on poorly dispersed catalysts. Much of the evidence for the nature of the adsorbed states of carbon monoxide on platinum has come from infrared spectroscopic studies [73]. Eischens and Pliskin [74] have suggested that, species adsorbed in the linear form give rise to bands above 2000 cm^{-1}, the bridged form gives bands below 2000 cm^{-1}. On this basis, the linear form appears to be the dominant state on platinum films [75], although a

band at 1874 cm^{-1} can be observed when platinum is evaporated in the presence of carbon monoxide at a pressure of 3 Torr. The appearance of this latter band was ascribed to changes in surface topography, a conclusion supported by the observation that highly disordered films gave broad, low frequency bands, which changed on sintering [76]. Carbon monoxide adsorbed on platinum/silica gives bands consistent with a linear species [77], whilst platinum/alumina gives a band at 1810 cm-1 [78], which may be due to a bridged species, although support effects or oxygen contamination may have been responsible [79]. Blyholder [80] strikes a note of caution in the interpretation of these low frequency bands, pointing out that significant back donation of electron charge from the metal to the adsorbed carbon monoxide may perturb the linear forms; he also states that surface atoms at edges and corners may be favorably positioned to produce such back donation. It has been shown that CO prefers coordination to a single atom rather than bridge coordinated CO on the Pt(111) face because of the relative large interaction of the CO 5σ orbital with the highly occupied *d*-valence electron band [80].

The CO:Pt value obtained for Pt/Al_2O_3, 0.7, is typical for the formation of linearly adsorbed CO(II), figure 126, and also in keeping with literature that the bridged species is not formed.

4.1.1.1.2. CO Pulses over Rh catalysts

The CO:M ratio was 0.9:1 for Rh/SiO_2 acetate suggesting that for almost every Rh atom a CO molecule was adsorbed. This could give an indication that CO is adsorbing linearly, however other combinations of (I), (II) and (III) are possible to give a value of 0.9. This will be re-addressed when the adsorption of H_2S over Rh/SiO_2 is considered.

A lower CO:M ratio of 0.6 was obtained for Rh/SiO_2 (nitrate) which may suggest that the bridge form predominates, however the presence of forms (I) and (II) cannot be ruled out as they may just be occurring to a lesser extent. The lower CO:M ratio obtained indicates that preparing the catalyst with a nitrate precursor rather than an acetate precursor has resulted in a more poorly dispersed catalyst.

Both Rh/Al_2O_3 (acetate) and Rh/Al_2O_3 (nitrate) have CO:Rh ratios exceeding 1:1, indicating the formation of the gem dicarbonyl species (III). The formation of $Rh^I(CO)_2$ is well-known and thought to arise from the adsorption of CO significantly perturbing the Rh-Rh coordination of the supported Rh clusters, leading to the formation of atomically dispersed Rh^I sites [83]. These isolated Rh sites are capable of adsorbing two CO molecules as a gem-dicarbonyl species. Yates et al found through spectroscopic methods that $Rh^I(CO)_2$ also formed on Rh/SiO_2 but to a much lesser extent than on Rh/Al_2O_3, higher temperatures and CO pressure are generally required for it to be formed to an appreciable extent [84]. Yates also provided direct evidence that specific OH groups on Al_2O_3 and SiO_2 are consumed as CO reacts with supported Rh crystallites to produce atomically dispersed $Rh^I(CO)_2$ suggesting the support is having a major influence.

4.1.1.2. H_2S Adsorption

4.1.1.2.1. H_2S Pulses over Pt catalysts

The S:Pt ratio obtained for Pt/SiO_2 was 0.9:1 and suggests that one sulphur atom adsorbs onto almost every Pt atom. A similar figure was obtained for the CO:Pt, suggesting the same sites are accessible to both CO and H_2S. Previously it was found that the S/Pt_S ratio was 1:1 on Pt/SiO_2 in a H_2S study by Jackson et al., which agrees well with coverage obtained here [85].

Over Pt/Al_2O_3 a S:Pt ratio of 1.2:1 was obtained. Where such values were acceptable on considering CO adsorption on Rh catalysts due to the formation of gem-dicarbonyl species, there have been no reports of an equivalent sulphur species formed on any metal. The high S:Pt ratio obtained, exceeding 1:1, is likely to be an artefact of having to perform a large subtraction; subtracting the amount of sulphur adsorbed onto the support from the total amount of sulphur adsorbed to determine sulphur adsorption onto Pt. Jackson et al. obtained a S/Pt_S ratio of 0.6:1 over Pt/Al_2O_3, much lower than the present results, therefore it appears the support subtraction is effecting the results to a large extent.

The alumina support was found to adsorb considerable quantities of H_2S, and this adsorption was associative i.e. no hydrogen was evolved. H_2S adsorption on alumina has been well documented and is considered in terms of H_2S adsorbing as a basic molecule onto isolated Lewis acid sites of the support. Incompletely coordinated aluminium atoms occur on the surface of gamma alumina and are strong Lewis acids, due to the electron accepting ability of the incomplete coordination sphere [86]. DeRosset et al. suggested that H_2S reacts with these sites to create an Al-S bond; this would satisfy energetic requirements [87].

The adsorption of H_2S on the alumina support was found to be associative, which is different from findings from other studies, where both types molecular and dissociative adsorption have been reported. However, Okamoto et al. found that when Al_2O_3 is exposed to a relatively high pressure of H_2S the molecular integrity of H_2S is conserved on adsorption and conclude H_2S chemisorbed associatively [88]. In the present study high pressures were used in order to saturate the catalysts, which may explain why H_2S adsorption on alumina was non-dissociative.

Importantly no hydrogen is evolved when H_2S is adsorbed onto the support alone, but hydrogen is evolved during adsorption on the catalysts, leading to the conclusion that only the metal has the ability to dissociate the H_2S molecule on adsorption. The degree of H_2S dissociation can be measured by examining the H_2 evolved : S adsorbed ratio. For Pt/Al_2O_3 and Pt/SiO_2 they are 0.6:1 and 0.2:1, respectively. It is clear H_2S is only partially dissociating with the catalysts retaining a good deal of the hydrogen, in the case of Pt/SiO_2 as much as 80% of the hydrogen retained. It has been previously cited that H_2S requires three adjacent metal sites in order to adsorb dissociatively[89], however as Pt begins to reach to saturation point it is likely three adjacent metal sites are no longer available. This may lead to the H_2S adsorbing close to saturation point not being able to dissociate and thereby retaining hydrogen. Hedge et al. observed this behaviour when H_2S was adsorbed on Rh (100).

4.1.1.2.2. H_2S Pulses over Rh catalysts

The S:M ratios obtained for Rh/SiO_2 (acetate) is 0.9:1 and suggests that one sulphur atom adsorbs onto almost every metal atom; whilst sulphur adsorption is significantly less over Rh/SiO_2 (nitrate) with approximately half of the Rh atoms adsorbing sulphur. These results are in good agreement with the CO adsorption results and strengthen our understanding of CO adsorption over Rh/SiO_2. There have been no reports of an equivalent gem-disulphide species the adsorbed species can only be bridged or linear sulphides. Therefore, since the ratios of S:Rh and CO:Rh are identical it is very likely that the same adsorbed species are formed on the catalyst and the gem-dicarbonyl species is not formed over Rh/SiO_2.

For the alumina supported catalysts the S:M ratios obtained indicates that approximately one sulphur atom adsorbs for every metal atom. A ratio of 1.1:1 was obtained for Rh/Al_2O_3 acetate and 0.9:1 for Rh/Al_2O_3 nitrate. In comparison to the results obtained over Rh/SiO_2 these values are slightly higher, and in the case of Rh/Al_2O_3 acetate exceeding 1:1. This may be attributed to the error associated with support subtraction, as cited in the case of Pt/Al_2O_3.

In general it can be seen that acetate prepared catalysts have the ability to adsorb more sulphur. The acetate catalysts were also evidenced to adsorb more CO than the nitrate catalysts. This may be because preparing the catalyst with an acetate precursor lead to a more highly dispersed catalyst. The table below compares the amount of sulphur atoms adsorbed/Rh atom to the amount of CO molecules adsorbed/ Rh atom.

Table 79 Comparison between CO and H_2S adsorption over Rh catalysts

Catalyst	S:Rh	CO:Rh
Rh/ SiO_2 acetate	0.9	0.9
Rh/ SiO_2 nitrate	0.6	0.6
Rh/ Al_2O_3 acetate	1.1	1.5
Rh/ Al_2O_3 nitrate	0.9	1.4

The values obtained for S:Rh are identical to the CO:Rh values for the silica supported catalysts, indicating exactly the same metal sites are used. If S and CO use the same metal site on the SiO_2 catalysts, then they probably use the same site on the Al_2O_3 catalysts as well. The excess in CO over the Al_2O_3 catalysts arises from the gem-dicarbonyl species due to the high dispersion of the catalysts.

From studies conducted on single crystal faces of Rh it was expected that the sulphur saturation coverage would be approximately 0.5 monolayer. The coverage value obtained for Rh/SiO_2 (nitrate) is fairly consistent with this; a value of 0.6 was obtained [89]. However, the saturation coverage obtained for Rh/SiO_2 acetate and the Rh/Al_2O_3 catalysts is considerably higher. Importantly, it should be noted that Hedge et al conducted the single crystal experiments at 100K whilst the present pulse flow experiments were conducted at room temperature, 293K. However, Hedge found on heating to 600K sulphur coverage increased which was attributed to physisorbed H_2S. This theory is discussed more fully below when considering hydrogen evolution and the dissociation of H_2S.

The hydrogen evolved during H_2S adsorption and consequently the degree of dissociation of H_2S varies considerably over the Rh catalysts. From table 34, H_2S almost fully dissociates over Rh/SiO_2 (acetate), whilst over Rh/SiO_2 (nitrate) H_2S appears to only partially dissociate. Over the Al_2O_3 supported catalysts the reverse occurred, with Rh/Al_2O_3 nitrate having a greater ability to dissociate H_2S.

The poorer dispersion of Rh/SiO_2 (nitrate), which has already been elucidated to, may have affected the catalyst's ability to dissociate H_2S resulting in the significantly lower H_2 evolved : S adsorbed ratio obtained. However, considering the Al_2O_3 catalysts, Rh/Al_2O_3 (acetate) dissociated H_2S to the lesser extent, despite having a higher dispersion. Consequently, there is no clear link between the degree of dissociation of H_2S and nature of the precursor or metal dispersion. Note that the high H_2:S ads indicate that even over Rh it is possible in a supported metal system for full dissociation to take place, possibly by using the interface between the metal and the support.

The reduced portion of H_2S dissociating may have indicated physisorbed H_2S, with reference to Hedge. However, with regard to the pulse flow system used to

produce the results presented here, it would not have been possible to produce physisorbed H_2S as this species is unstable in a flowing system.

In summary, the total amount of H_2S adsorbed on to the catalysts and consequently the amount of H_2 evolution was determined. Sulphur saturation coverages were determined and the degree of dissociation of H_2S. In general, the sulphur saturation coverages obtained in this study are considerably higher than those obtained in single crystal studies. Indeed, it is often found to be difficult to correlate the results between single crystal studies and polycrystalline and supported metal systems. The reasons for this are primarily twofold: (1) The saturation stoichiometry apparently depends upon P_{H2S} above about 0.1 ppm [90]; and (2) it varies with temperature [91]. Therefore when comparing the present study with the study conducted on Rh(100) it should be taken into account that a pressure of $<2 \times 10^{-7}$ torr was used in the single crystal study, whereas in the present study a pressure of typically 760 torr was used.

Changing the catalyst precursor has a significant effect on the catalysts' ability to dissociate H_2S. Whilst Rh/Al_2O_3 nitrate and Rh/Al_2O_3 actetate have similar dispersions, from the CO adsorption data, Rh/Al_2O_3 nitrate fully dissociates H_2S unlike Rh/Al_2O_3 acetate, which only partially dissociates H_2S. This suggests that H_2S adsorption is structurally sensitive as distinct to particle size dependent.

There also appears to be a slight support effect, the sulphur saturation coverage increased when the metal was supported on alumina. On average coverage increased by 0.2 monolyer. The support does not seem to have any clear effect on the dissociation of H_2S, H_2S dissociation is dominated by the effect of the precursor.

4.1.1.3. CH_3SH Adsorption

4.1.1.3.1. CH_3SH Pulses over SiO_2 Supported catalysts and comparison with H_2S

The only method available to analyse the amount of CH_3SH adsorbing onto the catalysts was to evaluate the quantity of hydrogen evolved. This assumed CH_3SH adsorbs dissociatively via:

$$2CH_3SH(g) \longrightarrow 2CH_3S_{(adsorbed)} + H_2(g)$$

The assumption was made that even if adsorption was occurring on the support, methanthiol would be adsorbing associatively, as was found with hydrogen sulphide over alumina. Therefore, this does not affect the method chosen to analyse methanthiol adsorption on the metal, since no hydrogen is produced from adsorption onto the support.

Based on the assumption above high coverages were obtained, giving a S:M ratio of 1:1, suggesting full dissociation did occur with no hydrogen being retained on the catalyst. It is unlikely that the hydrogen evolved is produced from the decomposition of the surface hydrocarbon fragment ($2CH_3S$) as it was seen over Ru (0001) that this fragment does not begin to decompose until temperature of 450K is reached [92]. The present adsorptions were conducted at 293K.

The table below details the S:M ratios obtained over the silica supported catalysts when methanthiol is pulsed over the catalysts and compares them to the ratios obtained from the H_2S pulses.

Table 80 S:M ratios obtained from methanthiol pulses over SiO_2 supported catalysts

Catalyst	Rh/SiO_2 acetate	Rh/SiO_2 nitrate	Pt/SiO_2
S:M CH_3SH	1.0	0.9	1.2
S:M H_2S	0.9	0.6	0.9

The sulphur saturation coverage achieved when CH_3SH is the adsorbent is slightly higher than when H_2S is the adsorbent. It is also apparent that the adsorption of CH_3SH is less influenced by changing the precursor.

4.1.1.3.2. CH_3SH Pulses over Al_2O_3 Supported catalysts and comparison with H_2S

The table below details the S:M ratios obtained over the alumina supported catalysts when methanthiol is pulsed over the catalysts and compares them to the ratios obtained from the H_2S pulses.

Table 81 S:M ratios obtained from methanthiol pulses over Al_2O_3 supported catalysts

Catalyst	Rh/Al_2O_3 acetate	Rh/Al_2O_3 nitrate	Pt/Al_2O_3
S:M CH_3SH	0.9	0.9	0.7
S:M H_2S	1.1	0.9	1.2

Over the alumina supported catalysts the dissociative adsorption of CH_3SH produces a saturation coverage slightly less than that produces by H_2S, except for Rh/Al_2O_3 nitrate where the dispersions are identical. However, it should be noted that there is a greater error associated with the S:M H_2S figures, owing to the support adsorption subtraction. This error should be taken into consideration when comparing the different sulphur species adsorbents.

To summarize high sulphur coverages approaching one monolayer are obtained when methanthiol is adsorbed onto the catalysts. Unfortunately, there is very little in the literature on the adsorption of methanthiol and no reported saturation coverages to compare with the present work. The high coverages obtained of approximately one CH_3S species for every metal atom, are indicitive of highly well dispersed catalysts, as evidenced from the CO and H_2S adsorption results.

4.1.1.4. Adsorption under Steam Reforming Conditions

4.1.1.4.1. The effect of H_2

To gauge the effect of hydrogen on the adsorption of H_2S the S:M ratios obtained when sulphur is adsorbed in a H_2 atmosphere are provided in tables 82 and 83, alongside the S:M ratios obtained during H_2S pulses.

Table 82 S:M ratios obtained when S is adsorbed in a H_2 atmosphere over SiO_2 supported catalyst and a comparison to the S:M ratios obtained during H_2S pulses

Catalyst	Rh/SiO_2 acetate	Rh/SiO_2 nitrate	Pt/SiO_2
S:M in H2/ H_2S	0.9	0.5	0.6
S:M H_2S	0.9	0.6	0.9

Table 83 S:M ratios obtained when S is adsorbed in a H_2 atmosphere over Al_2O_3 supported catalyst and a comparison to the S:M ratios obtained during H_2S pulses

Catalyst	Rh/Al_2O_3 acetate	Rh/Al_2O_3 nitrate	Pt/Al_2O_3
S:M in H2/ H_2S	0.7	1.2	0.7
S:M H_2S	1.1	0.9	1.2

Hydrogen does not appear to have any clear effect on the adsorption stoichiometry of hydrogen sulphide. In some cases the sulphur coverage remains unchanged (Rh/SiO_2 acetate), in others the coverage has decreased (Pt/SiO_2, Rh/Al_2O_3 acetate, Pt/Al_2O_3) and coverage was even seen to increase (Rh/Al_2O_3 nitrate).

It is important to note that in most cases the change in coverage was relatively small, and considering the errors associated with these measurements, particularly over the Al_2O_3 supported catalysts. Therefore, it is important to approach small changes with caution, as these are most likely within experimental error.

To examine the effect of hydrogen on the dissociation of H_2S tables 84 and 85 provide the H_2 evolved : S adsorbed values obtained, with and without a hydrogen atmosphere.

Table 84 Ratio of H_2 evolved : S adsorbed obtained in a H_2 atmosphere over SiO_2 supported catalysts and a comparison to the H_2 evolved : S adsorbed ratio obtained during H_2S pulses

Catalyst	H_2 evolved : S adsorbed H_2 /H_2S pulses	H_2 evolved : S adsorbed H_2S pulses
Rh/SiO_2 acetate	0.6	0.9
Rh/SiO_2 nitrate	0.5	0.6
Pt/SiO_2	1.2	0.6

Table 85 Ratio of H_2 evolved : S adsorbed obtained in a H_2 atmosphere over Al_2O_3 supported catalyst and a comparison to the H_2 evolved : S adsorbed ratio obtained during H_2S pulses

Catalyst	H_2 evolved : S adsorbed H_2 /H_2S pulses	H_2 evolved : S adsorbed H_2S pulses
Rh/Al_2O_3 acetate	0.7	0.5
Rh/Al_2O_3 nitrate	0.5	1.0
Pt/Al_2O_3	0.3	0.2

Again, on considering the dissociation of H_2S the presence of H_2 does most seem to be making an obvious impact. For half the catalysts the presence of H_2 has

decreased the dissociation, which can be explained by considering the dissociation of H_2S as an equilibrium:

$$H_2S \longleftrightarrow H_2 + H_2S$$

Effectively, the presence of H_2 is pushing the equilibrium to the left.

However, in other cases, particularly Pt/SiO_2, the dissociation of H_2S has considerably increased. In fact the value obtained for Pt/SiO_2 exceeds one, so hydrogen is being evolved from another source than the dissociation of H_2S alone. The only other possible source of H_2 is from the hydroxyl groups of the SiO_2 support, however it is highly unlikely that they play any role as the SiO_2 support was not seen to adsorb any H_2S. However, it is important to note that this experiment was not repeated and it would be desirable to do so to confirm if there definitely is an excess of hydrogen being produced.

4.1.1.4.2. The effect of temperature

By performing the adsorptions at 600°C instead of room temperature, the amount of H_2S adsorbed increased considerably over the silica supported catalysts. The saturation coverage obtained for the silica supported catalysts is approximately 1.5 as opposed to 1, which was obtained at room temperature. This generates a new stoichiometry, Rh_2S_3, suggesting the formation of bulk rhodium sulphide.

Rh has a relatively low free energy of formation of its bulk sulphides, indicating that relatively large gas-phase H_2S concentrations are required for stable bulk sulphides to exist [36]. The present adsorptions were conducted using a pulses of 100% H_2S, so the formation of the bulk sulphide is plausible. Moreover, the free energy of formation of Rh_xS is lower at increased temperatures, indicating the bulk sulphide is more stable at higher temperatures, which is in-keeping with the present results. The values for the free energy of formation for Rh_xS at 300K and 600K are quoted below:

Table 86 Values for the free energy of formation for Rh_xS and PtS_2 at 300K and 600K (36)

Sulphide	ΔG_f^o (kJ/g atom) at 300K	ΔG_f^o (kJ/g atom) at 600K
Rh_xS	-3.1	-10.9
PtS_2	+10.9	+23.0

However, from the table it can be seen that bulk Platinum sulphide has a higher free energy of formation at higher temperatures, which appears to be in conflict with the present results, which suggest bulk formation at 600°C. It may be that the kinetics of the adsorption process is having more influence than the thermodynamics. At higher temperatures the rate at which hydrogen desorbs from the catalyst increases, which may be driving the adsorption equilibrium in favour of producing the bulk sulphide:

$$H_2S + Pt \rightleftharpoons PtS_2 + H_2 \text{ DESORBING}$$

When the high temperature adsorptions were performed over the alumina supported catalysts, no increase in sulphur adsorption was apparent. The coverages obtained at 600°C were approximately 1, which was the coverage obtained at room temperature. It appears the support is strongly influencing the metals ability to form bulk sulphides.

However the alumina adsorption isotherm was significantly different (fig 3.2.8). Although the support adsorption was subtracted from overall adsorption, the shape and nature of the isotherm make accurate subtraction difficult. This change in adsorption properties of the alumina at 600°C may account for the metal not being able to form bulk sulphides at an increased temperature when it is supported on the alumina, because it has reduced the partial pressure of H_2S over the metal.

The extent of dissociation of H_2S increases over all the catalysts when the adsorption temperature is increased to 600°C, particularly over the alumina supported catalysts. Over the SiO_2 supported catalysts dissociation increased by 10-40%, whilst over the alumina supported catalysts dissociation of H_2S increased by typically 60%.

Adsorption at 600°C has increased the sulphur coverage at saturation, yet H_2S dissociation has increased. It was previously suggested that full dissociation of H_2S could not take place due to a lack of three adjacent sites, as the metal sites became saturated with sulphur. However as noted earlier it is indeed possible to obtain full dissociation over a supported metal crystallite. At 600°C this is made easier by the potential for sulphur to diffuse into the bulk, freeing up the surface site for dissociation of H_2S.

Certainly, diffusion into the bulk could explain the increased adsorption *and* the increased dissociation over the silica supported catalysts, where bulk formation was seen. However, no evidence for bulk formation was evidenced over the alumina supported catalysts, suggesting that a mechanism as outlined with the room temperature adsorption is still in operation.

4.1.1.4.3. The combined effect of temperature and H_2

The S:M ratios obtained over the silica supported catalysts are approximately 1:1 when the adsorption is carried out at 600°C and in hydrogen atmosphere. This value was also obtained when H_2S alone was adsorbed over the catalysts at room temperature, so it would appear the two variables are effectively cancelling each other out, as the effect of increasing the temperature was to increase coverage, whilst the effect of hydrogen was to generally decrease coverage.

Over the alumina supported catalysts the S:M ratios obtained are <1:1, and therefore less than the coverages obtained when H_2S alone is adsorbed at room temperature, which were generally found to be 1:1. This is not exceptional; since it was found increasing the temperature had no effect on the saturation coverage obtained over the alumina catalysts. However, the effect of hydrogen was, in general, to decrease the saturation coverage. It is clear that the

presence of hydrogen has lowered the S:M ratio whilst the temperature has had no effect over the alumina supported catalyst.

It becomes difficult to see the effect of the combination of increasing the temperature and adsorbing sulphur in hydrogen atmosphere on the dissociation of H_2S, as the effect is different for each catalyst. The effect as to whether dissociation increased or decreased in comparison to the original H_2S room temperature adsorptions are denoted in table 87.

Table 87 Effect of temperature and H_2 on the dissociation of H_2S in comparison with single H_2S pulses at room temperature.

Catalyst	Effect on dissociation
Rh/SiO_2 acetate	Decreased by 0.3
Rh/SiO_2 nitrate	Increased by 0.6
Pt/SiO_2	Decreased by 0.4
Rh/Al_2O_3 acetate	Increased by 0.4
Rh/Al_2O_3 nitrate	Decreased by 0.3
Pt/Al_2O_3	Increased by 0.5

This is similar to the dissociation results obtained when the effect of H_2 was examined independently of the temperature. It appears that the presence of hydrogen on the dissociation of H_2S is complex and without further study we are unable to interpret the data further.

4.1.1.5. Competitive Adsorption

4.1.1.5.1. H_2S pulses over CO saturated Rh Catalysts

H_2S is able to adsorb on CO saturated catalysts, however the percentage adsorbed in comparison to the fresh catalysts has been greatly reduced. Over the Rh/SiO_2 catalysts adsorption was decreased by 84-92%, and over the Rh/Al_2O_3 catalysts adsorption was decreased by 78-90%. This indicates that the support is not influencing competitive adsorption, or its effect is minimal compared to the effect the saturation layer of CO. This finding differs from

previous work conducted on Pt [43], where clear support effects were evidenced, it was found CO blocked H_2S adsorption on the metal sites on Pt/SiO_2, however did not block adsorption on Pt/Al_2O_3. It was proposed CO had a route to desorb over Pt/Al_2O_3 by utilising the hydoxyl groups of the support.

Earlier in this discussion (section: 4.2.1.1.2) it was concluded that gem-dicarbonyl species were formed when CO was pulsed over Rh/Al_2O_3. The formation of each gem-dicarbonyl species consumes one hydroxyl group of the support via the following equation:

$$(1/x)\ Rh0x + OH\ (a) + 2CO(g) \longrightarrow Rh^{I}(CO)_2\ (a) + (1/2)H_2(g)$$

The consumption of the hydoxyl groups during the initial saturation with CO means there is no route available for CO to desorb, thereby it remains on the surface and blocks the adsorption of H_2S. This also provides further evidence that gem-dicarbonyl is formed over Rh/Al_2O_3.

Rh/Al_2O_3 nitrate is the catalyst that has been able to adsorb the most H_2S, whilst saturated with CO, with a reduction in H_2S adsorption of 78%. Interestingly, on examination of the dissociation values of H_2S for all the CO saturated catalysts, the values are the same when compared to adsorption on the fresh catalyst, except for Rh/Al_2O_3 nitrate. When H_2S adsorbs on fresh Rh/Al_2O_3 nitrate the H_2 evolved:S adsorbed ratio is 1:1, it fully dissociates. However, when H_2S adsorbs on CO saturated Rh/Al_2O_3 nitrate this ratio is reduced to 0.3:1, this indicates the mode of adsorption has changed. The adsorption of H_2S is now more asscociative, and the ability for H_2S to change its mode of adsorption over Rh/Al_2O_3 nitrate has led to increased adsorption.

4.1.1.5.2. CO pulses over H_2S saturated Rh catalysts

Saturation of the Rh catalysts with H_2S has blocked most of the CO from adsorbing onto the catalysts. Over the Rh/SiO_2 catalysts CO adsorption was reduced by 85-96%, and over the Rh/Al_2O_3 catalysts CO adsorption was reduced by 93-96%.

Previously it has been cited that CO can adsorb on sulphur saturated Rh/SiO_2 catalyst, by the displacement of H_2S. The desorption of S requires hydrogen and it was proposed to be dependant on the precursor used. H_2S only partially dissociates on the oxide catalyst to produce an HS-* species, this would provide a source of hydrogen to allow for desorption.

A similar theory can be presented with the present results when considering the dissociation of H_2S over Rh/SiO_2. The following table details the amount of CO that adsorbs on the sulphur saturated catalysts alongside the dissociation values of H_2S on fresh catalyst.

Table 88 The amount of CO that adsorbs on the sulphur saturated catalysts and the dissociation values of H_2S on fresh catalyst

Catalyst	Reduction in CO adsorption (%)	H_2 evolved : S adsorbed
Rh/SiO_2 acetate	96	0.9
Rh/SiO_2 nitrate	85	0.6

The lower H_2 evolved : S adsorbed over Rh/SiO_2 nitrate indicates a greater degree of partial dissociation, so there is more hydrogen present on the catalyst surface. This hydrogen has provided the adsorbed sulphur with a route to desorb, and therefore allows a greater portion of CO to adsorb.

4.1.1.5.3. Co-Adsorption

When H_2S and CO are co-adsorbed over the Rh/SiO_2 catalysts, the amount of CO able to adsorb as approximately halved. Similarly, the amount of H_2 evolved, indicating dissociative adsorption of H_2S, has been reduced to less than half. In this experiment the amount of H_2S adsorbing was unable to be measured directly, but a comparison of the hydrogen evolved figures can be made to guage the change in dissociative adsorption.

All of the hydrogen evolved, and thereby dissociative adsorption occurred during the first pulse, hereafter no further adsorption of H_2S occurs. Most of the CO

adsorption that occurs also takes place during the first pulse, with small quantities start to adsorb at pulses 4 and 5.

Ultimately, both CO and H_2S are equally strong adorbates, with the requirement of H_2S to have three sites to adsorb dissociatively slightly hindering its ability to adsorb, which reduces its adsobitive ability to less than half in a competitive environment.

Unlike over the silica supported catalysts, when H_2S and CO are co-adsorbed over the Rh/Al_2O_3 catalysts, the amount of CO adsorbed is only slightly reduced in comparison to when only CO is pulsed over the catalysts. Meanwhile, the amount of H_2S dissociatively adsorbing (from H_2 evolved values) has been significantly reduced. H_2S adsorption was reduced by between 72-95% compared with adsorption when H_2S is pulsed solely over the catalysts.

Clearly the support is having a significant effect and most likely due to alumina's ability to adsorb significant quantities of H_2S. This has resulted in there being less competition for the metal sites, and so allowing CO to adsorb to a greater extent.

4.1.1.6. Summary of Adsorption

Excellent agreement was found between the CO and H_2S adsorption coverage's obtained over the catalysts, indicating the same metal sites are used for both adsorbents. Particularly over the Rh/SiO_2 catalysts, where the identical values obtained for H_2S and CO helped elucidate the identity of the adsorbed CO species, since there is a greater no. of possible CO adsorbed states, the information obtained from the H_2S pulses aided in narrowing down the possibilities.

The good agreement between the two sets of results also allows us to confidently produce a clear order of catalyst dispersity, for the Rh catalysts the order is:

Rh/Al_2O_3 acetate > Rh/Al_2O3 nitrate = Rh/SiO_2 acetate > Rh/SiO_2 nitrate

This allows two conclusions to be drawn; (i) the alumina catalysts are generally more disperse than the silica supported catalysts and (ii) the acetate prepared catalysts are more disperse than the nitrate prepared catalysts.

The agreement between the CO and H_2S results is less pronounced over the Pt catalysts. The SiO_2 supported catalyst is slightly more disperse than the alumina supported catalyst with regard to the CO results, but from the H_2S results the alumina supported catalyst appears more highly dispersed. This discrepancy has arisen due to the error associated with the subtraction of the adsorption onto the alumina support. In this case the result from the CO adsorption is more accurate; therefore the Pt/Al_2O_3 is slightly more disperse, in agreement with the results obtained over the Rh catalysts.

Whilst simulating steam reforming conditions, the effect of hydrogen was difficult to determine however, the effect increasing the temperature had on the adsorption of H_2S was much clearer to elucidate. The rise in temperature allowed the silica supported catalysts to form the bulk sulphide and both the silica and the alumina supported catalysts had an increased ability to dissoctiate the H_2S molecule.

Competitive adsorption examined the ability of H_2S to adsorb onto CO saturated catalysts. Adsorption of H_2S was limited by CO not having an accessible route to desorb. For H_2S to adsorb in any significant quantity the mode of adsorption changed and became more associative, this was seen over Rh/Al_2O_3 nitrate. The ability for CO to adsorb onto sulphur saturated catalysts was again governed by not having a route for H_2S to desorb. Here, the catalysts that retained more hydrogen during the adsorption of H_2S, had a greater ability to adsorb CO; and may attributed to changing the metal precursor.

A significant support effect was evidenced during the co-adsorption experiments where the adsorption of CO was largely un-effected over the alumina supported catalysts despite being in a competitive environment with sulphur. This was owing to alumina's large adsorpitive capacity and was effectively acting as sulphur sink, freeing up the metal sites for sulphur.

4.2. Steam Reforming Experiments

4.2.1. Standard reactions and effect of temperature

4.2.1.1. Conversion

In this section the conversion of ethane during the steam reforming reaction over the different catalysts is evaluated. The figure below compares the ethane conversions over the four catalysts tested.

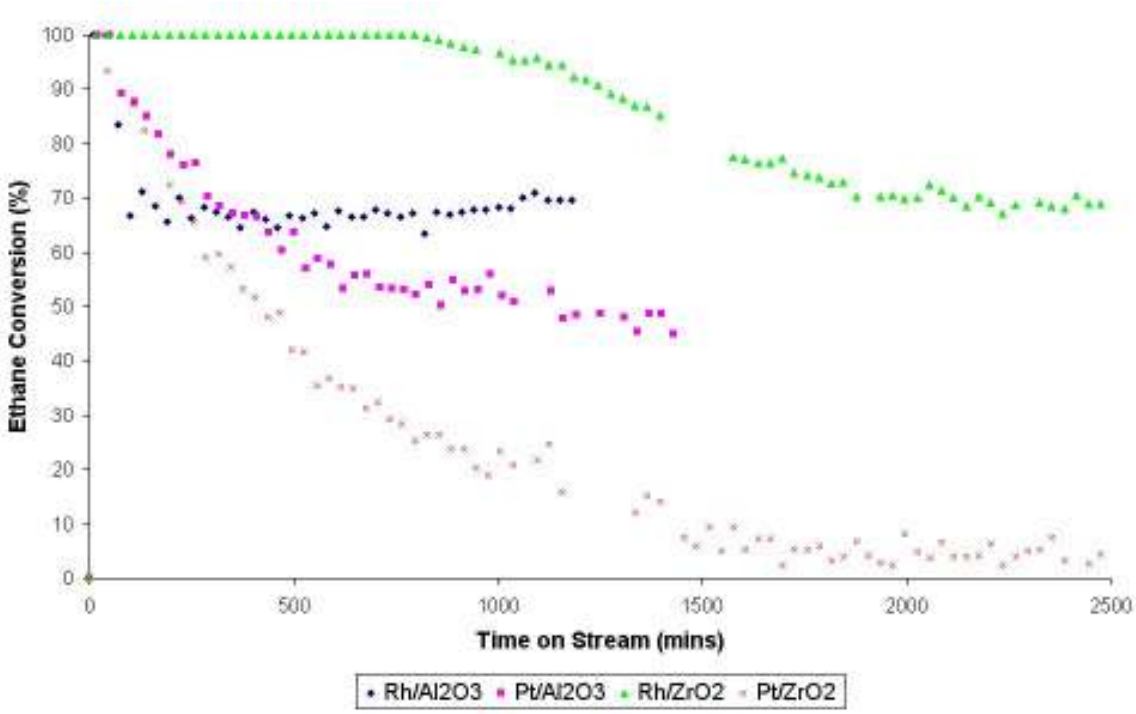

Figure 127 Comparison of conversion profiles over Rh/Al_2O_3, Pt/Al_2O_3, Rh/ZrO_2 and Pt/Al_2O_3

The alumina catalysts were not tested up to 2500 minutes on stream as conversion appeared stable at 1000 minutes on stream. The zirconia catalysts underwent a change in conversion at 1000 minutes and so were tested over a longer period. Rh/ZrO_2 began to deactivate at 1000 minutes and conversion did not begin to re-stabilise until 2000 minutes on stream. Pt/ZrO_2 deactivated from the beginning of the reaction, however deactivation appeared to slow for a short period at 1000 minutes on stream, before deactivation continued and the conversion was effectively stable at 2000 minutes on stream.

Rh/Al_2O_3 reached a stable conversion at 70%, whilst Pt/Al_2O_3 deactivated considerably and conversion did not stabilise until 50%. Rh exhibiting a much higher activity agrees with findings in the literature regarding Pt having lower reactivity towards higher hydrocarbons than Rh [11,13, further discussed in the Introduction section 1.2.2.1].

Rh/ZrO_2 initially converts all of the ethane, and after the period of deactivation conversion ultimately reaches the same level as Rh/Al_2O_3. Igarashi et al. [20] found Rh/ZrO_2 exhibited higher activity compared to Rh/Al_2O_3 for low temperature (500°C) steam reforming of *n*-butane. They found conversion of *n*-butane over Rh/ZrO_2 to be 82.6%, whilst over Rh/Al_2O_3 they obtained a conversion of only 31.3%. It is thought the presence of zirconia inhibits the Boudouard reaction and therefore reduces the amount of carbon deposition, this will be considered more fully in the product selectivity section. However, at this stage it appears this positive effect of zirconia is only transient during steam reforming, as by 2000 minutes on stream there is little difference between Rh/ZrO_2 and Rh/Al_2O_3.

Pt/ZrO_2 has a much lower conversion of ethane than Rh/ZrO_2, which from the results over the alumina catalysts, was to be expected. However, it was also found that Pt/ZrO_2 has a lower ethane conversion than Pt/Al_2O_3. This result differs from what was seen over the Rh catalysts, where zirconia had a positive effect on the conversion, and indeed findings in the literature, Souza et al. [27] found that zirconia supported Pt catalysts were more stable than the alumina supported catalysts during CO_2 reforming of CH_4.

It is important to point out that Souza was testing the reforming of CH_4 rather than C_2H_6. Comparing reforming of methane to reforming of ethane is non-trivial due to the breaking of the C-C bond that is required with ethane. Also, it should be noted that Souza [27] was examining dry reforming, while we are investigating steam reforming. However it is still the case that zirconia had a positive influence on conversion over Rh, but a negative influence over Pt.

4.2.1.1.1. Effect of Temperature on Conversion

In general, it was seen lowering the temperature decreased conversion and increased the rate of rate deactivation, however there were variations so each catalyst will be discussed in turn to examine in detail the effect temperature had. The table below shows how ethane conversion varies with a decrease in temperature over the four different catalysts.

Table 89 Conversion of ethane over the catalysts at three different temperatures 500, 550 and 500°C

	Conversion at steady state			
Catalyst / Temp	Rh/Al_2O_3	Pt/Al_2O_3	Rh/ZrO_2	Pt/ZrO_2
600°C	70%	50%	75%	10%
550°C	40%	10%	78%	-
500°C	20%	10%	75%	-

The conversion of ethane decreases with a decrease in temperature over Rh/Al_2O_3, Pt/Al_2O_3 and Pt/ZrO_2. The biggest decrease in conversion was seen going from a reaction temperature of 600 °C to 550°C. The drop in conversion is not as significant between 550°C and 500°C, particularly over the Pt catalysts where no further decrease in conversion occurs. This relationship between temperature and conversion is to be expected according to the Arrhenius equation.

Interestingly, lowering the reaction temperature does not appear to have much effect on the conversion of ethane over Rh/ZrO_2. In fact, it would seem decreasing the reaction temperature to 550°C slightly increases the conversion. On inspection of the conversion graph at 550°C, the initial period in which conversion is 100% has been extended by approximately 500 minutes, so when the reaction is switched off after 3000 minutes on stream the reaction is only just beginning to stabilise after a period of deactivation. This may account for the conversion being slightly higher, as conversion is not sufficiently stable and

has yet to reach steady state, therefore the Rh/ZrO_2 catalysts cannot be compared fairly.

Although the reaction performed at 500°C produced a similar conversion to those at higher temperatures, conversion was not seen to stabilise and it is likely deactivation would have continued past 2500 minutes on stream to produce a lower conversion.

4.2.1.2. Carbon Balances

The carbon mass balance for the steam reforming of ethane over Rh/Al_2O_3 at 600°C, figure 53, shows a steep rise within the first 100 minutes on stream to 70% before levelling off at 75% from 400 minutes on stream. As the carbon balance remains at 75%, this means that 25% of the carbon going in is not accounted for in the exit stream throughout the course of the reaction. The only explanation for the unaccounted carbon is that was laid down on the catalyst.

Carbon formation is a well documented occurrence during steam reforming, since carbon forming processes are in equilibrium under steam reforming conditions. They are known as methane cracking, Boubourd and CO reduction respectively:

$$CH_4 \longleftrightarrow C + 2H_2 \qquad (1)$$

$$2CO \longleftrightarrow C + CO_2 \qquad (2)$$

$$CO + H_2 \longleftrightarrow C + H_2O \qquad (3)$$

The formation of carbon is a major operational problem for the steam reforming industry as the carbon blocks active sites and decreases catalyst activity.

In the present circumstance, the formation of considerable quantities of carbon on Rh/Al_2O_3 has resulted in no catalyst deactivation. Rather than the carbon blocking active sites, it is likely that the deposited carbon has become an active site in itself. Kneal and Ross [9] also concluded that the mechanism for steam reforming of ethane over Ni/Al_2O_3 required the formation of surface carbon intermediates.

Compared to Rh/Al_2O_3, the carbon balance for Pt/Al_2O_3 at 600°C takes considerably longer to plateau out. Rh/Al_2O_3 reached a fairly stable balance within the first 200 minutes on stream, whilst the carbon balance for Pt/Al_2O_3 did not stabilise until 600 minutes on stream. The slower obtainment of a stable carbon balance may be due to the deactivation of catalyst, or rather the deactivation of Pt/Al_2O_3 is the result of carbon laydown.

Once stabilised the balance reaches 100%, all the carbon is accounted for. This suggests over Pt/Al_2O_3 the carbon deposited is behaving differently and rather than acting as an intermediate it is deactivating the catalyst.

The carbon balance for the reaction over Rh/ZrO_2 stabilises at 100% and then decreases at about 1000 minutes on stream to 85%. Interestingly, this coincides with a shift in the major product, from CH_4 to H_2 and thereby a change in the dominant reaction from CH_4 forming reaction to steam reforming. From the information obtained from the carbon balance over Rh/Al_2O_3, it would appear the balance falls from 100% to 85% due to carbon deposition on the catalyst surface and its utilisation as a new active site, in accordance with catalyst becoming more active towards steam reforming.

The carbon balance for steam reforming over Pt/ZrO_2 is similar to that over Pt/Al_2O_3, but takes even longer to reach 100%, 1500 minutes. This indicates carbon laydown was even more extensive over Pt/ZrO_2 and resulted in almost complete deactivation of the catalyst.

4.2.1.3. Catalyst Deactivation

No deactivation occurred over Rh/Al_2O_3 at 600°C.

Pt/Al_2O_3 and Pt/ZrO_2 both show catalyst deactivation and will be considered together as they have similar conversion profiles. Pt/Al_2O_3 deactivates throughout the entire reaction, although deactivation begins to slow considerably from 1000 minutes on stream. Pt/ZrO_2 also deactivates throughout the whole reaction and deactivation begins to slow at 1500 minutes on steam. Since the deactivation is over a much longer period of time than with Rh/Al_2O_3,

this can definitely be considered as deactivation rather than an artefact of the system taking time to adjust.

From figures 57 and 85 in section 3.3.2.2.1, deactivation of Pt/Al_2O_3 and Pt/ZrO_2 occurs in two stages. An initial fast period of deactivation, which ends at 600 minutes on stream over Pt/Al_2O_3 and 1000 minutes on stream over Pt/ZrO_2, followed by a slower period of deactivation. The rates of deactivation are given below for these two different periods over the two Pt catalysts.

Table 90 Rate of deactivation for two different stages of deactivation over Pt catalysts

Catalyst	Rate of 1st period of deactivation ($x10^{-4}$)	Rate of 2nd period of deactivation ($x10^{-4}$)
Pt/Al_2O_3	10	2
Pt/ZrO_2	14	6

From the deactivation rates it is clear that the zirconia supported Pt catalyst is deactivating faster, during both the first and second period of deactivation. In support of what was found when comparing the conversions of the Pt catalysts, the zirconia is having a negative impact on the ability of Pt to reform ethane.

Deactivation is also evident over Rh/ZrO_2, but does not occur until 1000 minutes on stream. The rate of deactivation was found to be 3 $x10^{-4}$, this deactivation rate is relatively low and is comparable with second, slower period of deactivation over the Pt catalysts. Deactivation stops at approximately 2200 minutes on stream and conversion re-stabilises.

4.2.1.3.1. Effect of Temperature on Deactivation

No deactivation occurred over Rh/Al_2O_3 at 600°C, however decreasing the reaction temperature definitely resulted in the catalyst beginning to deactivate. From figures 45 and 46 it appears deactivation occurs in two stages, as was the case over the Pt catalysts. Decreasing the reaction temperature from 550°C to 500°C resulted in the rate of deactivation over the first 200 minutes increasing, table 91.

Table 91 Effect of temperature on the individual deactivation periods over Rh/Al_2O_3

Reaction Temperature	Rate of 1st period of deactivation ($-1x10^{-4}$)	Rate of 2nd period of deactivation ($-1x10^{-4}$)
550°C	32	3
500°C	54	6

The second period of deactivation occurs considerably slower, approximately 1/10th of the first period of deactivation, and occurs over a much longer period. The second period begins at 200 minutes on stream and deactivation has not stopped by the time the reaction is switch off. It can also be seen from table 91 that decreasing the temperature resulted in the rate of the second period of deactivation increasing.

This effect of decreasing the reaction temperature causing the rates of deactivation to increase is also evident over the Pt catalysts, particularly when the temperature is decreased from 600°C to 550°C, see tables 92 and 93. By further decreasing the reaction temperature from 550°C to 500°C there is not much further change to the rate of deactivation, particularly over Pt/ZrO_2, whilst the deactivation rate decreases slightly over Pt/Al_2O_3.

Table 92 Effect of temperature on the individual deactivation periods over Pt/Al_2O_3

Reaction Temperature	Rate of 1st period of deactivation ($-1x10^{-4}$)	Rate of 2nd period of deactivation ($-1x10^{-4}$)
600°C	10	2
550°C	19	8
500°C	14	6

Table 93 Effect of temperature on the individual deactivation periods over Pt/ZrO_2

Reaction Temperature	Rate of 1st period of deactivation ($-1x10^{-4}$)	Rate of 2nd period of deactivation ($-1x10^{-4}$)
600°C	14	6
550°C	28	6
500°C	32	-

The effect of temperature on the deactivation of Rh/ZrO_2 is rather different. On decreasing the reaction temperature from 600°C to 550°C the rate of deactivation decreases marginally, from 3 ($-1x10^{-4}$) to 2 ($-1x10^{-4}$). A further reduction in the reaction temperature from 550°C to 500°C changes the deactivation profile, figure 74, and the deactivation of Rh/ZrO_2 now appears to be occurring in two stages rather than one, figures 72 and 73. Different to what was seen over the Pt catalysts, the first stage of deactivation occurs more slowly than the second stage. Even though the second stage is occurring faster, the actual deactivation rate 2 ($-1x10^{-4}$) is still slower than the deactivation at 600°C. Therefore decreasing the reaction temperature appears to be favourable over Rh/ZrO_2, as it becomes more resistant to deactivation. However, it is important to note that at lower temperatures the conversion had not yet re-stabilised after this period of deactivation and may continue to deactivate. To establish at what point the deactivation period ceases the reaction would need to be run for longer and a better comparison can be made.

4.2.1.4. Product Selectivity

Under the reaction conditions employed and the catalysts tested, along with steam reforming; methanation, hydrogenolysis and the water gas shift reaction also take place. The degree to which H_2, CO, CO_2 and CH_4 are formed over each catalyst give an indication to how favourable these reactions are.

4.2.1.4.1. Rh/Al_2O_3

The selectivity of the gaseous products formed during steam reforming of ethane over Rh/Al_2O_3 at 600°C is displayed in figure 47 in section 3.3.1. From this graph it is clear that hydrogen and CH_4 are the major products and form at relatively the same amounts. It may appear surprising that methane should be one of the major products from the reforming of ethane, however in a recent paper by Graf et al.[13] similar findings were reported. They reported methane to be one of the major products during ethane reforming over Rh supported on yttrium-stabilised zirconia at 600°C, and proposed its formation was due to the hydrogenolysis of ethane rather than the methanation reaction (Introduction figure 3).

The minor products of the reaction are CO and CO_2. Initially CO is formed as by-product from the steam reforming reaction, and with its formation the WGS reaction is then able to proceed under these conditions to produce CO_2.

To fully understand the reactions taking place and how they proceed with time, the rate of formation of the products will now be discussed.

The rate of formation of hydrogen begins to stabilise about 400 minutes on stream and then its formation starts to deactivate from 800 minutes. In comparison methane forms at a slower rate to begin with but is still increasing by the time the reaction is switched off. For methane to be formed, either by methanation or hydrogenolysis, hydrogen is required. This explains why methane is formed at a slower rate because the formation of hydrogen first had to be established, and then methane could be formed by a consecutive reaction. As the rate of formation of methane continues to increase a small effect is seen on the rate hydrogen formation in the form of a slow decay.

The rates of formation of CO and CO_2 are increasing up to 400 minutes on stream, thereafter the formation of CO_2 begins to stabilise and then decrease from 800 minutes on stream, whilst the formation of CO continues to increase throughout the course of the reaction. This would suggest that the water-gas shift reaction is yet to reach equilibrium, and towards the end of the reaction is favouring the formation of CO:

$$CO + H_2O \rightleftharpoons CO_2 + H_2$$

However, the equilibrium constant for the water-gas shift reaction at 600°C is 2.5, the equilibrium should definitely lie to the right. This would suggest the water gas shift reaction is deactivating as the equilibrium position would still favour CO_2 formation.

The fact that the formation of CO increases throughout the reaction is also indicative that methane is not formed via the methanation reaction. Since the methanation reaction consumes CO as well as hydrogen, you would expect to see the formation of CO begin to decrease, as was the case with hydrogen. This provides some evidence that hydrogenolysis was the route for making methane.

4.2.1.4.2. Pt/Al_2O_3

From figure 60 in section 3.3.1, hydrogen is clearly the major product from the steam reforming of ethane at 600°C over Pt/Al_2O_3. The next products to be formed in significant quantities are CH_4 and CO_2, which are formed in equal amounts. CO is only a minor product of this reaction over Pt/Al_2O_3.

In comparison to Rh/Al_2O_3, CH_4 is formed to a much lesser extent over Pt/Al_2O_3. Graf et al. [13] also carried out the reforming of ethane over a Pt supported on yttrium-stabilised zirconia catalyst and reported no methane was produced. Although the present results do report the formation of CH_4 and in significant quantities it was less than over Rh/Al_2O_3. In considering the production of CH_4 it should be remembered that it can be formed by both hydrogenolysis and methanation. The interaction of these two reactions will be discussed below.

The rate of formation of the products increases up to 400 minutes on stream, thereafter they begin to stabilise. The formation of H_2, CH_4 and CO_2 then begin to slowly decrease and by the same the rates which would suggest catalyst deactivation.

As outlined earlier CH_4 may be formed by hydrogenolysis and/or methanation. Previously, the activity of these catalysts towards the methanation reaction was examined by E.Opara [71]. It was found that both Rh/Al_2O_3 and Pt/Al_2O_3 were

active towards the methanation reaction, however although Rh showed the greatest activity it predominantly produced CO_2 over CH_4. Pt produced products in a lower yield than Rh, but produced more CH_4 than CO_2. The product ratio of CH_4:CO_2 for Rh and Pt from the methanation reaction is given in the table below, alongside the ratios obtained from the present steam reforming results.

Table 94 Comparison of product ratios, CH_4:CO_2, obtained from methanation and steam reforming

	Rh/Al_2O_3	Pt/Al_2O_3
CH_4:CO_2 product ratio methanation reaction [71]	0.25	1.67
CH_4:CO_2 product ratio steam reforming	2.5	1

Considering Rh/Al_2O_3, there is considerably more CH_4 formed in relation to CO_2 during steam reforming than during methanation alone. Therefore we suggest that the majority of the CH_4 is produced via hydrogenolysis rather than methanation. Over Pt/Al_2O_3 the reverse is true; more CH_4 is formed in relation to CO_2 via the methanation reaction. Either methanation is not so favourable under steam reforming conditions or the production of CO_2 (via WGS) has altered the ratio. In any case it is evident that an additional route for CH_4 formation does not need to be evoked over Pt/Al_2O_3.

If we examine the specific rates for hydrogenolysis of ethane to methane [93] there are eight orders of magnitude variation of catalytic activity, with Rh approximately four orders of magnitude more active than Pt. Therefore the literature is compatible with the above results and supports the conclusions drawn.

Previously over Rh/Al_2O_3 there seemed to be a link a between the formation CH_4 and the consumption of hydrogen, over Pt/Al_2O_3 no such relationship exists. This would suggest over Pt/Al_2O_3 that the steam reforming reaction is occurring faster than the methane forming reaction and perhaps because the methane forming reaction has changed i.e. rates of the reactions:

Hydogenolysis > Steam reforming > Methanation

↑ Only over Rh ↑ Occurs over Rh and Pt

If methanation is the only route for producing CH_4 over Pt, it may be expected that there is some impact on the formation of CO, as CO is consumed during methanation. It is found that CO is produced in very minor quantities over Pt/Al_2O_3 in comparison to the other products found over Rh/Al_2O_3. However, it cannot so easily be assigned as the result of the methanation reaction because the WGS reaction can also alter the concentration of CO present.

Over Pt/Al_2O_3 the formation of CO is low, whilst the formation of CO_2 is relatively high in comparison. This would indicate that Pt/Al_2O_3 is a highly active WGS catalyst, with the equilibrium lying to the right in favour of producing CO_2 (as predicted by thermodynamics) :

$$CO + H_2O \rightleftharpoons CO_2 + H_2$$

Indeed, Pt has been reported to have a higher activity than Rh towards the WGS reaction when supported on alumina, this can be seen from figure 4 in the introduction section.

4.2.1.4.3. Rh/ZrO_2

The selectivity graph for ethane reforming over Rh/ZrO_2 at 600°C, figure 75 section 3.3.1, is rather interesting as it takes of the form of sweeping curve, owing to the dramatic change in product selectivity through the course of the reaction. For the first half of the reaction CH_4 is the major product and as the reaction proceeds the major product changes to hydrogen. CO_2 can also be seen to be a fairly major product of the reaction, though its formation is more constant throughout the reaction, and CO is only a minor product of the reaction.

From the graph of the rate of formation of products, figure 35, it can be seen that the formation of CH_4 is extensive, particularly within the first 700 minutes on stream. By this point its formation is more than double that of hydrogen and approximately four times the formation of CH_4 over Rh/Al_2O_3, which was

considered extensive. CH_4 formation reaches a maximum at approximately 750 minutes on stream then undergoes significant deactivation before is begins to stabilise at about 2000 minutes on stream at a quarter of its original activity.

When Graff et al. [13] tested Rh/YSZ for its hydrogenolysis activity in a reaction independent of the steam reforming experiment, they observed that after a period of complete conversion fast deactivation occurred and the CH_4-yeild dropped to 68%. They ascribed this deactivation to coke formation on the catalyst. However, they found that during the ethane steam reforming experiment that methane formation was constant with time on stream and proposed that the presence of water limits coke formation on the Rh surface and a stable conversion of ethane to methane is obtained.

From the results presented here the fast deactivation of CH_4 formation is clearly evident, and in this case the presence of steam is not suppressing the formation of coke.

Although initially the rate of formation of hydrogen appears insignificant compared to CH_4, it is still a major product and nearly more than double of the formation of hydrogen over Rh/Al_2O_3. More over the rate of formation of hydrogen was seen to deactivate over Rh/Al_2O_3, which does not occur over Rh/ZrO_2. In fact, from about 1000 minutes on stream its formation begins to increase again before stabilising at 2000 minutes on stream. The increase in the rate of formation of hydrogen coincides with the deactivation of CH_4 formation, which is in agreement that hydrogen is required to form CH_4 by hydrogenolysis. Once the coke has formed on the catalyst, suppressing the formation of CH_4, hydrogen is no longer consumed to produce CH_4 and so the there is more hydrogen in the exit flow.

It is also interesting to note that whilst formation of coke has suppressed the methane forming reaction, the steam reforming reaction, in terms of hydrogen formation, appears unaffected as no deactivation is evident. This could indicate that different types of metal sites are required for the two different reactions, or that the methane forming reaction requires a larger ensemble.

The formation of CO_2 is also fairly considerable over Rh/ZrO_2 and reaches its maximum about 700 minutes on stream, hereafter its formation slowly

decreases. In comparison, CO formation is very small, and although it slowly increases up to 1500 minutes on stream it is still a minor product. The high level of CO_2/ low level of CO suggests that when Rh is supported on ZrO_2 rather than Al_2O_3 it becomes more active towards the WGS reaction. It was afore mentioned in the introduction that the role of the support is key when considering the WGS, as the support is important in the activation of water. A similar result was obtained by Igarashi et al. when carrying out low temperature steam reforming n-butane over Rh catalysts. They reported the water gas shift reaction occurs markedly faster over the Rh/ZrO_2 catalyst, in contrast to Rh/Al_2O_3 which exhibited slow oxidation of CO.

4.2.1.4.4. Pt/ZrO_2

The product selectivity graph for the reforming of ethane over Pt/ZrO_2 at 600°C, figure 88, shows a high selectivity towards hydrogen. The second most dominant product is CO_2, whilst CH_4 is only a minor product. There was no evolution of CO throughout the entire reaction.

The selectivity towards hydrogen appears relatively constant after the first 500 minutes on stream, however the graph of rate of formation of products, figure 47, reveals hydrogen formation begins to deactivate from approximately 500 minutes on stream. This is because in relation to the formation of the other products its selectivity is constant, i.e. the formation of the other products are also decreasing.

Prior to the decrease in hydrogen formation the production of hydrogen over Pt/ZrO_2 (~0.06 mmoles/s/g) is comparable to that obtained over Pt/Al_2O_3 However, whilst the formation of hydrogen also begins to deactivate over Pt/Al_2O_3, and from 500 minutes on stream, it occurs much slower than over Pt/ZrO_2. This indicates that using ZrO_2 in place of Al_2O_3 has had de-stabilising effect on the Pt catalyst, the reverse to what was seen over Rh.

The formation of CH_4 is very low over Pt/ZrO_2, which is in line with what was evidenced over Pt/Al_2O_3, CH_4 formation was considerably lower over Pt/Al_2O_3 than over Rh/Al_2O_3 as it was surmised hydrogenolysis does not occur over the Pt

catalyst. Over Pt/ZrO_2 CH_4 formation is even lower than over Pt/Al_2O_3 and this is probably due to the decreased levels of hydrogen which is necessary to produce CH_4 via the methanation reaction.

The high selectivity towards CO_2 and the lack for formation of CO suggests that Pt/ZrO_2 is a highly active WGS catalyst, indeed this trend also seen over Pt/Al_2O_3. The same trends regarding the formation of the products exist between Pt/Al_2O_3 and Pt/ZrO_2, indicating the same reaction mechanisms are occurring. The difference between the catalysts is that ZrO_2 has had a de-stabilising effect resulting in pronounced catalyst deactivation.

4.2.1.4.5. Effect of Temperature on Product Selectivity

Decreasing the reaction temperature had pronounced effects on the product selectivity over the alumina supported catalysts. Selectivity towards hydrogen increased whilst, selectivity towards CH_4 decreased. This would suggest the CH_4 forming reaction is not as favourable at lower temperatures, and consequently less hydrogen is being consumed by the reaction.

Another effect lowering the temperature had on the selectivity over the alumina catalysts was to decrease the selectivity towards CO and increase the selectivity towards CO_2. This indicates that the alumina catalysts are more active towards the WGS at lower reaction temperatures.

Lowering the reaction temperature had the opposite effect on the selectivity over Rh/ZrO_2. By comparing the later part of the reaction, once the H_2/CH_4 formation has re-stabilised, the selectivity towards hydrogen has *decreased* with decreasing the reaction temperature [However it is highly questionable whether selectivity has in fact re-stabilised at the lower temperatures]. Meanwhile, decreasing the reaction temperature has *increased* the selectivity towards CH_4, suggesting over Rh/ZrO_2 the CH_4 forming reaction is more favourable at lower reaction temperatures.

Similar to what was seen over the Al_2O_3 supported catalysts; the selectivity towards CO has also decreased considerably by lowering the reaction temperature. Though this may not necessarily be explained by increased activity towards the WGS reaction, since the selectivity towards CO_2 has also decreased

slightly. Rather, the culmination of decreased selectivity towards both CO hydrogen indicated that the steam reforming reaction is less favourable at lower temperatures over Rh/ZrO_2.

Over Pt/ZrO_2 product selectivity does not change considerably with the decreasing reaction temperature. The only marked difference between the selectivity graphs is an increase in the selectivity fluctuations due to considerable noise. This is evidenced in the graphs of the rate of formation of the products, particularly with regard to the production of CO_2. This problem arises when the G.C. measures very low detectable amounts of gas and the is more of a problem at lower reaction temperatures as the catalyst is more deactivated and even less gaseous product is evolved.

4.3. Sulphur Poisoning

4.3.1. Effect of Poison Identity

To compare the effects of the two poisons, methanthiol and hydrogen sulphide, the log of the rates of formation of hydrogen were taken during the period of deactivation due to sulphur because hydrogen was the desired product and the effect on hydrogen was of major concern. This assumed first order deactivation.

The formation of hydrogen was used to compare the deactivation rates rather than ethane conversion because generally the ethane conversion graphs have more noise than the rate of formation of hydrogen graphs, therefore are less accurate.

First, a comparison of the effect of the two poisons will be made over Pt/Al_2O_3. The graph below shows the deactivation of the rate of formation of hydrogen from when either H_2S (blue) or CH_3SH (pink) is introduced.

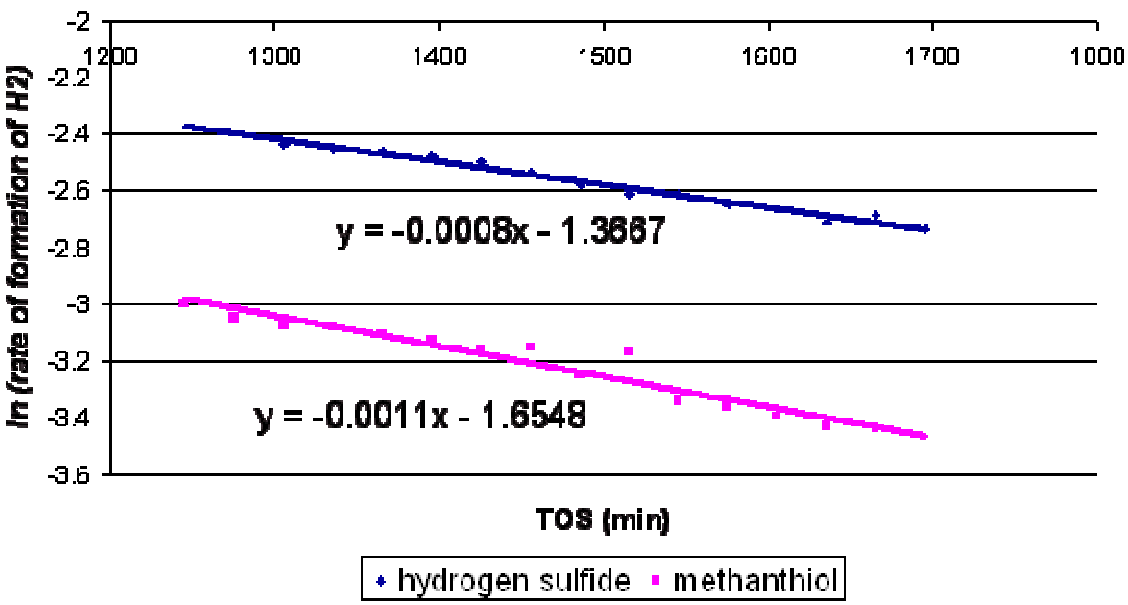

Figure 128 Effect of poisons on the ln(rate of formation of hydrogen) over Pt/Al_2O_3

Considering the deactivation rate constants obtained ($8.1x10^{-4}$ +/- $0.3x10^{-4}$ for H_2S and $10.7x10^{-4}$ +/- $0.7x10^{-4}$ for CH_3SH), methanthiol has produced a slightly faster rate of deactivation than hydrogen sulphide.

Following on, the effect of each poison will be discussed over Rh/Al_2O_3. Because the initial conversion of both the runs is different and also the rate of product formation have been altered it is not possible to make a direct comparison between H_2S and CH_3SH, therefore the effect of each poison will be discussed in turn, however the hydrogen production was stable and it was deemed appropriate to proceed with poisoning.

Initially, hydrogen production was stable, when H_2S was introduced immediate and marked deactivation takes place with a deactivation rate constant of $13x10^{-4}$ +/- $0.8x10^{-4}$.

Prior to the introduction of CH_3SH the conversion and rates of formation are at similar levels to the un-poisoned catalyst, however deactivation was occurring. Nevertheless once the poison was introduced the rate of deactivation undoubtedly increased to $46x10^{-4}$ +/- $1.3x10^{-4}$.

Rh/ZrO_2 was run for 3000 minutes before the H_2S was introduced. The rates of formation of H_2 and the other products were comparable to the rates found over the fresh catalyst at 3000 minutes on stream. The introduction of H_2S had very little effect, resulting in a small deactivation of the rate of formation of H_2.

Similarly when methanthiol was introduced, at 2317 minutes on stream, the rate of formation of hydrogen is comparable to that found in the standard run at 600°C at the same time on stream. Once the poison is introduced deactivation of the catalyst occurs rapidly. As the case with Rh/Al_2O_3, methanthiol is causing considerably more deactivation. H_2S does not have a significant deleterious effect in contrast to methanthiol, the reason for this will be discussed below:

Methanthiol resulting in faster catalyst deactivation is not surprising. With reference to the introduction (section 1.3.1.2.) the toxicity of the sulphur species increases with molecular weight. Methanthiol has a CH_3 group attached, which could be further deactivating the catalyst by:

a) Through bonding to the sulphur atom is anchored to the surface and is having an obstructive effect due to its proximity to the surface.

Or, b) The S-C bond has broken, leaving the alkyl group free to dissociate and laydown carbon on the catalyst surface.

If (b) occurred more carbon would be evident on the catalyst post reaction when methanthiol is the poison as opposed to hydrogen sulphide. This will therefore be re-visited when post reaction characterization is discussed.

4.3.2. The Effect of Poisoning on Individual Reactions: Steam Reforming, Hydrogenolysis and Water Gas Shift Reactions

It has previously been discussed that other reactions are in equilibrium with steam reforming under reaction conditions. These include the water-gas shift reaction and CH_4 forming reactions, namely hydrogenolysis and methanation. To examine the effect of sulphur poisoning on these individual reactions the deactivation of the formation of all the products are examined. The log is taken of the formation of each product, which assumes first order deactivation, this generates a straight line and from this the deactivation rate constant for each product is obtained. The period examined is from when the sulphur is introduced until deactivation begins to cease.

The effect of sulphur on the individual reactions will considered first over Pt/Al_2O_3, by examining the effect of both hydrogen sulphide and methanthiol. The table below shows the deactivation rate constants obtained from the deactivation of each of the gaseous products formed when hydrogen sulphide and methanthiol are introduced into the system.

Table 95 Deactivation rate contants ($-1x10^{-4}$) obtained for each product when H_2S and CH_3SH are introduced

	H_2S	CH_3SH
H_2	8	11
CO	2	9
CO_2	9	14
CH_4	16	24

It is clear that methanthiol has resulted in more deactivation than hydrogen sulphide. This was discussed in the previous section when solely considering the deactivation of hydrogen formation, now it is confirmed with regard to the formation of all the products.

The formation of CH_4 can be seen to deactivate most, it deactivates at almost double the rate of the other products, and this is true whether hydrogen sulphide or methanthiol is the poison. Therefore the CH_4 forming reaction appears to be the most sensitive reaction to sulphur.

The formation of H_2 and CO_2 are the products which deactivate second fastest. They exhibit very similar deactivation rate contants, both when hydrogen sulphide or methanthiol is the poison, which suggests the deactivation of these products are linked. Both H_2 and CO_2 are products of the water gas shift reaction; therefore it is likely that the water gas shift reaction is the second most sensitive reaction to the presence of sulphur.

The product exhibiting the least amount of deactivation is CO. CO is primarily a product of the steam reforming reaction, so this would suggest steam reforming is the reaction least effected by sulphur poisoning. Whilst hydrogen is also a product of steam reforming, it is also formed via water gas shift, which Pt/Al_2O_3 shows a high activity for. As a result the deactivation of hydrogen cannot be assigned solely to the deactivation of steam reforming or water gas shift, however from the deactivation rate constants it does appear to be closely related to the deactivation of CO_2 and therefore ultimately the water gas shift reaction.

The diagram below is a summary of the reactions involved during steam reforming and which ones are most susceptible to sulphur poisoning over Pt/Al_2O_3.

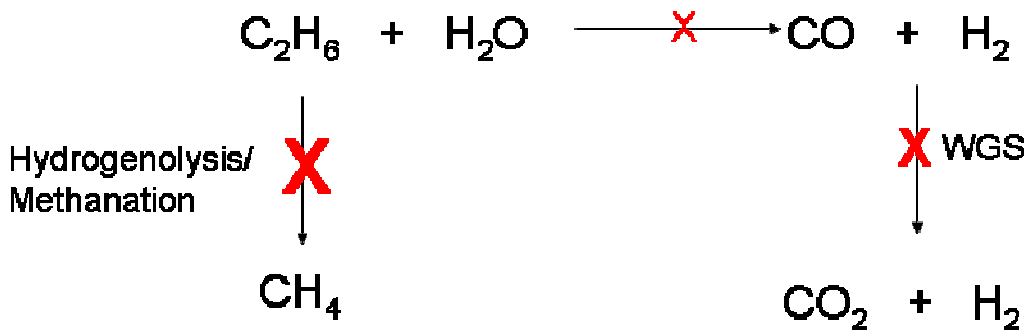

Figure 129 Reactions which take place during steam reforming and their relative suscepibility to sulphur over Pt/Al_2O_3

The same treatment of the formation of the products will now be carried out over Rh/Al_2O_3. The table below shows the deactivation rate constants obtained from the deactivation of each of the gaseous products formed when hydrogen sulphide and methanthiol are introduced into the system.

Table 96 Deactivation rate contants ($-1x10^{-4}$) obtained for each product when H_2S and CH_3SH are introduced

	H_2S	CH_3SH
H_2	13	46
CO	12	54
CO_2	16	36
CH_4	26	71

As found over Pt/Al_2O_3, the formation of CH_4 deactivates the fastest out of all the products, irrespective of the poison used. Unlike over Pt/Al_2O_3, there is much less distinction between the rates of deactivation of the other products.

When hydrogen sulphide is the poison the formation of CO_2 deactivates the second fastest, followed by H_2 and then CO. However, the difference in the rate constants is marginal, particularly between H_2 and CO, so it is concluded that the water gas shift and steam reforming reactions are deactivating at similar rates. This may be the result of Rh/Al_2O_3 not being a highly active water gas shift catalyst, as discussed in section 4.3.1.3.1. Therefore, the same extent of water gas shift deactivation, which occurred over Pt/Al_2O_3, cannot take place here.

When methanthiol is the poison, CO is the second fastest product to deactivate; previously it has always been the slowest product to deactivate. Here the

slowest product to deactivate is CO_2, suggesting there has been a shift in the order in which the reactions are poisoned. The methane forming reaction remains the most susceptible to CH_3SH, followed by the steam reforming reaction and *then* the water gas shift reaction. This new order of susceptibility has been summarized in the diagram below.

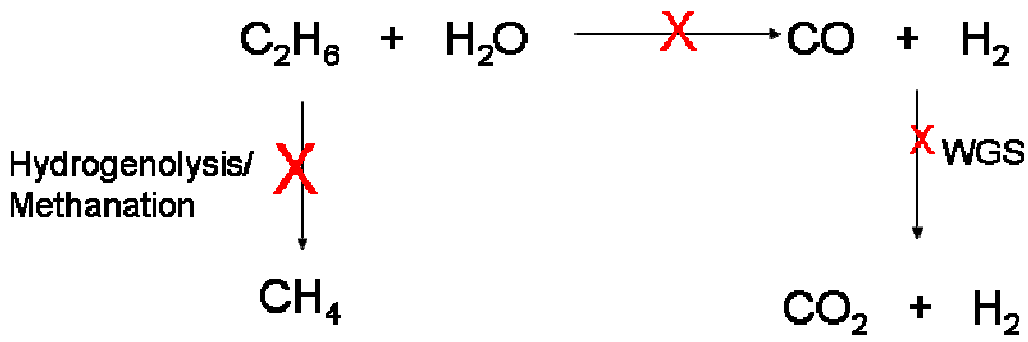

Figure 130 Reactions which take place during steam reforming and their relative suscepibility to CH_3SH over Rh/Al_2O_3

Interestingly, there is a clear distinction between the two poisons on the effect they are having on the individual reactions, which was not evident over Pt/Al_2O_3. This is in agreement with what was previously discussed that there was not much distinction between the poisons with regard deactivation of hydrogen formation over Pt/Al_2O_3, whilst a considerable difference between the poisons was seen over Rh/Al_2O_3.

The deactivation of the formation of the products will now be examined over Rh/ZrO_2. The table below shows the deactivation rate constants obtained from the deactivation of each of the gaseous products formed when hydrogen sulphide and methanthiol are introduced into the system.

Table 97 Deactivation rate contants ($-1x10^{-4}$) obtained for each product when H_2S and CH_3SH are introduced

	H_2S	CH_3SH
H_2	3	29
CO	0	22
CO_2	0	25
CH_4	9	39

The introduction of hydrogen sulphide into the system has resulted in very little or no deactivation with regard to the formation of products. Whilst, the

presence of methanthiol has caused considerable deactivation to the formation of all the products.

Again, it is the formation of CH_4 which deactivates the quickest, for both hydrogen sulphide and methanthiol poisoning. The deactivation rate constants obtained for the other products are all very similar. The formation of hydrogen deactivates slightly faster than CO and CO_2, irrespective of the poison introduced; and the formation of CO_2 deactivates marginally faster than CO during methanthiol poisoning.

When methanthiol poisons Rh/ZrO_2 the methane forming reaction is the most retarded, followed by the water-gas shift reaction and steam reforming, which appear to be affected to the same degree.

With all the catalysts (no matter what the initial state) it was seen that the formation of CH_4 deactivated the fastest, and there is a number of possible explanations for this:

- The formation of CH_4 requires a larger ensemble size than steam reforming or water-gas shift reaction. Rostrup-Nielsen [95] found steam reforming to involve ensembles of 3-4 nickel atoms, while the formation of CH4 required 6 or 7 atoms [95,96].

- Sulphur is selectively poisoning the CH_4 forming sites.

In the case of irreversible adsorption, the metal poisoning that would follow could either be selective or nonselective. A nonselective poison would present the same toxicity for all the reactions, whereas a selective poison would present considerable toxicity for any reaction occurring on sites where it is adsorbed, and negligible toxicity for all the reactions occurring on sites where it is not adsorbed. The notion of a selective poison whose adsorption would be sensitive to the structure of the catalyst is, in the case of sulphur, in perfect agreement with the energy values of adsorption, which show that this additive is energetically more tightly bound on the planes of low density. These are the same sites that seem to be most active for hydrogenolysis [94].

4.3.3. Catalyst Regeneration

The sulphur was removed from the feed water after six hours from when it was first introduced into the system to see if the catalysts recovered any of their initial activity. To gauge the recovery of the catalysts the formation of hydrogen was again examined. By taking logs of the rate of formation of hydrogen from when sulphur is removed straight lines are generated and rate constants of the catalysts regeneration are obtained. The regeneration of each catalyst along with the rate constants are displayed in the graph below.

Only the regeneration of the methanthiol poisoned catalysts are considered here since these were the catalysts, which exhibited the most severe catalyst deactivation.

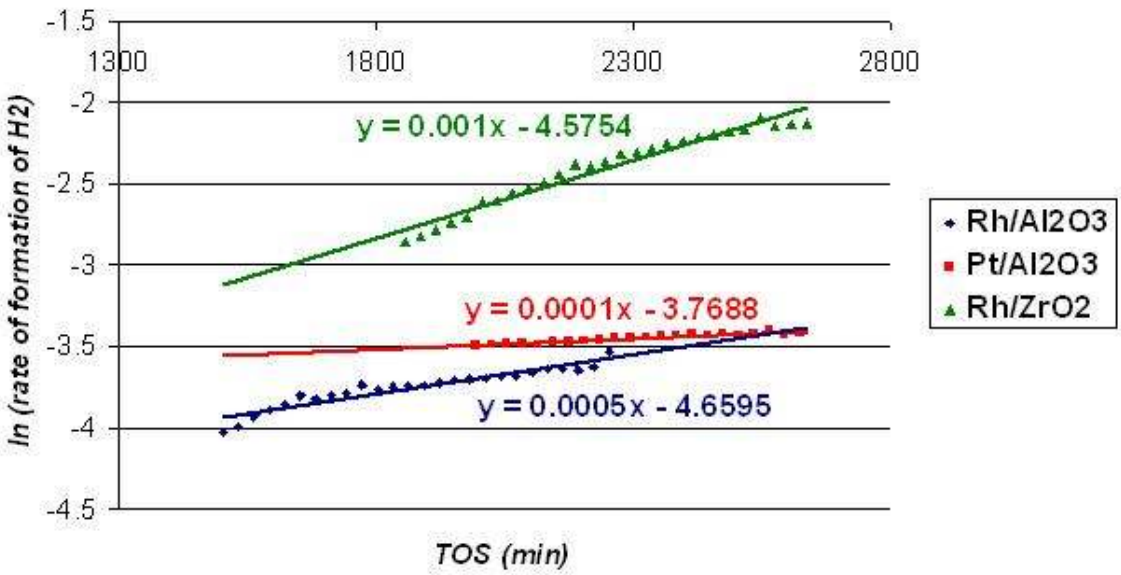

Figure 131 Graph showing the regeneration of the catalysts when sulphur is removed by examining the recovery in hydrogen formation

From the graph, Pt/Al_2O_3 is recovering the least in terms of the formation of hydrogen, whereas Rh/Al_2O_3 shows a great deal more recovery with the rate formation of hydrogen is 5 times faster than over Pt/Al_2O_3. The catalyst that regenerates at the fastest rate is Rh/ZrO_2, which exhibited the most severe catalyst deactivation. We have subjected the catalyst to1.49mg of methanthiol, this amount is in considerable excess to any sulphur that could have been accrued from previous testing (as determined by catalytic results).

The extent to which the catalysts recovered was also examined by comparing the highest value of the rate of formation hydrogen once the poison was removed to the initial rate of formation of hydrogen, before any sulphur was introduced. By this method a percentage by which each catalyst recovered was obtained and the values are displayed in the table below.

Table 98 Extent of catalyst recovery, recovery in the rate of formation of hydrogen

Catalyst	Pt/Al_2O_3	Rh/Al_2O_3	Rh/ZrO_2
% Recovery in terms of rate of formation of H_2	6	20	67

Rh/ZrO_2 regenerates considerably better than the other catalysts, suggesting the support is having a positive influence on the catalysts ability to remove sulphur. It was discussed in the introduction; section 1.2.2.2.3, that doping of the ZrO_2 support increased the number of oxygen vacancies and resulted in a faster rate of oxygen transfer to the metal. This oxygen can react with carbon deposited on the surface of the metal to produce CO_X species.

The Rh/ZrO_2 presently under discussion has been doped with La^{3+}, which could be promoting the catalysts redox properties in a similar manner. The cause of the catalysts deactivation may have been a combination of sulphur poisoning and carbon formation on the catalyst, particularly when considering methanthiol, which may be decomposing and laying down carbon. This is supported by the small effect H_2S has on the catalyst. If there is carbon formation there is mechanism to remove it due to the unique properties of the ZrO_2 support. Therefore, the regeneration of 67% of the catalyst may be from the removal of deposited carbon. The remaining 33% of the catalyst, which remains un-regenerated, could be the sites that have been poisoned by sulphur.

Another possibility exists whereby all the deactivation is due to the poisoning of sites with sulphur and no carbon formation took place. This would lead to the conclusion that there are two types of sulphur present on the catalyst: reversible and irreversibly adsorbed sulphur. In this case 67% of the sulphur is reversibly adsorbed and 33% is irreversibly adsorbed. Previous studies (67,68) have found that 80% of surface sulphur could be removed by regeneration using

steam and the heating the catalyst under hydrogen also regenerated 80% of the catalyst. Therefore, under the present steam reforming reaction conditions it should be possible to remove a portion of the sulphur from the catalyst surface.

Evidence was gained from the poisoning experiments that sulphur did promote carbon formation on the catalysts (see carbon mass balance, figure 101 in section 4.3.5), and therefore catalyst deactivation is the result of both sulphur poisoning and carbon laydown. This relationship between sulphur and coking has previously been cited, [63]; where it was inferred sulphur increases the amount of coke deposited on the support. It is likely that on removal of the poison from the feed, any regeneration is due to removal of deposited carbon.

As well as the support having a major impact on catalyst regeneration, the nature of the metal is also appeared to be a factor, with Rh/Al_2O_3 regenerating considerably more than Pt/Al_2O_3. This is likely to be because Pt had a lower original activity than Rh and had already begun to deactivate before sulphur was even introduced into the system.

4.3.4. Effect of Poison Concentration

To examine the effect halving the concentration of the poison had on catalyst deactivation, the deactivation of hydrogen formation at a poison concentration of 11.2ppm is compared to that of 5.6ppm. The rate formation of hydrogen prior to the introduction of poison was similar for both tests. The graph below contains this information from two reactions, one which was poisoned with 11.2ppm methanthiol and one which was poisoned with 5.6ppm methanthiol, both conducted over Rh/Al_2O_3.

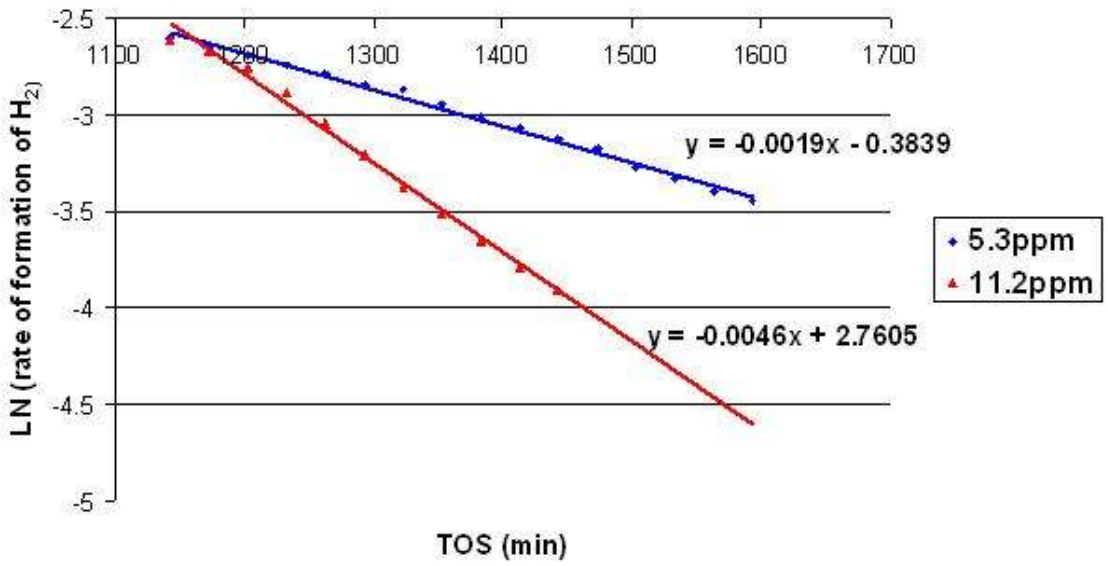

Figure 132 Deactivation of hydrogen formation over Rh/Al_2O_3 at two different poison concentrations

From the deactivation rate constants obtained it can be seen that halving the concentration of the poison approximately halves the rate of deactivation. This suggests that the catalyst deactivation is directly proportion to the amount of poison adsorbed onto the catalyst and that chemisorbed methanthiol poisons by blocking the metal surface for adsorption of reactants.

Evidence for this was also found during the steam reforming of ethane over 25wt.%Ni/$MgOAl_2O_3$, see table 3 of introduction section.

The deactivation rate constants of the other products for the two different concentrations can be compared in the same way.

Table 99 Deactivation rate constants for products at two different concentrations of methanthiol over Rh/Al_2O_3

Product	H_2	CO	CO_2	CH_4
Deactivation rate constant ($-1x10^{-4}$) 11.2ppm	46	54	36	71
Deactivation rate constant ($-1x10^{-4}$) 5.6ppm	19	19	19	28

It appears that the deactivation rates for all the products have approximately halved when the poison concentration was halved.

The same comparison of using two different methanthiol concentrations, 5.6ppm and 11.2ppm, was carried out over Rh/ZrO_2. The deactivation rate constants for all the products at the two different concentrations are provided in the table below.

Table 100 Deactivation rate constants for products at two different concentrations of methanthiol over Rh/ZrO_2

Product	H_2	CO	CO_2	CH_4
Deactivation rate constant ($-1x10^{-4}$) 11.2ppm	29	22	25	39
Deactivation rate constant ($-1x10^{-4}$) 5.6ppm	26	26	30	33

Over Rh/ZrO_2, it appears halving the poison concentration has had very little effect on the rate that products deactivate. This result is rather exceptional and disagrees with what was found over Rh/Al_2O_3 and findings in the literature, that there is direct relationship between sulphur coverage and catalyst deactivation. Unfortunately this experiment was not repeated and considering the inconsistency of this result with some of the literature it would be desirable to repeat it for further confirmation.

4.3.5. Effect of Sulphur on Carbon Formation

4.3.5.1. Influence of poison on carbon laydown

A comparison has been made between methanthiol and hydrogen sulphide on the formation of carbon over Rh/ZrO_2 during steam reforming. From table 19 in the characterization section,3.1.2.3.1, it is evident that in the presence of either poison, two types of carbon are formed on the catalyst surface. The amount of low temperature carbon deposited is the exact same for both the poisons. However, there is variation in the amount of high temperature carbon deposited. When methanthiol is the poison rather than hydrogen sulphide, the amount of high temperature carbon deposited has doubled. The deposition of extra carbon may have arisen from the cracking of the alkyl group in methanthiol.

4.3.5.2. Carbon deposition on Rh/Al_2O_3, Rh/ZrO_2 and Pt/Al_2O_3

When the amount of carbon deposited on Rh/ZrO_2 was compared to that deposited on Rh/Al_2O_3 during a H_2S poisoned steam reforming reaction, section 3.1.2.3.2, it was found there was significantly less deposition on Rh/ZrO_2. Also, the type of carbon deposited on each catalyst was different. From the TPO of Rh/ZrO_2, a lower temperature peak at 500°C dominated, whilst a higher temperature peak at 650°C was evident in the TPO of Rh/Al_2O_3. Therefore not only was there more carbon deposited on Rh/Al_2O_3, but the carbon was also more strongly bound.

Similarly, the results from methanthiol poisoned reactions show there was much less carbon deposition on Rh/ZrO_2 than on Pt/Al_2O_3. This provides evidence that doped Rh/ZrO_2 has unique redox properties and a mechanism whereby it can remove deposited carbon which is absent in the alumina supported catalysts.

5. Summary

From the adsorption studies conducted at room temperature there appeared to be little difference between the behaviour of H_2S and CH_3SH, both produced similar sulphur coverage's over the catalysts to generate a M:S ratio of approximately 1:1. However, with regard to the steam reforming results large differences were found between the poisons, with CH_3SH exhibiting a greater level of toxicity. This was attributed to the formation of carbon on the surface of the catalyst, which would have not occurred during room temperature adsorptions. Therefore, a better comparison would have been made if the CH_3SH adsorptions were also conducted at 600°C, as carbon laydown would likely be occurring.

Both the steam reforming experiments and the adsorption study lead to the conclusion that sulphur is very strong adsorber on the catalysts. From the competitive adsorption experiments it was apparent that adsorbed sulphur could not be displaced by the adsorption of other molecules such as CO. Whilst, during the poisoning experiments the alumina catalysts recovered little of their activity once the poison was removed, presumably because sulphur was still present on the catalyst surface. What activity that was recovered, is most likely to be from removal of deposited carbon rather than from the removal of adsorbed sulphur. Rh/ZrO_2, however, did show effective resistance to sulphur poisoning. H_2S had very little effect on the catalyst and although methanthiol did result in deactivation this was mainly attributed to carbon deposition.

Support effects were found to have positive influence on the catalysts resistance to sulphur, from both the steam reforming experiments and the adsorption studies. The adsorption study showed how the alumina support adsorbed large quantities of sulphur and this was found to be beneficial during co-adsorption of CO and H_2S as it free-ed up the metal sites for CO adsorption. Another property of the support was found to dominate the catalysts ability to recover activity after poisoning, ZrO_2s unique redox properties. Further understanding and manipulation of the catalyst support material could prove fruitful in the development of a sulphur tolerant catalyst.

6. References

[1] J. N. Armor, *Applied Catalysis a-General,* 176 (1999) 159-176
[2] L. Basini, *Catalysis Today* 106 (2005) 34-40.
[3] J.R.Rostrup-Nielsen, *Proceedings of the15th World Petroleum Congress*, John Wiley and Sons (1998) 767
[4] M.A. Pena, J.P.Gomez, J.L.G. Fierro, *App. Catal. A: Gen*, 144 (1996) 7
[5] D. L. Trimm, *Catalysis Today,* 37 (1997). 233-238.
6 D.E. Ridler, M.V. Twigg, in *Catalysis Handbook*, M.V. Twigg (Ed), Manson, London, 2nd Ed. (1997)
[7] J.R.H. Ross, in *Surface and Defect Properties of Solids*, senior reporters M.W. Roberts and J.M. Thomas (Specialist Periodical Report, The Chemical Society, London, 1975), vol. 4, pp 34-67.
[8] J.C. Yarze and T.E. Lockerbie, *Am. Chem. Soc.137th Meeting, Division of Gas and Fuel Chemistry*, 1960, p. 78.
[9] B. Kneal and J.R.H. Ross, *Faraday Discussion. Chem. Soc* (1981) 157-171
[10] P.O. Graff, B.L. Mojet, J.G. Ommen, L. Lefferts, *App. Catal. A*. 332 (2007) 310-317
[11] D.C. Grenoble, M.M. Estadt, *J. Catal*. 67 (1981) 90-102
[12] A. Igarashi, O. Takeshi, S. Motoki, *Catal. Letters*. 13 (1991) 189
[13] P.O. Graff, B.L. Mojet, L. Lefferts, *App. Catal. A*. 346 (2008) pp 90-95
[14] J.H. Sinfield, *J.Catal* 27 (1972) 468-471
[15] J.H. Sinfield, D.J.C. Yates, *J.Catal* 10 (1968) 362-367
[16] J.H. Sinfield, D.J.C. Yates, *J.Catal* 8 (1967) 82-90
[17] A.C. Zeigarnik, R.E. Valdes-Perez, O.N. Myatkovskaya, *J. Phys. Chem. B* 104 (2000) 10578
[18] E.H.v. Broekhoven, V. Ponec, *Prog. Surf. Sci*. 19 (1985) 351
[19] J.R. Rostrup-Nielsen, in *Catalysis Science and Technology* (J.R. Anderson, M. Boudart eds), Springer-Verlag, Vol 5 (1984)1
[20] A. Igarashi, T. Ohtaka, S. Motoki, *Catal. Letters*. 13 (1991) 189-194
[21] J.A. Dalmon, C. Mirodatos, P. Turlier, G.A. Martin, in *Spillover of Adsorbed Species*, G.M. Pajonk et al. (Eds.), Elsvier, Amsterdam (1983) 169
[22] D. Wang, O. Dewaele, A.M. De Groote, G.F. Froment, 159, *J. Catal*. (1996) 418
[23] D. Wang, Z. Li, C. Luo, W. Weng, H. Wan, *Chem. Eng. Sci.*, 58 (2003) 887
[24] R. Kramer, M, Andre, *J.Catal.*, 58 (1979) 287
[25] J.F. Cevallos,-Candau, J.L. Conner, *J.Catal.*, 106 (1987) 378
[26] P.Chiaranussati, L.F. Gladden, R.F. Griffiths, S.D. Jackson, G. Webb, *Trans. Inst. Chem. Eng.*, 71 (1993) 267
[27] M.M.V.M. Souza, D.A.G. Aranda, M. Schmal, *J. Catal*. 204 (2001) 498
[28] T. Horiuuchi, K. Sakuma, T. Fukui, Y. Kubo, T. Osaki, T. Mori. *Appl. Catal. A,* 144 (1996) 111
[29] Z.L. Zhang, X.E. Verykios, *Catal. Today,* 21 (1994) 589
[30] H.W. Wang, E. Ruckenstein, *Appl. Catal. A: General,* 204 (2000) 143
[31] L.V. Mattos, E. Rodina, D.E. Resasco, F.B. Passos, F.B. Noronha, *Fuel Process. Tech.*, 83 (2003) 147
[32] L. Wang, K. Murata, Y. Matsumura, M. Inaba, *Energy and Fuels*. 20 (2006) 1377-1381
[33] J. Sehested, *Catalysis Today*, 111 (2006) 103-110
[34] J.A. Moulijn, A.E. Van Diepen, F. Kapteijn, *Appl. Catal. A: Gen.,* 212 (2001) 3
[35] C. H. Bartholomew, *Applied Catalysis A: General,* 212 (2001) 17-60

[36] Bartholomew, C. H. Agrawal, P.K; Katzer, J.R. *Adv. Catal* (1982) *Sulphur poisoning of metals.*
[37] J.M. Saleh, C. Kemball, M.W. Roberts, *Trans. Faraday. Soc.* 57 (1961) 1771
[38] Den Besten, I. E., Selwood, P.W, *Journal of Catalysis* 1 (1962) 93-102
[39] J. R. Nielsen, Steam Reforming Catalysts, Danish Technical Press Inc. (1974)
[40] J.L. Oliphant, R.W. Fowler, R.B. Pannell, C.H. Bartholomew, J.*Catal*. 51 (1978) 229
[41] S. D. Jackson, P. Leeming, J. Grenfell, *J. Catal*. 150 (1994) 170-176
[42] S. D. Jackson, P. Leeming, G. Webb, *J.Catal*. 160 (1996) 235-243
[43] A.H. Uken, C.H. Bartholomew, *Appl. Catal* (1982)
[44] H.P. Bonzel, R. Ku, *J. Chem. Phys*. 58 (1973) 4617
[45] S. D. Jackson, J. Willis, G.D. McLellan,, G. Webb, M.B.T. Keegan, R.B. Moyes, S. Simpson, P.B. Wells, R. Whyman, *J.Catal*. 139 (1993) 207
[46] S.D. Jackson, B.J. Brandreth, D. Winstanley, *J. Chem. Soc. Faraday Trans. 1,* 83 (1987) 000-000
[47] L.D. Schmidt, D. Luss, *J.Catal*. 22 (1971) 269
[48] A-M. Lanzilotto, S.L. Bernasek, J. Chem.Phys. 84 (1986) 3553
[49] R.H. Hedge, J.M. White, *J. Chem. Phys*. 90 (1986) 296-300
[50] E.B Maxted, *Adv Catal*. 3 (1951) 129
[51]T.F.Garetto, A.Borgna, C.R. Apesteguia, *Surf. Sci*. 88 (1994) 369
[52] M.Guenin, M.Breysse, R.Frety, *J.Catal*. 105 (1987) 144-154
[53] P. Reyes, G. Pecchi', M.E. Kiinig and J.L,G. Fierro, *Rcact.Kinet.Catal.Lctt*. 67 (1999) 177-182
[54] G.A.del Angel, B.Coq, F.Figueras, *Nouveau Journal de Chimie*. 7 (1983) 173
[55] R. Torbati, S. Cimino, G. Russo, *Catal. Letters*. 127 (2009) 260-269
[56]P.Reyes, G.Pecchi, M.Morales, *App.Catal. A*. 163 (1997) 145-152
[57]Jackson, S. D., Winstanley, D, *J. Catal*. 121 (1990) 312-317
[58]L.Wang, K.Murata, M.Inaba, *App.Catal.B*. 48 (2004) 243-248
[59]Y. Li, X. Wang, C. Xie, C. Song, *App. Catal. A,* 357 (2009) 213
[60] J.R. Rostrup-Nielsen, *J. Catal*. 31 (1973) 173 READ
[61] J.R. Rostrup-Nielsen, 'Steam Reforming Catalysts' Teknisk Forlag. Copenhagen (1975)
[62] G. Delahay, D. Duprez, *Appl. Catal*. 53 (1989) 95-105
63 J.Barbier, D. Duprez, *Appl. Catal. B. Environ*. 4 (1994) 105
[64] J. Barbier, P. Marecot, *J.Catal,* 102 (1986) 21
[65] M. Ferrandon, J. Mawdsley, T. Kraus, *Appl. Catal. A: General*, 342 (2008) 69
[66] S.D. Jackson, B.J. Brandreth, D. Winstanley, *J. Catal*, 129 (1991) 540
[67] G.A. Somorjai, *J. Catal*. 27 (1972) 453
[68] J. Biswas, *catalysis review - science and engineering,* 30(2) (1988) 161.
[69] J.R. Rostrup-Nielsen, *J. Catal*. 21 (1971) 171
[70] M. Mathieu, M. Primet, *Applied Catalysis a-General* 9 (1984) 361-371.
[71] E.Opara, *Carbon forming reactions over precious metal steam reforming catalysts* (2005).
[72] T.A Dorling, R.L Moss, J. Catal, 7 (1967) 378
[73] L. H. Little, in *Chemisorption and Reactions of Metallic Films,* ed. J. R. Anderson (Academic ress, London, 1971), vol. 1, p. 489.
[74] R. P. Eischens and W. A. Pliskin, *Adv. Catalysis,* 10 (1958) 2.
[75] C. W. Garland, R. C. Lord and P. F. Troiano, *J. Phys. Chem, 69* (1965*)* 1188.
[76] J. F. Harrod, R. W. Roberts and E. F. Rissmann, J. *Phys. Chem.,* 71 (1967) 343.
[77] R. P. Eischens, S. A. Frances and W. A. Pliskin, J. *Phys. Chem.,* 60 (1956) 194.
[78] R. P. Eischens and W. A. Pliskin, *Adv. Catalysis,* 10 *(*1958) 2.
[79] L. H. Little, *Infra Red Spectra of Adsorbed Species* (Academic Press, London and New York), 1966
[80]. G. Blyholder, J. *Phys. Chem.,* 68 (1964) 2772

[81] S.J. Thomson, G. Webb.*Heterogeneous Catalysis*, (1968)
[82] Santen, R. J.*chem. Soc., Faraday Trans. I*, 83 (1987) 1915-1934
[83] Lemieux, R. U; Chu, N. J. Abstracts of Papers, 133rd National meeting of the American Chemical Society(1958)
[84] Basu, P; Panayotov, D; Yates, J.T. *J. Am. Chem. Soc*, 110 (1988) 2074-2081
[85] Jackson, S.D; Leeming, P; Grenfell, J. *J. Catal.*, 150 (1994) 170-176
[86] Tamele, M. W, *Discussion Faraday Soc.* 8 (1950) 270
[87] DeRosset, A. J; Finstrom, C. G; Adams, C. J, *J. Catal.* 1 (1962) 235-243
[88] Okamoto, Y; Oh-Hara, M; Maezawa, A; Imanaka, T; Teranishi, *J. Phys. Chem.* 90 (1986) 2396-2407
[89] R.I. Hedge, J.M. White, *J. Phys. Chem.* 90 (1986) 296
[90] Oliphant, J.L; Fowler, R.W; Pannell, R.B; Bartholomew, C.H., J.Catal. 51 (1978) 229
[91] Erekson, E.J; Bartholomew, C.H,. Appl.Catal (1982)
[92] Mullins, D.R; Lyman, P.F,. J. Phys. Chem. 97 (1993) 12008-12013
[93] G.A. Somorjai, Surf. Sci. 89 (1979) 496
[94] J. Oudar, H. Wise, *Deactivation and Poisoning of catalysts*, (1985)
[95] J.R. Rostrup-Nielsen, J. Catal., 85 (1984) 31
[96] J.R. Rostrup-Nielsen, Catalyst deactivation, in: C.H. Bartholomew, J.B. Butt (Eds.), Studies in Surface Science and Catalysis, vol. 68, Elsevier, Amsterdam, 1991.